

**Assessment of *in vitro* cardiotoxicity  
using metabolomics and  $^{13}\text{C}$  metabolic  
flux analysis**

Dissertation  
zur Erlangung des Grades  
des Doktors der Naturwissenschaften  
der Naturwissenschaftlichen-Technischen Fakultät III  
Chemie, Pharmazie, Bio- und Werkstoffwissenschaften  
der Universität des Saarlandes  
von

**Alexander Strigun**

Saarbrücken

2012

Tag des Kolloquiums: 20.07.2012

Dekan: Prof. Dr. Wilhelm F. Maier

Berichterstatter: Prof. Dr. Elmar Heinzle  
Prof. Dr. Manfred J. Schmitt

Vorsitz: Prof. Dr. Petra Bauer

Akad. Mitarbeiter: Dr. Gert-Wieland Kohring

*“All things are poison, and nothing is without poison, only the dose permits something not to be poisonous”*

**Paracelsus**

**Meinen Eltern**

# Acknowledgements

I owe my deepest gratitude to Prof. Dr. Elmar Heinzle for giving me the opportunity to work in the EU-project “Invitroheart”. I am thankful for his invaluable assistance and constant support throughout my thesis.

I am also thankful to Prof. Manfred Schmitt for his review of this thesis.

I would like to express my deepest appreciation to my scientific supervisor Dr. Fozia Noor for her time and patience as well as her invaluable contributions to the scientific manuscripts. I could storm her office at any given time and she always had an ear for me.

Thanks goes to Dr. Reiner Claß from Pharmacelsus GmbH for providing technical help on cytotoxicity assays. Thanks also to Dr. Sarina Arain from PreSens GmbH for her technical support on oxygen measurement devices.

I really would like to express my gratitude to all my colleagues at the Technische Biochemie. Without the help of you all this work would not have been possible. Many thanks go to Dr. Klaus Hollemeyer, Dr. Susanne Kohring, Michel Fritz and Robert Schmidt for their administrative and technical support. From my fellow Ph.D. students Averina Nicolae and Simone Beckers deserve a special mention here since they were not only very helpful and inspiring colleagues, but they also became very good friends. Thank you Averina! Thank you Simone! I am really glad I met you! I am sincerely grateful to Jens Niklas for many fruitful discussions and his help on <sup>13</sup>C metabolic flux analysis. I also want to express my gratitude to Judith Wahrheit for her invaluable experimental contributions during her diploma thesis. A thank you also goes to Alejandro Pironti for his patience during the medium optimisation experiments. I am also thankful to Angela Sudhoff for her contribution to respiration measurements on cardiomyocytes. I am sincerely grateful to Averina Nicolae, Christian Weyler, Steffen Krauser, Malina Orini as well as Daniel Müller, Georg Tascher, Christian Priesnitz and Saskia Müller for the nice atmosphere in the office upstairs and in the lab.

## Acknowledgements

---

I would like to thank my old university mate and friend Dr. Akuma Saningong for his moral support and the numerous enlightening discussions about “all the world and his brother”. A big thank you also goes to my friends Sebastian Sehn and Matthias Zenner as well as my old friends from Darmstadt.

Finally, I thank my beloved family for their constant encouragement and for their support in all its forms. Without you the present work would not have been possible.

## Abbreviations

AcCoA	Acetyl-Coenzyme A
AKG	Alpha-ketoglutarate
ALA	Alanine
AMM	Atom mapping matrices
ASN	Asparagine
ARG	Arginine
ASP	Aspartate
ATP	Adenosinetriphospate
CIT	Citrate
CM	Cardiomyocyte
CYS	Cysteine
DNA	Desoxyribonucleic acid
DXR	Doxorubicin
ECG	Electrocardiogram
FBS	Foetal bovine serum
GC/MS	Gas chromatography mass spectrometry
GLC	Glucose
GLN	Glutamine
GLU	Glutamate
GLY	Glycine
G6P	Glucose-6-phosphate
hESC-CM	Human embryonic stem cell derived cardiomyocyte
HIS	Histidine
HPLC	High performance liquid chromatography
ILE	Isoleucine
IMM	Isotopomer mapping matrices
LAC	Lactate
LDH	Lactate dehydrogenase
LEU	Leucine

## Abbreviations

---

LYS	Lysine
MAL	Malate
MBDSTFA	N-methyl-N-t-butyltrimethylsilyl-trifluoroacetamide
MET	Methionine
mM	Millimolar
MFA	Metabolic flux analysis
$\mu\text{M}$	Micromolar
$\text{NAD}^+$	Nicotinamide dinucleotide
$\text{NADH}+\text{H}^+$	Nicotinamide dinucleotide reduced form
NCE	New chemical entity
NSAID	Non-steroidal anti-inflammatory drug
OAA	Oxaloacetate
PBS	Phosphate buffered saline
PCA	Principal component analysis
PEP	Phosphoenolpyruvate
PHE	Phenylalanine
PPP	Pentose phosphate pathway
PRO	Proline
PYR	Pyruvate
ROS	Reactive oxygen species
RT	Room temperature
SER	Serine
SRB	Sulforhodamine B
SUCC	Succinate
TCA-cycle	Tricarboxylic acid cycle
TCA	Trichloroacetic acid
TdP	Torsades de pointes
THR	Threonine
TRP	Tryptophane
TYR	Tyrosine
VAL	Valine



# Table of contents

<b>ACKNOWLEDGEMENTS</b> .....	<b>I</b>
<b>ABBREVIATIONS</b> .....	<b>III</b>
<b>SUMMARY</b> .....	<b>1</b>
<b>ZUSAMMENFASSUNG</b> .....	<b>2</b>
<b>CHAPTER 1</b> .....	<b>3</b>
INTRODUCTION .....	3
Drug induced cardiotoxicity and the need for predictive <i>in vitro</i> models and assays.....	3
Cardiac <i>in vitro</i> models for preclinical drug testing .....	4
Respiration measurement in cardiac cells using oxygen sensitive sensors.....	5
Metabolomics in cardiac research .....	6
<sup>13</sup> C metabolic flux analysis.....	8
Objective of the thesis .....	10
<b>CHAPTER 2</b> .....	<b>12</b>
EC <sub>50</sub> DYNAMICS FOR A BETTER UNDERSTANDING OF TOXICITY .....	12
Abstract .....	12
Introduction .....	13
Material and methods .....	14
Results .....	16
Discussion .....	21
<b>CHAPTER 3</b> .....	<b>24</b>
METABOLIC PROFILING USING HPLC ALLOWS CLASSIFICATION OF DRUGS ACCORDING TO THEIR MECHANISMS OF ACTION IN HL-1 CARDIOMYOCYTES.....	24
Abstract .....	24
Introduction .....	25
Material and methods .....	28
Results .....	32
Discussion .....	41
<b>CHAPTER 4</b> .....	<b>44</b>
METABOLIC FLUX ANALYSIS GIVES AN INSIGHT ON VERAPAMIL INDUCED CHANGES IN CENTRAL METABOLISM OF HL-1 CELLS.....	44
Abstract .....	44
Introduction .....	45
Material and Methods.....	46
Results .....	51
Discussion .....	59

<b>CHAPTER 5</b> .....	<b>63</b>
DOXORUBICIN RESULTS IN INCREASED OXIDATIVE METABOLISM IN HL-1 CARDIOMYOCYTES AS SHOWN BY METABOLIC FLUX ANALYSIS.....	63
Abstract .....	63
Introduction .....	64
Material and Methods.....	66
Results .....	71
Discussion .....	80
<b>CHAPTER 6</b> .....	<b>85</b>
CHARACTERISATION OF THE CENTRAL METABOLISM IN CARDIOMYOCYTES DERIVED FROM HUMAN EMBRYONIC STEM CELLS IN RESPONSE TO DOXORUBICIN .....	85
Abstract .....	85
Introduction .....	86
Material and methods .....	88
Results .....	90
Discussion .....	96
<b>CHAPTER 7</b> .....	<b>99</b>
CONCLUDING REMARKS .....	99
Cytotoxicity screening of cardioactive drugs on murine HL-1 cardiomyocytes .....	99
Metabolic profiling of HL-1 cardiomyocytes in response to cardiotoxic drugs .....	100
<sup>13</sup> C metabolic flux analysis in HL-1 cells upon exposure to Doxorubicin and Verapamil .....	100
<sup>13</sup> C metabolic flux analysis in human embryonic stem cell derived cardiomyocytes upon exposure to Doxorubicin.....	102
<b>CHAPTER 8</b> .....	<b>103</b>
OUTLOOK.....	103
<b>REFERENCES</b> .....	<b>106</b>
<b>APPENDIX</b> .....	<b>121</b>
CHAPTER 2 .....	121
CHAPTER 3 .....	123
CHAPTER 4.....	125
CHAPTER 5.....	136
CHAPTER 6.....	143
<b>LIST OF PUBLICATIONS:</b> .....	<b>146</b>
<b>CURRICULUM VITAE</b> .....	<b>147</b>

# Summary

The potential of respiration measurements, metabolomics and  $^{13}\text{C}$  metabolic flux analysis ( $^{13}\text{C}$ -MFA) for the determination of drug-induced cardiotoxicity was analysed. Two cardiac *in vitro* models, namely murine HL-1 cells and human embryonic stem cell derived cardiomyocytes (hESC-CM) were applied for this purpose.

Respiration measurement in HL-1 cells upon drug treatment revealed distinct  $\text{EC}_{50}$  profiles. The toxicity occurred either fast or with a delay. This effect was dependant on the mechanism of toxicity of the respective drugs.

Metabolite profiling of HL-1 cells in response to sub-toxic drug concentrations was carried out by using HPLC. The considered metabolites included glucose, lactate, pyruvate and amino acids. The metabolic profiles were drug class dependant, as shown by multivariate statistics, thereby allowing classification of drugs according to their mechanisms of action.

$^{13}\text{C}$ -MFA was carried out to determine the effect of  $\text{Ca}^{2+}$  channel blocker verapamil and the cytostatic drug doxorubicin on the central metabolism at concentrations which were clinically relevant and non-toxic. Verapamil-treatment resulted in a highly efficient glucose metabolism in HL-1 cells. In both HL-1 cell and hESC-CM, doxorubicin-treatment resulted in an increased oxidative metabolism, most likely to avoid ATP-depletion.

The obtained results potentially have pharmacological relevancy, but also provide novel strategies for preclinical toxicity determination of new drug compounds.

# Zusammenfassung

In dieser Arbeit wurde das Potential von Respirationsmessungen, Metabolomics-Anwendungen und  $^{13}\text{C}$  basierten metabolischen Flussanalysen ( $^{13}\text{C}$ -MFA) zur Bestimmung von Medikamenten-induzierter Kardiotoxizität untersucht. Es wurden HL-1 Kardiomyozyten sowie aus humanen embryonalen Stammzellen gewonnene Herzzellen (hESC-CM) als *in vitro* Modelle verwendet.

Die Respirationsmessungen an HL-1 Zellen ergaben je nach Medikament sehr unterschiedliche  $\text{EC}_{50}$ -Dynamiken. Der toxische Effekt trat entweder sehr schnell oder mit einer zeitlichen Verzögerung ein. Die  $\text{EC}_{50}$ -Dynamiken waren von den Toxizitätsmechanismen der entsprechenden Medikamente abhängig.

Die Erstellung von Metabolit-Profilen in HL-1 Zellen wurde nach Gabe von subtoxischen Medikamentenkonzentrationen mittels HPLC durchgeführt. Es wurden Glukose, Laktat, Pyruvat sowie 20 Aminosäuren gemessen. Mit Hilfe multivariater statistischer Methoden konnten Medikamentenklassen-abhängige Metabolit-Profile bestimmt werden.

$^{13}\text{C}$ -MFA wurde angewandt, um den Einfluss des Kalziumkanal-Blockers Verapamil sowie des Zytostatikums Doxorubicin auf den Zentralstoffwechsel zu bestimmen. Die betrachteten Konzentrationen der Wirkstoffe waren sowohl klinisch relevant also auch nicht toxisch. Die Behandlung von HL-1 Zellen mit Verapamil resultierte in einer deutlich höheren Effizienz in der Glukosenutzung. Sowohl in hESC-CM als auch in HL-1 Zellen resultierte die Doxorubicin-Behandlung in einer Zunahme des oxidativen Stoffwechsels, welche wahrscheinlich der Aufrechterhaltung der intrazellulären ATP-Konzentration dient.

Die erzielten Ergebnisse haben pharmakologische Relevanz und zeigen des Weiteren auch neue Strategien für präklinische Kardiotoxizitäts-Messungen von neuen Wirkstoffen.

# Chapter 1

## Introduction

### **Drug induced cardiotoxicity and the need for predictive *in vitro* models and assays**

Drug induced cardiotoxicity may emerge as altered cardiac contractility, changes of cardiac rhythm or ischemia (Mandenius *et al.*, 2011). These potentially life threatening side effects still challenge the pharmaceutical industry as well as drug regulatory agencies (Darpo, 2007) and have resulted in drug withdrawal from the market in the past several years (Gwathmey *et al.*, 2009). The withdrawal of several cardiac and non-cardiac drugs due to cardiotoxic effects in man, while toxicity was observed in animals (Lasser *et al.*, 2002; Lexchin, 2005; Redfern *et al.*, 2003), has led to extended requirements by regulatory authorities concerning cardiotoxicity testing. Determination of cardiotoxicity in preclinical studies is therefore of high importance in the regulatory procedure. Cardiotoxicity assessment should be oriented on guidelines regarding repeated dose studies as well as cardiac safety pharmacology ((ICH) S4 guideline (ICH, 1997), EMEA (EMA, 2008; ICH, 2005). These guidelines suggest electrophysiological aspects *in vitro* and *in vivo* such as repolarisation and conduction abnormalities, heart rate and ECG. In addition, the assessment of endpoints such as blood pressure, heart rate or cardiac output is recommended. Preclinical *in vitro* determination of cardiac side effects mainly comprises electrophysiological measurements in canine or rabbit Purkinje fibers and cell lines which express the hERG ion channel (Braam *et al.*, 2010). Drug induced prolongation of the QT interval in an electrocardiogram (ECG) potentially produces a risk of cardiac arrhythmia, such as Torsades de Pointes (TdP), which can result in sudden death. In an ECG the QT-interval is defined as the time span between the start of the QRS-complex and the termination of the T-wave (Braam *et al.*, 2010).

Reliable electrophysiological measurements require appropriate cell models. The major drawback of animal models is the low predictability of cardiotoxic outcome in humans. Ideally, primary human cardiomyocytes represent a convenient cardiac model, as they possess all relevant ion channels. However, the use of primary human cardiomyocytes is limited by a shortage of available cells. Irrespective of the cardiac cell model, predictions of cardiotoxic outcome merely

based on electrophysiological measurements seem insufficient since molecular and energetic aspects of cardiotoxicity might be neglected. Characterization of functional parameters such as substrate usage and metabolic fluxes by using state of the art analysis on reliable cardiac cell types, such as hESC-CM may greatly improve the prediction potential of a test system, thus providing a more reliable test system.

### **Cardiac *in vitro* models for preclinical drug testing**

Determination of potential cardiac effects of new chemical entities (NCE) in man necessitates cardiac *in vitro* models which closely mimic the terminally differentiated, adult cardiomyocyte in terms of concerted ion channel activity (Mandenius *et al.*, 2011) but also in terms of the substrate spectrum for ATP generation. Ideally, such an *in vitro* model is of human origin which would circumvent interspecies variability, especially when considering the low predictive power of animal models. The use of human cardiomyocytes *ex vivo* is rather limited for drug testing purposes, since these cells are non-proliferating and their availability is very limited for obvious reasons. Human embryonic stem cells (ESCs) can be differentiated into spontaneously contracting cells with characteristics of cardiomyocytes (Jensen *et al.*, 2009; Kehat *et al.*, 2001; Synnergren *et al.*, 2008). It has been suggested that cardiomyocytes derived from human embryonic stem cells (hESC-CM) may be used as *in vitro* cardiac test models since their functionality makes them attractive and applicable for drug discovery and drug testing (Jensen *et al.*, 2009). To date the physiology of hESC-CM has been extensively characterised. One main advantage of hESC-CM over primary cardiomyocytes is that they can be maintained in culture while keeping a contractile phenotype. Besides that, functional synchronisation of contraction can be observed both in monolayer culture and in larger cell aggregates. In addition, gene expression levels of voltage-gated potassium channels (hERG) are similar as compared with human cardiac tissue (Asp *et al.*, 2010; Mandenius *et al.*, 2011). The presence of hERG channels is of high importance since drug-induced QT-prolongation can be the result of interaction with the hERG ion channel (Moss and Kass, 2005). Recent work on hESC-CM demonstrated the potential of these cells for predictive *in vitro* drug testing by using multielectrode arrays (MEA) (Braam *et al.*, 2010; Caspi *et al.*, 2009), a system which allows much higher and less costly throughput as compared with conventional patch clamp techniques using single cells.

Besides hESC-CM other animal cardiac cell models are available for use either for interspecies comparison, method optimisation or method validation. Primary cells from either chicken or rats

are widely used as a cardiac *in vitro* model. Murine HL-1 cardiomyocytes, a cardiac muscle cell line, derived from an atrial mouse tumour lineage (Claycomb *et al.*, 1998), represent a very convenient alternative to neonatal chicken heart cells or rat cardiomyocytes. These cells can be serially passaged, without losing their ability to contract. Besides, HL-1 cells maintain a differentiated cardiac phenotype, regarding biochemical and electrophysiological properties (Claycomb *et al.*, 1998; White *et al.*, 2004). HL-1 cells have been shown to be quite useful for studying cardiac physiology (Claycomb *et al.*, 1998; White *et al.*, 2004) since they express many genes typical for differentiated adult cardiomyocytes (Claycomb *et al.*, 1998). HL-1 cardiomyocytes express several cardiac ion channels, such as L- and T-Type  $\text{Ca}^{2+}$  channels (Xia *et al.*, 2004), ATP-sensitive  $\text{K}^+$  channels (Fox *et al.*, 2005) and inward rectifier  $\text{K}^+$  channels (Goldoni *et al.*, 2010). These properties make them attractive for preclinical studies on drug induced cardiotoxicity.

Nevertheless, the non-human origin of both HL-1 cells and animal derived primary cells might not allow any reproductive conclusions in man, as they do not mimic human cardiomyocytes (Mandenius *et al.*, 2010). Besides, HL-1 cells are highly relying on glycolysis (Monge *et al.*, 2009), while the adult human myocardium mainly relies on oxidative metabolism.

### **Respiration measurement in cardiac cells using oxygen sensitive sensors**

The healthy and resting human myocardium covers 70-80% of its energy demand by oxidation of fatty acids. The remainder is covered by catabolism of glucose and organic acids. This distribution is owed to the high amount of ATP which can be gained from oxidation of one mole of fatty acids. The stepwise process of  $\beta$ -oxidation of fatty acids leads to the formation of acetyl-CoA which enters the TCA-cycle to gain  $\text{NADH}+\text{H}^+$  and  $\text{FADH}_2$ . The reduction equivalents enter the respiratory chain in the inner mitochondrial membrane where they are oxidized at respiratory complex I or II. The electrons are transferred to molecular oxygen, a process which is coupled to phosphorylation of ADP to yield ATP. The rather high workload of the contracting cardiac tissue highly depends on oxidative metabolism. In ischemic heart disease altered cardiac respiration is the result of insufficient bloodflow and thus oxygen supply, which may result in energy deprivation. Besides cardiac disease, drug induced alterations of cardiac respiration can be the result of altered cardiac substrate usage. Changes in substrate metabolism may lead to contractile dysfunction (Stanley *et al.*, 2005). Both altered substrate usage and respiration have been observed in case of some drugs with potential or known cardiac risk.

Measuring cardiac respiration in response to new chemical entities (NCE) both *in vivo* and *in vitro* might reflect the cardiac energy status and thus provide information of potential cardiac risk. Determination of cardiac oxygen consumption might therefore complement well established preclinical measurements of cardiac electrophysiological of either single cells or isolated animal hearts.

Several methods for the determination of oxygen consumption are available, such as Clark electrodes or electrochemical cells (Ramamoorthy *et al.*, 2003). Clark electrodes are most commonly used. Though, the major drawback of this method is the oxygen consumption by the electrode (Ramamoorthy *et al.*, 2003; Wilson *et al.*, 1987). In addition, they are not easily applicable for high throughput measurements since several cost-intensive electrodes would be required. In preclinical *in vitro* drug testing on cardiac models, the use of *non-invasive* immobilised fluorescence based sensors (Bambot *et al.*, 1994; John *et al.*, 2003) would provide a convenient solution for high throughput drug testing, since they are now broadly available in high density well formats.

Use of oxygen sensitive optodes in drug screening has been shown to be very reliable (Beckers *et al.*, 2009; Deshpande *et al.*, 2005; Hynes *et al.*, 2003; Wodnicka *et al.*, 2000) On top of that, optodes allow the determination of dynamic toxic effects, as shown recently (Beckers *et al.*, 2009; Noor *et al.*, 2009; Wolf *et al.*, 2011).

### **Metabolomics in cardiac research**

Metabolomics or metabolite profiling includes the quantitative and qualitative analysis of the complete set of small molecules in a certain biological system, e.g. in prokaryotic or eukaryotic cells, body fluids and tissues (Koek *et al.*, 2011). Metabolome analysis involves quantitative or qualitative measurement of extracellular and/or intracellular metabolites. Most frequently, chromatographic techniques combined with mass spectrometry are applied, such as GC/MS or LC/MS. The measurement of small molecules potentially allows conclusions about alterations of metabolic pathways upon perturbation by either disease or pharmacological intervention. The metabolome may be more tractable than the proteome, due to its lower complexity (Lewis *et al.*, 2008). It is assumed that the human metabolome consists of approximately 3000 metabolites, while the complexity of post-translational modifications of proteins might give  $10^6$  protein species. The metabolome comprises many different compound classes, including metabolites which are anionic and cationic as well as lipophilic and hydrophilic (Lewis *et al.*, 2008).



Presently, several different strategies are applied in metabolomics research, i.e. metabolic target analysis, metabolic profiling, metabolic fingerprinting and metabolomics (Koeck *et al.*, 2011). According to Koeck *et al.* metabolic target analysis can be summarized as the quantitative (absolute or relative) analysis of one or only a few metabolites. Metabolic profiling refers to the quantitative and qualitative analysis of metabolically or analytically related metabolites. Metabolic fingerprinting was defined as the screening of samples to provide sample classification. Metabolomics aims at quantification and qualitative analysis of the total set of metabolites in a biological matrix (Koeck *et al.*, 2011).

Most metabolomics related studies result in high dimensional data sets. For the proper analysis of potential differences in the metabolite concentrations between healthy/untreated control groups and diseased/treated groups the respective sample or patient groups should be large enough to allow statistical reliability and furthermore necessitate proper statistical tools which allow analysis of multivariate data. These tools comprise either unsupervised or supervised algorithms (Blekherman *et al.*, 2011). Principal component analysis (PCA) is an unsupervised data analysis method which is used for dimension reduction and data visualisation, preferably in a 2-dimensional space. Other common unsupervised methods are hierarchical clustering and self-organizing maps. Supervised statistical methods are mainly used for generating classification models (healthy vs. diseased) based on observed sample readings, e.g. by linear regression in order to find the best linear predictor of a class (Blekherman *et al.*, 2011). Most popular supervised methods in metabolomic studies include ANOVA, partial-least square discriminant analysis (PLS-DA) and discriminant function analysis (DFA).

The use of metabolomic techniques and appropriate data analysis potentially allows the identification of novel biomarkers of drug induced cardiotoxicity and the respective mechanism of toxicity. Many cardiac diseases are related to alterations of cardiac substrate utilisation and energy deprivation (Ashrafian and Neubauer, 2009; Griffin *et al.*, 2011; Mayr, 2008; Stanley *et al.*, 2005). Thus, the number of metabolomic studies carried out in plasma and body fluids have increased in the past several years. Recently, MS-based measurement of metabolic changes in plasma/serum of patients in whom ischemia was either induced by stress or due to cardiac surgery were determined (Sabatine *et al.*, 2005; Turer *et al.*, 2009). Both studies suggested significant alterations of TCA-cycle activity in the course of ischemia and potentially provided targeted optimization in patients undergoing cardiac surgery.

Besides biomarker identification of cardiac diseases, it has also been used in toxicity assessments of drugs. By using  $^1\text{H}$ -NMR spectroscopy the effect of 3,4-methylenedioxymethamphetamine on the metabolism in rat hearts was determined (Perrine *et al.*, 2009). In addition, the effect of doxorubicin, an anticancer drug with high cardiotoxic side effects, has been assessed similarly (Andreadou *et al.*, 2009).

It can be assumed that metabolomic studies have high potential in preclinical studies on cardiotoxic side effects of new chemical entities. By mapping metabolic effects of compounds with known cardiac effects in humans, preferably by using hESC-CM, the risk of new chemical entities/pharmaceuticals for cardiac side effects might be reliably assessed, e.g. by applying pattern recognition techniques on the basis of clinically observed side effects, such as QT-prolongation or cardiac arrest.

### **$^{13}\text{C}$ metabolic flux analysis**

The quantification of cellular metabolism is of great interest in several fields of biotechnological research (Kohlstedt *et al.*, 2010; Niklas and Heinzle, 2011; Niklas *et al.*, 2010; Quek *et al.*, 2010; Wittmann, 2007; Zupke *et al.*, 1997). By applying metabolic flux analysis quantitative information on enzyme activity as well as substrate utilisation can be obtained (Vo and Palsson, 2006). Estimation of intracellular fluxes relies on both experimental measurements but also computational approaches. Metabolic fluxes can be determined either by flux balance analysis (Lee *et al.*, 2006) (FBA, metabolite balancing) or by applying  $^{13}\text{C}$ -labelled substrates (Lee *et al.*, 2006; Schmidt *et al.*, 1998) ( $^{13}\text{C}$  metabolic flux analysis). Determination of metabolic fluxes by using FBA is the least complicated method among all MFA methods in terms of both experimental and computational techniques. Experimentally, it mainly necessitates measurement of metabolite uptake and production rates of a cell population. A set of linear mass balance equations around intracellular metabolites is set up and the information in the metabolic network is stored in a stoichiometric matrix. This matrix contains information of known fluxes (measured extracellular uptake and production fluxes) and unknown intracellular fluxes. In case of determined systems the set of equations can easily be solved. In case of underdetermined systems, linear programming tools help finding an optimal solution space, depending on the defined objective function.

The main assumption in FBA is usually a metabolic steady-state, i.e. constant concentrations of intracellular metabolites. FBA has been successfully applied to study mammalian cell metabolism (Niklas *et al.*, 2009; Niklas *et al.*, 2010; Sidorenko *et al.*, 2008).

The major drawback of FBA is that it does not allow to resolve reversible, parallel or circular reactions (Niklas *et al.*, 2010). These drawbacks can be tackled with  $^{13}\text{C}$  metabolic flux analysis approaches. The use of  $^{13}\text{C}$  tracers (e.g.  $^{13}\text{C}$ -labelled glucose) combined with the GC/MS based analysis of  $^{13}\text{C}$ -enrichment in intra- or extracellular metabolites or in monomers from cellular polymers (e.g. amino acids in proteins) allows a more reliable determination of intracellular fluxes. For  $^{13}\text{C}$  metabolic flux analysis several modelling approaches have been established. These approaches are mainly optimization-based and fit an intracellular flux distribution to the measured  $^{13}\text{C}$  labelling pattern of the considered metabolites. These concepts mainly make use of atom mapping matrices (Zupke *et al.*, 1997) and isotopomer mapping matrices (IMM) (Schmidt *et al.*, 1997), which allow to track the carbon transfer in individual enzymatic reactions.

While metabolic flux analysis in prokaryotic cells is a well established procedure, e.g. in the field of metabolic engineering, application of this methodology in eukaryotic cells is still very limited, mainly due to compartmentation in these cells but also due to necessary biological conditions, such as metabolic and/or isotopically steady state, which are rather hard to achieve in these systems (Niklas *et al.*, 2010).

Nevertheless, metabolic flux analysis has been used for the analysis of mammalian metabolism mainly in the areas of cell culture technology as reviewed recently (Niklas *et al.*, 2010). Other applications include the physiological characterization of animal cell lines, such as hybridomas (Bonarius *et al.*, 2001), CHO-cells (Goudar *et al.*, 2010), human production cell lines (Henry *et al.*, 2011; Niklas *et al.*, 2011), hepatocytes (Maier *et al.*, 2009), kidney cells (Sidorenko *et al.*, 2008), the analysis of effects of drugs (Niklas *et al.*, 2009).

$^{13}\text{C}$  tracer studies have been carried out to determine the substrate metabolism and anaplerosis in the heart (Cohen and Bergman, 1997; Comte *et al.*, 1997a; Comte *et al.*, 1997b; Malloy *et al.*, 1996; Malloy *et al.*, 1987; Panchal *et al.*, 2001). In most of the studies the fluxes were analytically derived. It has been suggested that such analytical solutions are only applicable for small network models and not obtainable for some pathway structures (Vo and Palsson, 2006).

A  $^{13}\text{C}$ -based analysis of carbon substrate metabolism in the perfused mouse heart applying the IMM concept was recently described (Vo and Palsson, 2006). Detailed studies on the effect of cardiotoxic drugs on the cardiac metabolism by means of metabolic flux analysis hasn't been

carried out and is rather limited to toxicological studies in hepatic cell models (Maier *et al.*, 2009; Niklas *et al.*, 2009). Given that the failing heart changes its substrate spectrum (Stanley *et al.*, 2005), metabolic flux analysis using systemic approaches, as recently described (Vo and Palsson, 2006) might potentially be useful for the preclinical determination of a drug candidates influence on cardiac energy metabolism. Ideally, such studies would make use of reliable *in vitro* cell models, such as human embryonic stem cells derived cardiomyocytes.

### **Objective of the thesis**

The main objective of this thesis is to determine the potential of 1. dynamic respiration measurement systems, 2. metabolite profiling (metabolomics) and 3.  $^{13}\text{C}$ -metabolic flux analysis in preclinical *in vitro* cardiotoxicity testing of drug compounds. Two different cardiac *in vitro* models were used, namely HL-1 cardiomyocytes and cardiomyocytes derived from human embryonic stem cells (hESC-CM). For the assessment of the applicability of each method and *in vitro* model for drug testing a set of drugs with known pharmacology and cardiotoxic risk in man were considered. The applied drugs comprised several pharmacological classes such as antiarrhythmics, cytostatics, antihistamines and psychoactive drugs. Each of the methods was optimized by using HL-1 cardiomyocytes prior to the use of hESC-CM, since HL-1 cells are easier to maintain and their availability is not limited, due to their proliferating phenotype.

The first part of this thesis mainly consists of cytotoxicity screening of model drugs with known pharmacological effects. This cytotoxicity screening was carried out by applying dynamic respiration measurement in HL-1 cells or hESC-CM using oxygen sensitive optodes. Since the dynamic aspect of respiration measurement using optodes seems to have a high potential, corresponding dynamics of drugs tested on HL-1 cells and hESC-CM were established and compared. In addition, determination and comparison of  $\text{EC}_{50}$  dynamics of cardioactive drugs, oxygen measurement based cytotoxicity screening provided essential information for subsequent metabolomic and fluxomic studies, since it gave information on the toxicity range of a compound.

The second main objective was to assess whether metabolite profiling on HL-1 cells and hESC-CM allows the determination of potential cardiotoxic side effects of new drug compounds. Significant alterations in the metabolome at drug concentrations significantly below  $\text{EC}_{50}$  values where common toxicity screening assays fail to suggest potential harm in *in vitro* assays would illustrate the benefit of metabolomics as an additional tool for *in vitro* drug testing. This part of

the work comprised the exposure of HL-1 cells to drugs, analysis of the metabolome in the respective culture medium and finally the data evaluation using multivariate statistics, which are commonly used in this field. For this kind of analysis drug concentrations were considered which showed no significant alteration of cell respiration, as determined in the first part of the thesis.

The third main objective of the thesis was to determine whether  $^{13}\text{C}$  metabolic flux analysis on HL-1 cells and hESC-CM allows the determination of drug induced changes of fluxes in central metabolic pathways, such as glycolysis and TCA-cycle. Similar to the metabolite profiling approach,  $^{13}\text{C}$  MFA was carried out at drug concentrations which did not result in alterations of cell viability i.e. at sub-toxic concentrations.

## Chapter 2

### EC<sub>50</sub> dynamics for a better understanding of toxicity

#### Abstract

Determination of the EC<sub>50</sub> dynamic of a drug can give valuable information on the mechanism of its toxicity. Recent studies have reported the applicability of dynamic measurement of parameters such as dissolved oxygen or pH, as possible estimators of cellular respiration or metabolic activity. However, a direct comparison of EC<sub>50</sub> dynamics obtained from reported approaches with corresponding dynamics of common cytotoxicity assays hasn't been carried out yet. In addition, variability of EC<sub>50</sub> dynamics of drugs from the same and from different pharmacological classes has not been determined yet.

First, we assessed the performance of a recently described dynamic screening system (24 – well OxoDishes) by comparing time dependant EC<sub>50</sub> values with values obtained from two common cytotoxicity assays (SRB- and LDH assay) by screening four different drugs (amiodarone, desipramine, doxorubicin, terfenadine) on HL-1 cardiomyocytes. Secondly, we assessed to what extent EC<sub>50</sub> dynamics obtained from oxygen measurement were differing between model drugs belonging to different pharmacological classes. For this purpose, another five drugs from similar classes were screened by oxygen measurement and the data of nine different EC<sub>50</sub> dynamics were compared by calculating the Euclidean distance.

EC<sub>50</sub> values obtained from oxygen measurement showed no significant differences as compared to corresponding values from SRB- and LDH assays for all considered time points. Though, SRB showed the highest sensitivity of all three assays, while LDH assay was least sensitive. Comparison of EC<sub>50</sub> dynamics from an extended panel of tested drugs revealed distinct differences in the EC<sub>50</sub> profiles. Data analysis by means of hierarchical clustering revealed distinct grouping of drugs according to known toxic effects, for the majority of drugs. Considering EC<sub>50</sub> dynamics of a drug can give information on the time dependant toxicity of a drug. This information can not be obtained from sole consideration of individual EC<sub>50</sub> values at a certain time point. This approach might therefore be a valuable tool for the estimation of the potential mechanism of action and/or toxicity of a drug candidate.

**This chapter has been submitted as a manuscript in the Journal of Applied Toxicology.**

### Introduction

The pharmacological assessment of the toxicity of a drug is mainly carried out using routine toxicity assays during preclinical drug development. Most of these assays are carried out upon exposure of cells to a compound for a certain period and the half effective concentration (EC<sub>50</sub>) is determined for the respective time period. However, determination of EC<sub>50</sub> dynamics necessitates use and preparation of several cell culture plates in parallel (Beckers *et al.*, 2009). In addition, due to the invasive nature of many commonly used assays such as MTT, XTT or WST-1, in which a reagent is added to the cells, reduction of these dyes by media components or by reducing groups of drugs (Hynes *et al.*, 2003) cannot be excluded. The reagent may itself have an adverse effect which is not observed by commonly used assays.

To overcome these drawbacks non-invasive immobilised fluorescent based sensors (Bambot *et al.*, 1994; John *et al.*, 2003) for the measurement of dissolved oxygen have been developed and were described as a convenient solution. Use of oxygen sensitive optodes in drug screening using mammalian cell culture has been demonstrated as a potential alternative to commonly used cytotoxicity assays (Beckers *et al.*, 2009; Deshpande *et al.*, 2005; Hynes *et al.*, 2003; Wodnicka *et al.*, 2000). Furthermore, determination of EC<sub>50</sub> dynamics has been reported for several drugs and cell types (Beckers *et al.*, 2009; Noor *et al.*, 2009; Wolf *et al.*, 2011).

Although use of fluorescent dyes as a potential alternative to common cytotoxicity assays has been proposed, a direct comparison of EC<sub>50</sub> dynamics obtained *via* oxygen measurement and other common assays has not been carried out yet. Besides, to our knowledge no study has performed a direct comparison of EC<sub>50</sub> dynamic profiles within drugs of the same class and within different classes. Thus, it is not clear whether compounds from the same pharmacological class share similarities in their EC<sub>50</sub> dynamics. We addressed these issues and compared time dependant EC<sub>50</sub> values of amiodarone (antiarrhythmic), terfenadine (antihistamine), desipramin (antidepressant) and doxorubicin (antineoplastic) using a murine atrial cell line (HL-1 cells). We measured respiration/oxygen-consumption and compared the results with LDH and sulforhodamine B assay. The HL-1 cells were first described by Claycomb *et al.* (1998). HL-1 cells have been extensively used for toxicological and pharmacological studies (Andersson *et al.*, 2010; Deng *et al.*, 2009; Fox *et al.*, 2005; Fritzsche *et al.*, 2009; Strigun *et al.*, 2011a) and are quite useful for studying concentration dependant toxic drugs effects as shown recently (Fritzsche *et al.*, 2009; Strigun *et al.*, 2011a).

Due to the different mechanism of toxicity of the mentioned drugs which have known toxic side effects, we assumed that these different toxic mechanisms are also reflected in the respective EC<sub>50</sub> dynamics.

### **Material and methods**

#### *Cell Culture*

HL-1 cells (Claycomb *et al.*, 1998) were kindly provided by Dr. Claycomb (Louisiana State University) for research within the framework of EU-Invitroheart project (LSHB-CT-2007-037636). The cells were maintained in Claycomb medium (Sigma Chemical, USA) supplemented with 2 mM glutamine (PAA Laboratories, Austria), 100 U/ml penicillin 100 µg/ml streptomycin (PenStrep stock solution: CC Pro, Germany), 100 µM norepinephrine (Sigma Chemical, USA) in 30 mM L-ascorbic acid (Sigma Chemical, USA) and 10% FBS (JRH Biosciences, UK). Cells were passaged at confluency in a split ratio of 1:3. Culture flasks (75 cm<sup>2</sup>, Falcon, Germany) were pre-coated with a solution of 0.02% (wt./vol.) gelatine (AppliChem, Germany) containing 5 µg/ml fibronectin (Sigma Chemical, USA). The cells were maintained at standard culture conditions (37°C, 5% CO<sub>2</sub> and 95% relative humidity).

#### *Preparation of test solutions*

All drugs were purchased from Sigma Chemical USA with the highest purity available. Stock solutions of amiodarone (50 mM), verapamil (100 mM), daunorubicin (10 mM), terfandine (10 mM), astemizol (10 mM), diclofenac (500 mM), haloperidol (10 mM) and desipramin (10 mM) were prepared in DMSO (Sigma Chemical, USA). A 10 mM stock solution of doxorubicin was prepared in cell culture grade water (PAN Biotech, Germany). For the cytotoxicity screening all stock solutions were serially diluted in supplemented Claycomb medium. The end DMSO concentration did not exceed 1% (v/v) in any of the final test solutions.



### *Measurement of dissolved oxygen*

HL-1 cells were trypsinized at confluency and counted three times via trypan blue exclusion in a hemocytometer. Cells were seeded in 24-well OxoDishes (PreSens) which were pre-coated with 500 µl of a gelatine/fibronectine solution (see 2.1) for 24 h. Cells seeding density was  $1.5 \times 10^5$  cells in a total volume of 1 ml Claycomb medium (Sigma Chemical, USA) supplemented with 2 mM glutamine (PAA Laboratories, Austria), 100 U/ml penicillin 100 µg/ml streptomycin (PenStrep stock solution: CC Pro, Germany), 100 µM norepinephrine (Sigma Chemical, USA) in 30 mM L-ascorbic acid (Sigma Chemical, USA) and 10% FBS (JRH Biosciences, UK). After 24 h preincubation, the supernatant was removed and the cells were washed twice with Claycomb medium without any supplements. Afterwards, 1 ml of fresh medium containing drugs at different concentration was added to the cells. Untreated controls, DMSO-controls and drugs treated cells were tested in triplicates. To minimize evaporation, plates were covered with gas impermeable sticky foils. Cells were exposed to drugs for 48 h.

### *Sulforhodamine B and Lactate dehydrogenase release (LDH ) assay*

Cytotoxicity of the tested drugs on HL-1 cardiomyocytes was assessed using lactate dehydrogenase release (LDH-release assay) and proliferation (SRB-proliferation assay).  $1.5 \times 10^5$  cells/well were seeded in four gelatin/fibronectin-coated (see 2.3) 24-well plates (Greiner, Germany) in 1 ml Claycomb medium (containing 2 mM glutamine, 100 U/ml penicillin, 100 µg/ml streptomycin, 100 µM norepinephrine in 30 mM L-ascorbic acid and 10% fetal bovine serum (FBS). After 24 hours (h) incubation, the supernatant was removed and the cells were washed twice with Claycomb medium. Fresh medium containing different concentrations of the drugs was added to the cells in triplicates. The cells were exposed to the drugs for 48 h. Finally, lactate dehydrogenase assay (Cytotoxicity Detection Kit (LDH), Roche Applied Science, Germany) was carried out according manufacturer's instructions. Sulforhodamine B (SRB) assay, a colorimetric protein quantification assay (Skehan *et al.*, 1990) was carried out as recently described (Noor *et al.*, 2009).

Both assays were carried out after different exposure times (20 h, 30 h, 40 h, 48 h, referring to four plates). The SRB-assay was carried out as described recently (Strigun *et al.*, 2011a). Lactate dehydrogenase assay (Cytotoxicity Detection Kit (LDH), Roche Applied Science, Germany) was carried out according kit instructions on supernatants obtained from SRB-assay. All conditions, untreated controls and different drug concentrations, were tested in triplicates.

### *Calculation of EC<sub>50</sub>-values*

For the respective time points, EC<sub>50</sub> values were calculated with a four parameter sigmoidal concentration-response curve using Origin Pro Version 7.5G, exactly as described recently (Beckers *et al.*, 2009; Noor *et al.*, 2009).

### *Statistical analysis*

The similarity of the EC<sub>50</sub> dynamics as determined by oxygen measurement, LDH and SRB-assay for amiodarone, desipramin, doxorubicin and terfenadin was tested by repeated-measures one-way ANOVA following Tukey's posthoc test using Prism 5 V.5.04 (GraphPad Software, Inc., USA).

For the determination of the Euclidean distance of EC<sub>50</sub> dynamics of all drugs as determined by oxygen measurement, all EC<sub>50</sub> values were normalized to the respective EC<sub>50</sub> values obtained from 20 h time-point (100%). The dataset was then analysed by calculating the Euclidean distance between all tested drugs using XLSTAT 2010.3.06 (Addinsoft, Germany).

## **Results**

### *Continuous oxygen measurement gives similar EC<sub>50</sub> values and EC<sub>50</sub> dynamics as compared to SRB and LDH assay*

The time course of EC<sub>50</sub> values of amiodarone (class III antiarrhythmic), desipramin (tricyclic antidepressant), doxorubicin (cytostatic) and terfenadine (antihistamine) was determined by continuous measurement of dissolved oxygen measurement as well as SRB- and LDH-assay.

In case of oxygen measurement, the amount of dissolved oxygen decreased from 70-80 % to 20-30 % within 48 h incubation in medium containing untreated cells (Fig. 1 A-D). Medium controls remained steady at 80-90%. In case of cells treated with drugs a concentration dependant effect of each drug could be observed.

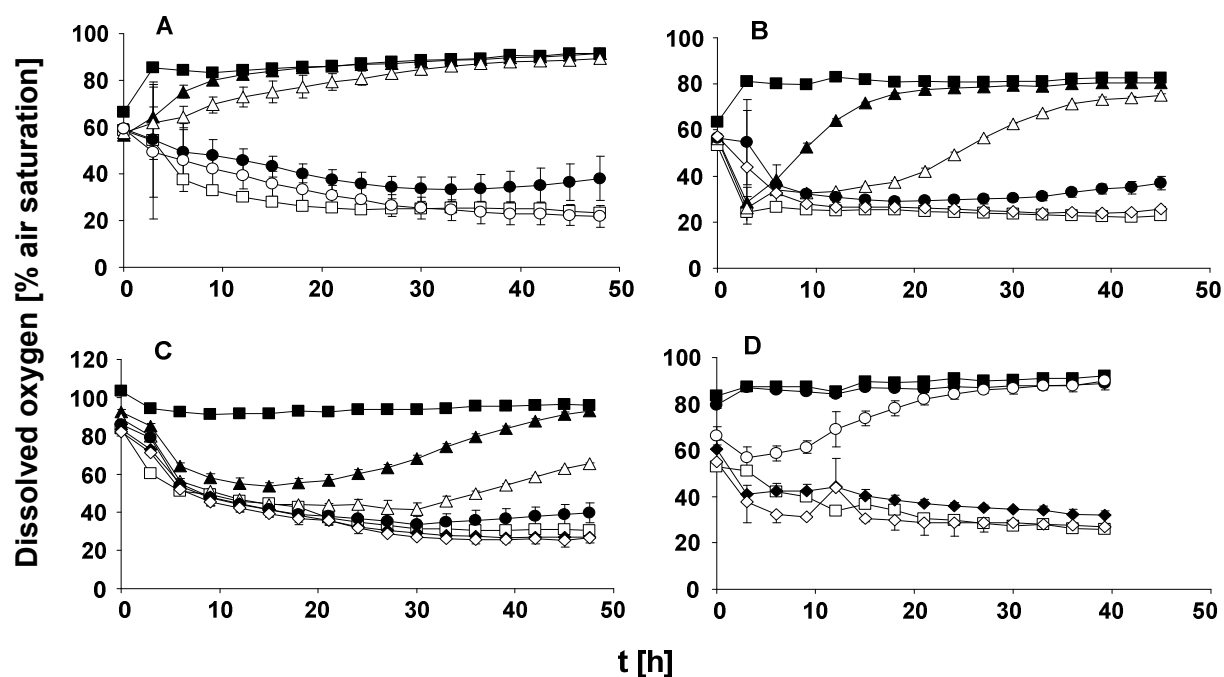


**Figure 1:** Time course of dissolved oxygen in culture medium containing HL-1 cells with different concentrations of (A) amiodarone (■: medium only; ▲: 100  $\mu$ M;  $\Delta$ : 33  $\mu$ M; ●: 11  $\mu$ M; ○: 3.7  $\mu$ M; □: 0  $\mu$ M); (B) desipramin (■: medium only; ▲: 100  $\mu$ M;  $\Delta$ : 50  $\mu$ M; ●: 25  $\mu$ M; ◇: 3.2  $\mu$ M; □: 0  $\mu$ M); (C) doxorubicin (■: medium only; ▲: 2.5  $\mu$ M;  $\Delta$ : 0.625  $\mu$ M; ●: 0.156  $\mu$ M; ◇: 3.2  $\mu$ M; □: 0  $\mu$ M) and (D) terfenadine (■: medium only; ●: 12.5  $\mu$ M; ○: 6.25  $\mu$ M; ●: 3.12  $\mu$ M; ◇: 0.002  $\mu$ M; □: 0  $\mu$ M). Cells were seeded in 24 – well OxoDishes (PreSens) and allowed to equilibrate for 24 h. Afterwards medium was removed and fresh medium containing drugs at different concentrations was added to the cells. Dissolved oxygen in culture medium was then continuously measured for 48 h. S.D. was determined from triplicate measurement.

Concentration-response curves were determined upon 20 h of exposure to the respective drugs. This initial time point allowed determination of a proper concentration dependant effect for each drug and assay. Subsequent considered time points for determination of concentration-response curves were 30 h, 40 h and 48h. Corresponding time courses were also determined by SRB- and LDH-assay. A direct comparison of concentration-response curves obtained by all three assays is shown using the example of doxorubicin (Fig. 2).

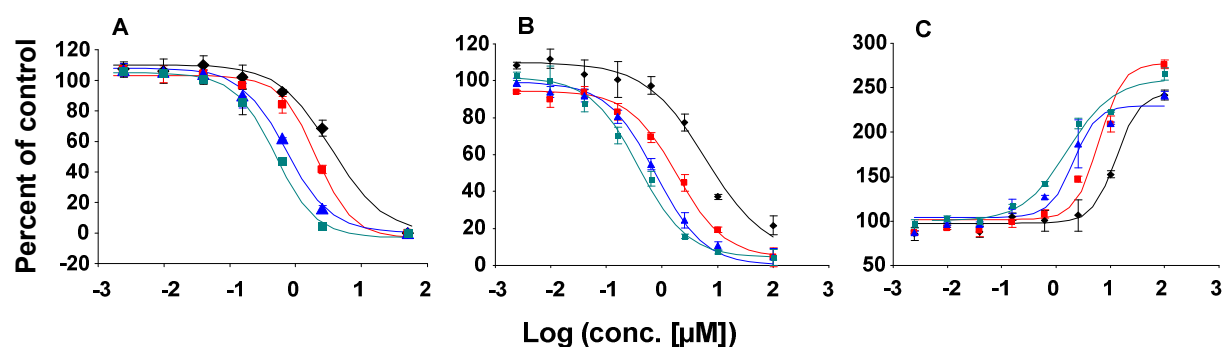


**Figure 2:** Concentration-response curves of doxorubicin screened on HL-1 cells by using (A) continuous oxygen measurement; (B) sulforhodamine B proliferation assay and (C) lactate dehydrogenase release assay. The concentration response was determined after 20 h (black symbols), 30 h (red symbols), 40 h (blue symbols) and 48 h (turquoise symbols) of exposure. Standard deviations were determined from triplicate measurement.

As apparent, a time-dependant shift of concentration-response curves towards decreasing concentrations was observed for all considered drugs in the three assays (Fig. 2 and Fig. S1 in the appendix for chapter 2), pointing towards an increasing toxic effect. This is reflected by decreasing EC<sub>50</sub> values (Tab. 1). The EC<sub>50</sub> values obtained for all four drugs were quite similar for all three tested assays and all considered time points.

The EC<sub>50</sub> value of amiodarone obtained from oxygen measurement was 19 µM at 20 h and decreased to 15 µM after 48 h. In SRB- and LDH-assay the corresponding value decreased from 18 µM (20 h) to 10 µM (48 h) and from 30 µM (20 h) to 12 µM (49h), respectively. EC<sub>50</sub> values at each time point obtained from all three assays were not significantly different.

The EC<sub>50</sub> value of desipramin obtained by oxygen measurement decreased from 64 µM after 20 h to 33 µM after 48 h. Corresponding values obtained by SRB and LDH-assay decreased from 35 µM (20 h) to 19 µM (48 h) and from 51 µM (20 h) to 30 µM (48 h), respectively (Tab. 1). The EC<sub>50</sub> values obtained by oxygen measurement were significantly higher at each time point as compared with SRB-assay ( $p < 0.01$ ), but not significantly different as compared with LDH-assay.

**Table 1:** EC<sub>50</sub> values of amiodarone, desipramin, doxorubicin and terfenadin tested on HL-1 cells for different exposure time points (20 h, 30 h, 40 h and 48 h). Cells were incubated in 24 – well OxoDishes and dissolved oxygen was continuously measured for 48. Corresponding EC<sub>50</sub> values were determined by using sulforhodamine B and LDH-release assay. The brackets represent 95% confidence intervals. \*\*: p < 0.01 (as compared with SRB assay)

EC <sub>50</sub> [μM]												
	Amiodarone			Desipramin			Doxorubicin			Terfenadin		
t [h]	oxygen	SRB	LDH	oxygen**	SRB	LDH	oxygen	SRB	LDH	oxygen	SRB	LDH
20	19(17-21)	18(16-20)	30(28-31)	64(61-67)	35(33-38)	51(45-57)	3.5(3.3-3.6)	6.1(3.8-7.7)	13(4.5-17.6)	5.3 (5.0-5.6)	5.3(5.0-5.4)	7.5(7-7.9)
30	18(17-19)	12(11-13)	16(15-18)	43(42-44)	25(23-27)	35(34-36)	2.1(2.2-3.3)	1.8(1.4-2.2)	6(5.1-7.1)	4.4 (4.2-4.6)	4(3.8-4.2)	5.7(5.2-6.1)
40	16(15-17)	9(8-10)	13(10-15)	35(34-36)	19(16-21)	30(27-33)	0.7(0.7-0.9)	0.77(0.62-0.88)	2.1(1.3-2.7)	4.3(4.1-4.5)	3.9(3.8-4.1)	4.5(4-4.9)
48	15(14-16)	10(9-11)	12(10-14)	33(32-34)	n.d.	n.d.	0.5(0.4-0.6)	0.39(0.31-0.44)	1.7(1.3-1.9)	4.1(3.8-4.4)	3.7(3.5-3.8)	4.5(4.2-4.8)

In case of doxorubicin, the EC<sub>50</sub> value decreased from 3.5 μM at 20 h to 0.5 μM after 48 h in oxygen measurement. In SRB- and LDH-assay the values decreased from 6.1 μM (20 h) to 0.4 μM (48 h) and from 12.7 μM (20 h) to 1.6 μM (48 h). No significant differences between EC<sub>50</sub> values at each time point could be determined.

For terfenadine, the EC<sub>50</sub> value obtained from oxygen measurement decreased from 5.3 μM (20 h) to 4.1 μM (48 h). In case of SRB and LDH assay the values decreased from 5.2 μM (20 h) to 3.7 μM (48 h) and from 7.5 μM (20 h) to 5.5 μM (48 h). EC<sub>50</sub> values obtained from oxygen measurement were not significantly different from LDH- and SRB assay.

### *Hierarchical clustering of EC<sub>50</sub> dynamics obtained from oxygen measurement allows distinction of drugs according to their mechanisms of toxicity*

We screened five additional drugs (astemizol, haloperidol, daunorubicin, diclofenac and verapamil) using oxygen measurement to perform a more detailed analysis of time dependant EC<sub>50</sub> profiles. Due to the differences of the actual EC<sub>50</sub> values of each drug and time point, EC<sub>50</sub> values were normalized to the first determined EC<sub>50</sub> at time point 20 h for better visual comparison of EC<sub>50</sub> dynamics. The EC<sub>50</sub> values for these drugs are given in Tab. S1 (Appendix for chapter 2). As apparent, the EC<sub>50</sub> dynamics of all considered drugs were quite diverse (Fig. 3A). While EC<sub>50</sub> values of some drugs remained constant after 20 h, such as astemizol, a merely slight decrease by 10–20% was observed in case of amiodarone or verapamil. A rather high

change of the EC<sub>50</sub> values was observed for daunorubicin and doxorubicin, where the EC<sub>50</sub> decreased by some 80% after 20 h.

For better visualisation of similarities between EC<sub>50</sub> dynamics of different drugs, hierarchical clustering was carried out on the data set by determination of the Euclidean distance (Fig. 3 B). This approach allowed the identification of three distinct drug groups with similarities in their EC<sub>50</sub> dynamics.

The first group, which was least related to the other two groups, consisted of daunorubicin and doxorubicin (both anthracyclines). This group revealed the lowest EC<sub>50</sub> range, which was between 3.5 and 0.1 μM (Tab. S1, appendix for chapter 2). Compared to the other groups, a distinct decrease of EC<sub>50</sub>-values characterized this group.

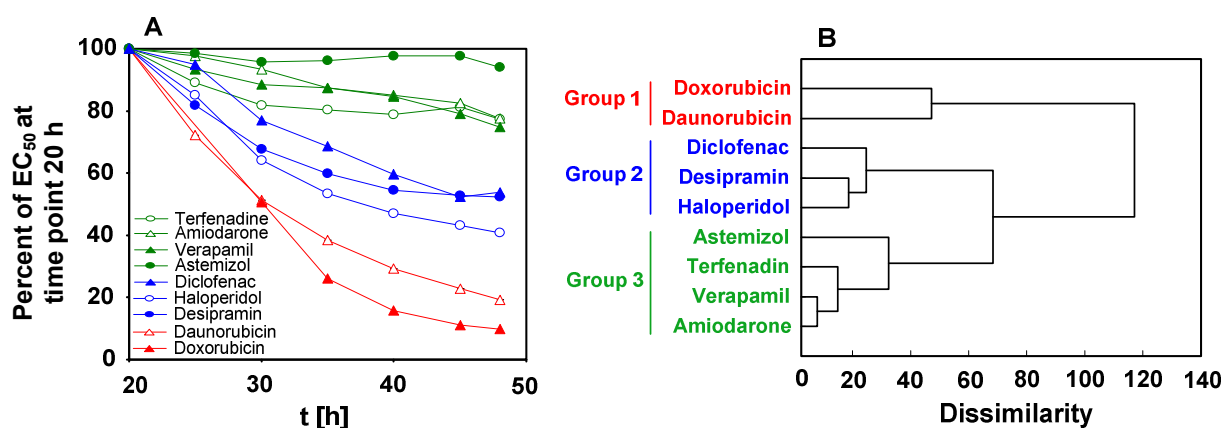


**Figure 3:** (A) EC<sub>50</sub> dynamics as percent of the respective EC<sub>50</sub> values at 20 h of several drugs determined by continuous measurement of dissolved oxygen using 24-well OxoDishes. Drugs were tested on HL-1 cardiomyocytes for 48 h. The underlying EC<sub>50</sub> values are given in Table S1 (Appendix for chapter 2); (B) Euclidean distance of drugs from tested groups calculated from EC<sub>50</sub> dynamics (Tab. S1 and Fig. 3 A).

The second group contained diclofenac (NSAID), desipramin (tricyclic antidepressant) and haloperidol (neuroleptic). Within this group haloperidol was closely related to desipramin. The actual EC<sub>50</sub> values, which were between 33 μM and 596 μM, revealed that these drugs are least toxic among all tested drugs (Tab. S1, appendix for chapter 2).

The third group contained amiodarone (class III antiarrhythmic), verapamil (class IV antiarrhythmic), astemizol and terfenadine (both antihistamines). Compared to the second group, this group had a lower EC<sub>50</sub> range (Tab. S1, appendix for chapter 2), which was between 4 μM and 44 μM.

### Discussion

The benefit of measurement systems which allow continuous measurement of metabolic parameters, such as respiration or acidification rate, was recently suggested as they avoid the need for multiplate seeding when determination of dynamic EC<sub>50</sub> values is desired (Beckers *et al.*, 2009; Wolf *et al.*, 2011). A direct comparison of EC<sub>50</sub> dynamics obtained from these approaches with corresponding dynamics obtained by commonly used cytotoxicity assays has not been carried out yet, least of all a comparison of EC<sub>50</sub> dynamics between drugs with distinct pharmacological properties.

We determined the EC<sub>50</sub> dynamics of four drugs using continuous oxygen measurement and compared them with the dynamics obtained from commonly used cytotoxicity assays (SRB- and LDH-assay). In case of oxygen measurement concentration-response curves were determined from the underlying dissolved oxygen profiles (Fig. 1), similarly as recently described (Beckers *et al.*, 2009; Wolf *et al.*, 2011). Using oxygen measurement a proper concentration dependant effect could be determined after 20 h of drug exposure. The response span at earlier time points did not cover the whole viability range (0% - 100 %). Though, concentration response curves determined after 20 h allowed accurate calculation of EC<sub>50</sub> values in case of oxygen measurement.

Independent of the applied assay the concentration response curves showed a time dependant shift towards lower drug concentrations (Fig. 2), similar as reported recently for the same measurement setup for hepatic cells (Beckers *et al.*, 2009). This shift is reflected by the time dependant decrease of EC<sub>50</sub> values independent of the applied assay (Tab. 1). This decrease of EC<sub>50</sub> values points towards a time dependant increase of toxicity depending on the drug and its mechanism of toxicity. The values obtained from all three approaches were similar for all considered time points which is represented by no significant differences of the time course of the corresponding EC<sub>50</sub> values, thus justifying comparative studies of EC<sub>50</sub> dynamics by using oxygen measurement and thereby eliminating the need for multiplate seeding.

Subsequent respiration measurements on an extended drug panel showed that EC<sub>50</sub> dynamics of the considered drugs were quite diverse (Fig. 3A). Hierarchical clustering on the respective EC<sub>50</sub> dynamics revealed a unique grouping of drugs (Fig. 3 B), which seemed to result from their known mechanism of action.

Group 3 (Fig. 3 B) consisted of amiodarone, verapamil (both channel blockers), astemizol and terfandine (both antihistamines). This group was characterized by a relatively low decrease of

EC<sub>50</sub> values (5%-22% within 24 h). It is well established that toxicity of astemizol, terfenadin and amiodarone is partially related to blockade of potassium and calcium channels (Tagliatalata *et al.*, 1999; Yap and Camm, 1999, Waldhauser *et al.*, 2006), while verapamil's main indication is the blockade of L-type calcium channels. Though, we haven't carried out mechanistic studies, it can be assumed that a toxic effect, which has partly been attributed to the interaction with ion channels, occurs relatively fast, as reflected by only decent decrease of the EC<sub>50</sub> values.

Group 2 (Fig. 3 B), which consists of both anthracyclines daunorubicin and doxorubicin formed a group with a distinct dissimilarity to all other drugs. As apparent from the underlying EC<sub>50</sub> dynamics (Fig. 3 A) a significant decrease of EC<sub>50</sub> values was observed after 20 h of exposure for both drugs (80%-90% within 24 h). This significant increase of toxicity with time is reflected by the versatile acute and chronic toxicity of both drugs, which might become synergistic in the course of exposure. Toxicity of anthracycline has been studied extensively. Its hallmark is the formation of reactive oxygen species due to a mechanism known as redox cycling. Consequences of oxidative stress include formation of reactive oxygen species (Bachur *et al.*, 1977; Sinha *et al.*, 1989) and consequently oxidative damage of DNA (Eliot *et al.*, 1984; Feinstein *et al.*, 1993). Besides, doxorubicin has been shown to deteriorate energy metabolism of cardiac cells both acutely and chronically (Tokarska-Schlattner *et al.* 2010), consequently leading to ATP depletion (Strigun *et al.*, 2011c; Pointon *et al.*, 2011). A significant decrease of EC<sub>50</sub> values, as observed in our study, might therefore be related to time dependant cumulative effects.

Group 1 (Fig. 3 B) contains the two psychoactive drugs, desipramin and haloperidol, as well as diclofenac. These drugs were least toxic as compared to all other drugs. Despite a higher similarity with the first group (amiodarone, verapamil, terfenadin and astemizol), these drugs also showed a significant decrease of EC<sub>50</sub> values (40% - 60% within 24 h), pointing towards a time dependant increase of their toxicity. The *in vitro* toxicity of these drugs has been described for several cell lines. While toxicity of desipramin potentially involves block of potassium channels, it was recently shown that diclofenac inhibits L-type calcium channels in ventricular myocytes. In spite of their channel blocking ability (Hong *et al.*, 2010; Staudacher *et al.*, 2011; Yarishkin *et al.*, 2009) they formed an individual cluster apart from the group which contains amiodarone, verapamil, astemizol and terfenadin. The reason for this difference remains to be assessed but is probably related to cumulative toxic effects, similarly as observed for the anthracyclines, resulting in a delayed toxic effect.



We conclude that determination of a drug's EC<sub>50</sub> dynamic allows a rough estimation whether the toxicity of a drug is either immediate or delayed. Simple consideration of an EC<sub>50</sub> value at a certain time point gives information on a drug's relative toxicity. However, measurement of the actual EC<sub>50</sub> dynamics will include the dynamic information, which is otherwise mostly neglected due to the necessity of multi-plate seeding when using common cytotoxicity assays (such as SRB- or LDH-assay). The presented approach can contribute to the understanding of the potential mechanism of toxicity of an unknown drug. However, accurate estimation of the mechanism of toxicity based on its dynamic EC<sub>50</sub> will necessitate an expanded set of training compounds with known toxicological and/or pharmacological properties. Work in this regard is underway in our laboratory.

## Chapter 3

### **Metabolic profiling using HPLC allows classification of drugs according to their mechanisms of action in HL-1 cardiomyocytes**

#### **Abstract**

Along with hepatotoxicity, cardiotoxic side effects remain one of the major reasons for drug withdrawals and boxed warnings. Prediction methods for cardiotoxicity are insufficient. High content screening comprising of not only electrophysiological characterization but also cellular molecular alterations are expected to improve the cardiotoxicity prediction potential. Metabolomic approaches recently have become an important focus of research in pharmacological testing and prediction. In this study, the culture medium supernatants from HL-1 cardiomyocytes after exposure to drugs from different classes (analgesics, antimetabolites, anthracyclines, antihistamines, channel blockers) were analyzed to determine specific metabolic footprints in response to the tested drugs. Since most drugs influence energy metabolism in cardiac cells, the metabolite “sub-profile” consisting of glucose, lactate, pyruvate and amino acids was considered. These metabolites were quantified using HPLC in samples after exposure of cells to test compounds of the respective drug groups. The studied drug concentrations were selected from concentration response curves for each drug. The metabolite profiles were randomly split into training/validation and test set; and then analysed using multivariate statistics (principal component analysis and discriminant analysis). Discriminant analysis resulted in clustering of drugs according to their modes of action. After cross validation and cross model validation, the underlying training data was able to predict 50%-80% of conditions to the correct classification group. We show that HPLC based characterisation of known cell culture medium components is sufficient to predict a drug’s potential classification according to its mode of action.

**This chapter has been published as: Strigun A, Wahrheit J, Beckers S, Heinzle E, Noor F, (2011). Metabolic profiling using HPLC allows classification of drugs according to their mechanisms of action in HL-1 cardiomyocytes. Toxicology and Applied Pharmacology 252: 183-191**

### Introduction

Cardiac injury, a severe side effect of drugs, is of extreme concern to the pharmaceutical industry and drug regulatory agencies (Darpo, 2007). Despite stringent regulations and guidelines for the assessment of cardiac injury, several drugs have been withdrawn from the market due to cardiotoxic side effects (Gwathmey *et al.*, 2009). Most traditional methods for preclinical assessment of cardiac side effects address electrophysiological aspects and involve determination of voltage-clamp analysis of ionic currents, action potential recordings in myocytes/tissues or measurement of QT-interval using whole animals (Sanguinetti and Mitcheson, 2005). Predictions on the basis of only electrophysiological screening have proved to be insufficient and at the same time may result in termination of lead compound development in preclinical assessment, even for compounds which may have been of beneficial value both to the patient and the pharmaceutical industry. In addition to electrophysiological evaluation, characterization of other cellular functional parameters such as substrate usage and metabolite trafficking may greatly improve the prediction potential of a test system. Over the years, extensive knowledge has been gained on cardiac substrate usage and metabolism; and its alterations in myocardial diseases (Ashrafian *et al.*, 2007; Gertz *et al.*, 1988; Mudge *et al.*, 1976; Panchal *et al.*, 2001; Randle *et al.*, 1964; Stanley *et al.*, 1997; Wisneski *et al.*, 1985), e.g. in myocardial ischemia (Depre and Taegtmeyer, 2000). There is growing evidence that changes in substrate metabolism lead to contractile dysfunction (Stanley *et al.*, 2005). These changes therefore more or less reflect cardiac pathological conditions or a drug's action/toxicity on the cardiac tissues (Ashrafian and Neubauer, 2009; Henney, 2009; Ho and Lieu, 2008; Nicholson and Wilson, 2003; Zhu *et al.*, 2008).

Metabolomic approaches have been successfully applied in cardiovascular research, for example, in profiling the metabolomic response of cardiac cells to induced ischemia (Sabatine *et al.*, 2005) and human atrial fibrillation (Mayr *et al.*, 2008b). Moreover, metabolic profiling has provided interesting insights on the response of microbial cells, mammalian cell cultures, other tissues or organs to drugs (Allen *et al.*, 2004; Tiziani *et al.*, 2009) and their mechanisms of toxicity (Andreadou *et al.*, 2009; Beger *et al.*, 2010; Clarke and Haselden, 2008; Kaddurah-Daouk *et al.*, 2008; Keun, 2006; Robertson, 2005; Wei *et al.*, 2009; West *et al.*, 2010). Similarly, metabolomics may also be useful for mapping specific metabolic responses of cardiac cells *in vivo* and *in vitro* upon exposure to drugs from specific groups classified according to their modes of action. Mapping groups of drugs with known cardiotoxic outcome in humans in terms of the

## Metabolite profiling of HL-1 cardiomyocytes

---

metabolic response of cardiac cell or tissue type can be helpful in identifying whether new drug candidates share similar metabolic profiles and therefore bear a potential risk to share similar toxic properties.

Assessment of drug induced toxicity using metabolomics requires cell or tissue models which closely reflect the *in vivo* system in humans. Immortalized cell lines respond in a different way than primary cells (Robertson, 2005). Human embryonic stem cell derived cell types, such as cardiomyocytes or hepatocytes have the potential to be applied as *in vitro* test models, since they have the required homogeneity and functionality to make them attractive for drug discovery (Jensen *et al.*, 2009) as well as for human relevant toxicity assessment. Nevertheless, suitable cell lines of human or non-human origin still prove to be useful for preliminary screening and method optimisation since they are less costly and easier to handle.

HL-1 cells have been shown to be quite useful for studying cardiac physiology (Claycomb *et al.*, 1998; White *et al.*, 2004) since they express many genes typical for differentiated adult cardiomyocytes (Claycomb *et al.*, 1998). HL-1 cardiomyocytes express several cardiac ion channels, such as L- and T-Type  $\text{Ca}^{2+}$  channels (Xia *et al.*, 2004), ATP-sensitive  $\text{K}^+$  channels (Fox *et al.*, 2005) and inward rectifier  $\text{K}^+$  channels (Goldoni *et al.*, 2010). Besides, there is evidence that HL-1 cardiomyocytes possess intracellular calcium release channels (Kim *et al.*, 2010), that are assumed to play a role in  $\text{Ca}^{2+}$  signaling and in excitation-contraction coupling in cardiomyocytes (Lipp *et al.*, 2000). These properties make them attractive for assessing metabolic responses upon targeting these cells with drugs which have channel blocking properties. In addition these cells are useful to study mechanisms of anthracycline induced apoptosis (Kim *et al.*, 2003) as well as in assessing damage of drugs on troponin T release (Andersson *et al.*, 2010). Besides, presence of inducible nitric oxide synthase in these cells (Sanders *et al.*, 2001) makes them attractive for studying drug induced disturbances of nitric oxide signalling pathways. Furthermore, cardiac adenosine receptors have been described in these cells, which are of high interest in studying effects of cardioprotective adenosine agonists on cardiomyocytes damage either induced by anthracyclines or due to hypoxia (Chaudary *et al.*, 2004; Keene *et al.*, 2010).

In this study, we investigated if selected drugs classified into groups; namely analgesics (acetaminophen, diclofenac), antimetabolites (methotrexate, 5-fluorouracil), anthracyclines (daunorubicin, doxorubicin), antihistamines (astemizol, terfenadin) and channel blockers (amiodarone, quinidine, verapamil); leave group specific profiles in culture supernatants of HL-1

cardiomyocytes. These drugs with the exception of acetaminophen have been associated with cardiac side effects. Diclofenac has been associated with cardiovascular risk (McGettigan and Henry, 2006; Waksman *et al.*, 2007). A recent study indicated that diclofenac inhibits L-type calcium channel in cardiac cells, which was suggested as a potential reason for diclofenac associated risk of heart failure (Yarishkin *et al.*, 2009). 5-fluoruracil is considered cardiotoxic (Senkus and Jassem, 2010), though the mechanism of is not well understood. Symptoms such as cardiac arrhythmias, congestive heart failure and sudden death due to 5-FU have been reported (Schimmel *et al.*, 2004). Although methotrexate is not definitely considered cardiotoxic, supraventricular and ventricular arrhythmias were associated with this drug (Gasser *et al.*, 1982; Kettunen *et al.*, 1995). Terfenadin has been withdrawn from the market due to cardiotoxicity. It is cardiotoxic in overdose or when its first pass metabolism (by hepatic CYP3A4) is impaired, resulting in QT-prolongation (Armstrong and Cozza, 2003). Terfenadin induced cardiotoxicity may involve inhibition of the delayed rectifier potassium channel in cardiac tissue (Tagliatela *et al.*, 1999; Yap and Camm, 1999). Astemizol also blocks potassium channels and prolongs the QT-interval (Yap and Camm, 1999). Cardiotoxicity has been extensively reviewed with the use of anthracyclines, daunorubicin and doxorubicin (Floyd *et al.*, 2005; Schimmel *et al.*, 2004; Simunek *et al.*, 2009). Anthracyclines have been reported to cause cardiomyopathy, congestive heart failure and QT-prolongation. Potential arrhythmic effects of antiarrhythmic drugs are well known (Lazzara, 1993). QT- prolongation, in particular after amiodarone and quinidine therapy has been described repeatedly (Hii *et al.*, 1992; McComb *et al.*, 1980; Schrickel *et al.*, 2003; Schrickel *et al.*, 2006; White, 2007).

In our study, unlike other recently reported studies using MS-based methods, we focused on HPLC quantification of metabolites which is accurate and precise (Hans *et al.*, 2003; Niklas *et al.*, 2009) based on selective derivatization of amino acids using ortho-phthaldehyde (OPA). We focused on common culture medium nutrients such as glucose, pyruvate and amino acids as well as lactate which is the most commonly secreted metabolite by cell lines. The presented data shows that this approach, combined with multivariate statistics (principal component analysis and discriminant analysis) is adequate for correct prediction of drug classification. It might prove useful in not only predicting a compound's potential classification based on mode of action but may also help in the assessment of risk of cardiac injury in clinical applications based on classification.

### Material and methods

#### *Cell Culture*

HL-1 cardiomyocytes were obtained from Dr. Claycomb (Louisiana State University) for research within the framework of EU-STREP (LSHB-CT-2007-037636) project “Invitroheart”(Claycomb *et al.*, 1998). The cells were maintained in Claycomb medium (Sigma Chemical, USA) supplemented with 2 mM glutamine (PAA Laboratories, Austria), 100 U/ml penicillin, 100 µg/ml streptomycin (PenStrep stock solution: CC Pro, Germany), 100 µM norepinephrine (Sigma Chemical, USA) in 30 mM L-ascorbic acid (Sigma Chemical, USA) and 10% foetal bovine serum (FBS, JRH Biosciences, UK). Cells were sub-cultured when confluent in a split ratio of 1:3. Culture flasks (75 cm<sup>2</sup>, Falcon, Germany) were pre-coated with a solution of 0.02% (w/v) gelatine (AppliChem, Germany) containing 5 µg/ml fibronectin (Sigma Chemical, USA). Beating HL-1 cardiomyocytes were maintained at standard cell culture conditions (37°C, 5% CO<sub>2</sub> and 95% relative humidity).

#### *Preparation of test solutions*

All drugs were purchased from Sigma Chemical (USA) with the highest purity available. Stock solutions of terfenadine (10 mM), diclofenac (500 mM), verapamil (100 mM), methotrexate (100 mM), 5-fluorouracil (100 mM), quinidine (100 mM), daunorubicin (10 mM), amiodarone (50 mM) were prepared in dimethylsulfoxide (DMSO) also purchased from Sigma Chemical, USA. A doxorubicin stock solution (10 mM) was prepared in cell culture grade water (PAN Biotech, Germany). The stock solution of acetaminophen (30 mM) was directly prepared in supplemented Claycomb medium. For the cytotoxicity screening all stock solutions were serially diluted in supplemented Claycomb medium. The end DMSO concentration did not exceed 1% (v/v) in any of the final test solutions. Solvent controls using DMSO (DMSO controls) at concentrations identical to the corresponding test concentrations were also tested. The concentrations analyzed for metabolic footprinting are given in table 1.

#### *Determination of concentration response curves*

HL-1 cardiomyocytes were trypsinized at confluency and counted using trypan blue exclusion method in a hemocytometer.  $1.5 \times 10^5$  cells/well were seeded in 24-well OxoDishes (PreSens, Germany) in a volume of 1 ml supplemented Claycomb medium per well. After 24 hours (h) incubation, the supernatant was removed and the cells were washed twice with Claycomb

## Metabolite profiling of HL-1 cardiomyocytes

---

medium without any supplements. Afterwards, fresh medium containing drugs at different concentrations was added to the cells. All conditions (untreated controls, DMSO controls, drugs) were tested in triplicates. For all drugs, cells were treated for 48h with the exception of antimetabolites, 5-fluorouracil (5-FU) and methotrexate, for which the exposure time was 96h. After the test period, cell culture supernatants were collected and spun down at 10000 x g for 5 minutes (min) at 4°C to remove cell debris. The samples were stored at -20°C until further analysis of metabolic footprints. After medium removal each well was washed thrice with 1 ml non-supplemented Claycomb medium. Cells were fixed at 4°C for one hour by adding 250 µl TFA-solution (50% trifluoroacetic acid (v/v) in water) into each well containing 1 ml of non-supplemented Claycomb medium. After fixation, the cells were washed carefully five times with deionized water. 250 µl of 0.4% sulforhodamine B (Sigma Chemical, USA) solution (w/v) in 0.1% acetic acid (Sigma Chemical) (v/v) was added for staining cellular proteins for 30 minutes at room temperature on a plate shaker set at 200 rpm. The staining solution was removed and the wells were washed thrice with 0.1% acetic acid (v/v) to remove unbound dye. The stained cells were then dried for 30 minutes and the dye was extracted from the cells with 500 µl of 10 mM Tris base (Roth, Germany) solution (pH 10). Extraction was performed for 10 minutes on a microplate shaker set at 200 rpm. The absorption of the dye was measured in 96 well microtiter plates using a fluorescence reader (iEMS, Labsystems) at a wavelength of 540 nm against a reference wavelength of 660 nm.

### *Sample preparation for metabolic footprint analysis*

The supernatant from each well was collected as described above. Serum proteins, such as albumin were removed by microfiltration using Microcon® Filter Devices (Millipore, Germany) with an exclusion size of 10kDa. Subsequently each filtrate was diluted 1:2 with  $\alpha$ -aminobutyric acid solution (400 µM in deionized water) which was used as internal standard.

### *Metabolic footprinting*

#### *Quantification of glucose, lactate and pyruvate*

Glucose, lactate and pyruvate were quantified as described recently (Hans *et al.*, 2003; Niklas *et al.*, 2009). In short, quantification was carried out using HPLC (Kontron Instruments, Germany) with an Aminex HPX 87H ion exchange column (300 mm x 7.8 mm, Biorad, USA). The isocratic separation was carried out using 7 mM sulfuric acid as eluent and a flow rate of 0.8 ml/min at a

## Metabolite profiling of HL-1 cardiomyocytes

---

column temperature of 60°C. Injection volume was 20 µl. Lactate and pyruvate were detected by UV-detection (UV-detector: HPLC 535, Biotek, Germany) at a wavelength of 210 nm. Glucose was determined by measuring the refractive index (ERC-7515A, ERC Inc, Germany). Standard solutions of glucose, lactate and pyruvate (Sigma Chemical, USA) were used for identification and quantification of these metabolites, respectively. The standard concentration of glucose, lactate and pyruvate included 10mM, 5mM, 2.5mM, 1.25mM, 0.625mM, 0.312mM, 0.156mM and 0.078mM. Retention times of these metabolites are given in Table 2.

### *Quantification of amino acids*

Amino acids were quantified as described earlier (Hans *et al.*, 2003; Kromer *et al.*, 2005; Niklas *et al.*, 2009). In short, quantification was carried out using HPLC (Agilent 1100 series, Agilent technologies, Germany) with a C18 RP-column (Gemini® 5u C18 110A, 150 mm x 4.6 mm, Phenomenex, Germany) at 40°C. A gradient separation was carried out (Eluent 1 : 40 mM Na<sub>2</sub>HPO<sub>4</sub>, pH 7.8; Eluent 2: methanol, acetonitrile, water 45:45:10 (v/v)) with a flow rate of 1 ml/min. Primary amino acids were derivatized by pre-column derivatisation using ortho-phthaldehyde (OPA) (Agilent, Germany) (excitation wavelength: 330 nm; emission wavelength: 450 nm). Proline, a secondary amino acid, was derivatized using 9-fluorenylmethyl-chloroform (FMOC) (Agilent, Germany) (excitation wavelength: 266 nm, emission wavelength: 305 nm). Amino acids were obtained from Sigma Chemical, USA. Standard solutions of amino acids were used for identification and quantification of these metabolites, respectively. The standard concentrations of amino acids included 1000µM, 500µM, 250µM, 125µM, 62.5µM, 31.25µM, 15.6µM and 7.8µM, respectively. Retention times of all amino acids are given in Table. 2.

### *Data handling and statistical analysis*

The changes in the metabolite concentrations (glucose, lactate and amino acids) upon exposure to the drugs were compared with the respective untreated controls using student's *t*-test. The changes were considered significant at  $p < 0.05$ .

The concentrations of each metabolite in the respective supernatants were normalized to the individual untreated controls (% of control) of each experiment. Principal component analysis (PCA) and discriminant analysis (DA) were carried out using XLSTAT 2010.3.06 (Addinsoft, Germany). For discriminant analysis, all conditions were assigned to specific classification, which represents the group labels. These are: 1) untreated controls 2) DMSO controls (cells



## Metabolite profiling of HL-1 cardiomyocytes

---

treated with concentrations of DMSO identical to those which were used in case of drugs) 3) channel blockers (amiodarone, quinidine & verapamil) 4) antihistamines (astemizol & terfenadine) 5) anthracyclines (daunorubicin & doxorubicin) 6) analgesics (acetaminophen & diclofenac) and 7) antimetabolites (5-fluorouracil & methotrexate). Cross model validation was carried out similar to a recently reported approach (Westerhuis *et al.*, 2008). Briefly, the data matrix, which consisted of 152 rows and 18 columns, was split into a test set (76 rows) and a second training/validation set (76 rows). From the training/validation set, which was used to determine discriminant models of drug groups, 35 observations were randomly selected and cross validation was carried out. This procedure was repeated until all conditions of the whole data set were part of the test set at least once. Thus, a total number of 76 prediction models were created. In no case, conditions from the test set were used to create a prediction model. The accuracy of each prediction model was assessed by determination of the percentage of correctly predicted groups in conditions from the test set. 95% confidence intervals were calculated with XLSTAT. In order to determine whether correct classification of conditions in the test set is random, a permutation test was carried out. Hereby, assignments of group labels in the training/validation set were permuted in a random way. Prediction quality was determined by comparing the accuracy of both permuted and non-permuted prediction models.

## Results

### Concentration response curves

A complete set of concentration response curves of the tested drugs is shown in Fig. 1. Each experiment was carried out with its individual untreated control. As apparent, the effective concentrations for different drugs were quite diverse, ranging from the nanomolar range in case of anthracyclines and antimetabolites to the upper micromolar range in case of analgesics. Along with anthracyclines and antimetabolites, the antihistamines (astemizol and terfenadine) were quite toxic, since the effective concentration range was in the lower micromolar range. The concentration response curves of both compounds were almost identical. Channel blockers amiodarone, quinidine and verapamil gave similar sigmoidal curves with similar shapes. However, they showed a shift in concentration response range. The effective concentration ranges for both analgesics (acetaminophen and diclofenac) were quite different, while corresponding curves for anthracyclines (daunorubicin and doxorubicin) were almost identical. Based on these concentration response results, drug concentrations were selected (Table 1) at specific points of the concentration response curve (ranging from 40%-100% of relative proliferation) for further HPLC quantification of metabolites in the supernatants.

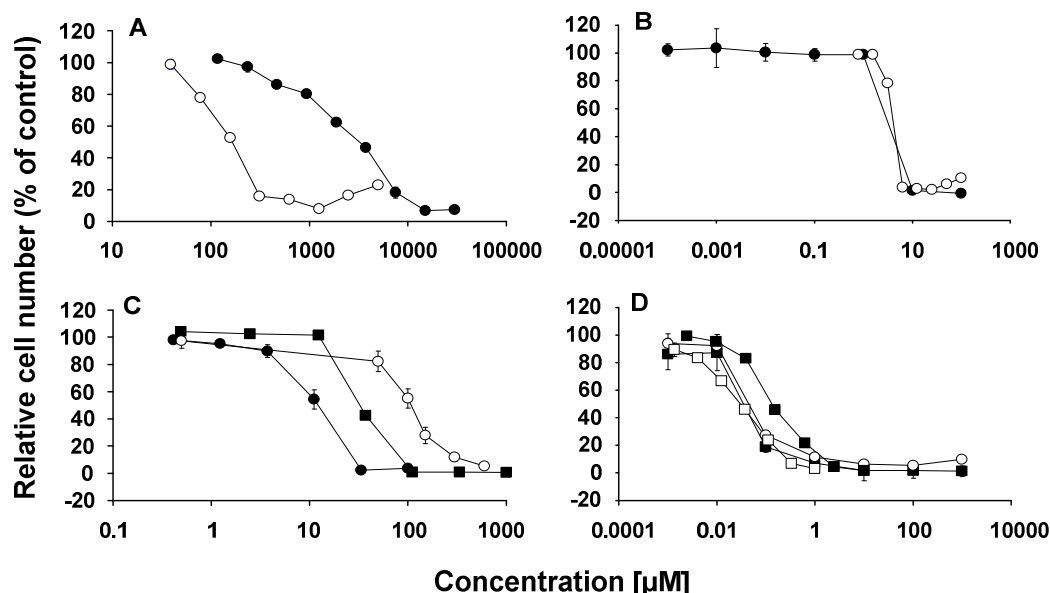


**Figure 1:** Concentration response curves of selected drugs **A.** Analgesics: acetaminophen (●) & diclofenac (○) **B.** Antihistamines: astemizol (●) & terfenadine (○) **C.** Channel blockers: amiodarone (●), quinidine (○) & verapamil (■) **D.** Anthracyclines/antimetabolites: methotrexate (●), 5-fluorouracil (○), doxorubicin (■) & daunorubicin (□). The drugs were tested on HL-1 cardiomyocytes for 48 h (except antimetabolites which were tested for 96 h) using sulforhodamine B proliferation assay. Error bars indicate  $\pm$  S.D. (n = 3).

## Metabolite profiling of HL-1 cardiomyocytes

---

**Table 1:** Drug concentrations considered for footprint analysis on culture supernatants of HL-1 cardiomyocytes after 48h of drug exposure (except for 5-fluorouracil and methotrexate for which the exposure time was 96h).

Drug class	Concentrations analysed for metabolic profiling [ $\mu\text{M}$ ]				
<b>Analgesics</b>					
Acetaminophen	940	470	235	117	
Diclofenac	80	40			
<b>Antihistamines</b>					
Astemizol	1	0.1	0.01	0.001	0.0001
Terfenadine	3.2	1.6	0.8		
<b>Channel blockers</b>					
Amiodarone	4	1.2	0.4		
Quinidine	50	0.5			
Verapamil	12.5	2.5	0.5		
<b>Anthracyclines</b>					
Daunorubicin	0.04	0.012	0.004	0.001	
Doxorubicin	0.04	0.01	0.0025		
<b>Antimetabolites</b>					
5-Fluorouracil	0.01	0.001			
Methotrexate	0.01	0.001			

*Since most drugs were dissolved in DMSO, the corresponding DMSO controls were also included in metabolic footprint analysis in addition to the untreated controls from each experiment.*

### *Metabolic footprinting (consumption and production of metabolites)*

Uptake and production of all considered metabolites (glucose, lactate, pyruvate and 19 amino acids) in untreated HL-1 cardiomyocytes is shown in Table 2. Average changes in glucose and lactate concentration within 48 h incubation were  $-5591 \pm 651 \mu\text{M}$  and  $9596 \pm 1184 \mu\text{M}$  respectively. Among amino acids, glutamine and alanine showed the highest changes in concentrations ( $-411 \pm 24 \mu\text{M}$  and  $190 \pm 17 \mu\text{M}$ ) followed by branched chain amino acids (BCAA) leucine, isoleucine and valine ( $-118 \pm 8 \mu\text{M}$ ,  $-104 \pm 8 \mu\text{M}$  and  $-70 \pm 9 \mu\text{M}$ ). Net concentration changes for the remaining amino acids ranged from 10 to 70  $\mu\text{M}$ . Concentration changes for asparagine ( $-6 \pm 3 \mu\text{M}$ ), aspartic acid ( $0 \pm 4 \mu\text{M}$ ) and glycine ( $8 \pm 6 \mu\text{M}$ ) were negligible.

## Metabolite profiling of HL-1 cardiomyocytes

**Table 2:** Retention time of metabolites and changes in extracellular metabolite concentrations in untreated HL-1 cardiomyocytes within 48h incubation. Quantification of metabolites was carried out according to methods part. Concentrations of metabolites were measured in cell culture supernatants using HPLC at t = 48h and t = 0h (medium without cells). Standard deviations were calculated from four replicates. Negative and positive values refer to uptake and production respectively.

Metabolite	$\Delta$ [ $\mu$ M]	$\pm$ S.D	Retention time [min]
Lactate	9596	1184	9.8
Glucose	-5591	651	7.0
Glutamine	-411	24	15.2
Alanine	190	17	21.7
Leucine	-118	8	39.7
Isoleucine	-104	8	37.5
Valine	-70	9	32.0
Lysine	-53	3	41.9
Pyruvate	-47	10	7.4
Serine	46	7	13.1
Proline	-38	10	45.6
Glutamic acid	34	10	7.0
Arginine	-31	3	19.4
Tyrosine	-30	5	26.0
Phenylalanine	-24	4	36.8
Methionine	-23	1	32.8
Threonine	-18	11	17.6
Histidine	-12	2	15.9
Tryptophan	-9	2	35.7
Glycine	8	6	17.0
Asparagine	-6	3	12.2
Aspartic acid	0	4	4.6

The metabolite uptake and production was quantified and analyzed for the drug treated cells as well. A detailed overview of the data is given in supplementary material (Appendix for Chapter 3, Table S1). Figure 2 shows changes in glucose and lactate concentrations induced by the highest analysed drug concentrations (Table 1) as percent of untreated controls. Since most of the drugs were dissolved in DMSO, the corresponding DMSO controls were analyzed for any changes due to the solvent (Fig. 2 A). No significant changes in glucose uptake and lactate production were observed for DMSO concentrations of 0.012 % or lower. Therefore, DMSO controls for drug concentrations containing less than 0.0012% of DMSO were not analyzed. Significant variations in glucose uptake and lactate production could be observed for most of the tested drugs, except for 5-fluorouracil (0.01  $\mu$ M) and methotrexate (0.01  $\mu$ M) (Fig. 2 H and I).

## Metabolite profiling of HL-1 cardiomyocytes

---

The highest impact on glucose uptake and lactate production was observed for channel blockers (amiodarone and verapamil) and analgesics (acetaminophen and diclofenac). Acetaminophen (940  $\mu\text{M}$ ) reduced glucose uptake as well as lactate production by 50% (Fig. 2 B). For this drug DMSO was not used as solvent. Amiodarone (4  $\mu\text{M}$ ) decreased relative uptake and production of glucose and lactate respectively by 35% (Fig. 2 C), while the corresponding DMSO control (0.04% v/v) resulted in a reduction of 11% for glucose uptake and 10% for lactate production (Fig. 2 A). In case of astemizol (1  $\mu\text{M}$ ), glucose uptake and lactate production was reduced by 20% and 25%, respectively (Fig. 2 D). Unlike doxorubicin (0.04  $\mu\text{M}$ ) which had no significant effect on both metabolites (Fig. 2 G), daunorubicin (0.04  $\mu\text{M}$ ) reduced glucose uptake and lactate production (Fig. 2 E) most significantly by 75% and 70%, respectively. In case of daunorubicin, the influence of DMSO was neglected as the DMSO concentration was below 0.0012%. Diclofenac (80  $\mu\text{M}$ ) reduced glucose uptake and lactate production by 60% and 55% respectively (Fig. 2 F), and was significantly different from untreated control and DMSO control, which contained 0.012 % (v/v) DMSO (Fig. 2 A). A slight increase in glucose uptake and lactate production was observed in response to channel blocker quinidine (8% and 12% respectively) (Fig. 2 J), which was however not significantly different from DMSO (0.012%) control. Terfenadine (3.2  $\mu\text{M}$ ) reduced glucose uptake by 35% and lactate production by 50%, as compared to untreated controls (Fig. 2 K). However, because of the larger error in glucose uptake measurement only reduced lactate production was significantly different from the corresponding DMSO control, which contained 0.04% (v/v) (Fig. 2 A). Verapamil (12.5  $\mu\text{M}$ ) decreased relative concentrations of glucose and lactate by about 50%, respectively (Fig. 2 L), while in corresponding DMSO (0.012%) controls no significant changes in glucose and lactate concentrations, as compared to the untreated controls, were observed. Amino acids which showed the highest uptake and production in untreated cells (glutamine, alanine, branched chain amino acids) were significantly affected by several of the tested drugs at the highest analysed concentration. A detailed overview of changes in measured amino acids in the presence of drugs is given in the supplementary material (Appendix for Chapter 3; Tab. S1 and S1.1).

## Metabolite profiling of HL-1 cardiomyocytes

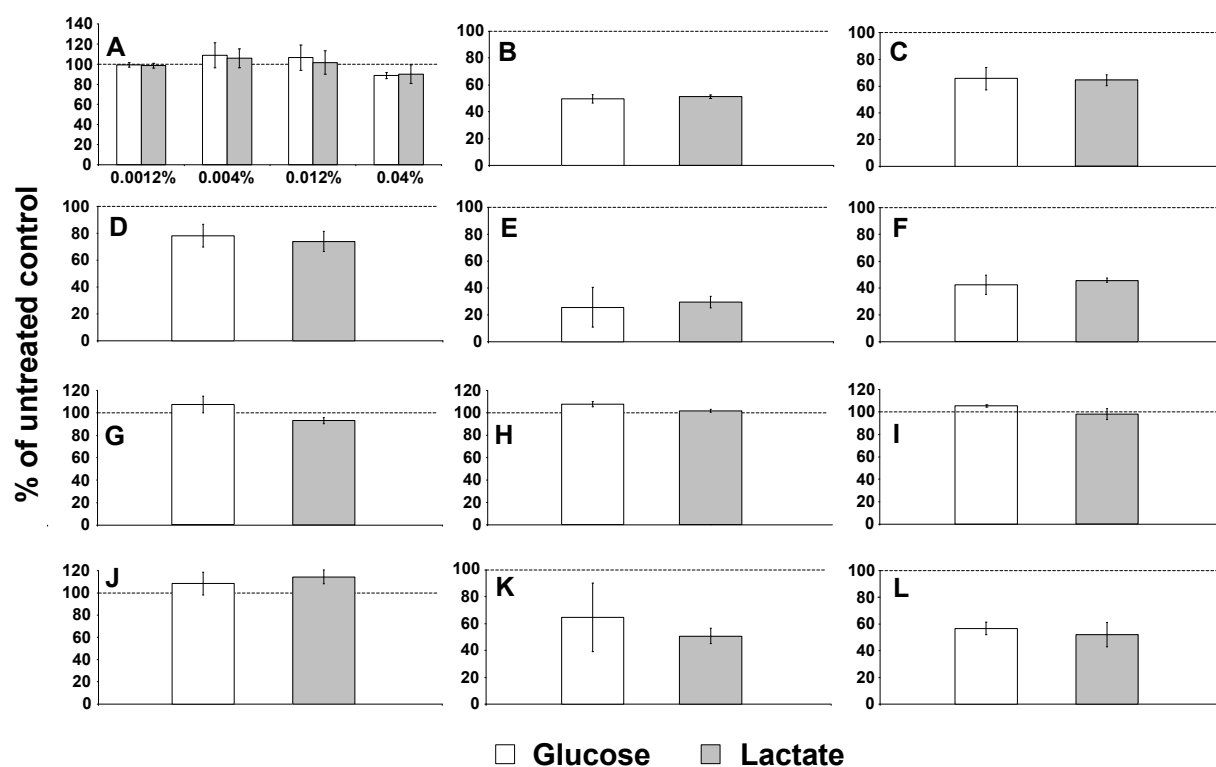


**Figure 2:** Drug induced changes in uptake/production of glucose and lactate in HL-1 cells as percent of untreated controls. HL-1 cells were incubated with the respective drugs for 48 h or 96h (in case of 5-fluorouracil and methotrexate). **A)** DMSO controls **B)** Acetaminophen (940  $\mu$ M) **C)** Amiodarone (4  $\mu$ M) **D)** Astemizol (1  $\mu$ M) **E)** Daunorubicin (0.04  $\mu$ M) **F)** Diclofenac (80  $\mu$ M) **G)** Doxorubicin (0.04  $\mu$ M) **H)** 5-Fluorouracil (0.01  $\mu$ M) **I)** Methotrexate (0.01  $\mu$ M) **J)** Quinidine (50  $\mu$ M) **K)** Terfenadine (3.2  $\mu$ M) **L)** Verapamil (12.5  $\mu$ M). Metabolites were quantified using HPLC and the metabolite concentration at  $t = 48$ h and  $t = 0$ h (negative control; medium without cells) was calculated. Standard deviations from triplicate measurements are indicated as error bars.

### *Principal component and discriminant analysis*

Using principal component analysis (PCA) the data set was analyzed for better visual inspection of differences in metabolite uptake and production (Fig. 3). The amino acids namely aspartate, asparagine, proline and tryptophan were not included in statistical analysis, since their uptake showed relatively high experiment to experiment variations in untreated cells.

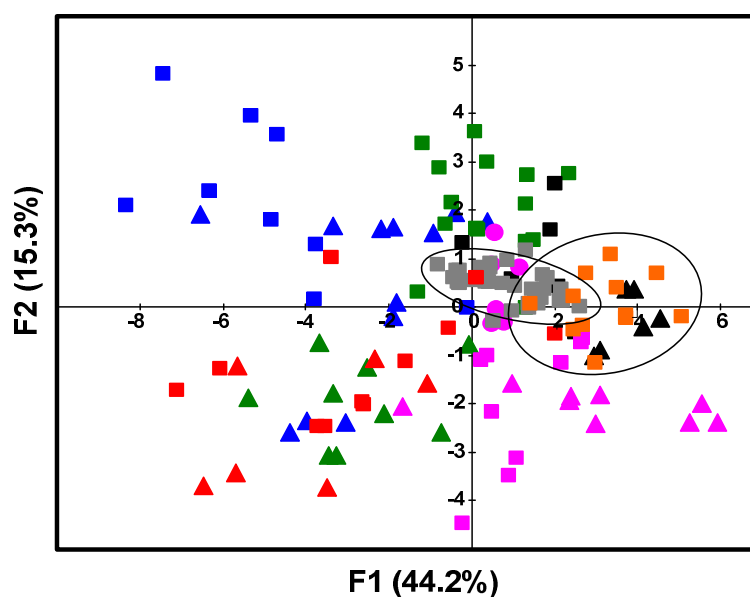


**Figure 3:** PCA score plot of the first two principal components (F1 and F2, 59.5% of the total variance in the data set). Metabolic profiling was carried out on supernatants from HL-1 cardiomyocytes upon exposure to drugs. Selected analyzed drugs from several classes (analgesics, channel blockers, antihistamines, anthracyclines, antimetabolites) are depicted; Amiodarone (pink squares), astemizol (green squares), acetaminophen (red squares), untreated controls (grey squares), daunorubicin (blue triangles), doxorubicin (blue squares), diclofenac (red triangles), DMSO (orange squares), 5-fluorouracil (black squares), methotrexate (black triangles), terfenadine (green triangles), quinidine (pink circles), verapamil (pink triangles). Untreated controls and DMSO controls are shown within 95% confidence ellipses.

In the score plot (Fig. 3), an approximate clustering of drugs from certain classes i.e. those with a similar mechanism of action is seen for the majority of the replicates for anthracyclines namely daunorubicin and doxorubicin (upper left quadrant), channel blockers namely amiodarone and verapamil (lower right quadrant), as well as most observations of analgesics (acetaminophen and diclofenac) (lower left quadrant). However, antihistamines (astemizol and terfenadine) were not located in a single quadrant but clearly grouped for the individual drugs. As apparent from loading coefficients (Fig. 4), the separation of drugs along the first component was mainly attributed to amino acids, especially those which are catabolised in TCA-cycle e.g. phenylalanine, branched chain amino acids (leucine, isoleucine, valine), glutamate (Fig. 4 A), while separation along the second component was mainly due to changes of glucose uptake and metabolites which are connected to intermediates from glycolysis (alanine, pyruvate, serine, lactate) (Fig. 4 B).

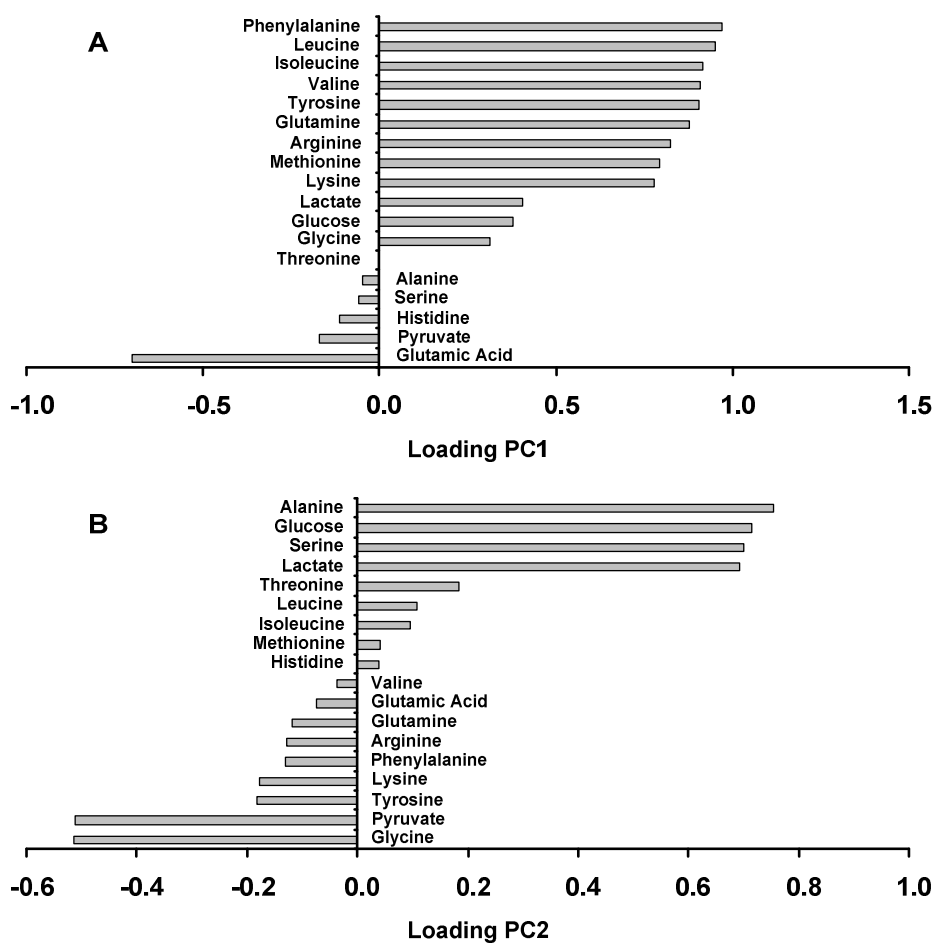


**Figure 4:** PCA-loading coefficients of 18 metabolites (glucose, lactate, pyruvate and 15 amino acids) from A) PC axis F1 and B) PC axis F2, obtained from the analysis shown in Figure. 3.

Discriminant analysis (DA) was carried out to further assess the clustering of the drugs. As depicted in figure 5, at least four distinct clusters were obtained. The first cluster includes the antihistamines, astemizol and terfenadine (Fig. 5, green symbols) while the second cluster includes analgesics, acetaminophen and diclofenac (Fig. 5, red symbols). The third cluster includes both anthracyclines daunorubicin and doxorubicin (Fig. 5, blue symbols), while the last cluster includes untreated controls, DMSO-controls, channel blockers and antimetabolites.



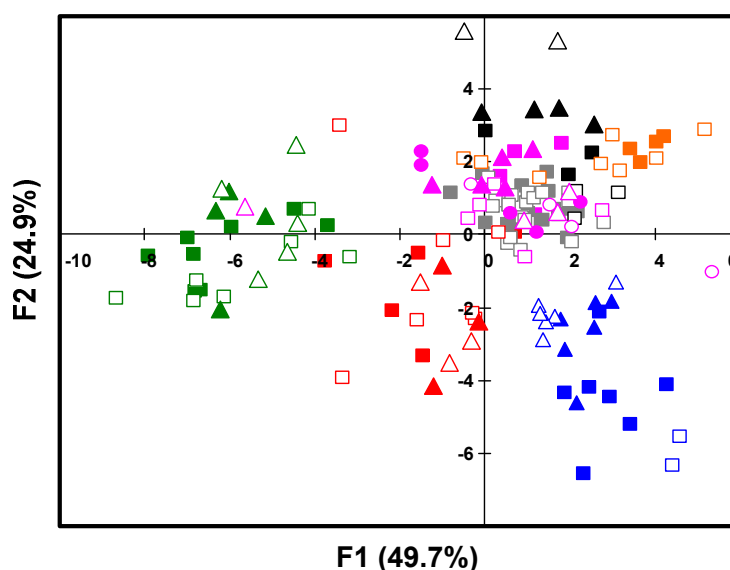


**Figure 5:** Discriminant analysis score plot of axis 1 and 2 (75% of the variance). Metabolic profiling was carried out on supernatants from HL-1 cardiomyocytes upon exposure to drugs from several classes (analgesics, channel blocker, antihistamines, anthracyclines, antimetabolites) represented by; Amiodarone (pink squares), astemizol (green squares), acetaminophen (red squares), untreated controls (grey squares), daunorubicin (blue triangles), doxorubicin (blue squares), diclofenac (red triangles), DMSO (orange squares), 5-fluorouracil (black squares), methotrexate (black triangles), terfenadine (green triangles), quinidine (pink circles), verapamil (pink triangles). The score plot is based on a prediction model which was created by using all 152 observations. Full symbols: training set; Empty symbols: cross validation data set.

### *Accuracy of prediction of classification/grouping*

We used discriminant analysis to see if it allows specific drug classification of conditions in a test data set based on prior determination and cross validation of discriminant models. The whole data set was split into training/validation data and test data. A total of 76 discriminant models was established (see methods), each with its own accuracy. Prediction of test data by using all 18 considered metabolites as variables in the training data was most reliable for the majority of the drugs in the test data (Fig. 6).

In the case of predictions, which are based on “non-permuted” assignments of groups in the training/validation data (Fig. 6, white bars), average accuracy of classification in the test data set is quite reliable in case of untreated controls ( $82\% \pm 9$ ), anthracyclines ( $78\% \pm 11$ ) and antihistamines ( $76\% \pm 10$ ). Accuracy of classification was  $54\% \pm 11$  for antimetabolites,  $62\% \pm 12$  for DMSO,  $59\% \pm 8$  for analgesics,  $50\% \pm 9$  for channel blockers.

## Metabolite profiling of HL-1 cardiomyocytes

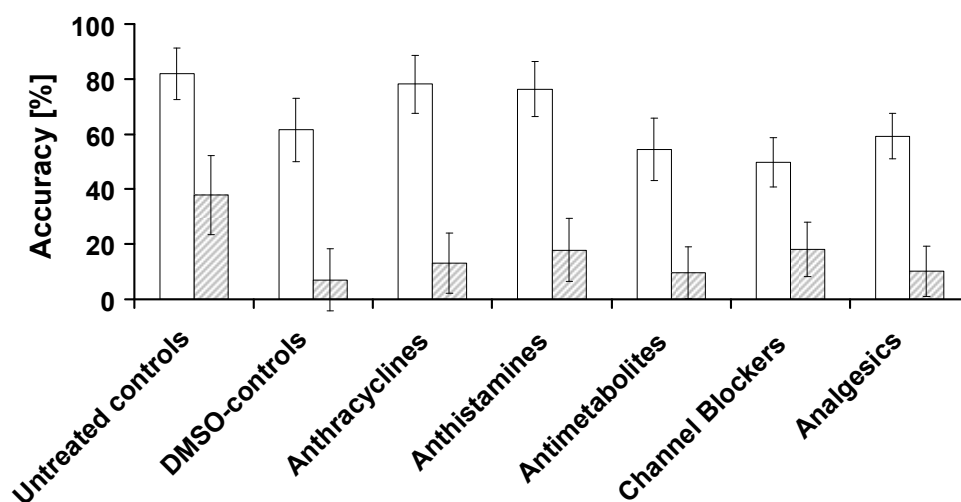


**Figure 6:** Discriminant analysis of extracellular metabolic footprints in HL-1 cardiomyocytes upon exposure to drugs from several classes/groups. The footprint data set (152 rows, 18 columns) was split into test data (76 rows) and a second set, which again was randomly split into training and validation data for cross validation. The average percent of correctly predicted classes/groups for each condition in the test data set and 95% confidence intervals were calculated from 76 evaluations i.e. discriminant functions. White bars indicate predictions which are based on models with correct assignment of group labels in the training/validation data set. Grey bars show predictions which are based on random i.e. permuted assignments of group labels to conditions in the training/validation data set.

Accuracy of classification was significantly better as compared with the corresponding predictions based on models in which classifications were randomly assigned (permuted) in the training/validation data set. Here, the accuracy of correctly predicted drug classes was 13%  $\pm$  10 (anthracyclines), 18%  $\pm$  11 (antihistamines), 10%  $\pm$  9 (antimetabolites), 38%  $\pm$  23 (untreated controls), 7%  $\pm$  11 (DMSO controls), 18%  $\pm$  10 (channel blockers) and 10%  $\pm$  9 (analgesics).

### Discussion

Since cardiac injury has been associated with alterations in substrate usage in cardiomyocytes (Stanley *et al.*, 2005), we assumed that the “sub-profile” of considered metabolites is unique for individual drug groups thereby allowing clustering of drugs according to their modes of action and for prediction of drug classification using supervised pattern recognition approach. Unlike recent metabolomic studies in which MS-based methods were used to monitor a whole spectrum of peaks of either known or unknown metabolites upon exposure of cells or tissues to toxic drugs (Allen *et al.*, 2003; Allen *et al.*, 2004; Dunn *et al.*, 2009; Henriques *et al.*, 2007; Kim *et al.*, 2010) we focused on HPLC measurement of known metabolites in common cell culture medium i.e. glucose, pyruvate and amino acids. Lactate secreted by cells was also taken into consideration. These metabolites not only serve anabolic functions (i.e. biomass synthesis) but to a high extent catabolic functions as well (oxidation in TCA-cycle). Uptake and secretion of metabolites relevant to glycolytic pathway (glucose, lactate, pyruvate, glycine and serine) as well as TCA-cycle (glutamine, BCAA, lysine, arginine etc.) showed both significant and non-significant changes induced by certain drugs. Changes in glucose uptake and lactate production represented the highest changes among the measured metabolites. Despite alterations in glucose uptake and lactate production in case of some drugs, the lactate/glucose ratio, which was  $1.8 \pm 0.2$  in untreated cells, was not significantly disturbed for any of the considered drugs concentrations. The observed lactate/glucose ratio in HL-1 cells is in accordance with recent observations (Monge *et al.*, 2009). It was argued that HL-1 cells share properties of cancer cells with a relatively high anaerobic glycolysis. The highest decrease in glucose uptake and lactate production was observed in case of channel blockers, analgesics and antihistamines. Since no significant alterations in lactate/glucose ratios were observed it can be assumed that the extent of glucose-derived pyruvate, which enters TCA-cycle where it is oxidized to CO<sub>2</sub>, was not disturbed at least by some of the tested drugs. However, additional tracer experiments using <sup>13</sup>C-labelled glucose might reveal actual alterations of glucose entering TCA-cycle upon treatment with the respective drug with higher accuracy. The actual decrease in glucose uptake observed in this study could be to some extent explained by reduced energy demand. Since HL-1 cells are spontaneously beating in culture, exposure to drugs which act on ion channels disturb excitation-contraction coupling in these cells, leading to decreased contraction and thereby reduced energy demand.

The changes in the metabolite concentrations were analyzed using PCA. PC1 and PC2 accounted for 60 % of the total variance observed in the data set. As depicted, several observations on supernatants from cells treated with drugs are plotted outside the 95% confidence ellipses of both untreated controls and DMSO treated cells (Fig. 3). There is a clear separation of treated cells from the untreated controls. An approximate clustering of individual drug classes, as indicated by different colours, could be observed in the corresponding PCA-scores plot (Fig. 3). Based on these results, the relevancy of each metabolite in the separation/formation was assessed by determination of the loading coefficients. Loading coefficients of the first two principal components (Fig. 4 A and B) revealed that separation of observations along the first two axis distinguishes between metabolites connected to glycolytic and TCA-cycle pathways. Separation of observations along principal component 1 was mainly attributed to metabolites which undergo degradation in TCA-cycle reactions, such as phenylalanine, branched chain amino acids (leucine, isoleucine, valine), tyrosine, glutamine and glutamic acid etc. On the other hand, separation along principal component 2 was mainly due to metabolites connected to the glycolytic pathway (glucose, lactate, alanine, glycine & serine).

Clustering could be improved by a supervised approach i.e. by assigning each drug to a specific drug group followed by discriminant analysis. Untreated controls and DMSO-controls were also treated as individual groups. Score plot of axis 1 and 2 (75% of the variance in the data) shows that some clusters could be obtained which refer to distinct drug classes (Fig. 5). Four clusters could be obtained by this supervised approach which included anthracyclines (daunorubicin & doxorubicin), antihistamines (astemizol & terfenadine) and analgesics (acetaminophen & diclofenac). The fourth cluster contained channel blockers, untreated controls, DMSO-controls and antimetabolites.

Average prediction quality was determined by applying cross model validation of both non-permuted and permuted group assignments, as described recently (Westerhuis *et al.*, 2008). Indeed the prediction of classes in this study worked quite well, which is reflected by high sensitivities of the calculated prediction models in the non-permuted prediction models. As predictions based on permuted class assignment should not be able to classify very well (Westerhuis *et al.*, 2008) (based on the assumption that no differences between the classes exist) an average of 14.3 % correctly predicted conditions was expected for each class, considering that the whole data set was split into seven distinct classes. Indeed, average accuracy observed in this

approach was 7%-38% for the majority of the classes. It can therefore be concluded that prediction accuracy is clearly not random but due to specific and unique metabolic profiles.

HPLC quantification of such metabolites was recently applied to study drug induced changes in extracellular fluxes (Niklas *et al.*, 2009) at subtoxic concentrations in a hepatic cell line. It was found that drug induced changes in metabolite uptake and production is linked to altered fluxes in central energy metabolism. The observed changes in metabolite uptake and production may therefore also be linked to changes in substrate usage i.e. to central metabolism and in turn probably effects fluxes through certain catabolic pathways for example in TCA-cycle reactions.

Despite the fact that we measured many different metabolites, measuring the relative uptake of fatty acids, a rich provider of ATP in cardiac cells, might increase the predictive power since it might give supportive insights in the extent of drug induced changes in energy metabolism. The approach used in the presented study allowed classification of drugs according to their modes of action. This can be very useful in the assessment of not only a new drug candidate's potential pharmacological properties according to group labels but also to assess its toxicity potential depending on the cell system used.

However, since HL-1 cells represent an immortalised atrial murine cell line, with some cardiac phenotype, its relevance in predicting potential cardiotoxic side effects in humans is limited. By using cell types which more closely reflect human tissue i.e. human embryonic stem cell derived cardiomyocytes, improvement in human specific and relevant prediction is expected. Moreover, using a similar profiling approach, even the risk of unknown compounds/new pharmaceuticals for cardiac side effects might be reliably assessed when applying pattern recognition techniques on the basis of clinically observed side effects, such as QT-prolongation or cardiac arrest.

## Chapter 4

### Metabolic flux analysis gives an insight on verapamil induced changes in central metabolism of HL-1 cells

#### Abstract

Verapamil has been shown to inhibit glucose transport in several cell types. However, the consequences of this inhibition on central metabolism are not well known. In this study we focused on verapamil induced changes in metabolic fluxes in a murine atrial cell line (HL-1 cells). These cells were adapted to serum free conditions and incubated with 4  $\mu$ M verapamil and [U- $^{13}$ C $_5$ ] glutamine. Specific extracellular metabolite uptake/production rates together with mass isotopomer fractions in alanine and glutamate were implemented into a metabolic network model to calculate metabolic flux distributions in the central metabolism. Verapamil decreased specific glucose consumption rate and glycolytic activity by 60%. Although the HL-1 cells show Warburg effect with high lactate production, verapamil treated cells completely stopped lactate production after 24 hours while maintaining growth comparable to the untreated cells. Calculated fluxes in TCA cycle reactions as well as NADH/FADH $_2$  production rates were similar in both treated and untreated cells. This was confirmed by measurement of cell respiration. Reduction of lactate production seems to be the consequence of decreased glucose uptake due to verapamil. In case of tumors, this may have two fold effects; firstly depriving cancer cells of substrate for anaerobic glycolysis on which their growth is dependent; secondly changing pH of the tumor environment, as lactate secretion keeps the pH acidic and facilitates tumor growth. The results shown in this study may partly explain recent observations in which verapamil has been proposed to be a potential anticancer agent. Moreover, in biotechnological production using cell lines, verapamil may be used to reduce glucose uptake and lactate secretion thereby increasing protein production without introduction of genetic modifications and application of more complicated fed-batch processes.

This chapter has been published as: Strigun A, Noor F, Pironti A, Niklas J, Yang TH, Heinze E (2011). Metabolic flux analysis gives an insight on verapamil induced changes in central metabolism of HL-1 cells. *Journal of Biotechnology* 155: 299-307.

### Introduction

Verapamil belongs to the class of calcium channel blockers (CCBs) and is clinically used for the treatment of hypertension (Kaplan, 1989) and angina pectoris (Broden and Benfield, 1996). In addition to calcium channel antagonism, verapamil has been reported to exert other physiological effects such as inhibition of glucose uptake in several cell types (skeletal muscle cells (Cartee, 1992), neuronal cells (Ardizzone *et al.*, 2002) and adipocytes (Bechtel *et al.*, 2008)) via several mechanisms. Many of the glucose uptake studies in diverse cell lines point towards a direct effect of verapamil on glucose transporters (Ardizzone *et al.*, 2002; Cartee *et al.*, 1992; Louters *et al.*, 2010). Verapamil's ability to inhibit glucose uptake makes it attractive in applications other than its intended use as calcium channel antagonist. For example, inhibition of glucose uptake is one of the potential targets in cancer therapy (Gatenby and Gillies, 2007). While none of the studies considering verapamil ability to inhibit glucose uptake were carried out in the context of cancer therapy, there is growing evidence that verapamil has an anticancer effect itself (Zhang *et al.*, 2009) as well as a synergistic effect on other anticancer agents (Tsuruo *et al.*, 1981; Zhang *et al.*, 2007). It was shown that verapamil reversibly inhibits cell proliferation of many tumor cell lines independent of calcium channel block (Schmidt *et al.*, 1988).

In addition, inhibition of glucose uptake may be exploited in biotechnological applications. In biotechnological production of biopharmaceuticals cell lines are used due to their ability to carry out posttranslational modifications. These cell lines are usually immortalized and show high glycolytic activity producing much lactate as by-product. Various approaches (such as genetic modifications or fed batch cultivations) are used to reduce substrate (glucose) uptake and by-product production to improve protein production. On smaller scales, a simple method to do this is desirable. Using a compound which inhibits glucose uptake such as verapamil in low non-toxic concentrations improving the efficiency of growth and thereby production could be very useful.

It is therefore of great importance to study physiological effects of glucose uptake inhibitors on metabolism especially with regard to substrate needs of cancer cells and cell lines. Taking verapamil as reference compound, in this study we used HL-1 cells to study its effects on central metabolism. HL-1 cells have been extensively characterized (Claycomb *et al.*, 1998; Eimre *et al.*, 2008; Monge *et al.*, 2009; Sartiani *et al.*, 2002; White *et al.*, 2004; Xia *et al.*, 2004) and were used in pharmacological (Deng *et al.*, 2009; Fox *et al.*, 2005) as well as toxicological studies (Andersson *et al.*, 2010; Fritzsche *et al.*, 2009). Glucose uptake studies on HL-1 cells in the presence of pharmacological compounds were carried out recently and it was found that HL-1

cells have relevant glucose transport isoforms (GLUT1 and GLUT4) (Shuralyova *et al.*, 2004), which also play a significant role in many cancer types. Moreover, the fact that HL-1 cells show high glycolytic activity (Monge *et al.*, 2009), a characteristic of many cancer cells and commercially available cell lines, makes them attractive for glucose uptake studies.

Metabolic flux analysis has been used for the analysis of mammalian metabolism mainly in the areas of cell culture technology as reviewed recently (Niklas *et al.*, 2010). Other applications include the physiological characterization of animal cell lines, such as hybridomas (Bonarius *et al.*, 2001), CHO-cells (Goudar *et al.*, 2010), human production cell lines (Henry *et al.*, 2010, Niklas *et al.*, 2011), hepatocytes (Maier *et al.*, 2009), kidney cells (Sidorenko *et al.*, 2008), the analysis of effects of drugs (Niklas *et al.*, 2009) and the physiological characterization of the whole murine myocardium (Vo and Palsson, 2006). In the present study we investigated the effect of verapamil on the glucose uptake and applied  $^{13}\text{C}$  metabolic flux analysis on HL-1 cells upon treatment with verapamil to estimate the influence of decreased glucose uptake induced by verapamil on intracellular fluxes in central metabolic pathways namely glycolysis and TCA cycle. The results of this study are discussed in the context of verapamil's potential application in the field of cancer therapy and biotechnology.

### Material and Methods

#### *Cell Culture*

HL-1 cells were kindly provided by Dr. Claycomb (Louisiana State University) for research within the framework of EU STREP-project "Invitroheart". The cells were maintained in Claycomb medium (Sigma Chemical, USA) supplemented with 2 mM glutamine (PAA Laboratories, Austria), 100 U/ml penicillin, 100 µg/ml streptomycin (PenStrep stock solution, C. C. Pro GmbH, Oberdorla, Germany), 100 µM norepinephrine (Sigma Chemical, USA) in 30 mM L-ascorbic acid (Sigma Chemical, USA) and 10% fetal bovine serum (FBS) (JRH Biosciences, UK). Cells were sub-cultured at confluency in a split ratio of 1:3. Culture flasks (75 cm<sup>2</sup>, Falcon, Germany) were pre-coated with a solution of 0.02% (w/v) gelatin (AppliChem, Germany) containing 5 µg/ml fibronectin (Sigma Chemical, USA). Beating cells were maintained at standard cell culture conditions (37°C, 5% CO<sub>2</sub> and 95% relative humidity) in a cell culture incubator (Memmert GmbH, Schwabach, Germany).



## Effect of verapamil on metabolic fluxes in HL-1 cells

---

### *Adaptation of HL-1 cells to serum free medium*

For metabolic flux analysis serum free culture conditions are desired, therefore, a modified composition of previously reported serum free medium for hESC cardiomyocytes (Xu *et al.*, 2006) was used. Carnitine, creatine and taurine were purchased from Sigma Aldrich. Stock solutions of taurine (100 mM), carnitine (100 mM), creatine (50 mM) were prepared in cell culture grade water (Invitrogen, Paisley, UK). Each solution was sterile filtered with a 0.2  $\mu\text{m}$  filter (Millipore, Billerica, USA). 2 mM taurine, 2 mM carnitine, 1 mM creatine, 0.1 mM norepinephrine, PenStrep and 2 mM glutamine were added to the basal Claycomb media (referred as CCT-medium henceforth). The HL-1 cells were gradually adapted to CCT-medium in four weeks. The standard supplemented Claycomb medium was step by step replaced with CCT-medium during the time of adaptation. The cells were passaged three times during this period.

### *Dose response curve for verapamil using cell proliferation assay*

HL-1 cells adapted to serum free conditions were trypsinized at confluency and counted using trypan blue exclusion method in a hemocytometer.  $3.0 \times 10^4$  cells/well were seeded in 96-well plates in a total volume of 200  $\mu\text{l}$  of CCT medium. After 24 hours (h) equilibration, the medium was removed. Fresh medium containing verapamil in five different concentrations (0.21  $\mu\text{M}$ , 1.04  $\mu\text{M}$ , 5.2  $\mu\text{M}$ , 26.2  $\mu\text{M}$ , 131  $\mu\text{M}$ ) in triplicates was added. Cells were incubated with verapamil at 37°C for 96 h in the incubator. A concentration response curve was plotted using the Sulforhodamine B assay according to a previously described method (Skehan *et al.*, 1990).

### *Experimental setup for studies on verapamil induced changes in metabolite uptake and production rates*

$1.5 \times 10^5$  HL-1 cells adapted to serum free medium were seeded per well in 24-well plates which were already coated with a gelatin/fibronectin solution for 24 h (five plates in total were seeded). The total medium volume per well was 500  $\mu\text{l}$ . After 24 h equilibration the medium was removed and the cells were carefully washed twice with 500  $\mu\text{l}$  of pre-warmed (37 °C) Claycomb medium without supplements. Afterwards, 500  $\mu\text{l}$  fresh medium with and without 4  $\mu\text{M}$  verapamil was added to the cells in triplicates, respectively. This medium contained 2 mM [U- $^{13}\text{C}_5$ ] glutamine (99 %) (Cambridge Isotope Laboratories, USA). Cell free medium served as blank. Plates were incubated under standard cell culture conditions (37 °C, 95 % relative humidity, 5 %  $\text{CO}_2$ ) in the

## Effect of verapamil on metabolic fluxes in HL-1 cells

---

incubator. Every 24 hours, one plate was taken out of the incubator, the supernatant was collected and the cells were fixed for protein quantification using sulforhodamine B (SRB) assay as explained above. Cell number was estimated using the standard population curve obtained with different cell numbers of HL-1 cells (data not shown).

### *Sample preparation for HPLC measurements*

Each of the collected supernatants was individually diluted (1:2) with  $\alpha$ -amino-butyric acid solution (400  $\mu$ M in deionized water) which was used as internal standard.

### *Quantification of glucose, lactate and pyruvate*

Quantification was carried out using HPLC (Kontron Instruments, Germany) with an Aminex HPX 87H ion exchange column (300x7.8mm, Biorad, USA). The isocratic separation was carried out using 7 mM sulfuric acid as eluent and a flow rate of 0.8 ml/min at a column temperature of 60°C. Injection volume was 20  $\mu$ l. Lactate and pyruvate were detected by UV-detection (UV-detector: HPLC 535, Biotek, Germany) at a wavelength of 210 nm. Glucose was determined by measuring the refractive index (ERC-7515A, ERC Inc., Germany). Standard solutions of glucose, lactate and pyruvate (Sigma Chemical, USA) were used for identification and quantification.

### *Quantification of amino acids*

Amino acids were quantified as described earlier (Hans *et al.*, 2003; Kromer *et al.*, 2005). Briefly, quantification was carried out using HPLC (Agilent 1100 series, Agilent technologies, Germany) with a C18 RP-column (Gemini® 5u C18 110A, 150 x 4.6 mm, Phenomenex, Germany) at 40 °C. A gradient separation was carried out (Eluent 1: 40 mM Na<sub>2</sub>HPO<sub>4</sub>, pH 7.8; Eluent 2: methanol, acetonitrile, water 45:45:10 (v/v)) with a flow rate of 1 ml/min. Primary amino acids were derivatized by pre-column derivatization using *ortho*-phthalaldehyde (OPA) (Agilent, Germany) (excitation wavelength: 330 nm; emission wavelength: 450 nm). Proline, a secondary amino acid, was derivatized using 9-fluorenylmethylchloroformate (FMOC) (Agilent, Germany) (excitation wavelength: 266 nm, emission wavelength: 305 nm).

Since glutamine is not stable at standard cell culture conditions (37°C) for longer time periods, its degradation was taken into account. Glutamine degradation was found to be a first order process having a rate constant ( $k_G$ ) of 0.0148  $\mu$ M h<sup>-1</sup> in the applied medium. The measured glutamine data was corrected for degradation using the following equation:

$$\frac{d[\text{Gln}]}{dt} = -(k_G \times [\text{Gln}] + r_{\text{Gln}}) \quad (1)$$

Where  $r_{\text{Gln}}$  is the actual glutamine uptake rate.

### *Sample preparation for mass isotopomer measurement*

100  $\mu\text{l}$  of collected supernatants were frozen in individual glass vials at  $-70^\circ\text{C}$  and lyophilized overnight. 50  $\mu\text{l}$  of dimethylformamide (Sigma Aldrich, Germany) containing 0.1% pyridine (Sigma Aldrich, Germany) (v/v) was added to the dried supernatants. For derivatization 50  $\mu\text{l}$  of *N*-methyl-*N*-*tert*-butyldimethylsilyl-trifluoroacetamide (MBDSTFA, Macherey-Nagel, Germany) were added and each sample was incubated for 1 h at  $80^\circ\text{C}$ . The derivatized samples were centrifuged at 6000 rpm and the supernatant (60  $\mu\text{l}$ ) was transferred into glass vials with micro-inlays for GC/MS analysis.

### *Mass isotopomer measurement using GC/MS*

Measurement of mass isotopomers was carried out using gas chromatography (HP 6890 Hewlett Packard, USA) equipped with a HP-5 MS column (5 % phenyl-methyl-siloxane-diphenylpolysiloxane, 30 m x 0.25 mm x 0.25  $\mu\text{m}$ , Agilent, Germany) and coupled with a quadrupole mass spectrometer (MS 5973, Agilent, Germany). The injection volume was 1  $\mu\text{l}$ . The separation was carried out with a flow rate of 1.1 ml/min (carrier gas: helium). The temperature gradient was as follows:  $135^\circ\text{C}$  for 7 minutes, temperature increase  $10^\circ\text{C}/\text{min}$  until  $160^\circ\text{C}$ ,  $7^\circ\text{C}/\text{min}$  until  $170^\circ\text{C}$ ,  $10^\circ\text{C}/\text{min}$  until  $325^\circ\text{C}$  which is held for 2.5 minutes. Ionization was carried out by electron impact at 70 eV.

Metabolites such as alanine and glutamate were silylated using MBDSTFA as previously described (Yang *et al.*, 2009). From the mass spectra of MBDSTFA derivatives, carbon mass isotopomer distributions were computed using the method described earlier (Yang *et al.*, 2009). The metabolic fluxes were computed from carbon mass isotopomer distributions obtained from the mass spectrometric labeling analysis of fragment ions of alanine and glutamate-derivatives, for which monoisotopic peaks were detected at  $m/z$  261 and 432, respectively. Mean mass isotopomer distributions for the phase considered for metabolic flux analysis were calculated according to the following equation:

$$(m+i)_{\text{corr}} = \frac{[m+i]}{\sum_{j=0}^n [m+j]} \quad n = n_c + 1, i = 0 \dots n \quad (2)$$

$(m+i)_{\text{corr}}$  represents the corrected mass isotopomer fraction (%) which was used for calculation of fluxes.  $[m+i]$  gives the concentration of each measured mass isotopomer,  $n_c$  is the numbers of carbon atoms in the metabolite.

### *Calculation of growth rate and specific uptake/production rates of metabolites*

Growth rate of HL-1 cells in serum free medium was calculated by using the following equation and plotting  $\ln(N)$  against time (t);

$$\ln(N) = \mu t + \ln(N_0)$$

$\mu$  represents the growth rate [ $\text{h}^{-1}$ ].  $N$  is the cell number at a defined time point and  $N_0$  is the initial cell number at  $t=0$ .

Yield coefficients ( $Y_i$ ) for each metabolite were calculated by the equation given below:

$$Y_i = \frac{dM_i}{dN} \quad (4)$$

where  $N$  represents the cell number and  $M_i$  concentration of metabolite  $i$ .

Specific consumption and production rates for measured metabolites ( $v$ ) were calculated from the growth rate  $\mu$  and the respective yield coefficients  $Y_i$  using the equation below:

$$v_{m,i} = Y_i \times \mu \quad (5)$$

### *<sup>13</sup>C flux analysis*

A carbon atom transition network model of the central metabolism was set up (Appendix for chapter 4, Tab. S1) and applied for <sup>13</sup>C metabolic flux analysis. Substrate metabolites which were only taken up for anabolic demand were excluded from the model since their carbon atoms were not entering central metabolic pathways. The model consisted of 41 reactions. 16 reactions were measured from extracellular uptake and production fluxes, while 25 reactions were intracellular rates of which 11 were defined as reversible. Anabolic fluxes were estimated from the growth rate and biomass composition which was taken from (Niklas *et al.*, 2009). Flux estimation was carried out using MATLAB 2008b (The Mathworks) using the elementary metabolite unit concept (Antoniewicz *et al.*, 2007) with a recently described method (Yang *et al.*, 2008).

In the applied stationary metabolic flux analysis approach, metabolic and isotopic steady state conditions are a prerequisite. To determine whether the pseudo steady state assumption is justified, metabolite and isotopomer concentrations at different time points of the cultivations were plotted against the corresponding number of cells, as described recently (Deshpande *et al.*, 2009).

### *Respiration measurement*

HL-1 cells were seeded with a density of  $3 \times 10^5$  cells/well in 24-well OxoDishes (PreSens, Germany). Cell free medium served control. After 24 h equilibration, fresh medium with and without 4  $\mu$ M verapamil was added to the cells in triplicates. Dissolved oxygen was continuously measured for 48 h as recently described (Beckers *et al.*, 2009). Afterwards cell number in each well was quantified by using SRB assay.

Specific oxygen consumption rate ( $qO_2$ ) was estimated using the liquid phase balance equation as follows:

$$\frac{d[O_2]}{dt} = k_L a \cdot ([O_2^{sat}] - [O_2]) - \frac{qO_2 \cdot X}{V} \quad (6)$$

$[O_2^{sat}]$  is the dissolved oxygen concentration at saturation in culture medium taken (6.23 mg/L; from (Oeggerli *et al.*, 1995) while  $[O_2]$  represents the actual dissolved oxygen concentration,  $X$  the number of cells per well and  $V$  the liquid volume per well. Equation (6) was integrated using MATLAB and statistical errors were estimated using Monte Carlo simulation (Further details are provided in the Appendix for chapter 4, Text S1, Figure S1 and S2).

### *Statistical analysis*

Extra- and intracellular fluxes in cells treated with 4  $\mu$ M verapamil were compared with the respective untreated controls using student's *t*-test. The changes were considered significant at  $p < 0.05$ .

## **Results**

### *Maintenance of HL-1 cells in serum free medium*

The HL-1 cells were successfully adapted to serum free Claycomb media. The cells were beating for more than six month after the complete removal of FBS.

## Effect of verapamil on metabolic fluxes in HL-1 cells

### *Cytotoxicity of verapamil*

Figure 1 shows the concentration response curve of verapamil obtained using sulforhodamine B assay for proliferation. The concentration range in which the relative cell number ranged from 100 to 20% of the control was between 5  $\mu\text{M}$  and 130  $\mu\text{M}$ . Based on the concentration response curve, a verapamil concentration of 4  $\mu\text{M}$  was chosen (95 % relative proliferation after 96 h of treatment) for further studies on specific uptake/production rates for glucose, lactate, pyruvate and amino acids.

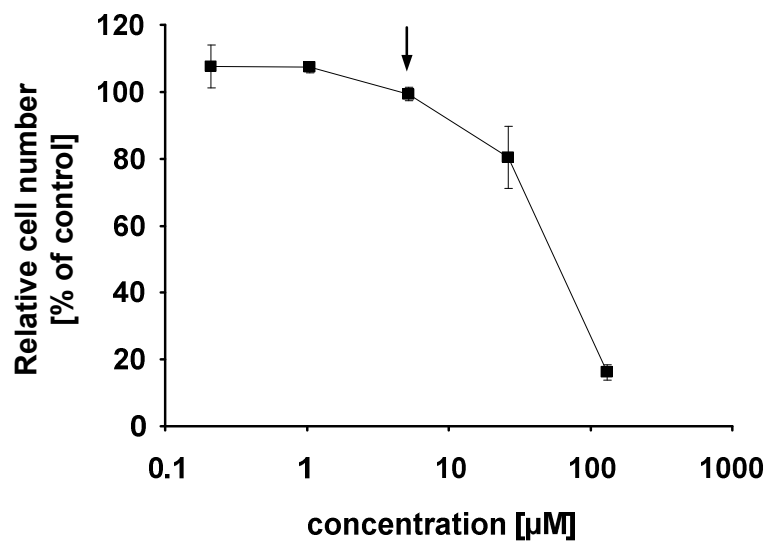


**Figure 1:** Effect of verapamil on proliferation of HL-1 cells adapted to serum free (CCT)-medium. Cells were seeded in 96-well plates and after 24 h equilibration; fresh medium with different concentrations of verapamil was added to the cells. Cells were fixed 96 h after exposure to verapamil and relative cell number was determined by sulforhodamine B staining. Standard deviations were determined from triplicate measurements. The arrow indicates the concentration (4  $\mu\text{M}$ ) which was used for subsequent flux analysis studies.

## Effect of verapamil on metabolic fluxes in HL-1 cells

---

### *Proliferation and metabolite profiles in HL-1 cells upon verapamil treatment*

Figure 2A shows the growth profiles of HL-1 cells in serum free medium with and without 4  $\mu\text{M}$  verapamil. Cell number increased from  $1.5 \times 10^5$  cells/well to  $8.0 \times 10^5$  (untreated control) and  $7.4 \times 10^5$  cells/well (verapamil) after 96h of incubation at standard incubation conditions. Although there was no significant change in the proliferation of HL-1 cells, exposure to verapamil (4 $\mu\text{M}$ ) resulted in complete arrest of microscopically observed beating.

The concentration of glucose in the medium decreased from 22.5 mM to 12.7 mM in case of untreated control in 96 h (Fig. 2B) showing high consumption of glucose. Whereas, in the presence of verapamil, glucose consumption by the cells was much lower. The concentration of glucose in the medium of treated cells was 17 mM after 96 h incubation (Fig 2B). As glucose was consumed from the medium, the concentration of lactate continuously increased to 10 mM in untreated control cells after 96 h. In the presence of verapamil an initial production of lactate (2.5 mM) was observed within the first 24 h of incubation. After 96 h of incubation lactate concentration slightly decreased to 2.2 mM. Therefore, lactate was slightly consumed at 96 h of treatment with verapamil. Pyruvate concentration continuously decreased from 60  $\mu\text{M}$  to 2  $\mu\text{M}$  (untreated control) and 3  $\mu\text{M}$  (verapamil treated cells) within the initial 48 h of incubation. Afterwards pyruvate concentration increased to 66  $\mu\text{M}$  (untreated control) and 11  $\mu\text{M}$  (verapamil) until 96 h of incubation (Fig. 2C). Alanine concentration continuously increased from 320  $\mu\text{M}$  (the initial concentration in the medium) to 922  $\mu\text{M}$  in untreated control and to 912  $\mu\text{M}$  in verapamil treated HL-1 cells (Fig 2D). No significant difference in glutamine consumption between untreated and treated HL-1 cells was observed (Fig. 2D). Glutamine concentration decreased from initially 2 mM to 1  $\mu\text{M}$  (control) and 12  $\mu\text{M}$  (treated cells). The profiles of all metabolites versus time are shown in the Appendix for chapter 4 (Figure S3).

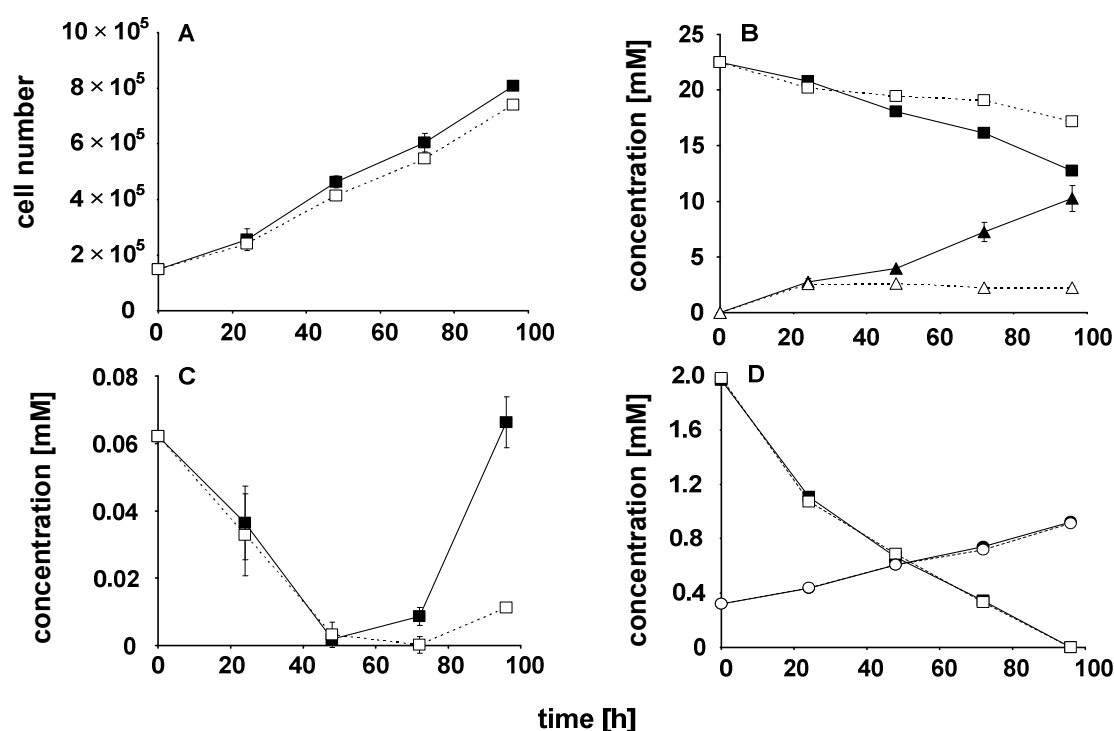


**Figure 2:** A) Growth of untreated control (closed symbols) and treated (4  $\mu\text{M}$  verapamil) HL-1 cells (open symbols). B) Concentration of glucose (squares) and lactate (triangles) in culture medium with (open symbols) and without (closed symbols) verapamil. C) Changes of concentration of pyruvate in untreated controls (closed symbols) and in cells treated with 4  $\mu\text{M}$  verapamil (open symbols) D) Changes of concentration of glutamine (squares) and alanine (circles) in culture medium with (open symbols) and without (closed symbols) verapamil. Standard deviations were calculated from triplicates measurements.

### *Influence of verapamil on uptake and production rates of metabolites*

Accumulation/depletion of metabolites versus cell number (Appendix for chapter 4, Fig. S4) showed a linear relationship, as apparent from correlation coefficients which were  $> 0.9$  for most of the considered metabolites (Appendix for chapter 4, Tab. S2). Based on the yields, average specific rates of metabolite uptake and production were calculated as shown in table 1. Glucose uptake rate was around 135 % higher in control cells as compared to the treated cells (Tab.1). Specific lactate production rate was  $213 \text{ fmol cell}^{-1} \text{ h}^{-1}$  in untreated HL-1 cells, whereas after initial production of lactate in the first 24 h, a slight uptake of lactate ( $11 \text{ fmol cell}^{-1} \text{ h}^{-1}$ ) was observed in HL-1 cells treated with verapamil. Lactate yield on glucose was  $1.0 \text{ mol}_{\text{lactate}}/\text{mol}_{\text{glucose}}$  in untreated control and  $-0.12 \text{ mol}_{\text{lactate}}/\text{mol}_{\text{glucose}}$  in treated HL-1 cells. Pyruvate was produced by untreated HL-1 cells ( $0.8 \text{ fmol cell}^{-1} \text{ h}^{-1}$ ) but was significantly consumed by treated cells ( $0.54 \text{ fmol cell}^{-1} \text{ h}^{-1}$ ,  $p < 0.01$ ). Glutamine, alanine and branched chain



## Effect of verapamil on metabolic fluxes in HL-1 cells

---

amino acids (isoleucine, leucine and valine) showed the highest uptake rates among all amino acids. With the exception of glycine, no significant differences of specific rates in controls and treated HL-1 cells were observed. Glycine production rate was  $0.7 \text{ fmol cell}^{-1} \text{ h}^{-1}$  in untreated and  $0.04 \text{ fmol cell}^{-1} \text{ h}^{-1}$  in treated HL-1 cells ( $p < 0.01$ ).

**Table 1:** Specific uptake and production rates of metabolites in untreated control and treated HL-1 cells ( $4 \mu\text{M}$  verapamil). Specific rates were calculated from specific growth rate and biomass yield. The biomass yield was constant for most of considered metabolites within 24 and 96 h of incubation (see Appendix for Chapter 4, Fig. S4 for biomass yield plots and Tab. S2 for correlation coefficients). Average rates were calculated from 24-96 h of incubation (see methods). Standard deviations (s.d.) were calculated from triplicate measurement. Rates were considered significantly different when  $p < 0.05$ , as calculated from two-tailed  $t$ -test. n.s.: not significant

Metabolite	Specific rate [ $\text{fmol cell}^{-1} \text{ h}^{-1}$ ]				
	control	$\pm$ s.d.	$4 \mu\text{M}$ verapamil	$\pm$ s. d.	$p$
GLC	-221.2	34.9	-94.3	15.8	< 0.01
LAC	213.5	48.0	-11.2	8.3	< 0.01
PYR	0.8	0.3	-0.5	0.3	< 0.01
ALA	13.8	2.0	14.3	0.7	n.s.
ARG	-2.5	0.4	-2.9	0.2	n.s.
ASN	-1.6	0.4	-1.8	0.2	n.s.
ASP	-0.5	0.7	-0.2	0.2	n.s.
GLU	2.7	1.0	2.9	0.3	n.s.
GLN	-31.3	4.6	-33.1	1.9	n.s.
GLY	0.7	0.3	0.04	0.2	< 0.01
HIS	-1.0	0.2	-1.2	0.4	n.s.
ILE	-8.6	1.5	-9.0	0.6	n.s.
LEU	-5.9	1.1	-6.4	1.0	n.s.
LYS	-3.6	1.0	-5.0	0.6	n.s.
MET	-2.0	0.3	-2.1	0.4	n.s.
PHE	-1.7	0.3	-2.0	0.4	n.s.
PRO	-7.6	6.5	-2.0	4.5	n.s.
SER	3.4	0.6	2.9	0.2	n.s.
THR	-2.6	1.0	-2.9	0.6	n.s.
TYR	-2.1	0.3	-2.1	0.7	n.s.
VAL	-5.6	1.4	-5.6	0.7	n.s.

### *Influence of verapamil on intracellular fluxes*

A time dependent increase of  $^{13}\text{C}$  mass isotopomer fractions in alanine and glutamate derived from  $[\text{U-}^{13}\text{C}_5]$  glutamine was observed in both treated and untreated HL-1 cells (Appendix for Chapter 4, Tab. S3 and S4). Figures 3 and 4 show the alanine and glutamate mass isotopomer concentrations plotted against the respective cell numbers at each time point of the cultivation. The slope of each plot represents the yield of the respective mass isotopomers. A linear relationship of alanine and glutamate mass isotopomer concentrations versus cell number is given in both untreated and verapamil treated cells ( $4\ \mu\text{M}$ ) as apparent from correlation coefficients  $> 0.9$  (Appendix for Chapter 4, Tab. S5 and S6).

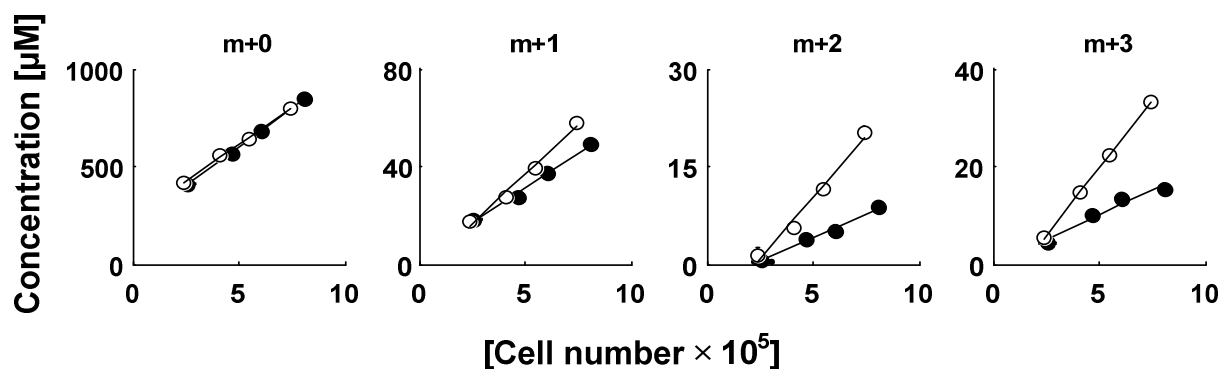


**Figure 3:** Concentrations of alanine  $^{13}\text{C}$ -mass isotopomers (unlabelled alanine (m+0), single labelled alanine (m+1), double labelled alanine (m+2) and fully labelled alanine (m+3)) versus cell number of untreated controls (closed symbols) and in cells treated with  $4\ \mu\text{M}$  verapamil (open symbols). Mass isotopomer concentrations were calculated by multiplication of alanine concentrations with corresponding mass distributions. The slope of each plot represents the yield coefficient ( $Y_i$ ) which was used for the calculation of the steady state mass distribution that was used as input data for estimation of intracellular fluxes in HL-1 cells. Enrichment of  $^{13}\text{C}$  in alanine was derived from  $[\text{U-}^{13}\text{C}_5]$  glutamine. The correlation coefficients for each mass isotopomer yield are shown in Tab. S5 (Appendix for Chapter 4). Error bars represent standard deviations determined from triplicate measurements.

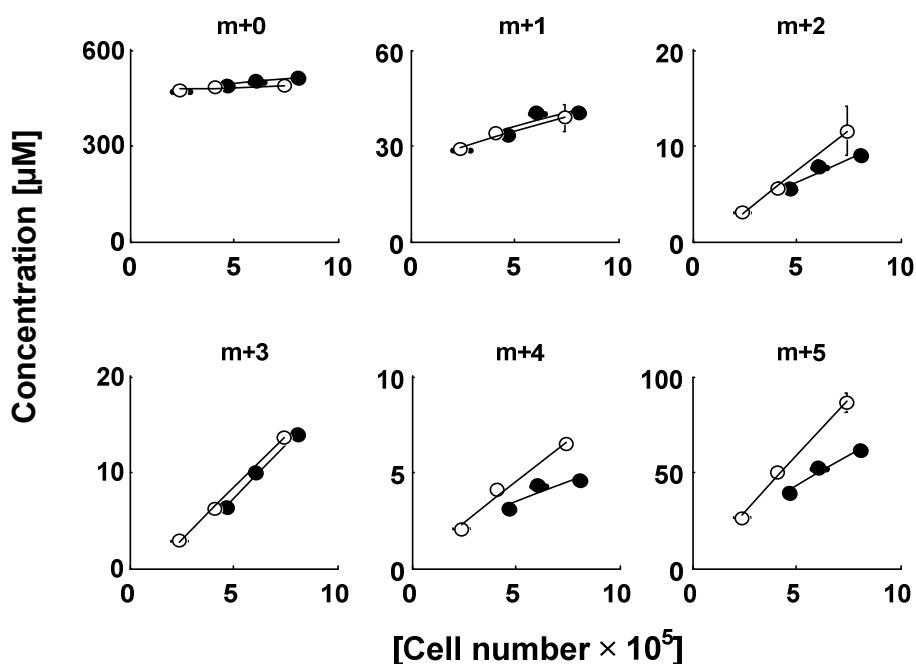


**Figure 4:** Concentrations of glutamate <sup>13</sup>C-mass isotopomers (unlabelled glutamate (m+0), single labelled glutamate (m+1), double labelled glutamate (m+2) and triple labelled glutamate (m+3), four fold labelled glutamate (m+4) and fully labelled glutamate (m+5)) versus cell number of untreated controls (closed symbols) and in HL-1 cells treated with 4 μM verapamil (open symbols). The slope of each plot represents the yield coefficient (Y<sub>i</sub>) which was used for calculation of the steady state mass distribution that was used as input data for estimation of intracellular fluxes in HL-1 cells. Enrichment of <sup>13</sup>C in glutamate was derived from [U-<sup>13</sup>C<sub>5</sub>] glutamine. The correlation coefficients for each mass isotopomer yield are shown in Tab. S6 (Appendix for Chapter 4). Error bars represent standard deviations determined from triplicate measurements.

Intracellular fluxes were estimated by using extracellular fluxes and labeling patterns of alanine and glutamate in a metabolic network model (Appendix for Chapter 4, Tab. S1). The fit between measured data and simulated data gives an estimate of the accuracy of the flux calculation. Figure S5 (Appendix for Chapter 4) shows the regression plots of simulated versus measured mass isotopomer distributions and extracellular fluxes from both untreated and treated cells. A good match of simulated and measured extracellular fluxes was found as most of the flux and mass distribution ranges were located on the angle bisector of the plot. The distribution of calculated intracellular steady state fluxes (containing reactions from glycolysis, TCA-cycle, amino acid metabolism and anaplerosis) is graphically depicted in Figure 5. The line widths are normalized to glucose uptake in untreated cells. The underlying flux values are given in Table S7 (Appendix for chapter 4). Flux rates through reactions of glycolysis (G6P→F6P, F6P→GAP, GAP→3PG and 3PG→PYR) were significantly decreased by about 60 % (P<0.01). Oxidative

## Effect of verapamil on metabolic fluxes in HL-1 cells

decarboxylation of pyruvate to acetyl-CoA was decreased by 17 % and TCA-cycle fluxes by 17-20 % in cells treated with verapamil. These changes, however, were not statistically significant (95 % confidence). Alterations of fluxes through reactions in amino acid metabolism were not significant for the majority of reactions. However, intracellular deamination of glutamine to glutamate was significantly increased by 27 % ( $p < 0.05$ ). Though not significant, the flux of glutamate to  $\alpha$ -ketoglutarate (AKG) was increased by 22 %.

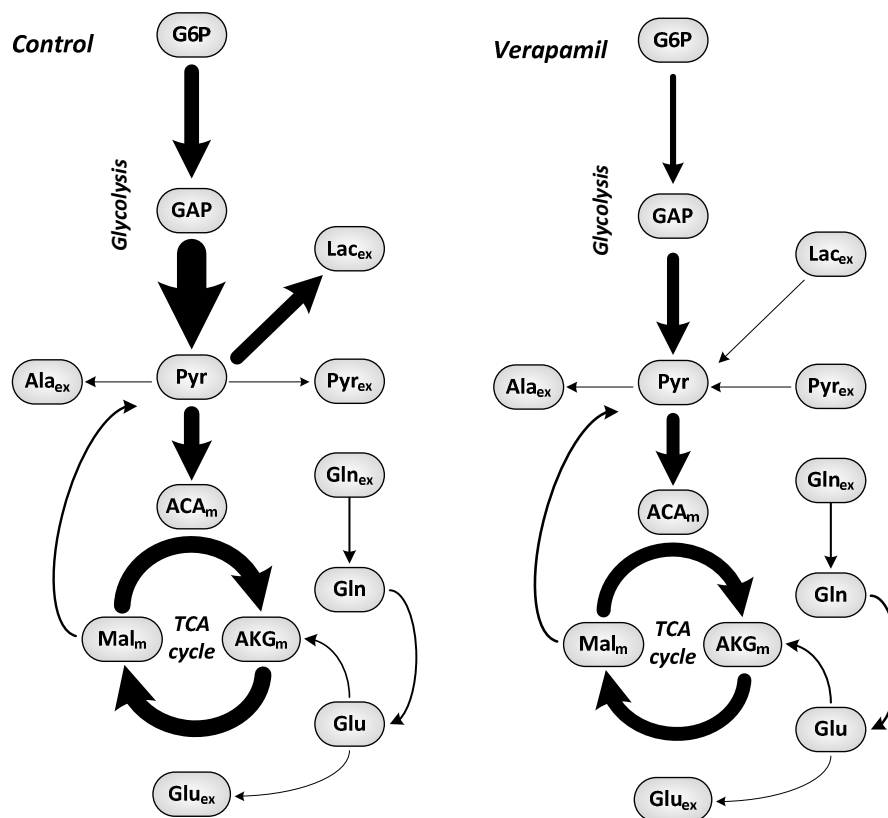


**Figure 5:** Impact of channel blocker verapamil (4  $\mu$ M) on reactions from glycolysis, TCA cycle and glutamine catabolism. Intracellular fluxes in HL-1 cells were calculated from extracellular rates and  $^{13}\text{C}$  mass isotopomer distribution in alanine and glutamate. The relative change of intracellular fluxes through individual reactions was normalised to glucose uptake rate in untreated control.

### *Influence of verapamil on respiration*

Respiration of HL-1 cells, i.e. the consumption of  $\text{O}_2$  was calculated from metabolic flux analysis, i.e. the surplus NADH/FADH<sub>2</sub> formation rate. The calculated specific oxygen uptake

## Effect of verapamil on metabolic fluxes in HL-1 cells

rate was decreased by 16 % in treated cells (untreated cells:  $750 \text{ fmol cell}^{-1} \text{ h}^{-1}$ , treated cells:  $630 \text{ fmol cell}^{-1} \text{ h}^{-1}$ , Appendix for chapter 4, Tab. S7). However, this change was not significant. Measured specific oxygen uptake rates as determined from continuous measurement of dissolved oxygen uptake rates accounted for  $582 \text{ fmol cell}^{-1} \text{ h}^{-1}$  in untreated cells and  $560 \text{ fmol cell}^{-1} \text{ h}^{-1}$  in treated cells (Tab. 2), corresponding to a decrease of about 4 % upon treatment with Verapamil (Appendix for Chapter 4, Fig. S1 and S2).

**Table 2:** Estimation of specific oxygen uptake rate,  $q_{O_2}$ , using optical measurement of dissolved oxygen in 24-well plates and simultaneous estimation of  $k_{L,a}$  in untreated control and treated HL-1 cells ( $4 \mu\text{M}$  verapamil). Details of measurement results and estimation of parameters are provided in the Appendix for Chapter 4 (Text S1, Fig S1 and S2).

	Untreated control	$4 \mu\text{M}$ verapamil	Assumed experimental error in oxygen measurement
$k_{L,a} [\text{h}^{-1}]$	$0.24 \pm 0.01$	$0.25 \pm 0.01$	5%
	$0.18 \pm 0.02$	$0.16 \pm 0.05$	10%
$q_{O_2} [\text{fmol cell}^{-1} \text{ h}^{-1}]$	$582 \pm 27$	$560 \pm 17$	5%
	$402 \pm 45$	$368 \pm 109$	10%

The differences between values determined via metabolic flux analysis and direct respiration measurement may be caused by some systematic deviations originating most likely from incomplete mixing in the static 24-well plates (Weiss *et al.*, 2002). Most importantly a similar trend between control and verapamil treated cells was observed.

### Discussion

Independent of the calcium channel blocking effect, verapamil has been shown to exert other physiological effects such as on the glucose uptake. Various studies have shown a potential effect of verapamil on glucose transporters such as GLUT1 and GLUT4. Using HL-1 cells, we investigated the influence of verapamil on specific uptake and production rates of a whole spectrum of metabolites and nutrients, such as lactate, pyruvate and amino acids in addition to glucose in serum free conditions.  $^{13}\text{C}$  labeled glutamine was used to obtain an insight into the central metabolism. Based on specific uptake rates and  $^{13}\text{C}$  enrichment in alanine and glutamate, we estimated the effect of verapamil on TCA cycle activity.

## Effect of verapamil on metabolic fluxes in HL-1 cells

---

Untreated control cells consumed glucose and produced lactate, resulting in a lactate/glucose ratio of 1 mol<sub>lactate</sub>/mol<sub>glucose</sub>. A recent study on HL-1 cells maintained in serum containing medium, reported a lactate/glucose ratio of 1.8 (Monge *et al.*, 2009) suggesting conversion of almost all glucose into lactate. This study suggested that HL-1 cells share properties with cancer cells and other immortalized cell lines, which often show Warburg effect, i.e. high anaerobic glycolysis. Secreted lactate may also serve to keep the tumor environment acidic which is commonly needed for tumor growth. We conducted our study in serum free conditions and our results indicate that the HL-1 cells adapted to serum free conditions seem to shuttle glucose carbon to a higher extent into the TCA cycle, as apparent from the lower lactate/glucose yield.

A significant decrease of specific glucose uptake rate in HL-1 cells was observed upon verapamil treatment. In addition, lactate production completely stopped after 24 h and a slight consumption of initially produced lactate was observed afterwards. The decrease in glucose uptake is probably partly caused by less energy demand due to arrest of myocyte beating i.e. the working state of the cardiomyocytes upon verapamil treatment. However, the fact that lactate was not produced in case of verapamil treated cells but even slightly consumed is a strong evidence that reduced glucose uptake is not solely due to reduced energy demand. A direct effect of verapamil on glucose uptake results in significantly reduced glycolytic flux. Recent studies suggest a direct effect of verapamil on glucose transporters (Ardizzone *et al.*, 2002; Cartee *et al.*, 1992; Louters *et al.*, 2010). Since HL-1 cells possess glucose transporters GLUT1 and GLUT4 (Shuralyova *et al.*, 2004) it can be assumed that the decreased glycolysis and halted lactate production are consequences of verapamil's effect on glucose uptake. Besides the reduction of lactate production, pyruvate is consumed in treated cells but not in untreated cells whereas glycine production was significantly decreased. As secreted pyruvate is probably linked to intracellular pyruvate pools and secreted glycine most probably derives from glycolytic intermediate 3-phosphoglycerate, it can be assumed that verapamil treated HL-1 cells try to make efficient use of available glucose. The complete halt of lactate production, which itself requires reduction of 1 mole of pyruvate on the expense of 1 mole NADH facilitates the maintenance of NADH production rate. In addition, slight uptake of lactate may yield additional NADH in verapamil treated cells.

These changes allow the cells to maintain TCA cycle activity, cell respiration (figure 2 and table 2) and cell growth almost comparable to untreated cells. However, despite a more efficient use of available glucose carbon in verapamil treated cells, the extent of carbon derived from glucose

entering TCA cycle doesn't seem sufficient to maintain TCA cycle activity at a similar level as in untreated cells, as calculated from a non-significant decrease in TCA cycle rates. This might explain the increased rate of deamination of glutamine to glutamate as well as the slight increase of transamination/deamination of glutamate to  $\alpha$ -ketoglutarate. This increased flux contributes to anaplerosis in the TCA cycle.

Verapamil's property to decrease glucose uptake and consequently glycolysis may be exploited in the fields of cancer therapy and biotechnology. It was recently suggested that verapamil has an anticancer effect itself (Zhang *et al.*, 2009) and also enhances the effect of other anticancer agents. Despite the fact that most studies regarding verapamil's antiproliferative effect were performed *in vitro*, which does not reflect tumor environment, verapamil induced reduction of glucose uptake and thereby glycolytic activity may contribute to decreased tumor growth. The interruption of tumor glycolytic metabolism is a potential strategy in cancer therapy (Gatenby and Gillies, 2007). In addition, lack of acidic environment may abolish selective advantage of tumor cells, as tumor invasion seems to favor  $H^+$  environment (Gillies and Gatenby, 2007). As apparent from our study, growth of untreated controls and verapamil treated cells was similar. We therefore assume that hypoxic conditions prevalent in tumor tissue, would favor verapamil's antiproliferative effect *in vivo*. Further experiments e.g. under hypoxic conditions would lead to a better insight since it can be expected that the HL-1 cells would not be able to maintain growth as was observed in our study.

Besides the field of cancer therapy verapamil (or compounds with similar properties i.e. phenylalkylamines) may have potential application from biotechnological point of view whereby cell lines are desired to efficiently use the substrate and produce minimum lactate as by product. Several strategies have been developed to reduce lactate formation in cell lines. It has been shown that lactate formation can be highly reduced in CHO cells by substitution of glucose by either fructose or galactose (Altamirano *et al.*, 2000). In addition, disruption of LDH-genes can significantly decrease lactate formation despite high glucose concentrations in the culture medium, while at the same time increasing both viable cell number and antibody production (Chen *et al.*, 2001). It was recently shown that down regulation of LDH-A gene via siRNA also allows significant reduction of lactate production (Kim and Lee, 2007). In addition, efficient use of glucose as substrate in mammalian cell culture can be achieved by fed-batch cultivation using low glucose concentrations (~0.5 mM) as described for several cell lines (Gambhir *et al.*, 1999; Maranga and Goochee, 2006; Zhou *et al.*, 1995). We assume that addition of verapamil or

## Effect of verapamil on metabolic fluxes in HL-1 cells

---

similarly acting compounds, to culture medium may serve as a potential alternative to the above mentioned approaches or an additional supplement for production efficiency. This is especially true in case of lab-scale production of proteins where the application of fed-batch cultivation would usually be considered too costly and where, therefore, batch cultivation of cells is preferentially applied necessitating rather high glucose concentrations. Reduction of glucose uptake by a compound and thereby elimination of lactate formation while maintaining cell growth and protein secretion at a high level might be very useful in such cases. Instead of optimizing cell lines by genetic modifications, simple addition of verapamil in non-toxic concentrations may result in lower glucose uptake rate and higher efficiency i.e. less production of lactate. Further experiments using verapamil and other glucose uptake inhibitors/modulators with cell lines used for biotechnological purposes are underway in our laboratory.



## Chapter 5

### **Doxorubicin results in increased oxidative metabolism in HL-1 cardiomyocytes as shown by metabolic flux analysis**

#### **Abstract**

Doxorubicin (DXR), an anticancer drug, is limited in its use due to severe cardiotoxic effects. These effects are partly caused by disturbed myocardial energy metabolism. We analyzed the effects of therapeutically relevant but non-toxic DXR concentrations for their effects on metabolic fluxes, cell respiration and intracellular ATP.  $^{13}\text{C}$  isotope labeling studies using [U- $^{13}\text{C}_6$ ]glucose, [1,2- $^{13}\text{C}_2$ ]glucose and [U- $^{13}\text{C}_5$ ]glutamine were carried out on HL-1 cardiomyocytes exposed to 0.01  $\mu\text{M}$  and 0.02  $\mu\text{M}$  DXR and compared with the untreated control. Metabolic fluxes were calculated by integrating production and uptake rates of extracellular metabolites (glucose, lactate, pyruvate, amino acids) as well as  $^{13}\text{C}$ -labeling in secreted lactate derived from the respective  $^{13}\text{C}$ -labeled substrates into a metabolic network model. The investigated DXR concentrations (0.01  $\mu\text{M}$  and 0.02  $\mu\text{M}$ ) had no effect on cell viability and beating of the HL-1 cardiomyocytes. Glycolytic fluxes were significantly reduced in treated cells at tested DXR concentrations. Oxidative metabolism was significantly increased (higher glucose oxidation, oxidative decarboxylation, TCA-cycle rates and respiration) suggesting a more efficient use of glucose carbon. These changes were accompanied by decrease of intracellular ATP. We conclude that DXR in nanomolar range significantly changes central carbon metabolism in HL-1 cardiomyocytes which results in a higher coupling of glycolysis and TCA-cycle. The myocytes probably try to compensate for decreased intracellular ATP which in turn may be the result of a loss of NADH electrons *via* either formation of reactive oxygen species or electron shunting.

This chapter has been published as: Strigun, A., Wahrheit, J., Niklas, J., Heinzle, E., Noor, F. (2011). Doxorubicin increases oxidative metabolism in HL-1 cardiomyocytes as shown by  $^{13}\text{C}$ -metabolic flux analysis. *Toxicological Sciences*, doi: 10.1093/toxsci/kfr298

### Introduction

Doxorubicin (DXR), an anthracycline antibiotic, is used in first line therapy of many human cancers. However, severe cardiotoxic side effects limit its clinical use (Simunek *et al.*, 2009). Multiple mechanisms of DXR toxicity *in vivo* and *in vitro* have been described (Gewirtz, 1999; Tokarska-Schlattner *et al.*, 2006). These include formation of reactive oxygen species (Bachur *et al.*, 1977; Sinha *et al.*, 1989), disturbances in nitric oxide pathway resulting in protein nitration (Fogli *et al.*, 2004), oxidative damage of DNA (Bates and Winterbourn, 1982; Eliot *et al.*, 1984; Feinstein *et al.*, 1993), lipid peroxidation (Gewirtz, 1999) and apoptosis (Ling *et al.*, 1993; Skladanowski and Konopa, 1993).

Yet, it is more and more evident that alterations in myocardial energy metabolism, especially due to mitochondrial dysfunction (Berthiaume and Wallace, 2007a), play an important role in the onset of DXR induced cardiac toxicity. DXR related acute and chronic cardiotoxicity has been associated with impaired cardiac high-energy phosphate metabolism. The compromising effect of DXR on cardiac energy metabolism is reflected by loss of mitochondrial ATP (Pointon *et al.*, 2010 ; Vidal *et al.*, 1996). Cardiac substrate usage for the generation of the ATP and its alterations in myocardial diseases has been extensively studied (Ashrafian *et al.*, 2007; Gertz *et al.*; 1988; Mudge *et al.*, 1976; Panchal *et al.*, 2001; Randle *et al.*, 1964; Stanley *et al.*, 1997; Wisneski *et al.*, 1985). It is well accepted that ATP is mainly generated from fatty acid oxidation in the healthy heart (Stanley *et al.*, 2005). Several studies have shown that DXR alters fatty acid and glucose metabolism in the myocardium (Abdel-aleem *et al.*, 1997; Bordoni *et al.*, 1999; Carvalho *et al.*, 2010; Wakasugi *et al.*, 1993). However, the effects of DXR on main energy generating pathways besides TCA cycle, such as glycolysis are contradictory. Recent *in vivo* and *in vitro* studies demonstrated increased mRNA of several glycolytic enzymes (Berthiaume and Wallace, 2007b) as well as increased glycolytic activity which is correlated to a decrease in the fatty acid oxidation (Carvalho *et al.*, 2010). In addition, it was recently demonstrated that DXR results in an up-regulation of mRNA from TCA-cycle relevant enzymes in perfused rat heart (Tokarska-Schlattner *et al.*, 2010). Contradictorily, decreased levels of TCA-cycle relevant mRNA has been described in another model (Berthiaume and Wallace, 2007b). Such conflicting data in this regard is most probably related to differences in the applied biological model and experimental setup. Moreover, these differences in observations regarding alterations in metabolic pathways may be partly due to either acute or chronic effects of DXR.

To our knowledge, holistic fluxome studies on DXR induced effects on central energy metabolism integrating reactions, such as glycolysis, TCA-cycle and amino acid degradation, have not been carried out at clinically relevant concentrations on myocardial cells. This can be very challenging with commonly used endpoint methods since therapeutic concentrations should not cause acute myocyte dysfunction or cytotoxicity. The plasma kinetics of DRX shows an initial half-life of ~8 minutes followed by a terminal half-life of about 30 hours (Greene *et al.*, 1983). The major exposure occurs during the terminal phase where drug concentrations are generally less than  $10^{-7}$  M. Following a 15 min infusion of DXR, the plasma concentration rapidly declines from 5 to 0.1  $\mu$ M within one hour and steadily declines until ~30 hours. Total plasma concentration ranges from 20nM to 2 $\mu$ M of which only 20-25 % is freely available i.e. the amount not bound to serum albumin. We assumed that DXR even at nanomolar concentrations exerts an effect on the central metabolism. To assess such effects sensitive methods and cutting edge technology is required. Using  $^{13}\text{C}$  metabolic flux analysis we analyzed the effect of DXR on the central metabolism in an *in vitro* model (HL-1 cardiomyocytes). The used methodology includes the measurement of a whole set of metabolite uptake and production rates as well as the measurement of  $^{13}\text{C}$  enrichment in metabolites derived from  $^{13}\text{C}$  labeled substrates. These data are implemented into a metabolic network model which allows the estimation of intracellular fluxes over metabolic pathways. This method has been successfully used to study the energy metabolism of mammalian cells *in vitro* (Forbes *et al.*, 2006; Goudar *et al.*, 2010; Maier *et al.*, 2009; Metallo *et al.*, 2009; Niklas *et al.* 2011; Strigun *et al.*, 2011b) and that of the whole myocardium, as shown earlier (Vo and Palsson, 2006). However, this method has not been yet applied to analyze the effect of DXR on cardiac metabolism. The advantage of  $^{13}\text{C}$  based fluxomic studies over transcriptomic or proteomic approaches is that activities of ATP-relevant pathways can be more reliably determined. Most importantly, specific rates of certain reactions cannot always be directly derived from changes of corresponding genes or proteins, due to the complex regulations of enzyme activities. We investigated the suitability of this method for the description of actual *in vivo* activities of metabolic pathways.

We furthermore complemented flux determinations with the measurement of cell respiration and intracellular ATP. The HL-1 cardiomyocytes is a murine cardiac cell line (Claycomb *et al.*, 1998; White *et al.*, 2004) which retains a differentiated morphology (Sartiani *et al.*, 2002, White *et al.*, 2004, Fukuda *et al.*, 2005, Clarke *et al.*, 2006). These cells have been used in the study of glucose and fatty acid metabolism (Palanivel *et al.*, 2006, Alfarano *et al.*, 2008) in addition to studying

DXR induced effects (Andersson *et al.*, 2010; Budde *et al.*, 2011). We used a dose response curve from an LDH release assay to determine the DXR concentrations which were not cytotoxic and did not inhibit myocyte beating. These concentrations have been reported to be clinically relevant corresponding to serum concentrations in patients undergoing DXR treatment (Greene *et al.*, 1983). These are also significantly lower than the DXR concentrations at which cardiac Troponin T release, an indicator for cardiac damage, has been recently reported in the HL-1 cardiomyocytes (Andersson *et al.*, 2010). The results of the present study are discussed in the context of current knowledge regarding DXR induced alterations of cardiac energy metabolism.

### Material and Methods

#### *Cell Culture*

HL-1 cardiomyocytes (Claycomb *et al.*, 1998; White *et al.*, 2004) were kindly provided by Dr. Claycomb (Louisiana State University) for research within the framework of EU STREP-project “Invitroheart”. The cells were maintained in Claycomb medium (Sigma Chemical, USA) which was supplemented with 2 mM glutamine (PAA Laboratories, Austria), 100 U/ml penicillin, 100 µg/ml streptomycin (PenStrep stock solution, C. C. Pro GmbH, Oberdorla, Germany), 100 µM norepinephrine (Sigma Chemical, USA) in 30 mM L-ascorbic acid (Sigma Chemical, USA) and 10% fetal bovine serum (FBS) (JRH Biosciences, UK). At confluency the cells were passaged in a split ratio of 1:3. Cells were cultivated in culture flasks (75 cm<sup>2</sup>, Falcon, Germany) which were pre-coated with a solution of 0.02% (w/v) gelatin (AppliChem, Germany) containing 5 µg/ml fibronectin (Sigma Chemical, USA). The cells were maintained at standard cell culture conditions (37 °C, 5% CO<sub>2</sub> and 95% relative humidity) in a cell culture incubator (Memmert GmbH, Schwabach, Germany).

#### *LDH assay*

A doxorubicin-HCl (DXR) (Sigma Chemical, USA) stock solution (10 mM) was prepared in cell culture grade water (PAN Biotech, Germany). Cytotoxicity of DXR on HL-1 cardiomyocytes was assessed using lactate dehydrogenase release (LDH-release assay).  $5 \times 10^4$  cells/well were seeded in gelatin/fibronectin-coated (see 2.1) 96-well plates (Greiner, Germany) in 200 µl Claycomb medium (containing 2 mM glutamine, 100 U/ml penicillin, 100 µg/ml streptomycin, 100 µM norepinephrine in 30 mM L-ascorbic acid and 10% FBS). After 24 hours (h) incubation, the supernatant was removed and the cells were washed once with Claycomb medium. Fresh

## Effect of doxorubicin on metabolic fluxes in HL-1 cells

---

supplemented Claycomb medium containing DXR at different concentrations (20  $\mu\text{M}$ , 10  $\mu\text{M}$ , 2.5  $\mu\text{M}$ , 0.6  $\mu\text{M}$ , 0.16  $\mu\text{M}$  and 0.004  $\mu\text{M}$ ) was added to the cells in triplicates. The cells were incubated with DXR for 48 h. Finally, lactate dehydrogenase assay (Cytotoxicity Detection Kit (LDH), Roche Applied Science, Germany) was carried out according to manufacturer's instructions.

### *Experimental setup for labeling studies on HL-1 cardiomyocytes*

A stock solution of 1 mM DXR in cell culture grade water (PAN Biotech, Germany) was diluted in supplemented Claycomb medium (see 2.2) to obtain 0.02  $\mu\text{M}$  or 0.01  $\mu\text{M}$  DXR final concentrations. For each test (0.02  $\mu\text{M}$ , 0.01  $\mu\text{M}$  or untreated control without DXR) four separate media containing different combinations of labeled glucose and glutamine substrates (enrichment 99%) (Cambridge Isotope Laboratories, USA) were prepared as follows; *medium 1*: 5 mM [U- $^{13}\text{C}_6$ ] glucose and 2 mM naturally labeled glutamine, *medium 2*: 5 mM [1,2- $^{13}\text{C}_2$ ] glucose and 2 mM naturally labeled glutamine, *medium 3*: 5 mM naturally labeled glucose and 2 mM [U- $^{13}\text{C}_5$ ] glutamine, *medium 4*: 5 mM naturally labeled glucose and 2 mM naturally labeled glutamine. Since the commercially available Claycomb medium already contains 20 mM glucose, the final glucose concentration in the media was 25 mM. In this way 12 different media in total were prepared (four media for controls, four for each 0.01  $\mu\text{M}$  and 0.02  $\mu\text{M}$  DXR, respectively).

$1.5 \times 10^5$  HL-1 cardiomyocytes in a volume of 1 ml were seeded per well in 24-well plates pre-coated with a gelatine/fibronectin solution (see 2.1) using Claycomb medium (25 mM naturally labeled glucose, 2 mM glutamine, 100 U/ml penicillin, 100  $\mu\text{g/ml}$  streptomycin, 100  $\mu\text{M}$  norepinephrine in 30 mM L-ascorbic acid and 10 % FBS). After 24 h equilibration the medium was removed and the cells were carefully washed twice with pre-warmed (37  $^\circ\text{C}$ ) Claycomb medium without supplements. The 12 different media containing 0.02  $\mu\text{M}$ , 0.01  $\mu\text{M}$  or no DXR and differently labeled glucose and glutamine substrates were added to the respective wells. Cell free medium served as blank. For each test condition (0.02  $\mu\text{M}$  DXR, 0.01  $\mu\text{M}$  DXR, untreated control, cell free medium control) four replicates per 24-well plate were prepared. Replicate 1 contained medium 1, replicate 2 contained medium 2, replicate 3 contained medium 3 and replicate 4 contained medium 4. Four 24-well plates were prepared in this way.

The plates were incubated under standard cell culture conditions (37  $^\circ\text{C}$ , 95 % relative humidity, 5 %  $\text{CO}_2$ ) in the incubator. After 2, 10, 24 and 34 h of incubation one plate was removed from the

incubator and the respective supernatants were collected and stored at -20 °C until further analysis. The cells of each plate were fixed and a protein quantification assay (SRB assay) was performed as described previously (Noor *et al.*, 2009). Cell number was estimated using a calibration curve obtained with different cell numbers of HL-1 cardiomyocytes.

### *Sample preparation for HPLC analysis*

Serum proteins, such as albumin were removed from the samples by microfiltration using Microcon<sup>®</sup> Filter Devices (Millipore, Germany) with an exclusion size of 10 kDa. Subsequently each filtrate was diluted 1:2 with  $\alpha$ -aminobutyric acid solution (400  $\mu$ M in deionized water) which was used as an internal standard for amino acid quantification.

### *Quantification of extracellular glucose, lactate, pyruvate, amino acids and total fatty acids*

Quantification of glucose, lactate and amino acids was carried out exactly as described recently (Strigun *et al.*, 2011b). Quantification of total free fatty acids was performed using a NEFA kit (Wako Chemicals, Germany) for the determination of non-esterified fatty acids. 300  $\mu$ l of each culture supernatant was lyophilized and reconstituted in 30  $\mu$ l cell culture grade water. Total free fatty acids in these samples were quantified according to the manufacturer's instructions. Briefly, 100  $\mu$ l of the prepared reaction solution were mixed with 10  $\mu$ l of the sample. After incubation for 10 minutes at room temperature (RT) the absorbance of the formed dye was measured at 550 nm using an iEMS reader (Labsystems, Finland). To exclude any influence of DXR on the measurement, reconstituted medium without cells was used. An oleic acid standard solution (Wako Chemicals, Germany) was used for calibration.

### *Mass isotopomer measurement using GC/MS*

Measurement of mass isotopomers was carried out using gas chromatography (HP 6890 Hewlett Packard, USA) equipped with a HP-5 MS column (5 % phenyl-methyl-siloxanediphenylpolysiloxane, 30 m x 0.25 mm x 0.25  $\mu$ m, Agilent, Germany) and coupled with a quadrupole mass spectrometer (MS 5973, Agilent, Germany). Sample preparation, measurement of mass distributions of lactate and calculation of mean mass isotopomer distributions was carried out using a recently reported procedure (Strigun *et al.*, 2011b).

### *<sup>13</sup>C flux analysis*

A carbon atom transition network of the central metabolism was set up for  $^{13}\text{C}$  metabolic flux analysis (Appendix of chapter 5, Tab. S6). The model consisted of 63 reactions of which 14 reactions represent extracellular uptake and production rates whereas 49 reactions were intracellular rates including 16 reversible reactions. Anabolic fluxes were estimated from the growth rate and biomass composition. Biomass composition was taken from literature (Niklas *et al.*, 2009). The estimation of fluxes was carried out with MATLAB 2008b (The Mathworks, USA) using the elementary metabolite unit concept (Antoniewicz *et al.*, 2007) applying a recently described method (Yang *et al.*, 2008).

### *Respiration measurement*

$1.5 \times 10^5$  HL-1 cardiomyocytes per well were seeded in 24-well OxoDishes (PreSens, Germany) pre-coated with gelatine/fibronectine solution (see 2.1). Cell free medium served as control. After 24 h equilibration, fresh Claycomb medium (25 mM naturally labeled glucose, 2 mM naturally labeled glutamine, 100 U/ml penicillin, 100  $\mu\text{g}/\text{ml}$  streptomycin, 100  $\mu\text{M}$  norepinephrine in 30 mM L-ascorbic acid and 10 % FBS) containing 0.01 and 0.02  $\mu\text{M}$  DXR was added to the respective wells. Untreated control was also included. The percentage of dissolved oxygen was measured continuously for 34 h using a recently described method (Beckers *et al.*, 2009). Specific oxygen consumption rate ( $q\text{O}_2$ ) [ $\text{fmol cell}^{-1} \text{h}^{-1}$ ] was estimated by fitting the time course of dissolved oxygen using equation (eq. 1).

$$\frac{d[\text{O}_2]}{dt} = k_L a \cdot ([\text{O}_2^{\text{sat}}] - [\text{O}_2]) - \frac{q\text{O}_2 \cdot X}{V} \quad (1)$$

$[\text{O}_2^{\text{sat}}]$  represents the dissolved oxygen concentration at saturation in culture medium i.e. 6.23 mg/L as previously reported (Oeggerli *et al.*, 1995), while  $[\text{O}_2]$  represents the actual dissolved oxygen concentration, X the number of cells per well and V the liquid volume per well. Curve fitting and estimation of the parameter  $q\text{O}_2$  was carried out using Berkeley Madonna V.8.3.14 (Berkeley Madonna Inc., USA). For each condition (control, 0.01  $\mu\text{M}$  DXR and 0.02  $\mu\text{M}$  DXR)  $q\text{O}_2$  was estimated thrice referring to each of the triplicate measurements.

## Effect of doxorubicin on metabolic fluxes in HL-1 cells

---

### *Measurement of intracellular ATP*

For determination of intracellular ATP HL-1 cardiomyocytes were seeded in two 96-well plates in a total volume of 100  $\mu$ l/well of Claycomb medium (containing 25 mM naturally labeled glucose, 2 mM naturally labeled glutamine, 100 U/ml penicillin, 100  $\mu$ g/ml streptomycin, 100  $\mu$ M norepinephrine in 30 mM L-ascorbic acid and 10 % FBS) in triplicates. After 24 h equilibration, the medium was replaced by 100  $\mu$ l of the above supplemented Claycomb medium containing 0.01  $\mu$ M and 0.02  $\mu$ M DXR was added to the cardiomyocytes. An untreated control was also included. Intracellular ATP was determined after 2 and 34 h of incubation using ATPlite 1Step assay (PerkinElmer, USA). 100  $\mu$ l of lysis solution containing substrate was added to the cells. After 10 minutes incubation at RT luminescence was measured using a LumiCount plate reader (Wallac 1420 Multilabel counter Victor<sup>3</sup>, PerkinElmer, USA). A standard curve with known ATP concentrations was used to estimate the ATP-concentration in samples. In parallel an SRB assay (see 2.3) was carried out for the estimation of cell number.

### *Statistical analysis*

All data, except respiration measurement, were compared using one-way ANOVA following Dunnett's posthoc analysis. Significance of altered cellular respiration was determined *via* two different methods. The time courses of dissolved oxygen in culture medium of all three conditions (control, 0.01  $\mu$ M DXR, 0.02  $\mu$ M DXR) was compared by repeated-measures two way ANOVA analysis following Bonferroni posthoc test. Secondly, all  $qO_2$  (3 for each condition, (see 2.8)), were compared by one-way ANOVA following Dunnett's posthoc analysis. One-way and two way ANOVA as well as posthoc tests were carried out using Prism 5 V.5.04 (GraphPad Software, Inc., USA). Statistical significance is reported at  $p < 0.05$ .



## Results

### *Cytotoxicity of doxorubicin*

Concentration dependent release of LDH was observed (Figure 1) after exposure to DXR for 48 h. DXR concentrations lower than 0.16  $\mu\text{M}$  did not show a significant release of LDH as compared with the control. However, 0.6  $\mu\text{M}$  and higher DXR concentrations led to approximately 1.5 to 1.9 fold higher release of LDH ( $p < 0.001$ ). Based on these results two DXR concentrations in an assumed sub-toxic range (0.01  $\mu\text{M}$  and 0.02  $\mu\text{M}$  DXR) were considered for the analysis of DXR-induced metabolic changes in HL-1 cardiomyocytes.

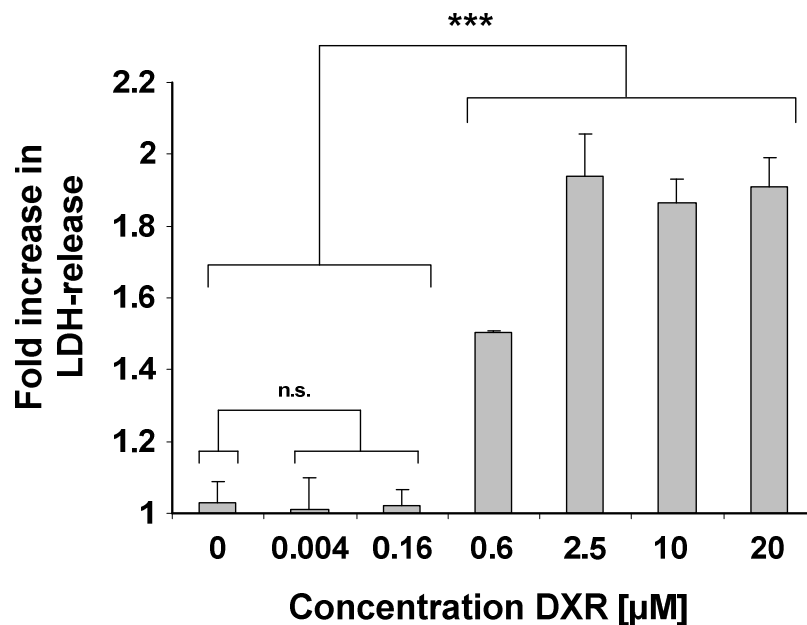


**Figure 1:** Concentration dependent release of LDH in DXR treated HL-1 cardiomyocytes determined in an LDH assay. Cells were exposed to DXR for 48 h. Values are given as fold increase of LDH release from the untreated control. Error bars indicate standard deviations ( $n=3$ ). Statistical significance was determined using one-way ANOVA following Dunnett's posthoc test. n.s.: not significant; \*\*\*:  $p < 0.001$ .

### *Cultivation profile and specific uptake/production rates of metabolites in HL-1 cardiomyocytes upon doxorubicin treatment*

Figure 2 A shows the growth profiles of HL-1 cardiomyocytes exposed to 0.01  $\mu\text{M}$  or 0.02  $\mu\text{M}$  DXR and the untreated control. Microscopically observed beating frequency in both DXR treated cells and controls were similar throughout the whole experiment. Cell number increased from  $1.5 \times 10^5$  cells per well seeding density to  $3.61 \times 10^5$  for untreated control,  $3.92 \times 10^5$  upon

## Effect of doxorubicin on metabolic fluxes in HL-1 cells

treatment with  $0.01 \mu\text{M}$  DXR and  $3.77 \times 10^5$  with  $0.02 \mu\text{M}$  DXR after 24 hours pre-incubation followed by 34 h drug exposure. Although cell growth seemed slightly increased in DXR treated cells the actual cell number at each time point was not significantly different from the control cells as shown by the SRB assay (figure 2A).

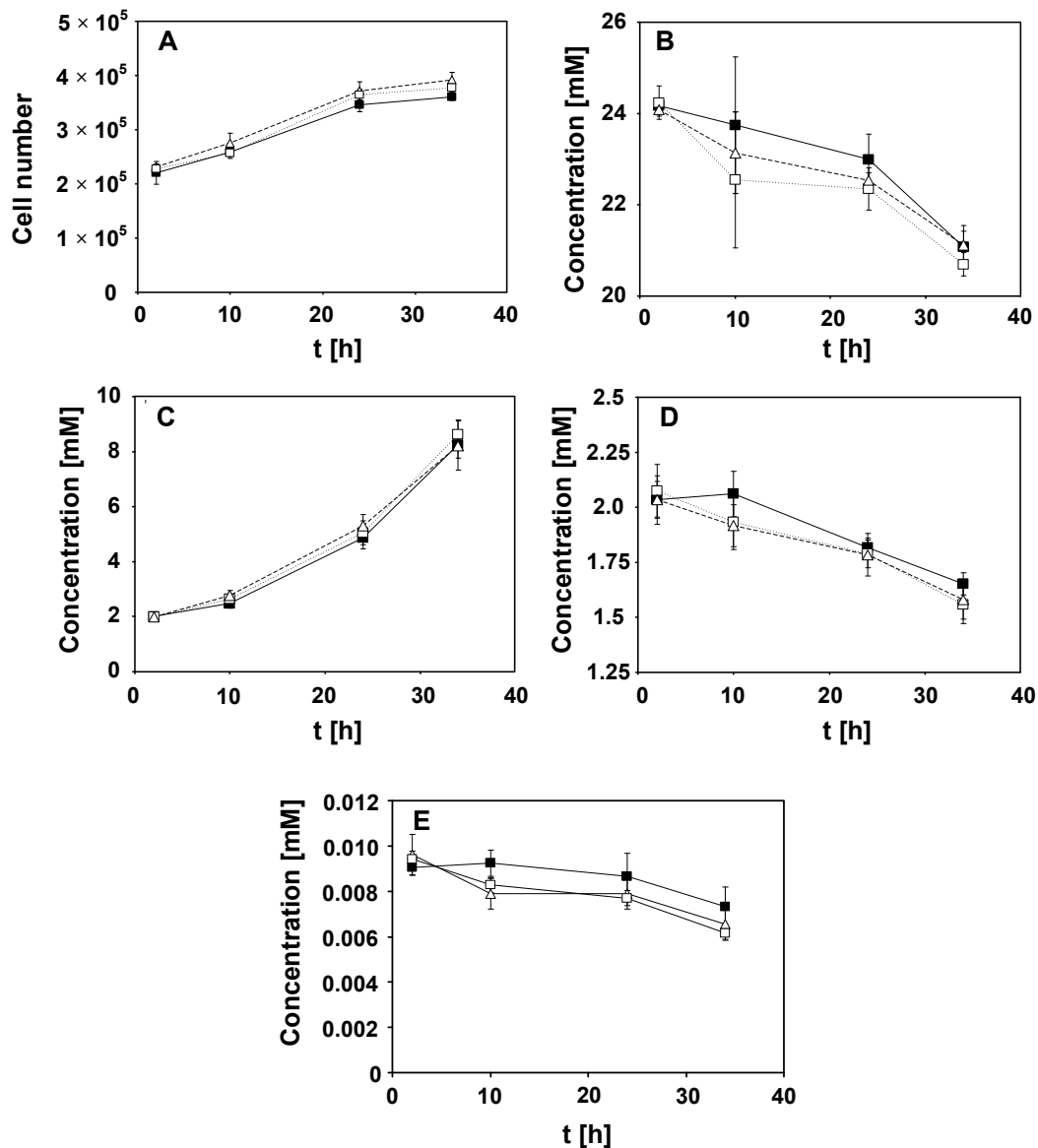


**Figure 2:** Cell number (A), glucose (B), lactate (C), glutamine (D) and oleic acid (E) concentrations versus time in culture medium of untreated HL-1 cardiomyocytes (■) and cells treated with  $0.01 \mu\text{M}$  (□) and  $0.02 \mu\text{M}$  ( $\Delta$ ) DXR. Error bars indicate standard deviations ( $n=4$ ). Statistical significance was determined using one-way ANOVA following Dunnett's posthoc test. The cell number was estimated using an SRB assay.

## Effect of doxorubicin on metabolic fluxes in HL-1 cells

---

Extracellular concentrations of glucose, lactate, glutamine, the 20 proteinogenic amino acids and total free fatty acids were similar in both controls and treated cells throughout DXR exposure (Figure 2 B, C, D, E and Figure S1 in the Appendix of Chapter 5). The time course of glucose, lactate, glutamine and oleic acid are depicted in figure 2 B-E. Despite slight differences of metabolite concentrations at each time point, these alterations were not statistically significant. Specific uptake or production rates of all metabolites were calculated from cell growth (Fig. 2 A) as well as metabolite concentrations and are given in Tab. S1 (Appendix of Chapter 5). Glucose, lactate and glutamine showed the highest specific uptake/production rates independent of DXR exposure. A trend towards decreased glucose uptake was observed in DXR treated cells (300  $\text{fmol cell}^{-1} \text{h}^{-1}$  in untreated control; 288  $\text{fmol cell}^{-1} \text{h}^{-1}$  with 0.01  $\mu\text{M}$  DXR; 262  $\text{fmol cell}^{-1} \text{h}^{-1}$  with 0.02  $\mu\text{M}$  DXR). A similar trend was observed for lactate production which was also slightly decreased in treated cells (642  $\text{fmol cell}^{-1} \text{h}^{-1}$  in untreated control; 604  $\text{fmol cell}^{-1} \text{h}^{-1}$  with 0.01  $\mu\text{M}$  DXR; 603  $\text{fmol cell}^{-1} \text{h}^{-1}$  with 0.02  $\mu\text{M}$  DXR). Glutamine consumption was similar in controls and treated cells (46  $\text{fmol cell}^{-1} \text{h}^{-1}$  in untreated control; 45  $\text{fmol cell}^{-1} \text{h}^{-1}$  with 0.01  $\mu\text{M}$  DXR; 38  $\text{fmol cell}^{-1} \text{h}^{-1}$  with 0.02  $\mu\text{M}$  DXR). For the majority of all other metabolites slight alterations due to DXR exposure were observed. Especially, pyruvate, arginine, lysine, leucine and isoleucine were consumed in slightly lower amounts as compared to the control. The uptake of oleic acid was relatively low in both treated and untreated cells and accounted on average for merely 0.1 % and 0.7 % of glucose and glutamine uptake, respectively. However, a statistically non-significant slight increase of uptake was observed in treated cardiomyocytes (0.16  $\text{fmol cell}^{-1} \text{h}^{-1}$  in controls; 0.29  $\text{fmol cell}^{-1} \text{h}^{-1}$  with 0.01  $\mu\text{M}$  DXR; 0.25  $\text{fmol cell}^{-1} \text{h}^{-1}$  with 0.02  $\mu\text{M}$  DXR).

### *Influence of clinically relevant concentrations of doxorubicin on metabolic flux distribution*

An enrichment of  $^{13}\text{C}$  in lactate derived from differently  $^{13}\text{C}$  labeled substrates (see material and methods, 2.3) was observed (Appendix of Chapter 5, Tab. S2-4). Intracellular fluxes were estimated by implementing extracellular uptake/production rates and the labeling pattern of secreted lactate into a metabolic network model (Appendix of Chapter 5, Tab. S6). In figure 3 simulated lactate mass isotopomer distributions are plotted against respective measured mass isotopomer distribution data for the three test conditions. Simulated mass isotopomer distribution, in this regard, refers to computed values of lactate mass isotopomer distributions, i.e. they represent the output with which lactate labeling theoretically can be expected from the used metabolic network model (Appendix of Chapter 5, Tab. S6) at a given set of measured metabolite

uptake and production rates. Thus, a good fit in a linear regression between measured and simulated mass distribution indicates that the used metabolic network model is suitable for the applied data and secondly, that the computed intracellular fluxes give a robust description of the actual flux distribution in the HL-1 cardiomyocytes.

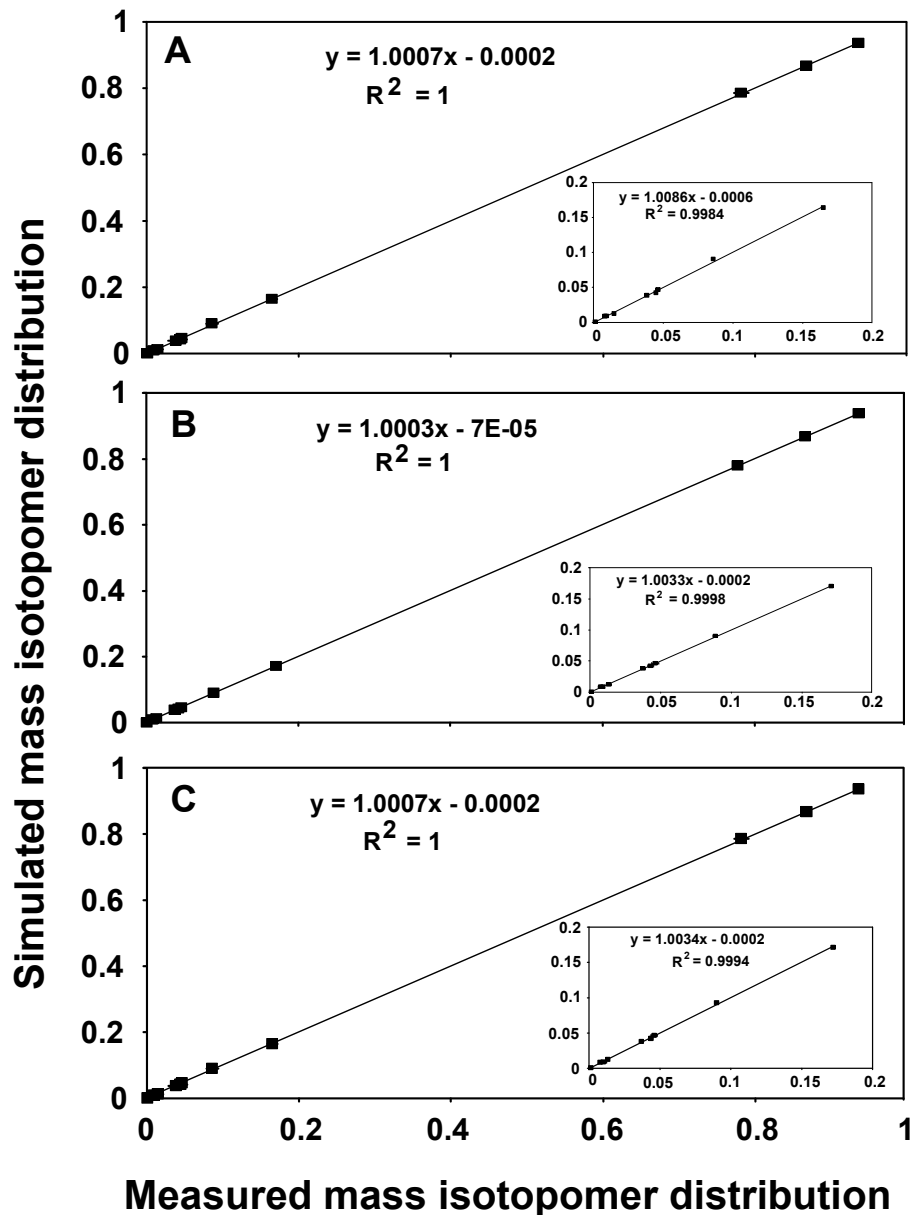


**Figure 3:** Calculated (simulated) lactate mass isotopomer distributions compared to experimentally measured lactate mass isotopomer distributions in untreated HL-1 cardiomyocytes (A) and in HL-1 cardiomyocytes treated with 0.01  $\mu\text{M}$  (B) and 0.02  $\mu\text{M}$  (C) DXR showing good correlation. The graphs inserts represent an enlargement of lower mass isotopomer distributions.

## Effect of doxorubicin on metabolic fluxes in HL-1 cells

---

A very good correlation was found as shown by a linear relationship of measured and calculated lactate mass distributions for treated cells and untreated control (linear correlation coefficients  $R^2 = 1.00$ ). The calculated distribution of intracellular steady state fluxes is depicted in figure 4. The network includes reactions from glycolysis, pentose-phosphate-pathway, TCA-cycle, anaplerosis and amino acid metabolism. The underlying flux values are given in the appendix of Chapter 5. (Table S5). The calculated intracellular flux distribution revealed significant changes in the metabolism of HL-1 cardiomyocytes upon DXR treatment at the tested concentrations.

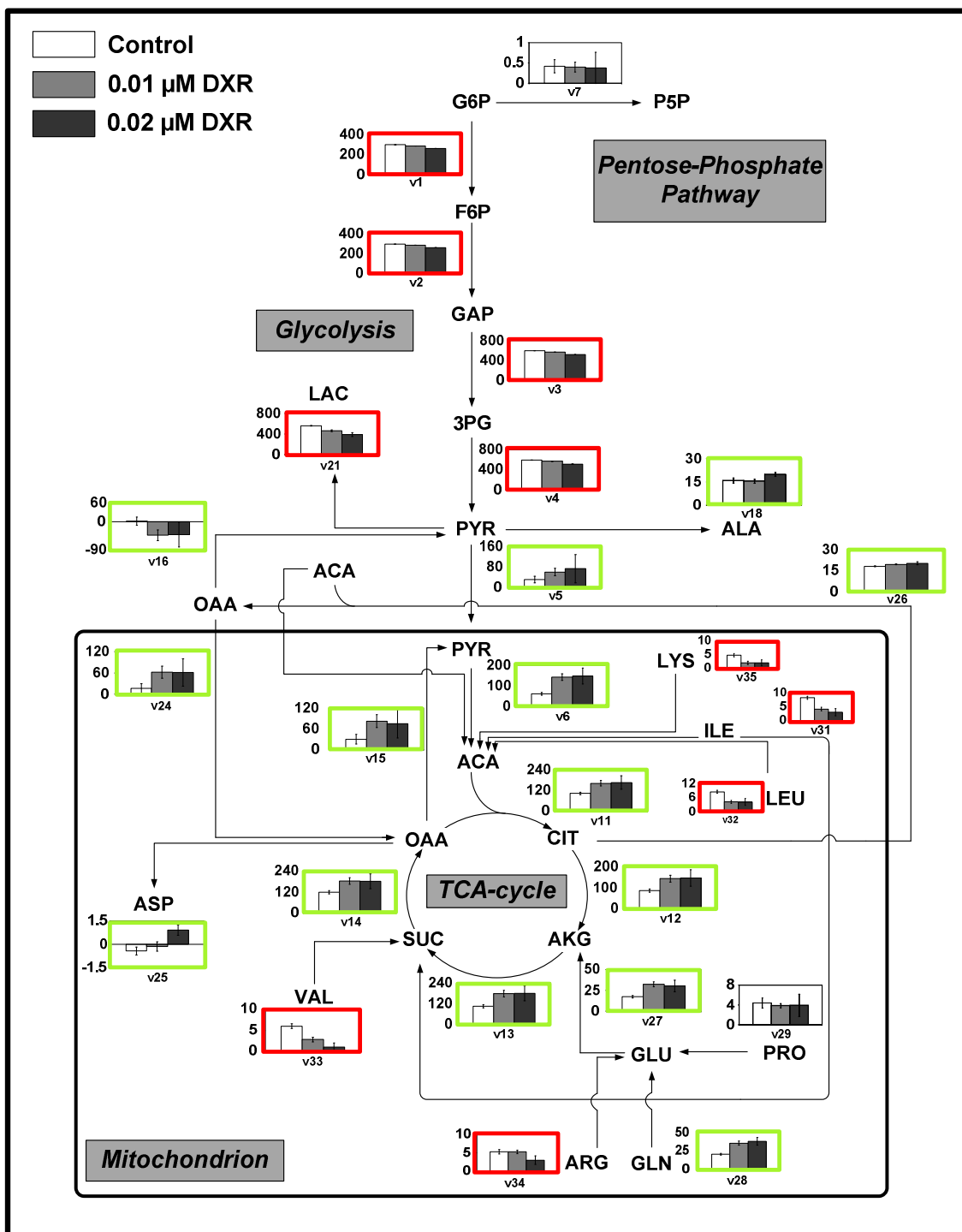


**Figure 4:** Metabolic flux distribution in untreated HL-1 cardiomyocytes and in cells treated with 0.01 μM and 0.02 μM DXR. Both DXR concentrations showed no significant effect on LDH release (figure 1). Cells were incubated for 34 h with 5 mM [U-<sup>13</sup>C<sub>6</sub>]glucose, 5 mM [1,2-<sup>13</sup>C<sub>6</sub>]glucose, 5 mM unlabeled glucose and 2 mM [U-<sup>13</sup>C<sub>5</sub>]glutamine in four parallel experimental setups. Cell number, metabolite concentrations and <sup>13</sup>C enrichment in secreted lactate

## Effect of doxorubicin on metabolic fluxes in HL-1 cells

---

were measured at specific time intervals. Metabolic fluxes were calculated by implementation of uptake and production rates of glucose, lactate, pyruvate and amino acids and the enrichment of  $^{13}\text{C}$  in lactate into a metabolic network model (Tab. S6, Appendix of chapter 5). All rates are given as  $\text{fmol cell}^{-1} \text{h}^{-1}$ . The denotations  $v1-v35$  represent simplified identifiers of the respective fluxes/reactions (see Appendix of Chapter 5 Tab. S5). Statistical significance was determined using one-way ANOVA following Dunnett's posthoc test. Most of the fluxes in DXR treated cells were significantly different from untreated controls ( $p < 0.05$ ). Red and green boxes refer to significantly decreased and increased fluxes as compared to controls ( $p < 0.05$ ). A detailed overview of the significance of individual fluxes is given in table S5 (Appendix of chapter 5).

Glycolytic flux ( $v1 - v4$ ) was dose dependently decreased in DXR treated cells to 96% (0.01  $\mu\text{M}$  DXR;  $p < 0.001$ ) and 87% (0.02  $\mu\text{M}$  DXR;  $p < 0.001$ ) of the control. Lactate production ( $v21$ ) was reduced by 17% (0.01  $\mu\text{M}$  DXR;  $p < 0.001$ ) and by 30% (0.02  $\mu\text{M}$  DXR;  $p < 0.01$ ). Alanine production ( $v18$ ) was increased by 24% in HL-1 cardiomyocytes treated with 0.02  $\mu\text{M}$  DXR ( $p < 0.01$ ).

However, connectivity between glycolysis and TCA-cycle was enhanced in DXR treated cardiomyocytes. Pyruvate transport into mitochondria ( $v5$ ) was increased to 197% and 239% of control in cardiomyocytes exposed to 0.01  $\mu\text{M}$  or 0.02  $\mu\text{M}$  DXR, respectively ( $p < 0.01$ ). Cytosolic flux from pyruvate to oxaloacetate ( $v16$ ) was activated upon drug exposure and caused a nearly four-fold increase ( $p < 0.01$ ) of oxaloacetate import into mitochondria *via* malate-shuttle ( $v24$ ;  $p < 0.001$ ) in treated cardiomyocytes. Activity of mitochondrial malic enzyme ( $v15$ ) producing mitochondrial pyruvate was low in control but increased in cells treated with DXR ( $p < 0.01$ ). Import of pyruvate into mitochondria was therefore increased *via* both direct pyruvate transport ( $v5$ ) and anaplerotic reactions ( $v15$ ,  $v16$ ,  $v24$ ). TCA-cycle fluxes ( $v11-v14$ ) were significantly increased by 54-72% ( $p < 0.001$ ) in treated cardiomyocytes compared to the untreated control. TCA-cycle was mainly sustained by oxidative decarboxylation of pyruvate into acetyl-CoA ( $v6$ ) indicating increased glucose oxidation, and glutaminolysis ( $v27$ ). Upon DXR treatment oxidative decarboxylation ( $v6$ ) was significantly increased to 234% (0.01  $\mu\text{M}$  DXR,  $p < 0.001$ ) or 243% (0.02  $\mu\text{M}$  DXR,  $p < 0.05$ ) so that carbons deriving from pyruvate accounted for more than 85% of TCA fluxes compared to only 60% in untreated control. Glutaminolysis ( $v28$ ) was significantly increased by 74-86% (0.01  $\mu\text{M}$  DXR,  $p < 0.01$ ; 0.02  $\mu\text{M}$  DXR,  $p < 0.05$ ). However, glutamine-derived carbons contributed to the same extent ( $\sim 20\%$ ) to the TCA cycle fluxes in treated cardiomyocytes and untreated control.

Whereas the specific rates of the anaplerotic reactions, the TCA-cycle fluxes, the major input fluxes into TCA cycle, oxidative decarboxylation and glutaminolysis were increased upon DXR exposure, consumption of other amino acids feeding into TCA-cycle such as lysine (v35), arginine (v34), branched chain amino acids (v31-v33) and aspartate (v25) was significantly decreased in treated cells ( $p < 0.05$ ). For valine, isoleucine, arginine and aspartate a dose-dependent effect of DXR was observed. Export of citrate via citrate-shuttle to produce cytosolic acetyl-CoA and oxaloacetate (v26) was slightly increased by 7% (0.01  $\mu\text{M}$  DXR;  $p < 0.01$ ) and 12% (0.02  $\mu\text{M}$  DXR;  $p < 0.001$ ) as compared to the untreated control.

### *Influence of DXR on cellular respiration*

Figure 5 A shows the dissolved oxygen for untreated control and cardiomyocytes treated with 0.01  $\mu\text{M}$  and 0.02  $\mu\text{M}$  DXR in the cultivation media. Dissolved oxygen in the media of both treated and untreated cardiomyocytes decreased due to consumption of oxygen by the cells. Dissolved oxygen in culture medium decreased from 0.19 mM to 0.096 mM (untreated control), 0.089 mM (0.01  $\mu\text{M}$  DXR) and 0.085 mM (0.02  $\mu\text{M}$  DXR). The time course of dissolved oxygen was significantly different after 24 h exposure in case of cardiomyocytes treated with 0.02  $\mu\text{M}$  DXR ( $p < 0.05$ ), but not for cardiomyocytes treated with 0.01  $\mu\text{M}$  DXR. Figure 5 B shows the corresponding specific oxygen uptake rates ( $q\text{O}_2$ ), which were derived from the profiles of dissolved oxygen as well as cell growth. The specific oxygen uptake rates were 66.5  $\text{fmol cell}^{-1} \text{h}^{-1}$  (untreated control), 78.5  $\text{fmol cell}^{-1} \text{h}^{-1}$  (0.01  $\mu\text{M}$  DXR;  $p < 0.05$ ) and 100  $\text{fmol cell}^{-1} \text{h}^{-1}$  (0.02  $\mu\text{M}$  DXR;  $p < 0.001$ ).



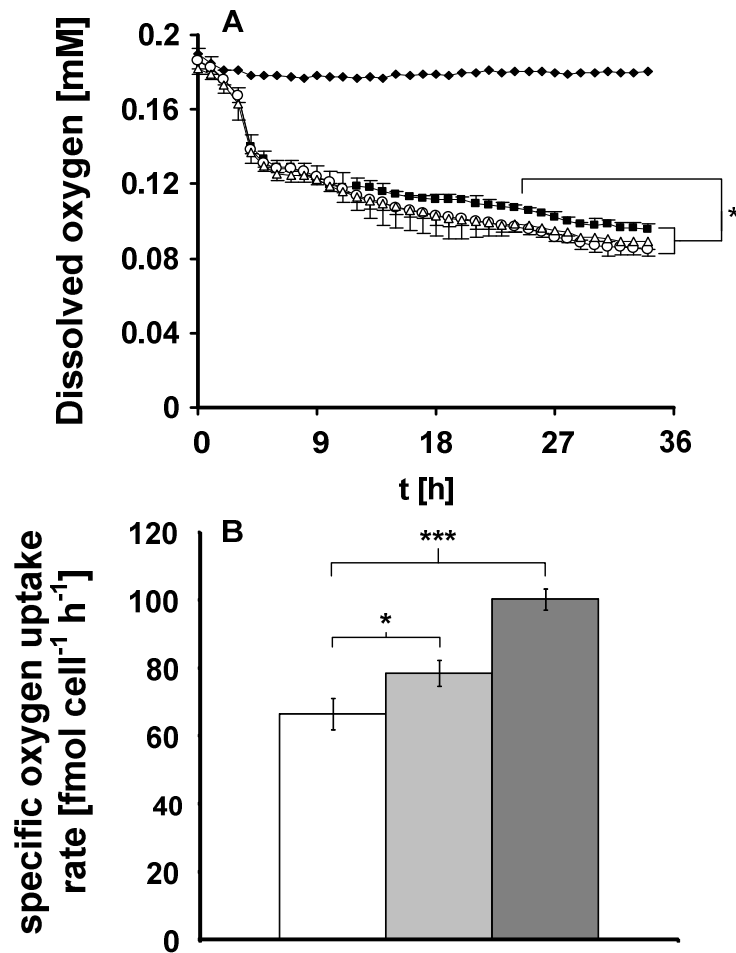


**Figure 5:** Influence of DXR on respiration in HL-1 cardiomyocytes. A) Course of dissolved oxygen in culture medium without cells (◆), untreated control (■), cells treated with 0.01 μM DXR (▲) and 0.02 μM DXR (●). Statistical significance was determined using repeated measures two-way ANOVA following Bonferroni posthoc test. B) Specific oxygen uptake rate in untreated cells (white bars), cells treated with 0.01 μM DXR (light grey bars) and cells treated with 0.02 μM DXR (dark grey bars). Significance was determined using one-way ANOVA following Dunnett's posthoc test. Measurements were carried out in triplicates. Significance is indicated at \*:  $p < 0.05$ ; \*\*\*  $p < 0.001$ .

#### *Influence of DXR on intracellular ATP concentration*

The influence of DXR on intracellular ATP concentration in whole cells extracts was measured at 2 h and 34 h after DXR exposure (Figure 6). After 2 h of incubation, ATP concentration was 16.2 pmol cell<sup>-1</sup> in untreated cells. In cells treated with 0.01 μM and 0.02 μM DXR, ATP concentrations was non-significantly decreased to 15.1 pmol cell<sup>-1</sup> and 15.2 pmol cell<sup>-1</sup> respectively. After 34 h ATP concentration was 13.7 pmol cell<sup>-1</sup> in untreated cells. No significant change of ATP concentration was observed in case of cells treated with 0.01 μM DXR (13 pmol

cell<sup>-1</sup>;  $p > 0.05$ ). However, in case of cells treated with 0.02  $\mu\text{M}$  a significant decrease of ATP concentration (11.2 pmol cell<sup>-1</sup>;  $p < 0.05$ ) was observed. The cell number was estimated using an SRB assay.

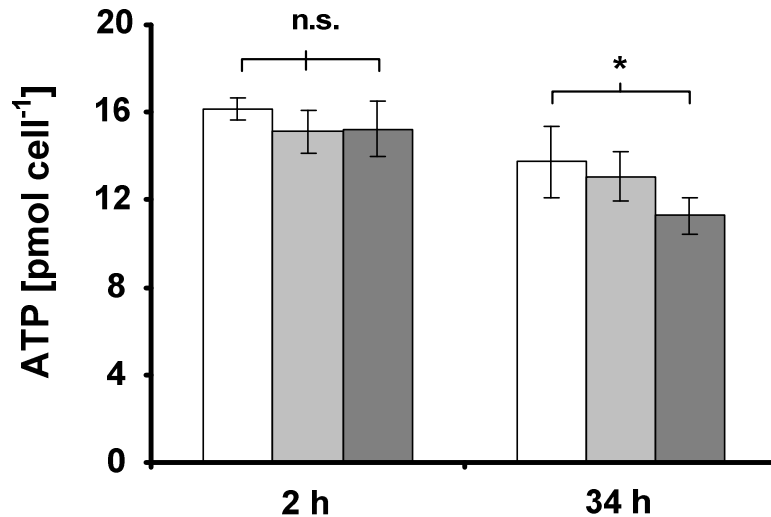


**Figure 6:** ATP-content (A) in untreated cells (white bars), cells treated with 0.01  $\mu\text{M}$  DXR (light grey bars) and 0.02  $\mu\text{M}$  DXR (dark grey bars) in HL-1 cardiomyocytes. ATP-concentration was determined using ATPlite assay. Cell number was estimated by sulforhodamine B staining. Error bars indicate standard deviations ( $n=4$ ). Statistical significance was determined using one-way ANOVA following Dunnett's posthoc test (\*:  $p < 0.05$ ).

### Discussion

In the present study we analyzed the effects of DXR on central energy metabolism in HL-1 cardiomyocytes. The DXR concentrations investigated were clearly not toxic in the LDH-release assay. Furthermore, it was recently shown that these concentrations do not result in significant Troponin T release (Andersson *et al.*, 2010). By using <sup>13</sup>C-metabolic flux analysis we found that DXR-concentrations as low as 0.01 and 0.02  $\mu\text{M}$  significantly affect glycolysis, TCA-cycle and amino acid catabolism *in vitro* in HL-1 cardiomyocytes.

Glycolytic rates in DXR treated cardiomyocytes decreased in a dose dependent manner. Down-regulation of phosphofructokinase at the transcriptional level upon DXR treatment was previously described in neonatal rat cardiomyocytes (Jeyaseelan *et al.*, 1997) and could partly explain decreased glycolytic rates. However, in the work of Jeyaseelan *et al.* DXR was applied at a concentration of 1  $\mu\text{M}$  which approximately represents the peak plasma concentration shortly after a bolus administration in cancer patients which declines relatively fast (within 1 h) to the lower nanomolar level (Greene *et al.*, 1983). DXR has a biphasic pharmacokinetic profile with

exposure of tissues without substantial clearance to extracellular free drug concentrations that are identical to plasma free drug exposure. Nowadays, *in vivo*, DXR is administered by intravenous infusion and the plasma concentration is much lower than 1  $\mu\text{M}$ . Most *in vitro* studies on DXR are carried out using high concentrations and do not necessarily reflect the situation *in vivo*. It is therefore important to investigate effects of DXR in the nanomolar range. Recent *in vivo* and *in vitro* transcriptomic studies at clinically relevant concentrations have demonstrated an upregulation of mRNA of several genes in the glycolytic pathway (Berthiaume and Wallace, 2007b; Tokarska-Schlattner *et al.*, 2010), which, at a first view, contradicts the observation of decreased glycolytic fluxes in our study. The level of the corresponding mRNA probably directly correlates with increased enzyme but not necessarily with enzymatic activity. While the upregulation of glycolytic genes in the work Berthiaume *et al.* and Tokarska-Schlattner *et al.* was in good agreement, corresponding data on TCA-cycle relevant mRNA from these two studies was conflicting. Contradictory data regarding DXR induced alterations in the fluxome or transcriptome might be related to different biological models or experimental setups. In addition, it has to be considered that DXR exerts diverse effects on energy metabolism both acutely and chronically. The transcriptomic *in vivo* study of Berthiaume *et al.* was carried out on isolated rat hearts upon 5 week chronic subcutaneous DXR treatment, whereby the heart weight was significantly decreased and the rats were in a poor health (Berthiaume and Wallace, 2007b). In the work of Tokarska-Schlattner *et al.* rat hearts were perfused with 2  $\mu\text{M}$  DXR for 2 h and the hearts showed mild cardiac dysfunction. This concentration highly exceeded the concentrations used in our study and the exposure to this relatively high concentration was longer than the observed peak plasma concentration in patients undergoing DXR treatment. Cardiac dysfunction independent of DXR exposure, contributes to increased glycolysis and glucose oxidation *in vivo* as shown previously (Lei *et al.*, 2004; Osorio *et al.*, 2002, review: Stanley, 2005). As such, care should be taken in the interpretation of results and cardiac damage should be taken into account. In our study there was no change in cell viability (LDH and SRB assays) and myocyte contraction/beating. Therefore, the changes in glycolytic fluxes in our study are due to DXR and not due to decreased cardiomyocyte viability and dysfunction.

In our study, the decreased glycolytic activity was accompanied by an increased oxidative decarboxylation (Pyruvate  $\rightarrow$  Acetyl-CoA) i.e. a higher flux of cytosolic pyruvate into mitochondria to form acetyl-CoA, which points towards an increase of glucose oxidation in DXR treated cells. Remarkably, the increased oxidative phosphorylation was facilitated by cytosolic

pyruvate entering the mitochondrion *via* two entry routes; firstly *via* direct entry into the mitochondrion through pyruvate transporter and secondly *via* cytosolic and mitochondrial malic enzyme. The anaplerotic entry of pyruvate into mitochondria *via* malic enzyme might make up for a saturated direct transport via mitochondrial pyruvate transporters and thus facilitate supply of TCA-cycle with sufficient carbon. An increased contribution of glucose carbon to mitochondrial acetyl-CoA upon DXR treatment was recently shown in a rat *in vivo* model (Carvalho *et al.*, 2010), which is in accordance with increased flux of pyruvate into mitochondrial acetyl-CoA, as observed in our study. In the study of Carvalho *et al.* it was shown that the increased contribution of glucose to acetyl-CoA is related to a decreased contribution of long chain fatty acids to acetyl-CoA. Decreased fatty acid oxidation has been generally linked to DXR-related cardiac toxicity (Abdel-aleem *et al.*, 1997; Bordoni *et al.*, 1999; Hong *et al.*, 2002; Iliskovic *et al.*, 1998). However, the uptake of fatty acids in HL-1 cardiomyocytes was relatively low for both untreated controls and DXR treated cells as compared to the glucose uptake (~0.1 %). Comparison of results should be considered with care as most studies on altered fatty acid uptake were carried out either on *in vivo* models or the applied DXR concentrations (Abdel-aleem *et al.*, 1997) highly exceeded the concentrations tested in our study. Nevertheless, it must be noted that the low uptake of fatty acids in HL-1 cardiomyocytes can be partly attributed to the low concentration of fatty acids in the used culture medium. Generally, glucose is the most abundant energy source in most cell culture media. The glucose concentration in the used culture medium was 25 mM. In contrast, the total fatty acid concentration in supplemented Claycomb medium mainly derived from 10% FBS, was only ~ 9  $\mu$ M, which is in the same range as recently reported for culture medium containing 10% FBS (Andersson *et al.*, 2008). In addition, cells cultured *in vitro* mainly use glucose to generate ATP (Marroquin *et al.*, 2007). However, the fact that fatty acid uptake was relatively low in both DXR-treated and untreated cardiomyocytes points to the fact that the higher contribution of glucose to acetyl CoA as observed in our considered *in vitro* model is most probably not related to altered fatty acid uptake.

The consequence of increased oxidative decarboxylation of mitochondrial pyruvate to form acetyl-CoA was significantly increased rates of TCA-cycle reactions in DXR treated cardiomyocytes. This increased oxidative metabolism was in accordance with an increased cell respiration. An up-regulation of TCA-cycle related genes upon DXR treatment was recently reported in perfused rat heart (Tokarska-Schlattner *et al.*, 2010) and might explain the increased TCA-cycle rates in our study, despite significant differences in the experimental setup. In

addition, a recent study (Pointon *et al.*, 2010) using a murine *in vivo* model showed increased activity of citrate synthase after acute DXR exposure which further supports the observation in our study. Though, several other studies on DXR induced alterations of respiration demonstrated decreased respiration (Bugger *et al.*, 2010; Nicolay and de Kruijff, 1987; Tao *et al.*, 2006). However, these studies were either carried out with much higher concentrations directly on whole cells (Tao *et al.*, 2006) or on isolated mitochondria, which have been shown to be different in their regulatory properties from mitochondria in the cell (Kuznetsov *et al.*, 2008; Picard *et al.*, 2010). Those reported effects, if occurring *in vivo*, might represent acute effects of DXR toxicity, e.g. when the concentration of DXR is relatively high in plasma within the initial hour of DXR application (Greene *et al.*, 1983).

The increase of TCA-cycle activity might be related to an early compensatory mechanism to the onset of functional defects as recently suggested (Tokarska-Schlattner *et al.*, 2010). Functional defects in conjunction with apoptotic events could include loss or depletion of high energy phosphates. Short term exposure (2 h) of cells to 0.01  $\mu\text{M}$  and 0.02  $\mu\text{M}$  DXR had no significant effect on cellular ATP concentration in our study. However, at 34 h, ATP concentration decreased at both concentrations of DXR, but only significantly at 0.02  $\mu\text{M}$  DXR. Recently decrease of ATP in murine *in vivo* model upon acute DXR exposure has been described (Pointon *et al.*, 2010). It can be assumed that increased TCA-cycle activity as well as respiration is a direct consequence of decreased levels of ATP. By increasing TCA-cycle activity the cells try to compensate for a decrease of intracellular ATP. However, we observed that increase of oxidative metabolism does not seem sufficient to completely compensate for ATP-decrease/depletion.

Besides depletion of ATP due to potential apoptotic events, reduction of DXR itself by mitochondrial NADH dehydrogenase by complex I in the respiratory chain might partially contribute to increased TCA-cycle activity. It is well established that DXR acts as an electron acceptor in reactions involving P450 reductase and NADH dehydrogenase (Doroshov, 1983; Goodman and Hochstein, 1977; Graham *et al.*, 1987). Addition of electrons to the DXR quinone group yields the semiquinone which after interaction with oxygen produces superoxides and other reactive oxygen species *in vitro* (Bates and Winterbourn, 1982; Doroshov, 1983; Sinha *et al.*, 1989) or results in electron shunting, more likely to occur *in vivo* as recently suggested (Pointon *et al.*, 2010). Pointon *et al.* argued that production of reactive oxygen species is more likely to occur *in vitro* than *in vivo* due to higher oxygen tension in most *in vitro* models. Electron shunting in case of DXR may involve electron transfer on DXR by complex I to form the

semiquinone and subsequent electron transfer downstream complex I, eventually to cytochrome C, thereby skipping electron transfer through complex II and III (Pointon *et al.*, 2010). Both scenarios would result in an uncoupling of electron transfer and building up of an H<sup>+</sup> gradient in the inner mitochondrial membrane and consequently decreased ATP concentration.

In brief, we show for the first time the effect of therapeutically relevant concentrations on the whole central metabolism including glycolysis, TCA-cycle and amino acid degradation in a cardiac cell model by means of <sup>13</sup>C metabolic flux analysis. Although <sup>13</sup>C flux studies have been carried out for the assessment of DXR's effect on the metabolism, the estimation of the flux distribution in cardiac cells upon DXR treatment *via* integration of a whole set of extracellular rates and <sup>13</sup>C labelling information into a metabolic network model has not been yet reported to our knowledge, least of all at concentrations as low as 0.01 μM. Most importantly, these concentrations had no significant effect on cell growth, beating frequency and cell morphology. Nevertheless, these tested therapeutically relevant concentrations result in an increased oxidative metabolism in HL-1 cardiomyocytes, i.e. a higher efficiency of glucose usage in TCA-cycle. This effect in HL-1 cardiomyocytes is most probably, not related to alterations in fatty acid uptake since it was negligible and was not significantly altered by DXR. In fact, changes in metabolic fluxes seem to occur due to decrease of intracellular ATP. The present work therefore complements and partly confirms recent *in vivo* data. Our results significantly contribute to the understanding of DXR induced cardiotoxicity which is more and more highlighted in the context of changes in energy metabolism. Further work including in depth studies of the role of reactive oxygen species in changes of metabolic fluxes would complement the observations in our study. In addition, it would be very interesting to apply <sup>13</sup>C metabolic flux analysis to human relevant system such as cardiomyocytes derived from human embryonic stem cells having both atrial and ventricular phenotypes which would more closely reflect the *in vivo* situation. This will greatly advance the understanding of mechanism of toxicity of DXR at the metabolic pathways level.

## Chapter 6

### Characterisation of the central metabolism in cardiomyocytes derived from human embryonic stem cells in response to Doxorubicin

#### Abstract

Doxorubicin (DXR) is a potent anticancer drug with severe cardiotoxic side effects, which are related to changes in the cardiac substrate spectrum, as shown in several animal *in vitro* models. However, animal models have a low validity in man. Therefore, human embryonic stem cell derived cardiomyocytes (hESC-CM) represent an ideal cardiac *in vitro* model for studying DXR induced cardiotoxicity. The purpose of this study was the metabolic characterization of untreated hESC-CM and of hESC-CM treated with a clinically relevant concentration of DXR by using <sup>13</sup>C metabolic flux analysis.

hESC-CM were incubated with and without 0.078  $\mu$ M DXR for 66 h. Uptake and production rates of glucose, lactate, pyruvate and amino acids from hESC-CM culture medium were determined using HPLC. The enrichment of <sup>13</sup>C in secreted lactate derived from feeding with [U-<sup>13</sup>C<sub>6</sub>]glucose was measured by GC/MS. Using metabolite rates, <sup>13</sup>C-labelling information in lactate and by presuming steady state conditions, intracellular fluxes were estimated in both untreated and DXR treated hESC CM.

Untreated hESC CM showed high activity of anaerobic glycolysis, which was reflected by a high lactate/glucose ratio (1.57) while fluxes in oxidative reactions were comparably low. Low TCA cycle activity was facilitated by high lactate and pyruvate production, but also by amino acid production i.e. by carbon loss from TCA-cycle. DXR treated cells showed reduced glycolytic fluxes and reduced lactate production. Though, the lactate/glucose ratio was increased (1.71). However, despite a higher lactate/glucose ratio, oxidative metabolism was significantly increased, which was facilitated by increased degradation of amino acids into TCA-cycle intermediates. These data partly agree with recent transcriptomic approaches. However, due to the high anaerobic glycolysis in the used hESC-CM, modifications in the cardiac differentiation protocol or design of adequate hESC-CM culture media should be considered for future studies.

**This chapter is in preparation for submission in *Toxicology and Applied Pharmacology*.**

## Introduction

Doxorubicin (DXR) is used as a potent anticancer drug. However, severe cardiotoxic side effects observed in cancer patients undergoing DXR treatment limit its clinical use (Simunek *et al.*, 2009). DXR-toxicity is related to formation of reactive oxygen species (Bachur *et al.*, 1977; Sinha *et al.* 1989), disturbances in nitric oxide pathway resulting in protein nitration (Fogli *et al.*, 2004), oxidative damage of DNA (Bates and Winterbourn, 1982; Eliot *et al.*, 1984; Feinstein *et al.*, 1993), lipid peroxidation (Gewirtz, 1999) and apoptosis (Ling *et al.*, 1993; Skladanowski and Konopa, 1993).

However, DXR induced cardiac toxicity also seems related to impaired cardiac energy metabolism, potentially leading to ATP-depletion. In the healthy myocardium ATP is mostly generated from oxidative metabolism (Stanley *et al.*, 2005). It was shown that DXR alters fatty acid and glucose metabolism in the myocardium (Abdel-aleem *et al.*, 1997; Bordoni *et al.*, 1999; Carvalho *et al.*, 2010; Wakasugi *et al.*, 1993). Recent transcriptomic approaches have shown alterations in the transcript levels of genes relevant in main catabolic pathways, such as glycolysis and TCA-cycle. It was recently shown that DXR results in increased transcripts of genes relevant in glycolysis (Berthiaume and Wallace, 2007b; Tokarska-Schlattner *et al.*, 2010). Though, results on TCA-cycle genes were contradictory. Such differences might be the result of differences in the biological models.

We have recently studied the effect of clinically relevant DXR concentrations on central metabolism of murine atrial HL-1 cardiomyocytes (Strigun *et al.*, 2011c). DXR resulted in an increased oxidative metabolism (increased TCA-cycle activity and respiration), probably as an attempt to compensate for a decreased intracellular ATP-concentration.

Despite the usefulness of HL-1 cells as a cardiac model system, the major drawback is their murine origin. Human embryonic stem cell derived cardiomyocytes (hESC-CM) have been suggested as an alternative for cardiac cell lines (Steel *et al.*, 2009). Primary cells from the human heart would be an alternative, but their availability is limited for obvious reasons. The use of hESC-CM probably circumvents the problem of species to species differences.

In terms of contractile characteristics hESC-CM have been shown to be similar to adult ventricular cells (Harding *et al.*, 2007). Though, it has been suggested that the maturation process of hESC-CM is not complete, since the Ca<sup>2+</sup>- handling properties in the excitation-contraction process do not seem to reflect the adult human myocardium (Binah *et al.*, 2007; Dolnikov *et al.*, 2006). Mature cardiomyocytes rely on intracellular sarcoplasmic Ca<sup>2+</sup> - stores for contraction,



while hESC-CM seem to rely on external calcium (Dolnikov *et al.*, 2006), most probably due to underdeveloped sarcoplasmic reticulum (Binah *et al.*, 2007; Satin *et al.*, 2008; Sedan *et al.*, 2008). However, a recent gene expression study has shown that hESC-CM clusters show similar expression patterns, compared to human cardiac tissue (Asp *et al.*, 2010). Ion channels, characteristic for the human myocardium, such as sodium channel SCN5A, the L-type calcium channel CACNA1C, the voltage-gated potassium channels KCNA4 and KCNH2 (hERG) have been found in hESC-CM (Sartiani *et al.*, 2007; Satin *et al.*, 2008). The availability of relevant ion channels as well as the ability for spontaneous contraction makes them attractive for preclinical drug testing based on electrophysiological measurement, as shown recently (Braam *et al.*, 2010; He *et al.*, 2003; Reppel *et al.*, 2005; Satin *et al.*, 2004).

Besides electrophysiological studies, hESC-CM can potentially be used to study drug-induced changes of cardiac energy metabolism and substrate usage. Although hESC-CM represent an attractive cardiac model system for metabolic, particularly metabolomic or fluxomic studies, a rather in depth quantification of central metabolism, i.e. in glycolysis, TCA-cycle or amino acid catabolism has not been carried out yet, least of all in the presence of drugs with known cardiotoxic properties, such as DXR.

The purpose of this study was the metabolic characterisation of untreated hESC-CM and DXR treated hESC-CM by means of <sup>13</sup>C metabolic flux analysis. The application of <sup>13</sup>C metabolic flux analysis has been shown to be useful for the determination of the effect of cardioactive drugs on HL-1 cardiomyocytes (Strigun *et al.*, 2011b; Strigun *et al.*, 2011c). The applicability of this method has been demonstrated in a recent study, which reported the flux distribution in the perfused mouse heart (Vo *et al.*, 2006). The results of the present study are compared with current knowledge of DXR induced effects on cardiac energy metabolism.

## Material and methods

### *hESC-CM cell culture*

The hESC-CMs were obtained from Cellartis (Sweden), within the framework of EU-STREP (LSHB-CT-2007-037636) project “Invitroheart”. The cells were delivered as adherent monolayer cultures and showed a beating phenotype. The cells were maintained in an optimized culture medium, referred to as hESC-CM medium in following chapters (The interested reader is asked to contact Cellartis for further information on the composition of the hESC-CM medium).

### *Determination of DXR cytotoxicity*

A doxorubicin-HCl (DXR) (Sigma Chemical, USA) stock solution (10 mM) was prepared in cell culture grade water (PAN Biotech, Germany).  $3 \times 10^4$  cells/well were maintained in 200  $\mu$ l medium containing 20% FBS. After ~72 hours (h) incubation, the supernatant was removed and the cells were washed once with fresh medium. Subsequently, medium containing DXR at different concentrations (1.25  $\mu$ M, 0.62  $\mu$ M, 0.32  $\mu$ M, 0.16  $\mu$ M, 0.078  $\mu$ M and untreated controls) was added to the cells in duplicates. Medium without cells served as medium control. For reduction of evaporation, the wells were covered with gas impermeable adhesive foils (Greiner, Germany). Subsequently, the cells were incubated for 66 h. Afterwards, the medium was removed and the cells were washed twice with 100  $\mu$ l of pre-warmed (37°C) PBS. Cells were then lysated in 100  $\mu$ l Cellytic M Cell Lysis reagent (Sigma Aldrich, USA) according to the manufacturer’s instructions. Total protein was determined with a detergent-compatible protein assay (Bio-Rad, Hercules, CA).

### *Experimental setup for labeling studies on hESC CM*

$3 \times 10^4$  cells/well were maintained in 200  $\mu$ l hESC-CM medium following 72 h incubation. Subsequently, the medium was removed and the cells were washed twice with 200  $\mu$ l of pre-warmed (37°C) PBS to remove contaminating lactate from the preincubation.

Instead of 25 mM naturally labeled glucose this medium contained 25 mM fully <sup>13</sup>C-labelled glucose ([U-<sup>13</sup>C<sub>6</sub>] glucose) (enrichment 99%) (Cambridge Isotope Laboratories, USA)). The plates were incubated under standard cell culture conditions (37 °C, 95 % relative humidity, 5 % CO<sub>2</sub>) in the incubator for 66 h. Afterwards, the supernatants were removed and stored at -20°C

until further analysis. The cells were washed once with 100 µl of pre-warmed (37°C) PBS and the total cell protein was quantified by using a protein assay (Bio-Rad, Hercules, CA).

### *Sample preparation for HPLC analysis and metabolite quantification*

Serum proteins, such as albumin were removed from the supernatants by microfiltration using Microcon<sup>®</sup> Filter Devices (Millipore, Germany) with an exclusion size of 10 kDa. Subsequently each filtrate was diluted 1:2 with α-aminobutyric acid solution (400 µM in deionized water) which was used as an internal standard for amino acid quantification. Quantification of glucose, lactate, pyruvate and amino acids was carried out exactly as described recently (Strigun *et al.*, 2011b).

### *Mass isotopomer measurement using GC/MS*

Measurement of mass isotopomers was carried out using gas chromatography (HP 6890 Hewlett Packard, USA) equipped with a HP-5 MS column (5 % phenyl-methyl-siloxanediphenylpolysiloxane, 30 m x 0.25 mm x 0.25 µm, Agilent, Germany) and coupled with a quadrupole mass spectrometer (MS 5973, Agilent, Germany). Sample preparation, measurement of mass distributions of lactate and calculation of mean mass isotopomer distributions was carried out using a recently reported procedure (Strigun *et al.*, 2011b).

### *<sup>13</sup>C flux analysis*

A carbon atom transition network of the central metabolism was set up for <sup>13</sup>C metabolic flux analysis for both untreated hESC-CM and DXR treated hESC-CM. (Appendix of chapter 6, Tab. S1 and Tab. S2). The estimation of fluxes was carried out with MATLAB 2008b (The Mathworks, USA) using the elementary metabolite unit concept (Antoniewicz *et al.*, 2007) applying a recently described method (Yang *et al.*, 2008).

*Statistical analysis*

Extra- and intracellular fluxes in HL-1 cardiomyocytes treated with 0.01  $\mu$ M and 0.02  $\mu$ M DXR were compared with the respective untreated controls using student's *t*-test. The changes were considered significant at  $p < 0.05$ .

**Results**

*Toxicity of Doxorubicin on hESC-derived cardiomyocytes*

DXR application on spontaneously beating hESC-CM resulted in a dose-dependant decrease of total cell protein after 66 h of exposure (Fig. 1). 0.078  $\mu$ M and 0.16  $\mu$ M DXR had no significant effect on cell protein compared to controls. 0.32 $\mu$ M, 0.62  $\mu$ M and 1.25  $\mu$ M DXR reduced total cell protein by 37%, 57% and 63%, respectively. The EC<sub>50</sub> value obtained from protein determination after 66 h of DXR exposure was 0.22  $\mu$ M (0.11  $\mu$ M – 0.44  $\mu$ M). A concentration of 0.078  $\mu$ M was considered for subsequent studies of metabolism in hESC-CM in response to DXR, since it resulted in no significant alteration of cellular protein and was clearly below the EC<sub>50</sub> value. At this concentration, the cells showed a beating phenotype comparably to untreated cells, as determined microscopically.

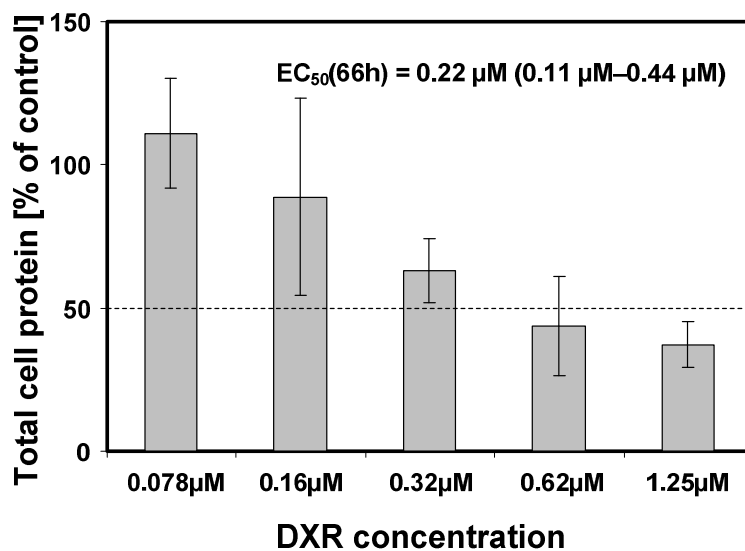


**Figure 1:** Effect of DXR on total cell protein of human embryonic stem cell derived cardiomyocytes after 66 h incubation. Total cell protein in each well was determined by Bradford assay. Measurements were carried out in duplicate measurement. The dotted line indicates 50% of viability as compared with untreated controls.

## *Metabolic response of hESC-CM to DXR treatment*

### *Glucose, lactate and pyruvate*

Figure 2A shows the effect of DXR on specific rates of glucose uptake as well as lactate and pyruvate production. Glucose was net consumed by both untreated and treated cells. Though, in treated cells glucose uptake was reduced by 28% (control: 53  $\mu\text{mol g}^{-1} \text{h}^{-1}$ ; DXR: 38  $\mu\text{mol g}^{-1} \text{h}^{-1}$ ;  $p < 0.01$ ). Lactate production was by 22% lower in treated cells (control: 84  $\mu\text{mol g}^{-1} \text{h}^{-1}$ ; DXR: 65  $\mu\text{mol g}^{-1} \text{h}^{-1}$ ). However, this change was not significant. Lactate/glucose yields were quite high in both treated and untreated cells. This ratio was 1.57 in untreated cells and 1.71 in treated cells.

Pyruvate was produced at both conditions, however, production was by 28% lower in treated cells (control: 15  $\mu\text{mol g}^{-1} \text{h}^{-1}$ ; DXR: 11  $\mu\text{mol g}^{-1} \text{h}^{-1}$ ;  $p < 0.05$ ).

### *Amino acids*

DXR treatment had diverse effects on amino acid consumption and production (Fig. 2 B). Amongst the amino acids, alanine, glutamine, glutamate, glycine, proline and arginine were net produced in untreated cells, while leucine and aspartate were net consumed from the culture medium. Most significant effects due to DXR were observed for alanine, glutamine, glycine, tyrosine, arginine, histidine, phenylalanine, lysine and leucine.

Alanine production was highly reduced in DXR treated cells (control: 5.7  $\mu\text{mol g}^{-1} \text{h}^{-1}$ ; DXR: 3.1  $\mu\text{mol g}^{-1} \text{h}^{-1}$ ;  $p < 0.001$ ). Glutamine was produced by untreated cells (3.9  $\mu\text{mol g}^{-1} \text{h}^{-1}$ ) but consumed by DXR treated cells (1.2  $\mu\text{mol g}^{-1} \text{h}^{-1}$ ,  $p < 0.001$ ). Production of glutamate and proline was not significantly different. Glycine was produced by controls (1.5  $\mu\text{mol g}^{-1} \text{h}^{-1}$ ) but consumed by treated cells (1.5  $\mu\text{mol g}^{-1} \text{h}^{-1}$ ;  $p < 0.001$ ). While no significant uptake of isoleucine could be determined, uptake of leucine was significantly higher in DXR treated cells (control: 1.75  $\mu\text{mol g}^{-1} \text{h}^{-1}$ ; DXR: 4.2  $\mu\text{mol g}^{-1} \text{h}^{-1}$ ;  $p < 0.05$ ). Similarly, uptake of aspartate and tryptophane was higher in DXR treated cells (Aspartate; control: 0.64  $\mu\text{mol g}^{-1} \text{h}^{-1}$ ; DXR: 1.3  $\mu\text{mol g}^{-1} \text{h}^{-1}$ ;  $p < 0.05$ ; Tryptophane; control: 0.1  $\mu\text{mol g}^{-1} \text{h}^{-1}$  DXR: 0.43  $\mu\text{mol g}^{-1} \text{h}^{-1}$ ). No significant uptake of lysine and phenylalanine could be determined. However, uptake of these amino acids was significantly increased in treated cells ( $p < 0.001$ , respectively)

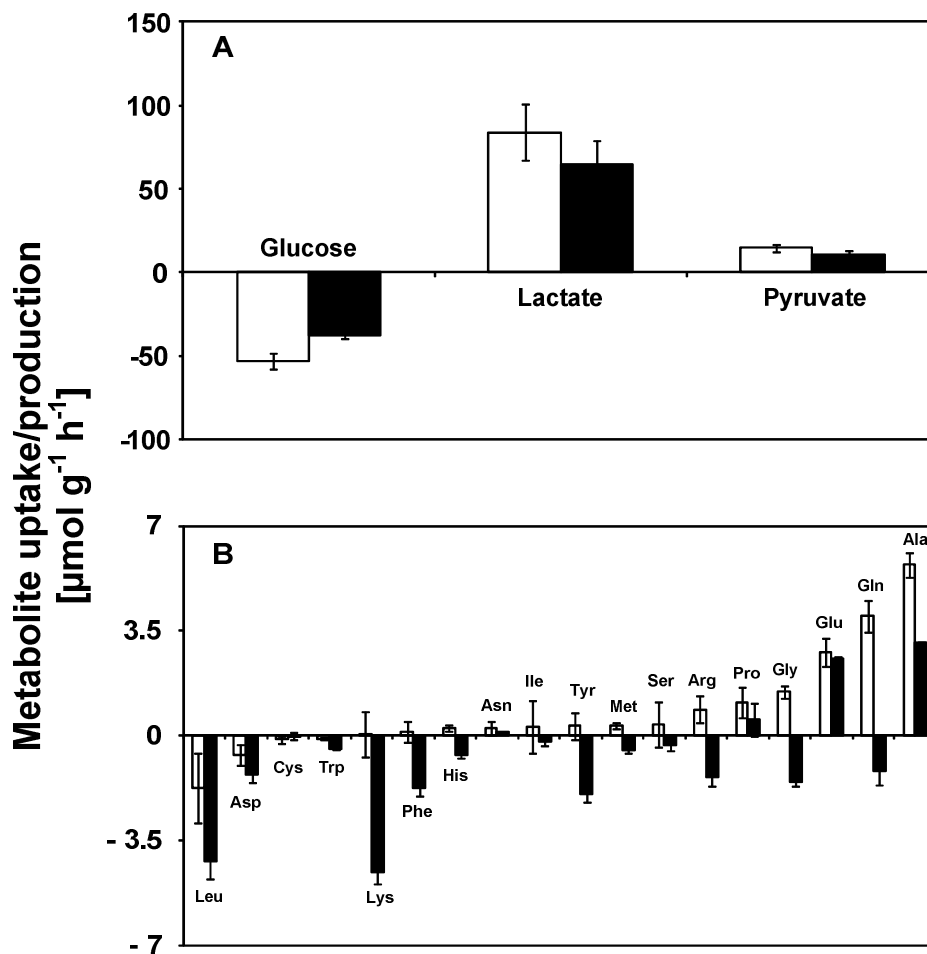


**Figure 2:** Metabolite uptake and production rates in untreated hESC-CM (white bars) and in hESC-CM treated with 0.078 μM DXR (black bars). (A) Effect of DXR on glucose, lactate and pyruvate rates, (B) Effect of DXR on amino acid rates. Negative and positive values refer to uptake and production, respectively. Rates were calculated from metabolite depletion/enrichment in culture medium and total protein amount after 66 h incubation. Measurements were carried out in duplicates.

### *Intracellular fluxes*

For the estimation of the influence of DXR on intracellular fluxes in hESC-CM, cells were fed with universally <sup>13</sup>C labelled glucose ([U-<sup>13</sup>C<sub>6</sub>]glucose) without DXR and with 0.078 μM DXR. The mass isotopomer distribution of lactate was measured upon 66 h of incubation using GC/MS. As apparent from Fig. 3 an enrichment of lactate containing single (m+1), double (m+2) and fully labelled lactate (m+3) could be observed. Though, independent of DXR treatment, the fraction of fully labelled lactate was highly exceeding both, single and double labelled lactate.

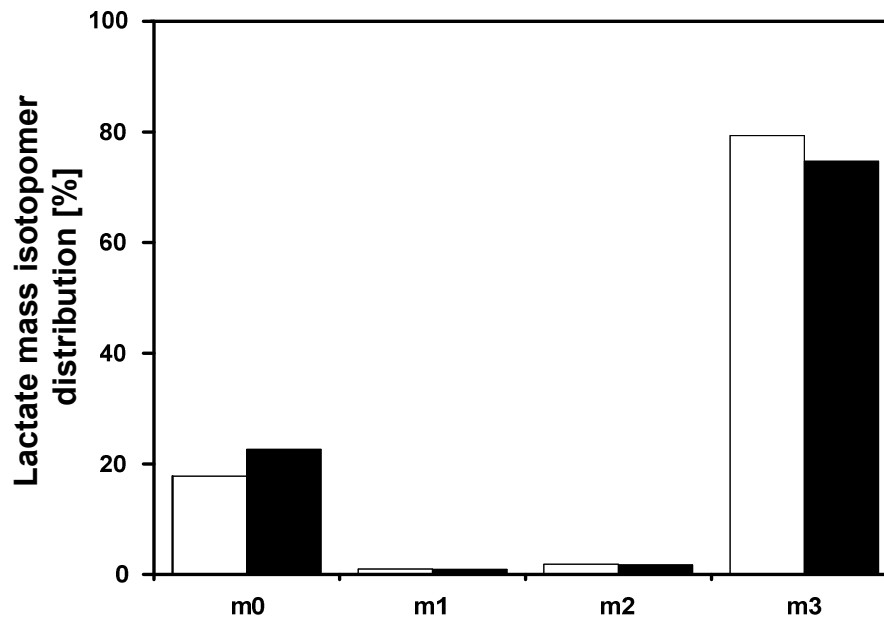


**Figure 3:** <sup>13</sup>C mass isotopomer distribution in lactate secreted by hESC-CM after 66 h incubation with fully <sup>13</sup>C-labelled glucose ([U-<sup>13</sup>C<sub>6</sub>]glucose) in controls (white bars) and in cells exposed to 0.078 μM DXR (black bars). All values were determined from duplicate measurement. The carbon skeleton of lactate consists of three carbon atoms, which gives four mass isotopomers (m0-m3). m0: unlabelled lactate; m1: single labelled lactate; m2: double labelled lactate; m3: fully/triple labelled lactate.

The mass distribution in secreted lactate together with the extracellular yields of glucose, lactate and amino acids were used for calculation of intracellular fluxes in untreated hESC-CM and in DXR treated hESC-CM using the metabolic network shown in table S1 and table S2 (Appendix of chapter 6).

Figure 4 shows the net intracellular fluxes in treated and untreated cells. Changes of fluxes were determined in all considered pathways (glycolysis, TCA-cycle, amino acid degradation). Glycolytic fluxes (G6P→3PG, 3PG→PYR) were decreased by 28% in treated cells ( $p < 0.001$ ). Oxidative decarboxylation (PYR→AcCoA) was relatively small in both treated and untreated cells and no significant difference could be determined. TCA-cycle fluxes in untreated cells were relatively small and merely accounted for 8%-17% of glycolytic fluxes. In DXR treated cells the flux of oxaloacetate and acetyl-CoA to form citrate in the TCA-cycle was significantly increased by 200% ( $p < 0.05$ ). This increase was facilitated by a significant increase of lysine and leucine degradation to acetyl-CoA ( $p < 0.05$ ), but also by reduced secretion of pyruvate. The fluxes in subsequent TCA-cycle reactions (CIT→AKG; AKG→SUC; SUC→OAA) were similarly increased ( $p < 0.05$ ). Unlike controls, TCA-cycle fluxes in DXR treated cells accounted for 40%-

80% of glycolytic fluxes. Apart from leucine and lysine, the relatively high uptake and catabolism of other amino acids also contributed to the higher TCA-cycle activity in DXR treated cells. The flux of phenylalanine and tyrosine into succinate was highly increased by 105% and 83%, respectively ( $p < 0.05$ ). Though, the most significant change was determined around TCA-cycle intermediate  $\alpha$ -ketoglutarate. While a net flux of  $\alpha$ -ketoglutarate towards glutamate was determined in untreated cells, which contributed to carbon loss in the TCA-cycle, this flux was reversed in treated cells ( $p < 0.05$ ), pointing towards increased anaplerosis of the TCA-cycle in case of treated cells. In addition, metabolism of arginine, histidine, glutamine and proline, which are catabolised to glutamate, also showed significant changes. Interestingly, a net flux of glutamate to glutamine was observed in untreated cells. This flux was reversed in DXR-treated cells ( $p < 0.001$ ).



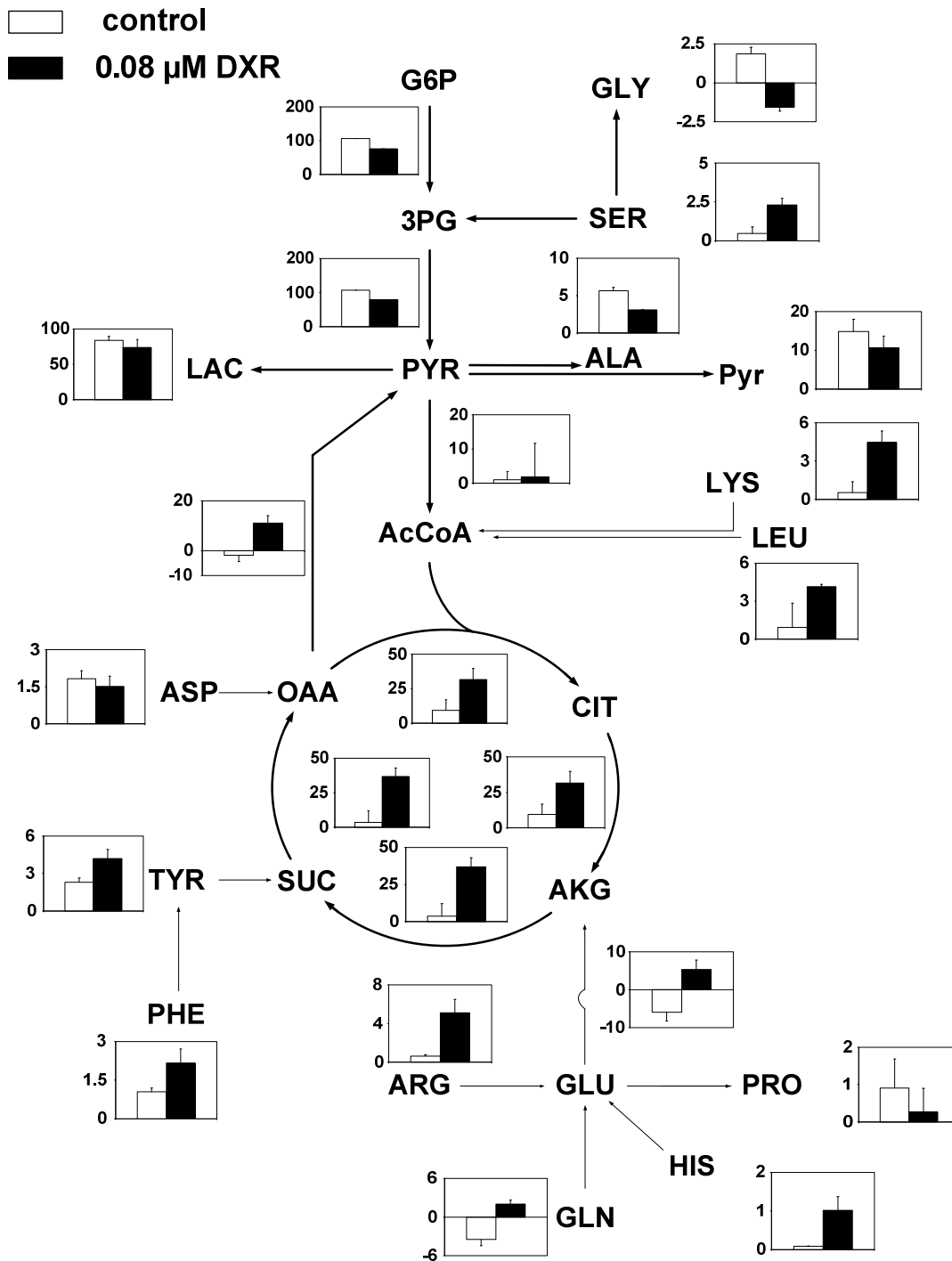


**Figure 5:** Effect of DXR (0.078 μM) on main catabolic pathways of human embryonic stem cell derived cardiomyocytes. hESCM were incubated with and without DXR in the presence of fully <sup>13</sup>C labelled glucose ([U-<sup>13</sup>C<sub>6</sub>]glucose) for 66 h. Metabolite uptake and production in hESC-CM culture medium as well as <sup>13</sup>C enrichment in secreted lactate were then measured by HPLC and GC/MS. The data was then implemented into a simplified metabolic model containing main reactions from glycolysis, TCA-cycle and amino acid catabolism for calculation of fluxes. All rates are given in μmol g<sup>-1</sup> protein h<sup>-1</sup>.

## Discussion

The presented work shows the effect of DXR on the metabolism of cardiomyocytes derived from human embryonic stem cells (hESC-CM). Similar to our recent work using a murine cardiac cell line (HL-1 cells) the considered DXR concentration for metabolic studies was clearly below the EC<sub>50</sub> value, which was approximately between 0.11 μM – 0.44 μM after 66 h of exposure. The lowest concentration of 0.078 μM DXR had no significant effect on the amount of cell protein after 66 h exposure and was used for further analysis of the effect of DXR on hESC-CM metabolism. As in our recent study regarding metabolic effect of DXR in HL-1 cells, this concentration was also in the range of clinical relevancy (Greene *et al.*, 1983).

The rather high lactate/glucose ratio in untreated cells (1.57) as well as <sup>13</sup>C metabolic flux analysis suggest a high anaerobic metabolism in untreated cells. This is substantiated by a high extracellular enrichment of fully/triple labelled lactate, which is directly derived from the fully labelled glucose and which approximately accounted for ~80% of total produced lactate. The high anaerobic metabolism in untreated cells was accompanied by a quite low TCA-cycle activity, though loss of carbon via secretion of pyruvate as well as net synthesis and secretion of amino acids derived from TCA-cycle intermediates contributed its low activity. The observed “Warburg-like effect” in untreated cells was rather surprising, given that the healthy myocardium generates the vast majority of its ATP by oxidative metabolism (Stanley *et al.*, 2005). Generally, anaerobic glycolysis seems to be sufficient for embryonic stem cell homeostasis (Chung *et al.*, 2007). However, engagement of oxidative metabolism seems to be a prerequisite for the differentiation of stem cells into a functional cardiac phenotype (Chung *et al.*, 2007). Dissolved oxygen concentration in our experimental setup was sufficient to exclude hypoxia as a potential reason for the high anaerobic glycolysis (dissolved oxygen > 50% air saturation, data not shown). However, the observed anaerobic glycolysis still allowed a contracting phenotype.

The presented data suggests that the used hESC-CM somehow share similarities with pluripotent stem cells on the metabolic level. While similarities of hESC-CM with human cardiac tissue on the transcriptomic level was recently demonstrated (Asp *et al.*, 2010), other recent studies on hESC-CM have suggested that these cells differ from adult human myocardium regarding the Ca<sup>2+</sup>-handling in excitation-contraction coupling (Binah *et al.*, 2007; Dolnikov *et al.*, 2006), most probably due to an immature sarcoplasmic reticulum capacity (Binah *et al.*, 2007).

hESC-CM treated with DXR showed a decreased glycolytic flux. A similar effect could also be observed in a recent study using HL-1 cardiomyocytes (Strigun *et al.*, 2011c). The reason for the

observed decrease of glycolytic flux remains to be determined, but may involve DXR induced alterations of relevant mRNA levels of glycolytic genes. In fact, it has been shown that DXR alters mRNA levels of glycolytic genes in animal cardiac *in vivo* models (Berthiaume and Wallace, 2007b; Tokarska-Schlattner *et al.*, 2010).

Despite a decreased glucose uptake and lactate production in DXR treated cells, the average amount of mole lactate per mole glucose was slightly higher (lactate/glucose ratio: 1.71). This points towards a decreased oxidation of glucose carbon in the TCA-cycle. Nevertheless, the flux of pyruvate to acetyl-CoA (oxidative decarboxylation) was similar at both conditions. Thus, the higher lactate/glucose ratio was mainly facilitated by a significant increase of the TCA-cycle activity as well as a high cataplerotic flux from either malate or oxaloacetate to cytosolic pyruvate. A higher cataplerotic flux to pyruvate might circumvent depletion of cytosolic pyruvate pools, as a result of decreased glucose uptake. This would also explain the slightly decreased secretion of alanine and pyruvate, which additionally prevents a depletion of intracellular pyruvate. The maintenance of intracellular pyruvate pools might allow the cells to still rely on anaerobic glycolysis, since this energy-pathway needs pyruvate for NADH-oxidation to form lactate. The higher TCA-cycle activity in DXR treated cells is mainly due to an increased catabolism of amino acids into relevant intermediates, such as leucine and lysine flux to acetyl-CoA but also  $\alpha$ -ketoglutarate and succinate. Most importantly, glutamine was secreted by untreated cells, while DXR treated cells showed a net uptake of glutamine, which therefore contributed to an increased TCA-cycle activity. Thus, DXR treated cells revealed a significant shift towards oxidative metabolism independent of glucose carbon. However, an increased TCA-cycle flux might also prevent DXR-induced depletion of intracellular ATP, as suggested recently (Strigun *et al.*, 2011c; Tokarska-Schlattner *et al.*, 2010).

In summary, this work shows for the first time the influence of a clinically relevant concentration of DXR on the metabolism of hESC-CM. However, the clinical relevancy of the observed effect is questioned by the fact that both untreated and DXR-treated hESC-CM highly rely on anaerobic glycolysis. Preferably, the used hESC-CM should mimic adult myocardial cells in terms of their energy metabolism, especially when considering that the healthy myocardium mainly relies on oxidative metabolism. However, by using medium design strategies the metabolism of the hESC-CM potentially could be altered to a state which more reflects the metabolism of the adult human cardiomyocyte. In the used hESC-CM medium, glucose was the dominating substrate and its concentration highly exceeded the concentration of other metabolites (e.g. amino acids). The

relatively high concentration of glucose, which was 25 mM (standard glucose concentration in commercially available DMEM medium), might partly contribute to the observed high anaerobic glycolysis. In fact, this glucose concentration exceeds the blood glucose concentration in healthy, non-diabetic adults (4.0–5.9 mM)(Ceriello *et al.*, 2008) Thus, future studies on hESC-CM energy metabolism should take into account an adequate glucose concentration. Besides, fatty acids and lipids are the main energy source in the human myocardium and it has been shown that the average fatty acid concentration in human plasma is in the lower mM range (Kuriki *et al.*, 2006). However, culture medium which contains 10%-20% FBS (as was used for this study) merely contains fatty acids in the lower  $\mu$ M range (as shown in Chapter 5 and in (Andersson *et al.*, 2008)). Thus, when applying metabolic studies on hESC-CM, a higher concentration of fatty acids should be considered. An optimal ratio between fatty acids and glucose, which mimics the ratio in human plasma, might result in a substrate usage which more reflects the cardiac *in vivo* situation in man and thus, gives more reliable results, when the assessment of the effect of drugs on cardiac energy metabolism is desired.

## Chapter 7

### Concluding remarks

It is assumed that alterations in cardiac energy metabolism either due to disease or drugs result in cardiac dysfunction (Stanley *et al.*, 2005). While several studies report alterations of metabolism in the diseased heart (Ashrafian *et al.*, 2007; Gertz *et al.*, 1988; Mudge *et al.*, 1976; Panchal *et al.*, 2001; Randle *et al.*, 1964; Stanley *et al.*, 1997; Wisneski *et al.*, 1985), holistic descriptions of the cardiac energy metabolism in response to cardioactive/toxic drugs are rare.

The presented work describes the assessment of the effects of drugs with known clinical cardiac toxicity on two cardiac *in vitro* model systems, namely HL-1 cardiomyocytes and human embryonic stem cell derived cardiomyocytes (hESC-CM) by using metabolic profiling (metabolomics) and <sup>13</sup>C-metabolic flux analysis. In addition, respiration measurement was used for cell viability measurements. The combination of all three methodologies allowed the assessment of the effect of cardiotoxic drugs on the metabolism of the two model cell types. However, the focus was clearly set on HL-1 cells due to their ready availability. Unlike hESC-CM the source of HL-1 cells is not limited. Due to the limited availability of hESC-CM not all studies could be carried out on these cells in such detail as for HL-1 cells.

Parts of the thesis were published as three scientific papers (Strigun *et al.*, 2011a; Strigun *et al.*, 2011b; Strigun *et al.*, 2011c). Two manuscripts are in preparation for submission.

#### **Cytotoxicity screening of cardioactive drugs on murine HL-1 cardiomyocytes**

In the first part of this study the effect of cardioactive drugs on the respiration in HL-1 cardiomyocytes was determined by using oxygen-sensitive fluorescent sensors (Optodes). These optodes have been described as a convenient alternative to common cytotoxicity assays (e.g. WST-1, MTT, Alamar Blue) when the determination of EC<sub>50</sub> dynamics of drugs is desired (Beckers *et al.* 2009; Noor *et al.*, 2009; Wolf *et al.*, 2011). However, a direct comparison of EC<sub>50</sub> dynamics of drugs with similar or different mechanism of action or toxicity has not been reported yet. The first part of the thesis shows for the first time EC<sub>50</sub> dynamics of several cardioactive/toxic drugs. Significant differences in the EC<sub>50</sub>-dynamic profiles could be determined, which partly depend on the mechanism of action or toxicity of the drugs. The

distinct differences in the dynamic profiles suggest that preclinical *in vitro* studies on drug toxicity (independent of the cell model) should include measurement of EC<sub>50</sub> dynamics, since such profiles potentially allow conclusions whether the toxic effect of a drug occurs directly or with a certain delay. The presented results suggest that the determination of EC<sub>50</sub> dynamics gives information on the mechanism of toxicity of a drug or chemical.

### **Metabolic profiling of HL-1 cardiomyocytes in response to cardiotoxic drugs**

In the second part of this study HPLC-based metabolomics was used to assess whether drugs create specific profiles in the extracellular metabolome of HL-1 cells. The metabolome was measured at drug concentrations which were not cytotoxic. This methodology included the measurement of culture medium metabolites after a specific time of exposure and the subsequent data evaluation using common statistical multivariate procedures e.g. principal component analysis. This study shows that a targeted metabolomics approach, in which the considered sub-profile merely consists of nutrients available in most common cell culture media (glucose, pyruvate, amino acids), is sufficient to classify drugs according to their known mechanism of action. The presented results suggest that this approach also provides indications on the mechanism of toxicity of a new drug compound.

### **<sup>13</sup>C metabolic flux analysis in HL-1 cells upon exposure to Doxorubicin and Verapamil**

The first drug which was considered in the flux analysis approach was the calcium channel blocker verapamil. Although clinical cardiotoxic reports on this drug are rare and mainly involve overdoses, this drug was quite interesting for flux studies for several reasons. First, metabolic profiling revealed a unique effect of verapamil on glucose and lactate metabolism and second, fluxomic studies clarified the consequences of this effect on the central metabolism. <sup>13</sup>C flux analysis on HL-1 with and without verapamil was successfully carried out and gave a holistic description of the effect of verapamil on central metabolism. At the applied conditions, verapamil resulted in a highly decreased glucose uptake which was accompanied by a halt of lactate production. This effect allowed the cells to maintain the TCA-cycle- as well as respiratory activity and thereby maintenance of cell growth similar to untreated cells. Thus, the verapamil-induced decrease of glucose uptake resulted in an efficient use of available glucose

carbon. This is especially of importance when considering that HL-1 cells highly rely on anaerobic glycolysis under normal conditions (i.e. high lactate production). These results were published (Strigun *et al.*, 2011a) and have been discussed extensively there. However, although verapamil highly influenced glucose and lactate metabolism of HL-1 cardiomyocytes, a direct correlation to clinically observed toxicity of verapamil could not be made. Although, several recent reports showed an inhibiting influence of verapamil on glucose uptake in several cell types, these studies were not carried out in the context of cardiotoxicity related research. Thus, in the published work, the effects of verapamil on HL-1 metabolism were not discussed in the context of cardiotoxic research, but in the context of cancer research and of potential biotechnological applications. Inhibition of glucose uptake along with the observed effects on lactate metabolism might contribute to verapamil's potential usefulness as an anticancer drug which has been recently proposed (Zhang *et al.*, 2009). Second, verapamil induced inhibition of glucose uptake and the observed halt of lactate production might be exploited in the field of bioproduction of therapeutical proteins using mammalian cell lines, which often show high lactate production i.e. inefficient use of glucose. Further work is necessary on relevant cell lines to assess this potential.

Like verapamil, doxorubicin highly influenced the extracellular metabolome of HL-1 cardiomyocytes at sub-toxic concentrations. The fact that doxorubicin shows high cardiotoxicity in cancer patients undergoing DXR treatment and the assumption that doxorubicin highly influences cardiac energy metabolism (Tokarska-Schlattner *et al.*, 2006) additionally motivated an extended fluxomic characterisation by means of  $^{13}\text{C}$ -metabolic flux analysis. The most important finding of this study was that doxorubicin significantly increases activity of the TCA-cycle as well as respiration, apparently to prevent doxorubicin induced depletion of ATP in HL-cells. Unlike most recent studies, the analysis was carried out at clinically relevant concentrations that are considered non-toxic. This was facilitated by the high sensitivity of the GC/MS-based flux analysis approach. The results of this study were recently published (Strigun *et al.*, 2011c) and have been extensively discussed in the context of current knowledge regarding doxorubicin cardiotoxicity. The presented results give additional weight to the assumption that doxorubicin deteriorates cardiac energy metabolism. If occurring *in vivo* in patients undergoing doxorubicin treatment, depletion of cardiac ATP might be exacerbated by other reported metabolic effects, such as doxorubicin-induced decrease of fatty acid oxidation.

### **<sup>13</sup>C metabolic flux analysis in human embryonic stem cell derived cardiomyocytes upon exposure to Doxorubicin**

Reliable *in vitro* cardiotoxicity testing necessitates cardiac models which closely mimic human cardiac tissue. Human embryonic stem cell derived cardiomyocytes have been suggested as a convenient alternative to isolated primary cells from either human or animal origin.

Since the healthy human heart covers the majority of its ATP demand by oxidative metabolism, *in vitro* cardiac cell models should also share this metabolic phenotype. This is especially of importance when the reliable *in vitro* determination of drug induced changes in cardiac energy metabolism is desired.

In this work the central energy metabolism of hESC-CM and its alteration due to the anticancer drug doxorubicin was studied by using <sup>13</sup>C metabolic flux analysis.

Untreated cells seemed to cover the majority of their ATP-demand by anaerobic glycolysis i.e. the flux of glucose carbon into the TCA-cycle was relatively low. The TCA-cycle was mainly fuelled by catabolism of amino acids. This result suggests further optimisation of the cardiac differentiation process, or alternatively, a proper design of adequate cultivation media.

However, treatment of the cells with doxorubicin showed significant alterations of the intracellular metabolism, similar to HL-1 cells treated with doxorubicin. The cells showed a more efficient use of glucose carbon, i.e. less lactate secretion and increase oxidative decarboxylation as well as a higher TCA-cycle flux. This increase might be the result of either formation of reactive oxygen species or electron shunting (uncoupling of respiration), and consequently, an attempt of the cells to compensate for ATP-depletion.

In summary, the presented study shows that application of metabolic profiling and <sup>13</sup>C metabolic flux analysis, combined with respiration measurement, allows the assessment of drug induced changes of cardiac energy metabolism. The presented results suggest that preclinical *in vitro* studies regarding drug-induced cardiotoxicity by electrophysiologically based methods should be complemented by assessment of cardiac energy metabolism.



## Chapter 8

### Outlook

Respiration measurement was carried out on HL-1 cells by using oxygen-sensitive fluorescent optodes. The EC<sub>50</sub> dynamics of the considered drugs could partly be explained by current literature knowledge regarding their general toxicity or more specifically, their cardiotoxicity. However, when the EC<sub>50</sub> dynamic of a new chemical/drug with unknown mechanism of toxicity is determined it will merely give information whether the onset of toxicity occurs either fast or slow. Prediction of its mechanism of general toxicity or cardiotoxicity might necessitate the screening of a rather extensive library of training compounds with known *in vitro* or *in vivo* toxicity/cardiotoxicity. Besides that, EC<sub>50</sub> values should be determined as exactly as possible, i.e. the number of considered drug concentrations should be higher than the number considered in this study (6-9 drug concentrations). Such an approach would require a higher throughput format, such as 384-well plates or even higher. In addition to the potential prediction of the toxicity mechanism of a drug, one could also establish mathematical models that describe the relationships between drug concentrations, death kinetics, toxicity delay time and the course of dissolved oxygen. Such relationships might show distinct characteristics (linear, asymptotical, sigmoidal etc.) depending on the toxicity mechanism of a drug. Such information might be very useful for *in vitro* safety pharmacological studies, but could also be used for a more detailed determination of a drug's toxicity mechanism.

Metabolic profiling of culture supernatants containing HL-1 cells was carried out upon exposure to drugs. The metabolic profiles were dependant on the drug class, thereby allowing classification of drugs according to their mechanism of toxicity. However, the used data set in the present work was limited and included merely a set of ten drugs. The establishment of extensive models for prediction of completely unknown compounds classification would probably need a rather extended set of training compounds. Moreover, using a similar profiling approach with an extended set of drugs, the risk of unknown compounds/new pharmaceuticals for cardiac side effects might be reliably assessed when applying classification on the basis of clinically observed side effects, such as QT-prolongation or cardiac arrest.

<sup>13</sup>C metabolic flux analysis has shown a clear effect of the cardioactive drug verapamil on the central metabolism of HL-1 cardiomyocytes. The actual mechanism by which verapamil inhibited glucose uptake was not determined in this study, but may involve direct inhibition of glucose transporters. Additionally there is evidence that verapamil and other channel blockers inhibit expression of hypoxia inducible factor (HIF1) at normoxic and hypoxic conditions (Bharadwaj *et al.*, 2002). Elevated glucose consumption, has been associated with elevated (HIF1- $\alpha$ ) levels in human breast cancer cell lines, while depression of HIF1-  $\alpha$  levels resulted in an inhibition of anaerobic glycolysis (Robey *et al.*, 2005). This might be an explanation for verapamil induced reduction in glucose uptake, which, however, has not been studied so far to our knowledge and should be the focus of following research in this regard.

The effect of doxorubicin on the central metabolism of HL-1 cells was determined by <sup>13</sup>C metabolic flux analysis. In the presented work it was pointed out that either doxorubicin induced production of reactive oxygen species or a mechanism referred to as “electron shunting” might be responsible for increased TCA-cycle activity and respiration. Both effects would result in an uncoupling of electron transfer to oxygen from oxidative phosphorylation and thus, decreased ATP-production. While formation of reactive oxygen species is highly associated with doxorubicin-cardiotoxicity (Simunek *et al.*, 2009), more recent studies have suggested that electron shunting is more likely to occur *in vivo* (Pointon *et al.*, 2011). It will be interesting to determine whether formation of reactive oxygen species occurs in the tested experimental setup and whether the application of appropriate antioxidants compensates the observed effects.

<sup>13</sup>C metabolic flux analysis on human embryonic stem cell derived cardiomyocytes revealed that these cells highly rely on anaerobic glycolysis. However, by using medium design strategies the metabolism of the hESC-CM potentially could be altered to a state which more reflects the metabolism of the adult human cardiomyocyte (i.e. aerobic metabolism). In the used medium, glucose was the dominating substrate and its concentration highly exceeded the concentration of other metabolites (e.g. amino acids) which might contribute to the observed high anaerobic glycolysis. In fact, glucose concentration in common culture media (e.g. DMEM) exceeds the blood glucose concentration in healthy, non-diabetic adults (Ceriello *et al.*, 2008)). Future studies on hESC-CM energy metabolism should take into account an adequate glucose concentration. In addition, fatty acids and lipids are the main energy source in the human myocardium and it has been shown that the fatty acid concentration in culture medium containing FBS is much lower than in human plasma. Thus, when applying metabolic studies on hESC-CM, a higher

concentration of fatty acids should be used. An optimal ratio between fatty acids and glucose, which mimics the ratio in human plasma, might result in a substrate usage which more reflects the cardiac *in vivo* situation in man and thus, gives more reliable results, when the assessment of the effect of drugs on cardiac energy metabolism is desired. However, treatment of the cells with doxorubicin showed significant alterations of the intracellular metabolism, similar to HL-1 cells treated with doxorubicin. Though, besides ATP-measurement, it will be interesting to study whether the altered TCA-cycle activity is accompanied by altered cell respiration and whether ROS-formation plays a significant role in the observed effects.

---

## References

- Abdel-aleem, S., el-Merzabani, M. M., Sayed-Ahmed, M., Taylor, D. A. and Lowe, J. E. (1997). Acute and chronic effects of adriamycin on fatty acid oxidation in isolated cardiac myocytes. *J. Mol. Cell Cardiol.* 29, 789-97.
- Alfarano, C., Sartiani, L., Nediani, C., Mannucci, E., Mugelli, A., Cerbai, E., Raimondi, L. (2008). Functional coupling of angiotensin II type 1 receptor with insulin resistance of energy substrate uptakes in immortalized cardiomyocytes (HL-1 cells). *Br. J. Pharmacol.* 153, 907-14.
- Allen, J., Davey, H. M., Broadhurst, D., Heald, J. K., Rowland, J. J., Oliver, S. G. and Kell, D. B. (2003). High-throughput classification of yeast mutants for functional genomics using metabolic footprinting. *Nat. Biotechnol.* 21, 692-696.
- Allen, J., Davey, H. M., Broadhurst, D., Rowland, J. J., Oliver, S. G. and Kell, D. B. (2004). Discrimination of modes of action of antifungal substances by use of metabolic footprinting. *Appl. Environ. Microbiol.* 70, 6157-6165.
- Altamirano, C., Paredes, C., Cairo, J.J., Godia, F. (2000). Improvement of CHO cell culture medium formulation: simultaneous substitution of glucose and glutamine. *Biotechnol. Prog.* 16, 69-75.
- Andersson, H., Kagedal, B. and Mandenius, C. F. (2010). Monitoring of troponin release from cardiomyocytes during exposure to toxic substances using surface plasmon resonance biosensing. *Anal. Bioanal. Chem.* 398, 1395-1402.
- Andersson, C., Al-Turkmani, M. R., Savaille, J. E., Alturkmani, R., Katrangi, W., Cluette-Brown, J. E., Zaman, M. M., Laposata, M. and Freedman, S. D. (2008). Cell culture models demonstrate that CFTR dysfunction leads to defective fatty acid composition and metabolism. *J. Lipid Res.* 49, 1692-1700.
- Andreadou, I., Papaefthimiou, M., Zira, A., Constantinou, M., Sigala, F., Skaltsounis, A. L., Tsantili-Kakoulidou, A., Iliodromitis, E. K., Kremastinos, D. T. and Mikros, E. (2009). Metabonomic identification of novel biomarkers in doxorubicin cardiotoxicity and protective effect of the natural antioxidant oleuropein. *NMR Biomed.* 22, 585-92.
- Antoniewicz, M. R., Kelleher, J. K. and Stephanopoulos, G. (2007). Elementary metabolite units (EMU): a novel framework for modeling isotopic distributions. *Metab. Eng.* 9, 68-86.
- Ardizzone, T.D., Lu, X.H., Dwyer, D.S. (2002). Calcium-independent inhibition of glucose transport in PC-12 and L6 cells by calcium channel antagonists. *Am. J. Physiol. Cell Physiol.* 283, C579-586.
- Armstrong, S. C. and Cozza, K. L. (2003). Antihistamines. *Psychosomatics* 44, 430-434.
- Ashrafian, H. and Neubauer, S. (2009). Metabolomic profiling of cardiac substrate utilization: fanning the flames of systems biology? *Circulation* 119, 1700-2.
- Ashrafian, H., Frenneaux, M. P. and Opie, L. H. (2007). Metabolic Mechanisms in Heart Failure. *Circulation* 116, 434-448.

- Asp, J., Steel, D., Jonsson, M., Ameen, C., Dahlenborg, K., Jeppsson, A., Lindahl, A. and Sartipy, P. (2010). Cardiomyocyte clusters derived from human embryonic stem cells share similarities with human heart tissue. *J. Mol. Cell Biol.* 2, 276-83.
- Bachur, N. R., Gordon, S. L. and Gee, M. V. (1977). Anthracycline antibiotic augmentation of microsomal electron transport and free radical formation. *Mol. Pharmacol.* 13, 901-10.
- Bambot, S., Holavanahali, R., Lakowicz, J. R., Carter, G. M. and Rao, G. (1994). Optical oxygen sensor using fluorescence lifetime measurement. *Adv. Exp. Med. Biol.* 361, 197-205.
- Bates, D. A. and Winterbourn, C. C. (1982). Deoxyribose breakdown by the adriamycin semiquinone and H<sub>2</sub>O<sub>2</sub>: evidence for hydroxyl radical participation. *FEBS Lett.* 145, 137-42.
- Bechtel, L.K., Haverstick, D.M., Holstege, C.P. (2008). Verapamil toxicity dysregulates the phosphatidylinositol 3-kinase pathway. *Acad. Emerg. Med.* 15, 368-374.
- Beckers, S., Noor, F., Muller-Vieira, U., Mayer, M., Strigun, A. and Heinzle, E. (2009). High throughput, non-invasive and dynamic toxicity screening on adherent cells using respiratory measurements. *Toxicol. In Vitro* 24, 686-94.
- Beger, R. D., Sun, J. and Schnackenberg L. K. (2010). Metabolomics approaches for discovering biomarkers of drug-induced hepatotoxicity and nephrotoxicity. *Toxicol. Appl. Pharmacol.* 243, 154-166.
- Berthiaume, J. M. and Wallace, K. B. (2007a). Adriamycin-induced oxidative mitochondrial cardiotoxicity. *Cell. Biol. Toxicol.* 23, 15-25.
- Berthiaume, J. M. and Wallace, K. B. (2007b). Persistent alterations to the gene expression profile of the heart subsequent to chronic Doxorubicin treatment. *Cardiovasc. Toxicol.* 7, 178-91.
- Bharadwaj, L. A., Davies, G. F., Xavier, I. J. and Ovsenek, N. (2002). l-carnosine and verapamil inhibit hypoxia-induced expression of hypoxia inducible factor (HIF-1 alpha) in H9c2 cardiomyoblasts. *Pharmacol. Res.* 45, 175-81.
- Binah, O., Dolnikov, K., Sadan, O., Shilkrot, M., Zeevi-Levin, N., Amit, M., Danon, A., and Itskovitz-Eldor, J. (2007). Functional and developmental properties of human embryonic stem cells-derived cardiomyocytes. *J Electrocardiol* 40, S192-6.
- Blekherman, G., Laubenbacher, R., Cortes, D. F., Mendes, P., Torti, F. M., Akman, S., Torti, S. V. and Shulaev, V. (2011). Bioinformatics tools for cancer metabolomics. *Metabolomics* 7, 329-343.
- Bonarius, H. P., Ozemre, A., Timmerarends, B., Skrabal, P., Tramper, J., Schmid, G. and Heinzle, E. (2001). Metabolic-flux analysis of continuously cultured hybridoma cells using <sup>13</sup>CO<sub>2</sub> mass spectrometry in combination with <sup>13</sup>C-lactate nuclear magnetic resonance spectroscopy and metabolite balancing. *Biotechnol. Bioeng.* 74, 528-38.
- Bordoni, A., Biagi, P. and Hrelia, S. (1999). The impairment of essential fatty acid metabolism as a key factor in doxorubicin-induced damage in cultured rat cardiomyocytes. *Biochim. Biophys. Acta* 1440, 100-6.
- Braam, S. R., Tertoolen, L., van de Stolpe, A., Meyer, T., Passier, R. and Mummery, C. L. (2010). Prediction of drug-induced cardiotoxicity using human embryonic stem cell-derived cardiomyocytes. *Stem Cell Res.* 4, 107-16.

- Brogden, R. N., Benfield, P. (1996). Verapamil: a review of its pharmacological properties and therapeutic use in coronary artery disease. *Drugs* 51, 792-819.
- Budde, T., Haney, J., Bien, S., Schwebe, M., Riad, A., Tschöpe, C., Staudt, A., Jedlitschky, G., Felix, S. B., Kroemer, H. K. and Grube, M. (2011). Acute exposure to doxorubicin results in increased cardiac P-glycoprotein expression. *J. Pharm. Sci.* 100, 3951-8.
- Bugger, H., Guzman, C., Zechner, C., Palmeri, M., Russell, K. S. and Russell, R. R., 3<sup>rd</sup> (2010). Uncoupling protein downregulation in doxorubicin-induced heart failure improves mitochondrial coupling but increases reactive oxygen species generation. *Cancer Chemother. Pharmacol.* 67, 1381-8.
- Cartee, G.D., Briggs-Tung, C., Holloszy, J.O. (1992). Diverse effects of calcium channel blockers on skeletal muscle glucose transport. *Am. J. Physiol.* 263, R70-75.
- Carvalho, R. A., Sousa, R. P., Cadete, V. J., Lopaschuk, G. D., Palmeira, C. M., Bjork, J. A. and Wallace, K. B. (2010). Metabolic remodeling associated with subchronic doxorubicin cardiomyopathy. *Toxicology* 270, 92-8.
- Caspi, O., Itzhaki, I., Kehat, I., Gepstein, A., Arbel, G., Huber, I., Satin, J. and Gepstein, L. (2009). *In vitro* electrophysiological drug testing using human embryonic stem cell derived cardiomyocytes. *Stem Cells Dev.* 18, 161-72.
- Ceriello, A., Colagiuri, S., Gerich, J. and Tuomilehto, J. (2008). Guideline for management of postmeal glucose. *Nutr. Metab. Cardiovasc. Dis.* 18, S17-33.
- Chaudary, N., Naydenova, Z., Shuralyova, I. and Coe, I. R. (2004). Hypoxia regulates the adenosine transporter, mENT1, in the murine cardiomyocyte cell line, HL-1. *Cardiovasc. Res.* 61, 780-788.
- Chen, K., Liu, Q., Xie, L., Sharp, P.A., Wang, D.I. (2001). Engineering of a mammalian cell line for reduction of lactate formation and high monoclonal antibody production. *Biotechnol. Bioeng.* 72, 55-61.
- Chung, S., Dzeja, P. P., Faustino, R. S., Perez-Terzic, C., Behfar, A., and Terzic, A. (2007). Mitochondrial oxidative metabolism is required for the cardiac differentiation of stem cells. *Nat Clin Pract Cardiovasc Med* 4 Suppl 1, S60-7.
- Clarke, C. J. and Haselden, J. N. (2008). Metabolic profiling as a tool for understanding mechanisms of toxicity. *Toxicol. Pathol.* 36, 140-147.
- Clarke, T. C., Thomas, D., Petersen, J. S., Evans, W. H., Martin, P. E. M. (2006). The antiarrhythmic peptide rotigaptide (ZP123) increases gap junction intracellular communication in cardiac myocytes and HeLa cells expressing connexin. *Br. J. Pharmacol.* 147,486-95.
- Claycomb, W. C., Lanson, N. A., Jr., Stallworth, B. S., Egeland, D. B., Delcarpio, J. B., Bahinski, A. and Izzo, N. J., Jr. (1998). HL-1 cells: a cardiac muscle cell line that contracts and retains phenotypic characteristics of the adult cardiomyocyte. *Proc. Natl. Acad. Sci. U. S. A.* 95, 2979-84.
- Cohen, D. M. and Bergman, R. N. (1997). Improved estimation of anaplerosis in heart using <sup>13</sup>C NMR. *Am. J. Physiol.* 273, E1228-42.

- Comte, B., Vincent, G., Bouchard, B. and Des Rosiers, C. (1997a). Probing the origin of acetyl-CoA and oxaloacetate entering the citric acid cycle from the  $^{13}\text{C}$  labeling of citrate released by perfused rat hearts. *J. Biol. Chem.* 272, 26117-24.
- Comte, B., Vincent, G., Bouchard, B., Jette, M., Cordeau, S. and Rosiers, C. D. (1997b). A  $^{13}\text{C}$  mass isotopomer study of anaplerotic pyruvate carboxylation in perfused rat hearts. *J. Biol. Chem.* 272, 26125-31.
- Darpo, B. (2007). Detection and reporting of drug-induced proarrhythmias: room for improvement. *Europace* 9 Suppl, 23-36.
- Deng, C., Rao, F., Wu, S., Kuang, S., Liu, X., Zhou, Z., Shan, Z., Lin, Q., Qian, W., Yang, M., Geng, Q., Zhang, Y., Yu, X., Lin, S. (2009). Pharmacological effects of carvedilol on T-type calcium current in murine HL-1 cells. *Eur. J. Pharmacol.* 621, 19-25.
- Depre, C. and Taegtmeyer, H. (2000). Metabolic aspects of programmed cell survival and cell death in the heart. *Cardiovasc. Res.* 45, 538-548.
- Deshpande, R. R., Koch-Kirsch, Y., Maas, R., John, G. T., Krause, C. and Heinzle, E. (2005). Microplates with integrated oxygen sensors for kinetic cell respiration measurement and cytotoxicity testing in primary and secondary cell lines. *Assay Drug Dev. Technol.* 3, 299-307.
- Deshpande, R., Yang, T.H., Heinzle, E. (2009). Towards a metabolic and isotopic steady state in CHO batch cultures for reliable isotope-based metabolic profiling. *Biotechnol. J.* 4, 247-263.
- Dolnikov, K., Shilkrut, M., Zeevi-Levin, N., Gerecht-Nir, S., Amit, M., Danon, A., Itskovitz-Eldor, J., and Binah, O. (2006). Functional properties of human embryonic stem cell-derived cardiomyocytes: intracellular  $\text{Ca}^{2+}$  handling and the role of sarcoplasmic reticulum in the contraction. *Stem Cells* 24, 236-45.
- Doroshov, J. H. (1983). Anthracycline antibiotic-stimulated superoxide, hydrogen peroxide, and hydroxyl radical production by NADH dehydrogenase. *Cancer Res.* 43, 4543-51.
- Dunn W. B., Brown M., Worton S. A., Crocker I. P., Broadhurst D., Horgan R., Kenny L. C., Baker P. N., Kell D. B. and Heazell A. E. (2009). Changes in the metabolic footprint of placental explant-conditioned culture medium identifies metabolic disturbances related to hypoxia and pre-eclampsia. *Placenta* 30, 974-980.
- Eimre, M., Paju, K., Pelloux, S., Beraud, N., Roosimaa, M., Kadaja, L., Gruno, M., Peet, N., Orlova, E., Remmelkoor, R., Piirsoo, A., Saks, V., Seppet, E. (2008). Distinct organization of energy metabolism in HL-1 cardiac cell line and cardiomyocytes. *Biochim. Biophys. Acta* 1777, 514-524.
- Eliot, H., Gianni, L. and Myers, C. (1984). Oxidative destruction of DNA by the adriamycin-iron complex. *Biochemistry* 23, 928-36.
- Feinstein, E., Canaani, E. and Weiner, L. M. (1993). Dependence of nucleic acid degradation on in situ free-radical production by adriamycin. *Biochemistry* 32, 13156-61.
- Floyd, J. D., Nguyen, D. T., Lobins, R. L., Bashir Q., Doll D. C. and Perry M. C. (2005). Cardiotoxicity of cancer therapy. *J Clin Oncol* 23, 7685-7696.
- Fogli, S., Nieri, P. and Breschi, M. C. (2004). The role of nitric oxide in anthracycline toxicity and prospects for pharmacologic prevention of cardiac damage. *Faseb J.* 18, 664-75.

- Forbes, N. S., Meadows, A. L., Clark, D. S. and Blanch, H. W. (2006). Estradiol stimulates the biosynthetic pathways of breast cancer cells: detection by metabolic flux analysis. *Metab. Eng.* 8, 639-52.
- Fox, J. E., Jones, L. and Light, P. E. (2005). Identification and pharmacological characterization of sarcolemmal ATP-sensitive potassium channels in the murine atrial HL-1 cell line. *J. Cardiovasc. Pharmacol.* 45, 30-5.
- Fritzsche, M., Fredriksson, J.M., Carlsson, M., Mandenius, C.F. (2009). A cell-based sensor system for toxicity testing using multiwavelength fluorescence spectroscopy. *Anal. Biochem.* 387, 271-275.
- Fukuda, K., Davies, S. S., Nakajima, T., Ong, B. H., Kuperschmidt, S., Fessel, J. et al. (2005). Oxidative mediated lipid peroxidation recapitulates proarrhythmic effects on cardiac sodium channels. *Circ. Res.* 97, 1262-69.
- Gambhir, A., Europa, A.F., Hu, W.S. (1999). Alteration of cellular metabolism by consecutive fed-batch cultures of mammalian cells. *J. Biosci. Bioeng.* 87, 805-810.
- Gasser, A. B., Tieche, M. and Brunner, K. W. (1982). Neurologic and cardiac toxicity following iv application of methotrexate. *Cancer Treat. Rep.* 66, 1561-1562.
- Gatenby, R.A., Gillies, R.J. (2007). Glycolysis in cancer: a potential target for therapy. *Int. J. Biochem. Cell. Biol.* 39, 1358-1366.
- Gertz, E. W., Wisneski, J. A., Stanley, W. C. and Neese, R. A. (1988). Myocardial substrate utilization during exercise in humans. Dual carbon-labeled carbohydrate isotope experiments. *J. Clin. Invest.* 82, 2017-2025.
- Gewirtz, D.A. (1999). A critical evaluation of the mechanisms of action proposed for the antitumor effects of the anthracycline antibiotics adriamycin and daunorubicin. *Biochem. Pharmacol.* 57, 727-741.
- Gillies, R.J., Gatenby, R.A. (2007). Adaptive landscapes and emergent phenotypes: why do cancers have high glycolysis? *J. Bioenerg. Biomembr.* 39, 251-257.
- Goldoni, D., Zhao, Y., Green, B. D., McDermott, B. J., and Collins, A. (2010). Inward rectifier potassium channels in the HL-1 cardiomyocyte-derived cell line. *J. Cell Physiol.* 225, 751-6.
- Goodman, J. and Hochstein, P. (1977). Generation of free radicals and lipid peroxidation by redox cycling of adriamycin and daunomycin. *Biochem. Biophys. Res. Commun.* 77, 797-803.
- Goudar, C., Biener, R., Boisart, C., Heidemann, R., Piret, J., de Graaf, A., and Konstantinov, K. (2010). Metabolic flux analysis of CHO cells in perfusion culture by metabolite balancing and 2D [<sup>13</sup>C, <sup>1</sup>H] COSY NMR spectroscopy. *Metab. Eng.* 12, 138-49.
- Graham, M. A., Newell, D. R., Butler, J., Hoey, B., and Patterson, L. H. (1987). The effect of the anthrapyrazole antitumour agent CI941 on rat liver microsome and cytochrome P-450 reductase mediated free radical processes. Inhibition of doxorubicin activation *in vitro*. *Biochem. Pharmacol.* 36, 3345-51.
- Greene, R. F., Collins, J. M., Jenkins, J. F., Speyer, J. L. and Myers, C. E. (1983). Plasma pharmacokinetics of adriamycin and adriamycinol: implications for the design of *in vitro* experiments and treatment protocols. *Cancer Res.* 43, 3417-21.



- Griffin, J. L., Atherton, H., Shockcor, J. and Atzori, L. (2011). Metabolomics as a tool for cardiac research. *Nat. Rev. Cardiol.* 8, 630-43.
- Gwathmey, J. K., Tsaïoun, K. and Hajjar, R. J. (2009). Cardionomics: a new integrative approach for screening cardiotoxicity of drug candidates. *Expert Opin. Drug Metab. Toxicol.* 5, 647-60.
- Hans, M.A., Heinzle, E., Wittmann, C. (2003). Free intracellular amino acid pools during autonomous oscillations in *Saccharomyces cerevisiae*. *Biotechnol. Bioeng.* 82, 143-151.
- Harding, S. E., Ali, N. N., Brito-Martins, M., and Gorelik, J. (2007). The human embryonic stem cell-derived cardiomyocyte as a pharmacological model. *Pharmacol Ther* 113, 341-53.
- He, J. Q., Ma, Y., Lee, Y., Thomson, J. A., and Kamp, T. J. (2003). Human embryonic stem cells develop into multiple types of cardiac myocytes: action potential characterization. *Circ Res* 93, 32-9.
- Henney, A. M. (2009). Who will take up the gauntlet? Challenges and opportunities for systems biology and drug discovery. *EMBO Rep.* 10 Suppl, S9-13.
- Henriques, I. D., Aga, D. S., Mendes, P., O'Connor, S. K. and Love N. G. (2007). Metabolic footprinting: a new approach to identify physiological changes in complex microbial communities upon exposure to toxic chemicals. *Environ. Sci. Technol.* 41, 3945-3951.
- Henry, O., Jolicoeur, M. and Kamen, A. (2011). Unraveling the metabolism of HEK-293 cells using lactate isotopomer analysis. *Bioprocess Biosyst. Eng.* 34, 263-73.
- Hii, J. T., Wyse, D. G., Gillis, A. M., Duff, H. J., Solylo, M. A. and Mitchell, L. B. (1992). Precordial QT interval dispersion as a marker of torsade de pointes. Disparate effects of class Ia antiarrhythmic drugs and amiodarone. *Circulation* 86, 1376-1382.
- Ho, R. L. and Lieu, C. A. (2008). Systems biology: an evolving approach in drug discovery and development. *Drugs R. D.* 9, 203-216.
- Hong, H. K., Park, M. H., Lee, B. H., Jo, S. H. (2010). Block of the human ether-a-go-go-related gene (hERG) K<sup>+</sup> channel by the antidepressant desipramine. *Biochem. Biophys. Res. Commun.* 394, 536-541.
- Hong, Y. M., Kim, H. S. and Yoon, H. R. (2002). Serum lipid and fatty acid profiles in adriamycin-treated rats after administration of L-carnitine. *Pediatr. Res.* 51, 249-55.
- Hynes, J., Floyd, S., Soini, A. E., O'Connor, R. and Papkovsky, D. B. (2003). Fluorescence-based cell viability screening assays using water-soluble oxygen probes. *J. Biomol. Screen.* 8, 264-72.
- Iliskovic, N., Li, T., Khaper, N., Palace, V. and Singal, P. K. (1998). Modulation of adriamycin-induced changes in serum free fatty acids, albumin and cardiac oxidative stress. *Mol. Cell. Biochem.* 188, 161-6.
- Jensen, J., Hyllner, J. and Bjorquist, P. (2009). Human embryonic stem cell technologies and drug discovery. *J. Cell. Physiol.* 219, 513-9.
- Jeyaseelan, R., Poizat, C., Wu, H. Y. and Kedes, L. (1997). Molecular mechanisms of doxorubicin-induced cardiomyopathy. Selective suppression of Reiske iron-sulfur protein, ADP/ATP translocase, and phosphofructokinase genes is associated with ATP depletion in rat cardiomyocytes. *J. Biol. Chem.* 272, 5828-32.

- John, G. T., Klimant, I., Wittmann, C. and Heinzle, E. (2003). Integrated optical sensing of dissolved oxygen in microtiter plates: a novel tool for microbial cultivation. *Biotechnol. Bioeng.* 81, 829-36.
- Kaddurah-Daouk, R., Kristal, B. S. and Weinshilboum, R. M. (2008). Metabolomics: A Global Biochemical Approach to Drug Response and Disease. *Annual Review of Pharmacology and Toxicology* 48, 653-683.
- Kaplan, N.M. (1989). Calcium entry blockers in the treatment of hypertension. Current status and future prospects. *Jama* 262, 817-823.
- Keene, A. M., Balasubramanian, R., Lloyd, J., Shainberg, A. and Jacobson, K. A. (2010). Multivalent dendrimeric and monomeric adenosine agonists attenuate cell death in HL-1 mouse cardiomyocytes expressing the A(3) receptor. *Biochem. Pharmacol.* 80, 188-196.
- Kehat, I., Kenyagin-Karsenti, D., Snir, M., Segev, H., Amit, M., Gepstein, A., Livne, E., Binah, O., Itskovitz-Eldor, J. and Gepstein, L. (2001). Human embryonic stem cells can differentiate into myocytes with structural and functional properties of cardiomyocytes. *J. Clin. Invest.* 108, 407-14.
- Kettunen, R., Huikuri, H. V., Oikarinen, A. and Takkunen, J. T. (1995). Methotrexate-linked ventricular arrhythmias. *Acta Derm. Venereol.* 75, 391-392.
- Keun, H. C. (2006). Metabonomic modeling of drug toxicity. *Pharmacol. Ther.* 109, 92-106.
- Kim, D. H., Jarvis, R. M., Xu, Y., Oliver, A. W., Allwood, J. W., Hampson, L., Hampson, I. N. and Goodacre R. (2010). Combining metabolic fingerprinting and footprinting to understand the phenotypic response of HPV16 E6 expressing cervical carcinoma cells exposed to the HIV anti-viral drug lopinavir. *Analyst.* 135, 1235-1244.
- Kim, J. C., Son, M. J., Subedi, K. P., Kim, do H. and Woo, S. H. (2010). IP3-induced cytosolic and nuclear Ca<sup>2+</sup> signals in HL-1 atrial myocytes: possible role of IP3 receptor subtypes. *Mol. Cells* 29, 387-395.
- Kim, S.H., Lee, G.M. (2007). Down-regulation of lactate dehydrogenase-A by siRNAs for reduced lactic acid formation of Chinese hamster ovary cells producing thrombopoietin. *Appl. Microbiol. Biotechnol.* 74, 152-159.
- Kim, Y., Ma, A. G., Kitta, K., Fitch, S. N., Ikeda, T., Ihara, Y., Simon, A. R., Evans, T. and Suzuki Y. J. (2003). Anthracycline-induced suppression of GATA-4 transcription factor: implication in the regulation of cardiac myocyte apoptosis. *Mol. Pharmacol.* 63, 368-377.
- Koek, M. M., Jellema, R. H., van der Greef, J., Tas, A. C. and Hankemeier, T. (2011). Quantitative metabolomics based on gas chromatography mass spectrometry: status and perspectives. *Metabolomics* 7, 307-328.
- Kohlstedt, M., Becker, J. and Wittmann, C. (2010). Metabolic fluxes and beyond-systems biology understanding and engineering of microbial metabolism. *Appl. Microbiol. Biotechnol.* 88, 1065-75.
- Kromer, J. O., Fritz, M., Heinzle, E. and Wittmann C. (2005). *In vivo* quantification of intracellular amino acids and intermediates of the methionine pathway in *Corynebacterium glutamicum*. *Anal. Biochem.* 340, 171-173.

- Kuriki, K., Tajima, K., and Tokudome, S. (2006). Accelerated solvent extraction for quantitative measurement of fatty acids in plasma and erythrocytes. *Lipids* 41, 605-14.
- Kuznetsov, A. V., Veksler, V., Gellerich, F. N., Saks, V., Margreiter, R. and Kunz, W. S. (2008). Analysis of mitochondrial function in situ in permeabilized muscle fibers, tissues and cells. *Nat. Protoc.* 3, 965-76.
- Lasser, K. E., Allen, P. D., Woolhandler, S. J., Himmelstein, D. U., Wolfe, S. M. and Bor, D. H. (2002). Timing of new black box warnings and withdrawals for prescription medications. *Jama* 287, 2215-20.
- Lazzara, R. (1993). Antiarrhythmic drugs and torsade de pointes. *Eur. Heart J.* 14 Suppl, 88-92.
- Lee, J. M., Gianchandani, E. P. and Papin, J. A. (2006). Flux balance analysis in the era of metabolomics. *Brief Bioinform.* 7, 140-50.
- Lei, B., Lionetti, V., Young, M. E., Chandler, M. P., d'Agostino, C., Kang, E., Altarejos, M., Matsuo, K., Hintze, T. H., Stanley, W. C., Recchia, F. A. (2004). Paradoxical downregulation of the glucose oxidation pathway despite enhanced flux in severe heart failure. *J. Mol. Cell. Cardiol.* 36, 567-76.
- Lewis, G. D., Asnani, A. and Gerszten, R. E. (2008). Application of metabolomics to cardiovascular biomarker and pathway discovery. *J. Am. Coll. Cardiol.* 52, 117-23.
- Lexchin, J. (2005). Drug withdrawals from the Canadian market for safety reasons, 1963-2004. *Cmaj* 172, 765-7.
- Ling, Y. H., Priebe, W. and Perez-Soler, R. (1993). Apoptosis induced by anthracycline antibiotics in P388 parent and multidrug-resistant cells. *Cancer Res.* 53, 1845-52.
- Lipp, P., Laine, M., Tovey, S. C., Burrell, K. M., Berridge, M. J., Li W. and Bootman, M. D. (2000). Functional InsP3 receptors that may modulate excitation-contraction coupling in the heart. *Curr. Biol.* 10, 939-942.
- Louters, L.L., Stehouwer, N., Rekman, J., Tidball, A., Cok, A., Holstege, C.P. (2010). Verapamil Inhibits the Glucose Transport Activity of GLUT1. *J. Med. Toxicol.* 6, 100-105.
- Maier, K., Hofmann, U., Bauer, A., Niebel, A., Vacun, G., Reuss, M. and Mauch, K. (2009). Quantification of statin effects on hepatic cholesterol synthesis by transient <sup>13</sup>C-flux analysis. *Metab. Eng.* 11, 292-309.
- Malloy, C. R., Jones, J. G., Jeffrey, F. M., Jessen, M. E. and Sherry, A. D. (1996). Contribution of various substrates to total citric acid cycle flux and anaplerosis as determined by <sup>13</sup>C isotopomer analysis and O<sub>2</sub> consumption in the heart. *Magma* 4, 35-46.
- Malloy, C. R., Sherry, A. D. and Jeffrey, F. M. (1987). Carbon flux through citric acid cycle pathways in perfused heart by <sup>13</sup>C NMR spectroscopy. *FEBS Lett.* 212, 58-62.
- Mandenius, C. F., Steel, D., Noor, F., Meyer, T., Heinzle, E., Asp, J., Arain, S., Kraushaar, U., Bremer, S., Class, R. and Sartipy, P. (2011). Cardiotoxicity testing using pluripotent stem cell-derived human cardiomyocytes and state-of-the-art bioanalytics: a review. *J. Appl. Toxicol.* 31, 191-205.
- Maranga, L., Goochee, C.F. (2006). Metabolism of PER.C6 cells cultivated under fed-batch conditions at low glucose and glutamine levels. *Biotechnol. Bioeng.* 94, 139-150.

- Marroquin, L. D., Hynes, J., Dykens, J. A., Jamieson, J. D. and Will, Y. (2007). Circumventing the Crabtree effect: replacing media glucose with galactose increases susceptibility of HepG2 cells to mitochondrial toxicants. *Toxicol. Sci.* 97, 539-47.
- Mayr, M. (2008a). Metabolomics: Ready for the Prime Time? *Circ. Cardiovasc. Genet.* 1, 58-65.
- Mayr, M., Yusuf, S., Weir, G., Chung, Y. L., Mayr, U., Yin, X., Ladroue, C., Madhu, B., Roberts, N., De Souza, A., Fredericks, S., Stubbs, M., Griffiths, J. R., Jahangiri, M., Xu, Q. and Camm A. J. (2008b). Combined metabolomic and proteomic analysis of human atrial fibrillation. *J. Am. Coll. Cardiol.* 51, 585-594.
- McComb, J. M., Logan, K. R., Khan, M. M., Geddes, J. S. and Adgey, A. A. (1980). Amiodarone-induced ventricular fibrillation. *Eur. J. Cardiol.* 11, 381-385.
- McGettigan, P. and Henry, D. (2006). Cardiovascular risk and inhibition of cyclooxygenase: a systematic review of the observational studies of selective and nonselective inhibitors of cyclooxygenase 2. *Jama* 296, 1633-1644.
- Metallo, C. M., Walther, J. L. and Stephanopoulos, G. (2009). Evaluation of  $^{13}\text{C}$  isotopic tracers for metabolic flux analysis in mammalian cells. *J. Biotechnol.* 144, 167-74.
- Monge, C., Beraud, N., Tepp, K., Pelloux, S., Chahboun, S., Kaambre, T., Kadaja, L., Roosimaa, M., Piirsoo, A., Tourneur, Y., Kuznetsov, A. V., Saks, V. and Seppet, E. (2009). Comparative analysis of the bioenergetics of adult cardiomyocytes and nonbeating HL-1 cells: respiratory chain activities, glycolytic enzyme profiles, and metabolic fluxes. *Can. J. Physiol. Pharmacol.* 87, 318-26.
- Moss, A. J. and Kass, R. S. (2005). Long QT syndrome: from channels to cardiac arrhythmias. *J. Clin. Invest.* 115, 2018-24.
- Mudge, G. H., Jr., Mills, R. M., Jr., Taegtmeier, H., Gorlin, R. and Lesch, M. (1976). Alterations of myocardial amino acid metabolism in chronic ischemic heart disease. *J. Clin. Invest.* 58, 1185-92.
- Nicholson, J. K. and Wilson, I. D. (2003). Opinion: understanding 'global' systems biology: metabolomics and the continuum of metabolism. *Nat. Rev. Drug Discov.* 2:668-676.
- Nicolay, K. and de Kruijff, B. (1987). Effects of adriamycin on respiratory chain activities in mitochondria from rat liver, rat heart and bovine heart. Evidence for a preferential inhibition of complex III and IV. *Biochim. Biophys. Acta* 892, 320-30.
- Niklas, J. and Heinzle, E. (2011). Metabolic Flux Analysis in Systems Biology of Mammalian Cells. *Adv. Biochem. Eng. Biotechnol.* DOI: 10.1007/10\_2011\_99.
- Niklas, J., Noor, F. and Heinzle, E. (2009). Effects of drugs in subtoxic concentrations on the metabolic fluxes in human hepatoma cell line Hep G2. *Toxicol. Appl. Pharmacol.* 240, 327-36.
- Niklas, J., Sandig, V. and Heinzle, E. (2011). Metabolite channeling and compartmentation in the human cell line AGE1.HN determined by  $^{13}\text{C}$  labeling experiments and  $^{13}\text{C}$  metabolic flux analysis. *J. Biosci. Bioeng.* 10.1016/j.jbiosc.2011.07.021.
- Niklas, J., Schneider, K. and Heinzle, E. (2010). Metabolic flux analysis in eukaryotes. *Curr Opin. Biotechnol.* 21, 63-9.

- Niklas, J., Schrader, E., Sandig, V., Noll, T. and Heinzle, E. (2011). Quantitative characterization of metabolism and metabolic shifts during growth of the new human cell line AGE1.HN using time resolved metabolic flux analysis. *Bioprocess Biosyst. Eng.* 34, 533-45
- Noor, F., Niklas, J., Muller-Vieira, U. and Heinzle, E. (2009). An integrated approach to improved toxicity prediction for the safety assessment during preclinical drug development using Hep G2 cells. *Toxicol. Appl. Pharmacol.* 237, 221-31.
- Oeggerli, A., Eyer, K., Heinzle, E. (1995). On-line gas analysis in animal cell cultivation: I. Control of dissolved oxygen and pH. *Biotechnol. Bioeng.* 45, 42-53.
- Osorio, J. C., Stanley, W. C., Linke, A., Castellari, M., Diep, Q. N., Panchal, A. R., Hintze, T. H., Lopaschuk, G. D., Recchia, F. A. (2002). Impaired myocardial fatty acid oxidation and reduced protein expression of retinoid X receptor-alpha in pacing-induced heart failure. *Circulation* 106, 606-12.
- Palanivel, R., Eguchi, M., Shuralyova, I., Coe, I., Sweeney, G. (2006). Distinct effects of short and long-term leptin treatment on glucose and fatty acid uptake and metabolism in HL-1 cardiomyocytes. *Metabolism* 55, 1067-75.
- Panchal, A. R., Comte, B., Huang, H., Dudar, B., Roth, B., Chandler, M., Des Rosiers, C., Brunengraber, H. and Stanley, W. C. (2001). Acute hibernation decreases myocardial pyruvate carboxylation and citrate release. *Am. J. Physiol. Heart Circ. Physiol.* 281, H1613-20.
- Perrine, S. A., Michaels, M. S., Ghoddoussi, F., Hyde, E. M., Tancer, M. E., and Galloway, M. P. (2009). Cardiac effects of MDMA on the metabolic profile determined with <sup>1</sup>H-magnetic resonance spectroscopy in the rat. *NMR Biomed.* 22, 419-25.
- Picard, M., Ritchie, D., Wright, K. J., Romestaing, C., Thomas, M. M., Rowan, S. L., Taivassalo, T. and Hepple, R. T. (2010). Mitochondrial functional impairment with aging is exaggerated in isolated mitochondria compared to permeabilized myofibers. *Aging Cell* 9, 1032-46.
- Pointon, A. V., Walker, T. M., Phillips, K. M., Luo, J., Riley, J., Zhang, S. D., Parry, J. D., Lyon, J. J., Marczylo, E. L. and Gant, T. W. (2010). Doxorubicin in vivo rapidly alters expression and translation of myocardial electron transport chain genes, leads to ATP loss and caspase 3 activation. *PLoS One* 5, e12733.
- Quek, L. E., Dietmair, S., Kromer, J. O. and Nielsen, L. K. (2010). Metabolic flux analysis in mammalian cell culture. *Metab. Eng.* 12, 161-71.
- Ramamoorthy, R., Dutta, P. K., and Akbar, S. A. (2003). Oxygen sensors: Materials, methods, designs and applications. *Journal of Materials Science* 38, 4271-4282.
- Randle, P. J., Newsholme, E. A. and Garland, P. B. (1964). Regulation of glucose uptake by muscle. 8. Effects of fatty acids, ketone bodies and pyruvate, and of alloxan-diabetes and starvation, on the uptake and metabolic fate of glucose in rat heart and diaphragm muscles. *Biochem. J.* 93, 652-665.
- Redfern, W. S., Carlsson, L., Davis, A. S., Lynch, W. G., MacKenzie, I., Palethorpe, S., Siegl, P. K., Strang, I., Sullivan, A. T., Wallis, R., Camm, A. J. and Hammond, T. G. (2003). Relationships between preclinical cardiac electrophysiology, clinical QT interval prolongation and torsade de pointes for a broad range of drugs: evidence for a provisional safety margin in drug development. *Cardiovasc. Res.* 58, 32-45.

- Reppel, M., Pillekamp, F., Brockmeier, K., Matzkies, M., Bekcioglu, A., Lipke, T., Nguemo, F., Bonnemeier, H., and Hescheler, J. (2005). The electrocardiogram of human embryonic stem cell-derived cardiomyocytes. *J Electrocardiol* 38, 166-70.
- Robertson, D. G. (2005). Metabonomics in toxicology: a review. *Toxicol. Sci.* 85, 809-822.
- Robey, I. F., Lien, A. D., Welsh, S. J., Baggett, B. K. and Gillies, R. J. (2005). Hypoxia-inducible factor-1 $\alpha$  and the glycolytic phenotype in tumors. *Neoplasia* 7, 324-30.
- Sabatine, M. S., Liu, E., Morrow, D. A., Heller, E., McCarroll, R., Wiegand, R., Berriz, G. F., Roth, F. P. and Gerszten, R. E. (2005). Metabolomic identification of novel biomarkers of myocardial ischemia. *Circulation* 112, 3868-75.
- Sanders, D. B., Larson, D. F., Hunter, K., Gorman, M. and Yang, B. (2001). Comparison of tumor necrosis factor- $\alpha$  effect on the expression of iNOS in macrophage and cardiac myocytes. *Perfusion* 16, 67-74.
- Sanguinetti, M. C. and Mitcheson, J. S. (2005). Predicting drug-hERG channel interactions that cause acquired long QT syndrome. *Trends Pharmacol. Sci.* 26, 119-124.
- Sartiani, L., Bochet, P., Cerbai, E., Mugelli, A., Fischmeister, R. (2002). Functional expression of the hyperpolarization-activated, non-selective cation current  $I_f$  in immortalized HL-1 cardiomyocytes. *J. Physiol.* 545, 81-92.
- Satin, J., Itzhaki, I., Rapoport, S., Schroder, E. A., Izu, L., Arbel, G., Beyar, R., Balke, C. W., Schiller, J., and Gepstein, L. (2008). Calcium handling in human embryonic stem cell-derived cardiomyocytes. *Stem Cells* 26, 1961-72.
- Satin, J., Kehat, I., Caspi, O., Huber, I., Arbel, G., Itzhaki, I., Magyar, J., Schroder, E. A., Perlman, I., and Gepstein, L. (2004). Mechanism of spontaneous excitability in human embryonic stem cell derived cardiomyocytes. *J Physiol* 559, 479-96.
- Sedan, O., Dolnikov, K., Zeevi-Levin, N., Leibovich, N., Amit, M., Itskovitz-Eldor, J., and Binah, O. (2008). 1,4,5-Inositol trisphosphate-operated intracellular  $Ca^{2+}$  stores and angiotensin-II/endothelin-1 signaling pathway are functional in human embryonic stem cell-derived cardiomyocytes. *Stem Cells* 26, 3130-8.
- Schimmel, K. J., Richel, D. J., van den Brink, R. B. and Guchelaar H. J. (2004). Cardiotoxicity of cytotoxic drugs. *Cancer Treat. Rev.* 30, 181-191.
- Schmidt, K., Carlsen, M., Nielsen, J. and Villadsen, J. (1997). Modeling isotopomer distributions in biochemical networks using isotopomer mapping matrices. *Biotechnol. Bioeng.* 55, 831-40.
- Schmidt, W.F., Huber, K.R., Ettinger, R.S., Neuberg, R.W. (1988). Antiproliferative effect of verapamil alone on brain tumor cells *in vitro*. *Cancer Res.* 48, 3617-3621.
- Schmidt, K., Marx, A., de Graaf, A. A., Wiechert, W., Sahn, H., Nielsen, J. and Villadsen, J. (1998).  $^{13}C$  tracer experiments and metabolite balancing for metabolic flux analysis: comparing two approaches. *Biotechnol. Bioeng.* 58, 254-7.
- Schrickel J. W., Schwab J. O., Yang A., Bitzen A., Luderitz B. and Lewalter T. (2006). "Torsade de pointes" in patients with structural heart disease and atrial fibrillation treated with amiodarone, beta-blockers, and digitalis. *Pacing Clin. Electrophysiol.* 29, 363-366.
- Schrickel, J., Bielik, H., Yang, A., Schwab, J. O., Shlevkov, N., Schimpf, R., Luderitz, B. and Lewalter, T. (2003). Amiodarone-associated "torsade de pointes". Relevance of concomitant

- cardiovascular medication in a patient with atrial fibrillation and structural heart disease. *Z. Kardiol.* 92, 889-892.
- Senkus, E. and Jassem, J. (2010). Cardiovascular effects of systemic cancer treatment. *Cancer Treat. Rev.*
- Shuralyova, I., Tajmir, P., Bilan, P.J., Sweeney, G., Coe, I.R. (2004). Inhibition of glucose uptake in murine cardiomyocyte cell line HL-1 by cardioprotective drugs dilazep and dipyridamole. *Am. J. Physiol. Heart Circ. Physiol.* 286, H627-632.
- Sidorenko, Y., Wahl, A., Dauner, M., Genzel, Y. and Reichl, U. (2008). Comparison of metabolic flux distributions for MDCK cell growth in glutamine- and pyruvate-containing media. *Biotechnol. Prog.* 24, 311-20.
- Simunek, T., Sterba, M., Popelova, O., Adamcova, M., Hrdina, R. and Gersl, V. (2009). Anthracycline-induced cardiotoxicity: overview of studies examining the roles of oxidative stress and free cellular iron. *Pharmacol. Rep.* 61, 154-71.
- Sinha, B. K., Mimnaugh, E. G., Rajagopalan, S. and Myers, C. E. (1989). Adriamycin activation and oxygen free radical formation in human breast tumor cells: protective role of glutathione peroxidase in adriamycin resistance. *Cancer Res.* 49, 3844-8.
- Skehan, P., Storeng, R., Scudiero, D., Monks, A., McMahon, J., Vistica, D., Warren, J.T., Bokesch, H., Kenney, S., Boyd, M.R. (1990). New colorimetric cytotoxicity assay for anticancer-drug screening. *J. Natl. Cancer. Inst.* 82, 1107-1112.
- Skladanowski, A. and Konopa, J. (1993). Adriamycin and daunomycin induce programmed cell death (apoptosis) in tumour cells. *Biochem. Pharmacol.* 46, 375-82.
- Stanley, W. C., Lopaschuk, G. D., Hall, J. L. and McCormack, J. G. (1997). Regulation of myocardial carbohydrate metabolism under normal and ischaemic conditions. Potential for pharmacological interventions. *Cardiovasc. Res.* 33, 243-57.
- Stanley, W. C., Recchia, F. A. and Lopaschuk, G. D. (2005). Myocardial substrate metabolism in the normal and failing heart. *Physiol. Rev.* 85, 1093-129.
- Staudacher, I., Wang, L., Wan, X., Obers, S., Wenzel, W., Tristram, F., Koschny, R., Staudacher, K., Kisselbach, J., Koelsch, P., Schweizer, P.A., Katus, H.A., Ficker, E., Thomas, D. (2011). hERG K<sup>+</sup> channel-associated cardiac effects of the antidepressant drug desipramine. *Naunyn. Schmiedebergs Arch. Pharmacol.* 383, 119-139.
- Steel, D., Hyllner, J., and Sartipy, P. (2009). Cardiomyocytes derived from human embryonic stem cells - characteristics and utility for drug discovery. *Curr Opin Drug Discov Devel* 12, 133-40.
- Strigun, A., Noor, F., Pironti, A., Niklas, J., Yang, T. H. and Heinzle, E. (2011a). Metabolic flux analysis gives an insight on verapamil induced changes in central metabolism of HL-1 cells. *J. Biotechnol.* 155, 299-307.
- Strigun, A., Wahrheit, J., Beckers, S., Heinzle, E., Noor, F. (2011b). Metabolic profiling using HPLC allows classification of drugs according to their mechanisms of action in HL-1 cardiomyocytes. *Toxicol. Appl. Pharmacol.* 252, 183-191.

- Strigun, A., Wahrheit, J., Niklas, J., Heinzle, E. and Noor, F. (2011c). Doxorubicin increases oxidative metabolism in HL-1 cardiomyocytes as shown by  $^{13}\text{C}$ -metabolic flux analysis. *Toxicol Sci* doi: 10.1093/toxsci/kfr298.
- Synnergren, J., Akesson, K., Dahlenborg, K., Vidarsson, H., Ameen, C., Steel, D., Lindahl, A., Olsson, B. and Sartipy, P. (2008). Molecular signature of cardiomyocyte clusters derived from human embryonic stem cells. *Stem Cells* 26, 1831-40.
- Tagliatalata, M., Castaldo, P., Pannaccione, A., Giorgio, G., Genovese, A., Marone, G., Annunziato, L. (1999). Cardiac ion channels and antihistamines: possible mechanisms of cardiotoxicity. *Clin. Exp. Allergy* 29 Suppl 3, 182-189.
- Tao, Z., Withers, H. G., Penefsky, H. S., Goodisman, J. and Soud, A. K. (2006). Inhibition of cellular respiration by doxorubicin. *Chem. Res. Toxicol.* 19, 1051-8.
- Tiziani, S., Lodi, A., Khanim, F. L., Viant, M. R., Bunce, C. M. and Gunther, U. L. (2009). Metabolomic profiling of drug responses in acute myeloid leukaemia cell lines. *PLoS One* 4, e4251.
- Tokarska-Schlattner, M., Lucchinetti, E., Zaugg, M., Kay, L., Gratia, S., Guzun, R., Saks, V., and Schlattner, U. (2010). Early effects of doxorubicin in perfused heart: transcriptional profiling reveals inhibition of cellular stress response genes. *Am. J. Physiol. Regul. Integr. Comp. Physiol.* 298, R1075-88.
- Tokarska-Schlattner, M., Wallimann, T. and Schlattner, U. (2006). Alterations in myocardial energy metabolism induced by the anti-cancer drug doxorubicin. *C. R. Biol.* 329, 657-68.
- Tsuruo, T., Iida, H., Tsukagoshi, S., Sakurai, Y. (1981). Overcoming of Vincristine Resistance in P388 Leukemia *in Vivo* and *in Vitro* through Enhanced Cytotoxicity of Vincristine and Vinblastine by Verapamil. *Cancer Res.* 41, 1967-1972.
- Turer, A. T., Stevens, R. D., Bain, J. R., Muehlbauer, M. J., van der Westhuizen, J., Mathew, J. P., Schwinn, D. A., Glower, D. D., Newgard, C. B. and Podgoreanu, M. V. (2009). Metabolomic profiling reveals distinct patterns of myocardial substrate use in humans with coronary artery disease or left ventricular dysfunction during surgical ischemia/reperfusion. *Circulation* 119, 1736-46.
- Vidal, R. F., Eksborg, S., Sundberg, M., Carlberg, M., Elfsson, B. and Andersson, B. S. (1996). Doxorubicin- and daunorubicin-induced energy deprivation and nucleotide degradation in isolated cardiomyocytes. *Toxicology* 114, 1-10.
- Vo, T. D. and Palsson, B. O. (2006). Isotopomer analysis of myocardial substrate metabolism: a systems biology approach. *Biotechnol. Bioeng.* 95, 972-83.
- Wakasugi, S., Fischman, A. J., Babich, J. W., Callahan, R. J., Elmaleh, D. R., Wilkinson, R. and Strauss, H. W. (1993). Myocardial substrate utilization and left ventricular function in adriamycin cardiomyopathy. *J. Nucl. Med.* 34, 1529-35.
- Waksman, J. C., Brody, A. and Phillips, S. D. (2007). Nonselective nonsteroidal antiinflammatory drugs and cardiovascular risk: are they safe? *Ann. Pharmacother.* 41, 1163-1173.



- Waldhauser, K.M., Torok, M., Ha, H.R., Thomet, U., Konrad, D., Brecht, K., Follath, F., Krahenbuhl, S. (2006). Hepatocellular toxicity and pharmacological effect of amiodarone and amiodarone derivatives. *J. Pharmacol. Exp. Ther.* 319, 1413-1423.
- Wei, L., Liao, P., Wu, H., Li, X., Pei, F., Li, W. and Wu, Y. (2009). Metabolic profiling studies on the toxicological effects of realgar in rats by (1)H NMR spectroscopy. *Toxicol. Appl. Pharmacol.* 234, 314-325.
- Weiss, S., John, G.T., Klimant, I., Heinzle, E. (2002). Modeling of mixing in 96-well microplates observed with fluorescence indicators. *Biotechnol. Prog.* 18, 821-830.
- West, P. R., Weir, A. M., Smith, A. M., Donley, E. L. and Cezar, G. G. (2010). Predicting human developmental toxicity of pharmaceuticals using human embryonic stem cells and metabolomics. *Toxicol. Appl. Pharmacol.* 247, 18-27.
- Westerhuis, J., Hoefsloot, H., Smit, S., Vis, D., Smilde, A., van Velzen, E., van Duijnhoven J. and van Dorsten F. (2008). Assessment of PLS-DA cross validation. *Metabolomics* 4, 81-89.
- White, N. J. (2007). Cardiotoxicity of antimalarial drugs. *Lancet Infect. Dis.* 7, 549-558.
- White, S. M., Constantin, P. E. and Claycomb, W. C. (2004). Cardiac physiology at the cellular level: use of cultured HL-1 cardiomyocytes for studies of cardiac muscle cell structure and function. *Am. J. Physiol. Heart Circ. Physiol.* 286, H823-829.
- Wilson, D. F., Vanderkooi, J. M., Green, T. J., Maniara, G., DeFeo, S. P. and Bloomgarden, D. C. (1987). A versatile and sensitive method for measuring oxygen. *Adv. Exp. Med. Biol.* 215, 71-7.
- Wisneski, J. A., Gertz, E. W., Neese, R. A., Gruenke, L. D., Morris, D. L. and Craig, J. C. (1985). Metabolic fate of extracted glucose in normal human myocardium. *J. Clin. Invest.* 76, 1819-1827.
- Wittmann, C. (2007). Fluxome analysis using GC-MS. *Microb. Cell Fact.* 6, 6.
- Wodnicka, M., Guarino, R. D., Hemperly, J. J., Timmins, M. R., Stitt, D. and Pitner, J. B. (2000). Novel fluorescent technology platform for high throughput cytotoxicity and proliferation assays. *J. Biomol. Screen.* 5, 141-52.
- Wolf, P., Hartl, F., Brischwein, M. and Wolf, B. (2011). Determination of dynamic doxorubicin-EC<sub>50</sub> value in an automated high-content workstation for cellular assays. *Toxicol. In Vitro* 25, 1889-94.
- Xia, M., Salata, J. J., Figueroa, D. J., Lawlor, A. M., Liang, H. A., Liu, Y. and Connolly, T. M. (2004). Functional expression of L- and T-type Ca<sup>2+</sup> channels in murine HL-1 cells. *J. Mol. Cell Cardiol.* 36, 111-9.
- Xu, C., He, J.Q., Kamp, T.J., Police, S., Hao, X., O'Sullivan, C., Carpenter, M.K., Lebkowski, J., Gold, J.D. (2006). Human embryonic stem cell-derived cardiomyocytes can be maintained in defined medium without serum. *Stem Cells Dev.* 15, 931-941.
- Yang, T.H., Bolten, C.J., Coppi, M.V., Sun, J., Heinzle, E. (2009). Numerical bias estimation for mass spectrometric mass isotopomer analysis. *Anal. Biochem.* 388, 192-203.
- Yang, T. H., Frick, O. and Heinzle, E. (2008). Hybrid optimization for <sup>13</sup>C metabolic flux analysis using systems parametrized by compactification. *BMC Syst. Biol.* 2, 29.

- Yap Y. G. and Camm A. J. (1999). The current cardiac safety situation with antihistamines. *Clin. Exp. Allergy* 29 Suppl, 15-24.
- Yarishkin, O.V., Hwang, E.M., Kim, D., Yoo, J.C., Kang, S.S., Kim, D.R., Shin, J.H., Chung, H.J., Jeong, H.S., Kang, D., Han, J., Park, J.Y., Hong, S.G. (2009). Diclofenac, a Non-steroidal Anti-inflammatory Drug, Inhibits L-type Ca Channels in Neonatal Rat Ventricular Cardiomyocytes. *Korean J. Physiol. Pharmacol.* 13, 437-442.
- Zhang, C., Lv, F., Zhou, L., Li, X., Wu, X. X. and Hoffman, R. M. (2009). Effect of verapamil on the expression of EGFR and NM23 in A549 human lung cancer cells. *Anticancer Res.* 29, 27-32.
- Zhang, L., Yang, Y., Wei, X.Y., Shi, Y.R., Liu, H.Y., Niu, R.F., Hao, X.S. (2007). Reversing adriamycin resistance of human breast cancer cells by hyperthermia combined with Interferon alpha and Verapamil. *J. Exp. Clin. Cancer Res.* 26, 201-207.
- Zhou, W., Rehm, J., Hu, W.S. (1995). High viable cell concentration fed-batch cultures of hybridoma cells through on-line nutrient feeding. *Biotechnol. Bioeng.* 46, 579-587.
- Zhu, J., Zhang, B. and Schadt, E. E. (2008). A systems biology approach to drug discovery. *Adv. Genet.* 60, 603-635.
- Zupke, C., Tompkins, R., Yarmush, D. and Yarmush, M. (1997). Numerical isotopomer analysis: estimation of metabolic activity. *Anal. Biochem.* 247, 287-93.

# Appendix

## Chapter 2

**Table S1:** EC<sub>50</sub> values of several drugs determined by continuous measurement of dissolved oxygen using 24 – well OxoDishes. Drugs were tested on HL-1 cardiomyocytes for 48 h. n.d.: not determined.

t [h]	EC <sub>50</sub> [μM]								
	Terfenadin	Verapamil	Daunorubicin	Amiodarone	Diclofenac	Desipramin	Haloperidol	Astemizol	Doxorubicin
20	5.3	44.3	0.8	18.8	596.8	63.5	87.7	4.6	3.5
25	4.7	41.4	0.5	18.3	566.6	51.9	74.6	4.5	n.d.
30	4.4	39.3	0.4	17.5	458.9	43.0	56.2	4.4	2.7
35	4.3	38.8	0.3	16.4	409.7	38.0	47.0	4.4	1.4
40	4.2	37.6	0.2	15.9	355.9	34.6	41.2	4.5	0.8
45	4.3	35.1	0.2	15.5	312.0	33.6	38.0	4.5	0.6
48	4.1	33.2	0.1	14.5	321.3	33.2	35.8	4.3	0.5

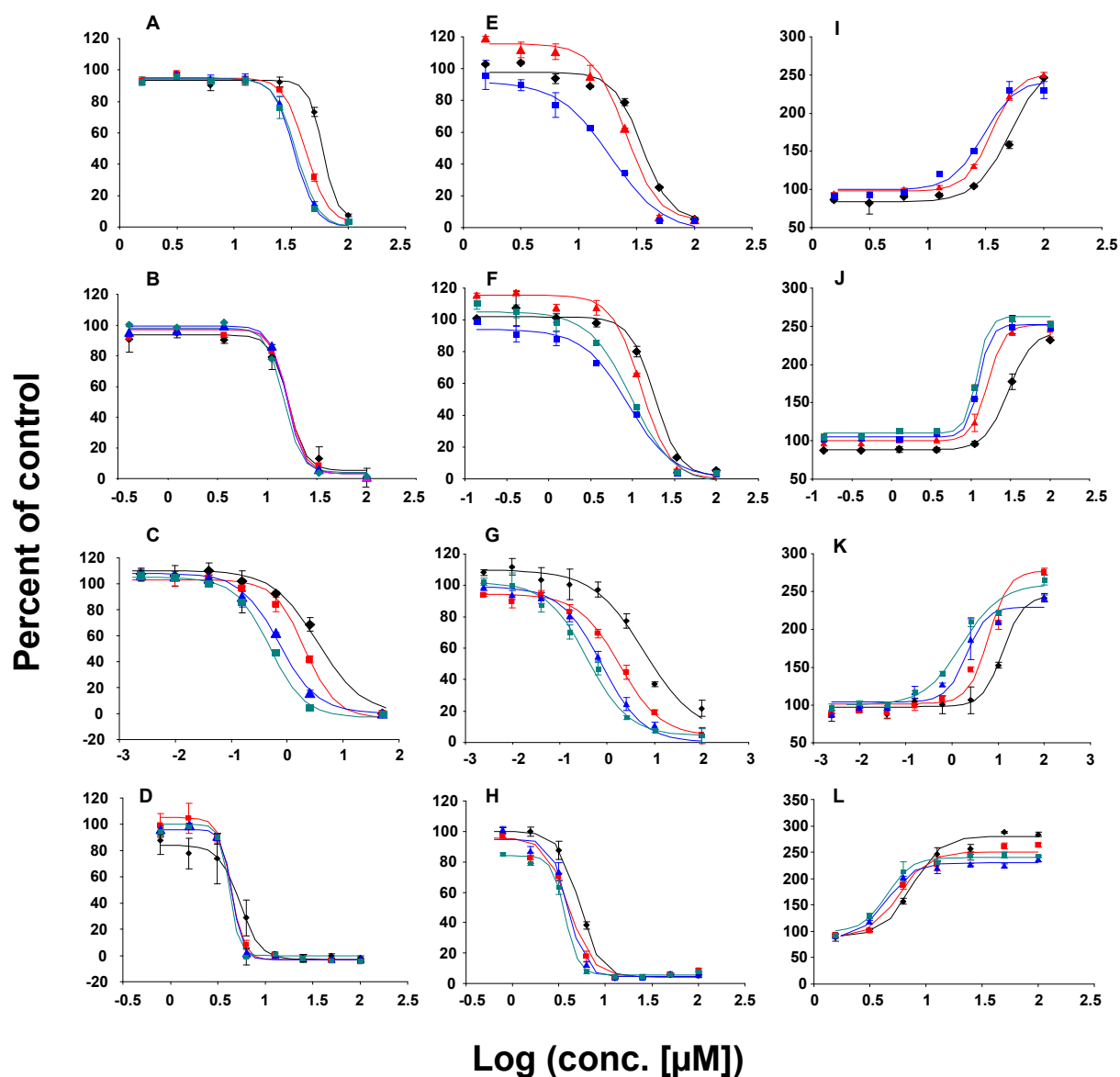


**Figure S1:** Concentration-response curves of amidarone (B,F,J), desipramin (A,E,I), doxorubicin (C,G,K) and terfenadin (D,H,L) screened on HL-1 cells by using continuous oxygen measurement (A,B,C,D); sulforhodamine B proliferation assay (E,F,G,H) and lactate dehydrogenase release assay (I,J,K,L). The concentration response was determined after 20 h (black symbols), 30 h (red symbols), 40 h (blue symbols) and 48 h (turquoise symbols) of exposure. Standard deviations were determined from triplicate measurement.





## Chapter 4

### Text S1: Oxygen uptake rate measurement

Specific oxygen consumption rate per cell ( $qO_2$ ) was estimated using the liquid phase balance:

$$\frac{d[O_2]}{dt} = k_L a \cdot ([O_2^{sat}] - [O_2]) - \frac{qO_2 \cdot X}{V}$$

$[O_2^{sat}]$  is the dissolved oxygen concentration at saturation in culture medium while  $[O_2]$  represents the actual dissolved oxygen concentration,  $X$  the number of cells per well and  $V$  the liquid volume per well.  $k_L a$  is the oxygen transfer coefficient. It was additionally assumed that oxygen uptake follows Michaelis-Menten Kinetics. Additionally, exponential growth of cells was considered resulting in the set of equations (MATLAB listing)

$$\text{OUR} = (qO_2 \cdot X) \cdot (O / (K_O + O));$$

$$\text{DODT} = K_L a \cdot (O_S - O) - \text{OUR} / \text{Volume};$$

$$\text{DXDT} = \mu_{\text{max}} \cdot X;$$

$K_O$  was set to 0.001 mM,  $X$  was the experimentally determined cell number,  $O_S$  is the saturation concentration of dissolved oxygen as taken from Oeggerli et al. (1995) and Volume is the volume per well.

Equation (6) was integrated using MATLAB (routine *od15s*) and statistical errors were estimated using Monte Carlo simulation. Experimental data were fitted using least square criterion and the optimization routine *fmincon* of MATLAB. For each experiment two Monte-Carlo-runs (each with 200 simulations) were computed, one with a standard deviation of dissolved oxygen measurement of 5% and one with 10%. It was observed that the parameters  $k_L a$  and  $qO_2$  are significantly correlated with each other. Therefore, combinations of parameter values estimated by the Monte-Carlo method were dependent on the specified measurement error. In parameter estimation the four parameters  $qO_2$ ,  $K_L a$ ,  $\mu_{\text{max}}$  and the initial value of  $O$ , the dissolved oxygen concentration, were estimated simultaneously.

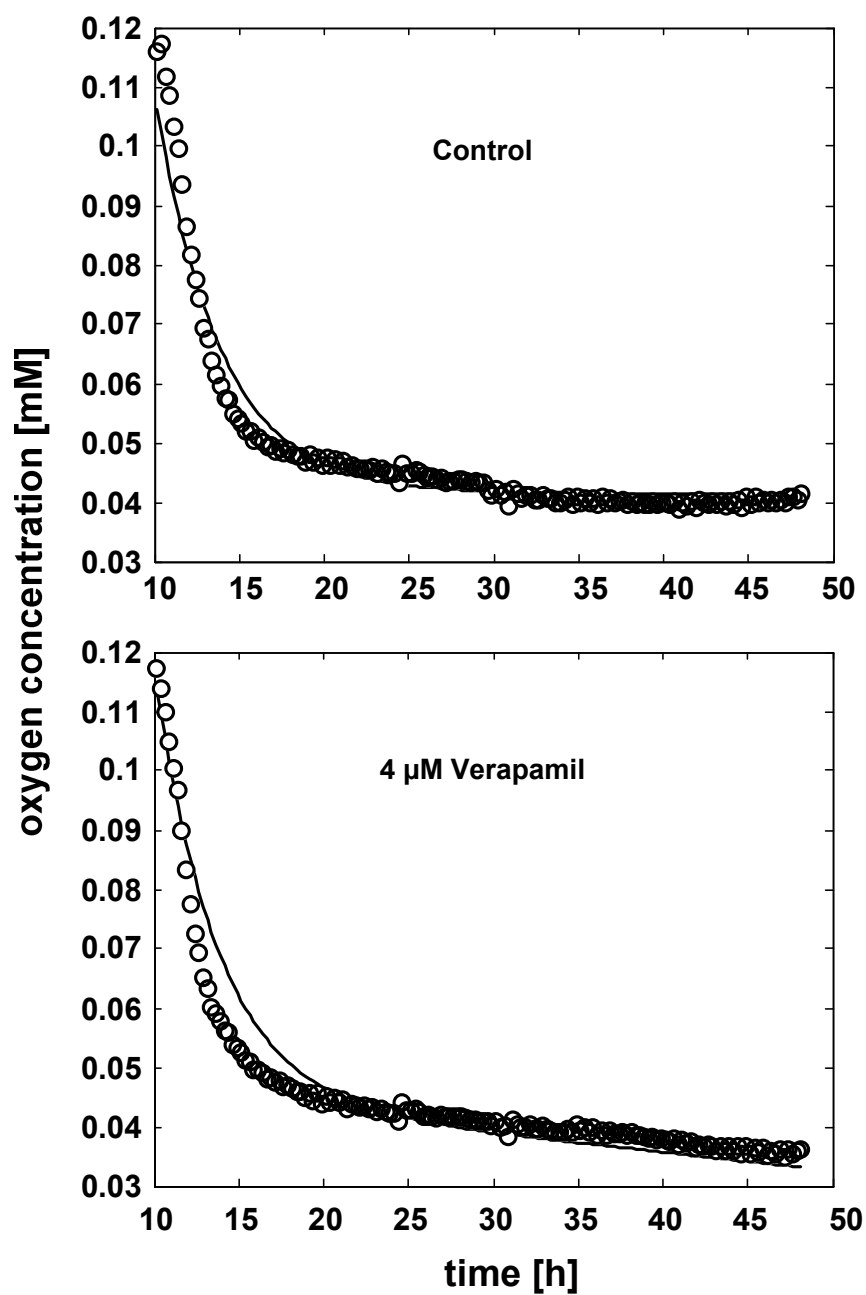


**Figure S1:** Experimental (symbols) and model calculated (full line) dissolved oxygen concentration profiles in untreated control and treated HL-1 cells (4  $\mu$ M verapamil).



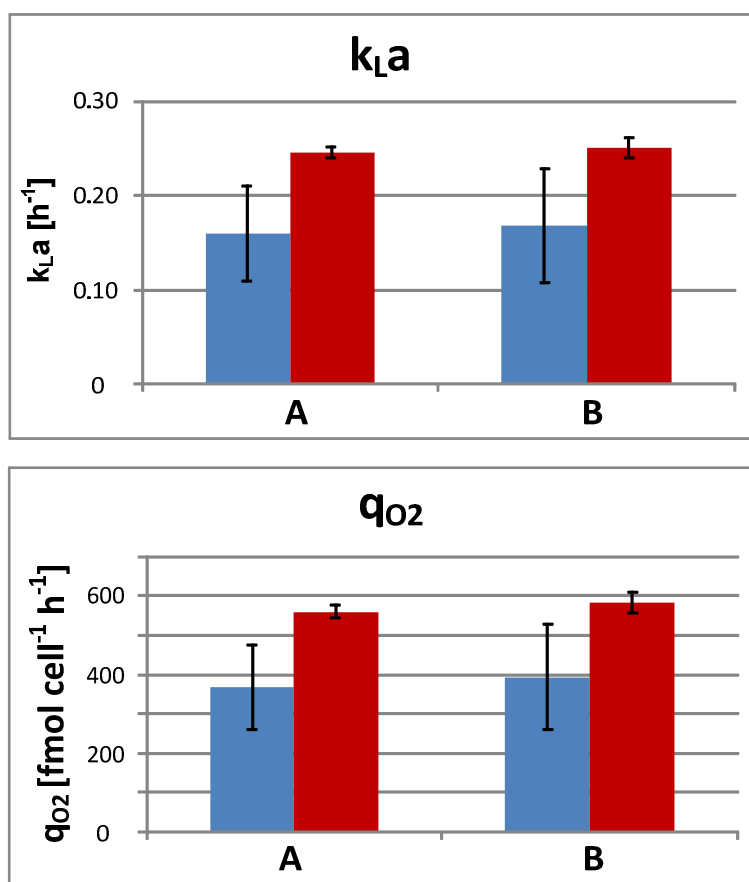


**Figure S2:** Monte-Carlo calculations of mass transfer coefficient,  $k_{La}$ , and specific oxygen uptake rate,  $q_{O_2}$ , in HL-1 cells treated with 4  $\mu\text{M}$  verapamil (A) and in untreated control (B). Light (blue) columns represent estimations assuming 10% standard deviation of dissolved oxygen concentration and dark (red) columns estimations assuming 5% error. Error bars show the resulting error in estimated parameters resulting from 200 Monte-Carlo runs.

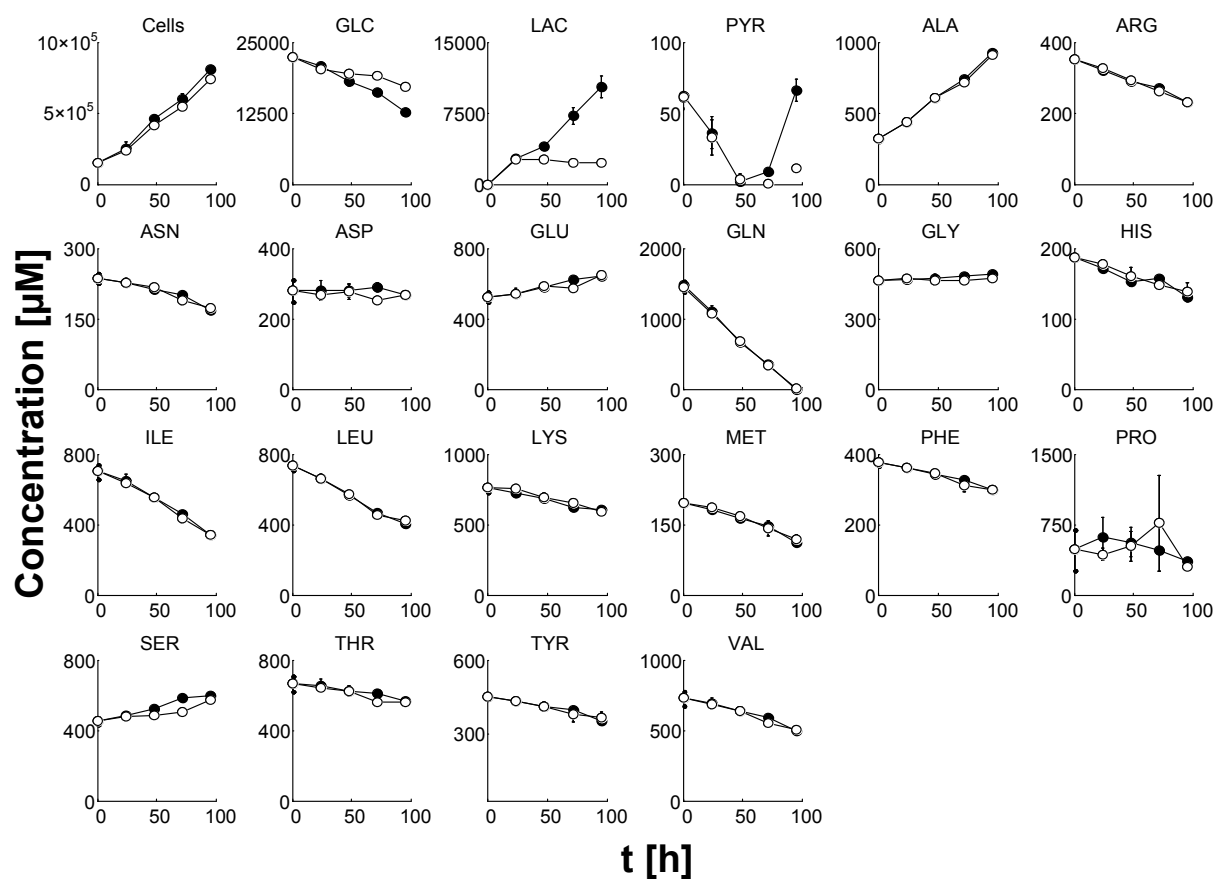


**Figure S3:** Concentrations of all considered metabolites versus time in culture medium of untreated (filled symbols) and in HL-1 cells treated with 4  $\mu\text{M}$  verapamil (open symbols). Error bars represent standard deviations from triplicate measurement.

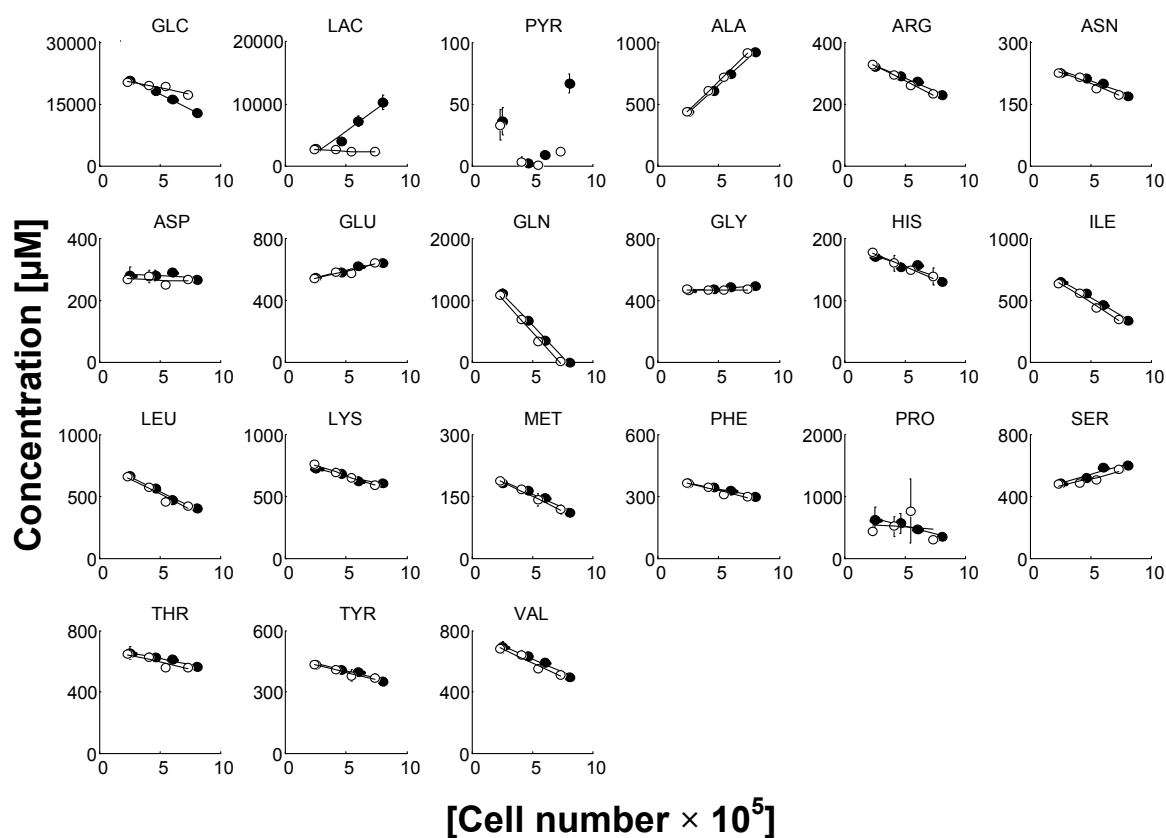


**Figure S4:** Concentrations of all considered metabolites versus cell number at each time point of the cultivation in culture medium of untreated HL-1 cells (filled symbols) and in HL-1 cells treated with 4  $\mu\text{M}$  verapamil (open symbols). The slope of each plot represents the yield coefficient ( $Y_i$ ) which was used for calculation of uptake and production rates (see Tab. 1, Chapter 4) according to equation 5 (Chapter 4). The correlation coefficients for each yield are shown in Tab. S2. Error bars represent standard deviations determined from triplicate measurement.

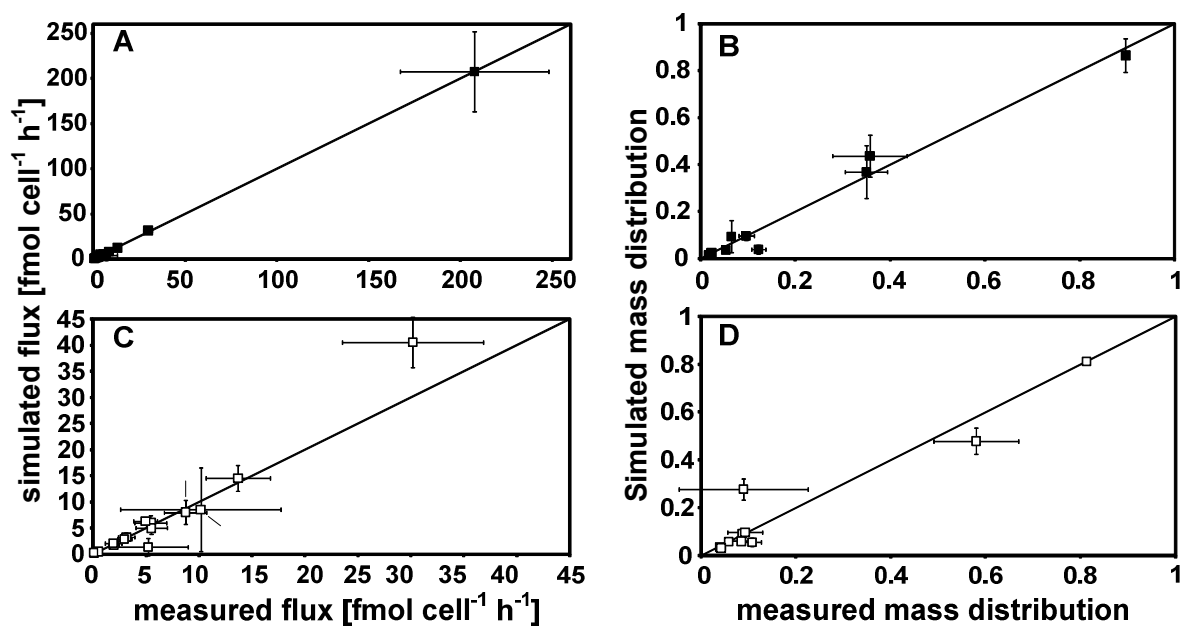


**Figure S5:** Calculated (simulated) intracellular fluxes and mass distributions as compared to experimentally measured fluxes and mass distributions in untreated controls (A and B) and in HL-1 cells treated with 4 μM verapamil (C and D).

**Table S1:** List of reactions in the metabolic network model used for the calculation of intracellular fluxes showing reactants, products, carbon transfer atom products and the metabolic pathway.

reactant	product	Atomic mechanism		pathway
		reactant carbon	product carbon	
G6P <sub>in</sub>	F6P <sub>in</sub>	[1*2*3*4*5*6]	[1*2*3*4*5*6]	Glycolysis
F6P <sub>in</sub>	G6P <sub>in</sub>	[1*2*3*4*5*6]	[1*2*3*4*5*6]	Glycolysis
F6P <sub>in</sub>	GAP <sub>in</sub>	[1*2*3*4*5*6]	[4*5*6]	Glycolysis
F6P <sub>in</sub>	GAP <sub>in</sub>	[1*2*3*4*5*6]	[3*2*1]	Glycolysis
GAP <sub>in</sub>	3PG <sub>in</sub>	[1*2*3]	[1*2*3]	Glycolysis
3PG <sub>in</sub>	PYR <sub>in</sub>	[1*2*3]	[1*2*3]	Glycolysis
PYR <sub>in</sub>	mACA <sub>in</sub>	[1*2*3]	[2*3]	TCA-cycle
mOAA <sub>in</sub>	mCIT <sub>in</sub>	[1*2*3*4]	[4*3*2*0*0*1]	TCA-cycle
mACA <sub>in</sub>	mCIT <sub>in</sub>	[1*2]	[0*0*0*2*1*0]	TCA-cycle
mCIT <sub>in</sub>	mAKG <sub>in</sub>	[1*2*3*4*5*6]	[1*2*3*4*5]	TCA-cycle
mAKG <sub>in</sub>	mSUC <sub>in</sub>	[1*2*3*4*5]	[2*3*4*5]	TCA-cycle
mSUC <sub>in</sub>	mOAA <sub>in</sub>	[1*2*3*4]	[1*2*3*4]	TCA-cycle
mSUC <sub>in</sub>	mOAA <sub>in</sub>	[1*2*3*4]	[4*3*2*1]	TCA-cycle
mOAA <sub>in</sub>	mSUC <sub>in</sub>	[1*2*3*4]	[1*2*3*4]	TCA-cycle
mOAA <sub>in</sub>	PYR <sub>in</sub>	[1*2*3*4]	[1*2*3]	Anaplerosis
PYR <sub>in</sub>	mOAA <sub>in</sub>	[1*2*3]	[1*2*3*0]	Anaplerosis
mCIT <sub>in</sub>	mOAA <sub>in</sub>	[1*2*3*4*5*6]	[6*3*2*1]	Intracellular
mCIT <sub>in</sub>	ACA <sub>in</sub>	[1*2*3*4*5*6]	[4*5]	Intracellular
mOAA <sub>in</sub>	mCIT <sub>in</sub>	[1*2*3*4]	[4*3*2*0*0*1]	Intracellular
ACA <sub>in</sub>	mCIT <sub>in</sub>	[1*2]	[0*0*0*2*1*0]	Intracellular
PYR <sub>in</sub>	LAC <sub>in</sub>	[1*2*3]	[1*2*3]	Intracellular
mOAA <sub>in</sub>	ASP <sub>in</sub>	[1*2*3*4]	[1*2*3*4]	Intracellular AA Metabolism
ASP <sub>in</sub>	mOAA <sub>in</sub>	[1*2*3*4]	[1*2*3*4]	Intracellular AA Metabolism
GLU <sub>in</sub>	mAKG <sub>in</sub>	[1*2*3*4*5]	[1*2*3*4*5]	Intracellular AA Metabolism
mAKG <sub>in</sub>	GLU <sub>in</sub>	[1*2*3*4*5]	[1*2*3*4*5]	Intracellular AA Metabolism
PYR <sub>in</sub>	ALA <sub>in</sub>	[1*2*3]	[1*2*3]	Intracellular AA Metabolism
ALA <sub>in</sub>	PYR <sub>in</sub>	[1*2*3]	[1*2*3]	Intracellular AA Metabolism
3PG <sub>in</sub>	SER <sub>in</sub>	[1*2*3]	[1*2*3]	Intracellular AA Metabolism
SER <sub>in</sub>	3PG <sub>in</sub>	[1*2*3]	[1*2*3]	Intracellular AA Metabolism
SER <sub>in</sub>	GLY <sub>in</sub>	[1*2*3]	[1*2]	Intracellular AA Metabolism
GLY <sub>in</sub>	SER <sub>in</sub>	[1*2]	[1*2*0]	Intracellular AA Metabolism
GLN <sub>in</sub>	GLU <sub>in</sub>	[1*2*3*4*5]	[1*2*3*4*5]	Intracellular AA Metabolism
GLU <sub>in</sub>	GLN <sub>in</sub>	[1*2*3*4*5]	[1*2*3*4*5]	Intracellular AA Metabolism
GLU <sub>in</sub>	PRO <sub>in</sub>	[1*2*3*4*5]	[1*2*3*4*5]	Intracellular AA Metabolism
PRO <sub>in</sub>	GLU <sub>in</sub>	[1*2*3*4*5]	[1*2*3*4*5]	Intracellular AA Metabolism
ILE <sub>in</sub>	mACA <sub>in</sub>	[1*2*3*4*5*6]	[5*6]	Intracellular AA Metabolism
ILE <sub>in</sub>	mSUC <sub>in</sub>	[1*2*3*4*5*6]	[0*2*3*4]	Intracellular AA Metabolism
LEU <sub>in</sub>	mACA <sub>in</sub>	[1*2*3*4*5*6]	[1*2]	Intracellular AA Metabolism
LEU <sub>in</sub>	mACA <sub>in</sub>	[1*2*3*4*5*6]	[3*4]	Intracellular AA Metabolism
LEU <sub>in</sub>	mACA <sub>in</sub>	[1*2*3*4*5*6]	[5*6]	Intracellular AA Metabolism
VAL <sub>in</sub>	mSUC <sub>in</sub>	[1*2*3*4*5]	[2*3*4*5]	Intracellular AA Metabolism
LYS <sub>in</sub>	mACA <sub>in</sub>	[1*2*3*4*5*6]	[2*3]	Intracellular AA Metabolism
LYS <sub>in</sub>	mACA <sub>in</sub>	[1*2*3*4*5*6]	[4*5]	Intracellular AA Metabolism
PHE <sub>in</sub>	TYR <sub>in</sub>	[1*2*3*4*5*6*7*8*9]	[1*2*3*4*5*6*7*8*9]	Intracellular AA Metabolism
TYR <sub>in</sub>	mOAA <sub>in</sub>	[1*2*3*4*5*6*7*8*9]	[6*7*8*9]	Intracellular AA Metabolism
TYR <sub>in</sub>	mACA <sub>in</sub>	[1*2*3*4*5*6*7*8*9]	[4*5]	Intracellular AA Metabolism
TYR <sub>in</sub>	mACA <sub>in</sub>	[1*2*3*4*5*6*7*8*9]	[2*3]	Intracellular AA Metabolism
LAC <sub>in</sub>	LAC <sub>ex</sub>	[1*2*3]	[1*2*3]	Secretion
PYR <sub>in</sub>	PYR <sub>ex</sub>	[1*2*3]	[1*2*3]	Secretion
ALA <sub>in</sub>	ALA <sub>ex</sub>	[1*2*3]	[1*2*3]	Secretion
GLU <sub>in</sub>	GLU <sub>ex</sub>	[1*2*3*4*5]	[1*2*3*4*5]	Secretion
GLY <sub>in</sub>	GLY <sub>ex</sub>	[1*2]	[1*2]	Secretion
SER <sub>in</sub>	SER <sub>ex</sub>	[1*2*3]	[1*2*3]	Secretion
GLC <sub>ex</sub>	G6P <sub>in</sub>	[1*2*3*4*5*6]	[1*2*3*4*5*6]	Uptake
GLN <sub>ex</sub>	GLN <sub>in</sub>	[1*2*3*4*5]	[1*2*3*4*5]	Uptake
ILE <sub>ex</sub>	ILE <sub>in</sub>	[1*2*3*4*5*6]	[1*2*3*4*5*6]	Uptake
LEU <sub>ex</sub>	LEU <sub>in</sub>	[1*2*3*4*5*6]	[1*2*3*4*5*6]	Uptake
VAL <sub>ex</sub>	VAL <sub>in</sub>	[1*2*3*4*5]	[1*2*3*4*5]	Uptake
ASP <sub>ex</sub>	ASP <sub>in</sub>	[1*2*3*4]	[1*2*3*4]	Uptake
PRO <sub>ex</sub>	PRO <sub>in</sub>	[1*2*3*4*5]	[1*2*3*4*5]	Uptake
LYS <sub>ex</sub>	LYS <sub>in</sub>	[1*2*3*4*5*6]	[1*2*3*4*5*6]	Uptake
PHE <sub>ex</sub>	PHE <sub>in</sub>	[1*2*3*4*5*6*7*8*9]	[1*2*3*4*5*6*7*8*9]	Uptake
TYR <sub>ex</sub>	TYR <sub>in</sub>	[1*2*3*4*5*6*7*8*9]	[1*2*3*4*5*6*7*8*9]	Uptake

**Table S2:** Correlation coefficients of metabolite yields (see Fig. S4, Chapter 4)

Metabolite	correlation coefficients (d[M]/d[N])	
	Untreated control	4 $\mu$ M Verapamil
GLC	-0.998	-0.96244
LAC	0.974	-0.84193
PYR	0.420	-0.57672
ALA	0.999	0.99936
ARG	-0.994	-0.99544
ASN	-0.972	-0.97336
ASP	-0.467	-0.26242
GLU	0.985	0.92923
GLN	-0.998	-0.99641
GLY	0.986	0.082844
HIS	-0.926	-0.98624
ILE	-0.997	-0.99307
LEU	-0.991	-0.96915
LYS	-0.977	-0.99958
MET	-0.986	-0.99524
PHE	-0.995	-0.96709
PRO	-0.984	-0.15852
SER	0.955	0.92734
THR	-0.984	-0.91537
TYR	-0.971	-0.97156
VAL	-0.990	-0.9765

**Table S3:** Mass isotopomer distribution of alanine in untreated control and HL-1 cells treated with 4  $\mu$ M verapamil derived from [U- $^{13}$ C $_5$ ] glutamine. Mass distribution of alanine, which was secreted by the cells into the culture medium, was analysed in samples by GC/MS. The data was used for calculation of mass isotopomer yields, as shown in Fig. 3.

alanine mass distribution [%] in untreated control				
t [h]	m+0	m+1	m+2	m+3
0	95.8 $\pm$ 1.02	3.74 $\pm$ 0.12	0.46 $\pm$ 0.23	0 $\pm$ 0.21
24	94.65 $\pm$ 0.07	4.19 $\pm$ 0.09	0.14 $\pm$ 0.11	1.01 $\pm$ 0.04
48	93.14 $\pm$ 0.1	4.56 $\pm$ 0.1	0.62 $\pm$ 0.07	1.69 $\pm$ 0.06
72	92.46 $\pm$ 0.09	5.02 $\pm$ 0.13	0.69 $\pm$ 0.14	1.82 $\pm$ 0.09
96	92.04 $\pm$ 0.35	5.33 $\pm$ 0.14	0.96 $\pm$ 0.07	1.67 $\pm$ 0.14
alanine mass distribution [%] in treated cells				
t [h]	m+0	m+1	m+2	m+3
0	95.8 $\pm$ 1.57	3.74 $\pm$ 0.21	0.46 $\pm$ 0.22	0 $\pm$ 0.11
24	94.42 $\pm$ 0.5	3.99 $\pm$ 0.2	0.33 $\pm$ 0.24	1.26 $\pm$ 0.06
48	92.12 $\pm$ 0.12	4.58 $\pm$ 0.05	0.9 $\pm$ 0.05	2.4 $\pm$ 0.03
72	89.77 $\pm$ 0.15	5.49 $\pm$ 0.19	1.63 $\pm$ 0.01	3.12 $\pm$ 0.03
96	87.79 $\pm$ 0.35	6.36 $\pm$ 0.21	2.2 $\pm$ 0.11	3.65 $\pm$ 0.03

**Table S4:** Mass isotopomer distribution of glutamate in untreated control and HL-1 cells treated with 4  $\mu\text{M}$  verapamil derived from  $[\text{U-}^{13}\text{C}_5]$  glutamine. Cells were incubated for 96 h. Mass distribution of alanine, which was secreted by the cells into the culture medium, was analysed in samples by GC/MS. The data was used for calculation of mass isotopomer yields, as shown in Fig. 4 (Chapter 4).

glutamate mass distribution [%] in untreated control						
t [h]	m+0	m+1	m+2	m+3	m+4	m+5
0	94.05 $\pm$ 1.34	4.55 $\pm$ 0.17	0.00 $\pm$ 0.00	0.03 $\pm$ 1.47	0.03 $\pm$ 0.04	0.20 $\pm$ 0.28
24	85.16 $\pm$ 0.39	7.15 $\pm$ 0.03	1.96 $\pm$ 0.17	0.64 $\pm$ 0.05	0.33 $\pm$ 0.01	4.77 $\pm$ 0.14
48	84.85 $\pm$ 0.21	5.81 $\pm$ 0.04	0.95 $\pm$ 0.01	1.10 $\pm$ 0.02	0.53 $\pm$ 0.01	6.74 $\pm$ 0.16
72	81.40 $\pm$ 0.14	6.54 $\pm$ 0.18	1.26 $\pm$ 0.10	1.61 $\pm$ 0.04	0.70 $\pm$ 0.01	8.47 $\pm$ 0.14
96	79.90 $\pm$ 0.12	6.25 $\pm$ 0.1	1.39 $\pm$ 0.10	2.18 $\pm$ 0.01	0.71 $\pm$ 0.02	9.54 $\pm$ 0.1
glutamate mass distribution [%] in cells treated with 4 $\mu\text{M}$ verapamil						
t [h]	m+0	m+1	m+2	m+3	m+4	m+5
0	94.05 $\pm$ 1.34	4.55 $\pm$ 0.17	0.00 $\pm$ 0.00	0.03 $\pm$ 1.47	0.03 $\pm$ 0.04	0.20 $\pm$ 0.28
24	88.30 $\pm$ 0.28	5.37 $\pm$ 0.01	0.57 $\pm$ 0.05	0.53 $\pm$ 0.02	0.38 $\pm$ 0.02	4.89 $\pm$ 0.21
48	82.90 $\pm$ 0.28	5.80 $\pm$ 0.02	0.95 $\pm$ 0.11	1.08 $\pm$ 0.02	0.70 $\pm$ 0.00	8.60 $\pm$ 0.16
72	80.25 $\pm$ 1.48	5.69 $\pm$ 0.65	1.14 $\pm$ 0.30	1.59 $\pm$ 0.02	0.83 $\pm$ 0.09	10.55 $\pm$ 0.49
96	75.65 $\pm$ 1.91	6.03 $\pm$ 0.64	1.79 $\pm$ 0.40	2.12 $\pm$ 0.03	1.00 $\pm$ 0.04	13.45 $\pm$ 0.78

**Table S5:** Correlation coefficients of alanine mass isotopomer yields (see Fig. 3)

Mass isotopomer	correlation coefficients (d[M]/d[N])	
	Untreated control	4 $\mu\text{M}$ Verapamil
m+0	0.999	0.999
m+1	0.996	0.993
m+2	0.995	0.989
m+3	0.973	1.000

**Table S6:** Correlation coefficients of glutamate mass isotopomer yields (see Fig. 4)

Mass isotopomer	correlation coefficients (d[M]/d[N])	
	Untreated control	4 $\mu$ M Verapamil
m+0	0.97	0.93
m+1	0.78	0.99
m+2	0.95	1.00
m+3	1.00	1.00
m+4	0.89	0.99
m+5	0.97	1.00



**Table S7:** Intracellular rates of main catabolic pathway in untreated control and in cells treated with 4  $\mu\text{M}$  verapamil. Metabolic fluxes were estimated from uptake and production rates and the mass isotopomer distribution of alanine and glutamate, derived from  $[\text{U-}^{13}\text{C}_5]$  glutamine. Standard deviations were calculated from Monte-Carlo simulation (see methods in Chapter 4). Rates were considered significantly different when  $p < 0.05$ , as calculated from two-tailed  $t$ -test.

Reaction	Specific rate [ $\text{fmol cell}^{-1} \text{h}^{-1}$ ]				$p$
	untreated control	$\pm$ s. d.	4 $\mu\text{M}$ verapamil	$\pm$ s. d.	
G6P $\rightarrow$ F6P	218.0	0.1	90.4	0.4	<0.001
F6P $\rightarrow$ GAP	218.0	0.1	90.4	0.4	<0.001
GAP $\rightarrow$ 3PG	434.5	0.2	179.1	1.0	<0.001
3PG $\rightarrow$ PYR	420.3	0.5	163.4	2.5	<0.001
PYR $\rightarrow$ ACA	228.9	39.3	191.9	13.1	n.s.
OAA+ACA $\rightarrow$ CIT	246.2	39.2	207.6	12.4	n.s.
CIT $\rightarrow$ AKG	211.4	39.4	165.9	15.4	n.s.
AKG $\rightarrow$ SUC	235.8	38.6	195.7	20.1	n.s.
SUC $\rightarrow$ OAA	247.2	44.4	205.7	21.3	n.s.
OAA $\rightarrow$ PYR	35.6	4.3	38.4	6.9	n.s.
CIT $\rightarrow$ OAA	34.7	0.7	41.7	4.6	<0.05
PYR $\rightarrow$ LAC	209.8	40.2	-8.5	8.0	<0.01
OAA $\rightarrow$ ASP	1.6	0.5	2.4	0.5	<0.05
GLU $\rightarrow$ AKG	24.4	2.6	29.8	5.9	n.s.
PYR $\rightarrow$ ALA	16.3	0.6	19.0	2.4	n.s.
3PG $\rightarrow$ SER	14.2	0.4	15.7	1.5	n.s.
SER $\rightarrow$ GLY	7.0	0.4	7.8	0.9	n.s.
GLN $\rightarrow$ GLU	29.4	1.9	37.3	5.0	<0.05
GLU $\rightarrow$ PRO	0.1	1.6	1.0	1.6	n.s.
ILE $\rightarrow$ ACA	7.2	0.8	6.7	2.3	n.s.
LEU $\rightarrow$ ACA	2.4	0.6	2.3	1.2	n.s.
VAL $\rightarrow$ SUC	4.1	1.0	3.3	1.2	n.s.
LYS $\rightarrow$ ACA	0.0	0.0	0.0	0.1	n.s.
PHE $\rightarrow$ TYR	0.5	0.2	0.3	0.3	n.s.
TYR $\rightarrow$ OAA	1.4	0.2	1.1	0.7	n.s.
NAD $^+$ +2H $^+$ +2e $^-$ $\rightarrow$ NADH+H $^+$	1207	208	1008	88	n.s.
FAD+2H $^+$ +2e $^-$ $\rightarrow$ FADH $_2$	256	46	214	25	n.s.
4e $^-$ +O $_2$ $\rightarrow$ 2O $_2^{2-}$	750	127	630	60	n.s.
ADP+P $_i$ $\rightarrow$ ATP	5640	760	4150	340	<0.05

## Chapter 5

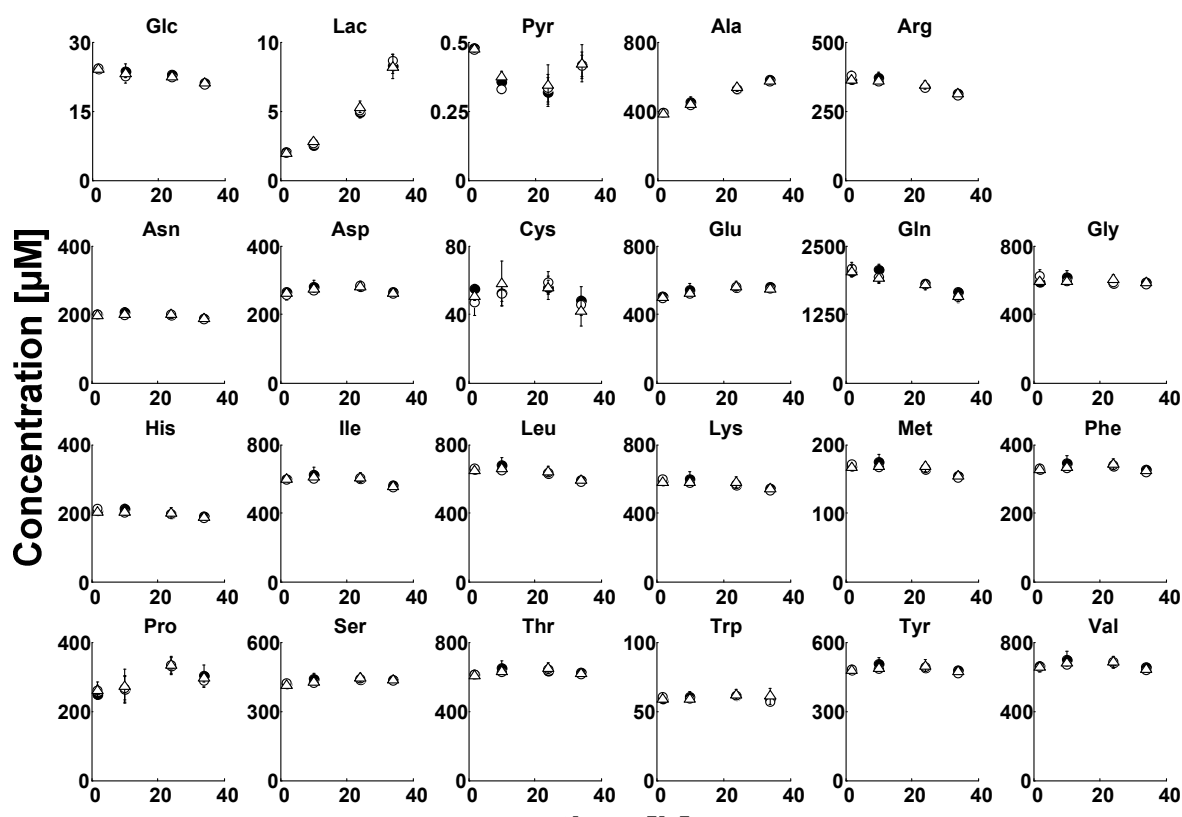


**Figure S1:** Concentration of glucose, lactate, pyruvate and 20 amino acids versus time in culture medium of untreated HL-1 cardiomyocytes (●) and cells treated with 0.01  $\mu\text{M}$  (○) and 0.02  $\mu\text{M}$  (△) Doxorubicin. Error bars indicate standard deviations from four biological replicates.

**Table S1:** Specific uptake and production rates of metabolites in HL-1 cardiomyocytes upon exposure of cells to doxorubicin at different sub-toxic concentrations. Cells were incubated for 34 h (n=4).

Metabolite	Specific rate [fmol cell <sup>-1</sup> h <sup>-1</sup> ]					
	Untreated control		0.01 $\mu$ M DXR		0.02 $\mu$ M DXR	
Glc	-299.7	$\pm$ 107.9	-288.2	$\pm$ 96.7	-262.1	$\pm$ 68.6
Lac	641.5	$\pm$ 150.4	604.3	$\pm$ 94.3	603.0	$\pm$ 94.0
Pyr	-9.5	$\pm$ 5.6	-5.2	$\pm$ 5.4	-7.6	$\pm$ 7.3
Ala	20.0	$\pm$ 4.1	18.2	$\pm$ 2.8	19.3	$\pm$ 2.5
Arg	-6.0	$\pm$ 2.3	-6.7	$\pm$ 1.9	-4.2	$\pm$ 1.4
Asn	-1.2	$\pm$ 0.7	-1.1	$\pm$ 0.6	-0.8	$\pm$ 0.8
Asp	0.1	$\pm$ 1.1	1.1	$\pm$ 1.4	0.2	$\pm$ 0.9
Cys	-0.1	$\pm$ 0.7	0.3	$\pm$ 1.0	-1.1	$\pm$ 1.1
Glu	5.9	$\pm$ 2.4	6.5	$\pm$ 2.4	6.6	$\pm$ 1.9
Gln	-45.6	$\pm$ 17.0	-44.5	$\pm$ 14.7	-38.4	$\pm$ 13.6
Gly	-1.4	$\pm$ 2.6	-4.9	$\pm$ 4.4	0.7	$\pm$ 2.1
His	-1.8	$\pm$ 1.0	-2.4	$\pm$ 0.8	-1.4	$\pm$ 1.1
Ile	-4.2	$\pm$ 2.7	-2.8	$\pm$ 2.4	-3.1	$\pm$ 1.9
Leu	-7.5	$\pm$ 4.0	-6.7	$\pm$ 2.2	-4.7	$\pm$ 2.4
Lys	-5.7	$\pm$ 3.2	-5.7	$\pm$ 2.1	-3.0	$\pm$ 2.9
Met	-1.5	$\pm$ 0.8	-1.5	$\pm$ 0.5	-0.9	$\pm$ 0.6
Phe	-0.7	$\pm$ 1.2	-0.3	$\pm$ 0.9	0.7	$\pm$ 1.1
Pro	8.6	$\pm$ 3.3	6.0	$\pm$ 2.8	6.6	$\pm$ 3.4
Ser	1.5	$\pm$ 1.4	1.5	$\pm$ 0.9	2.9	$\pm$ 1.3
Thr	0.6	$\pm$ 3.3	0.7	$\pm$ 2.5	1.4	$\pm$ 2.3
Trp	0.0	$\pm$ 0.0	0.0	$\pm$ 0.0	0.4	$\pm$ 0.5
Tyr	-0.9	$\pm$ 2.1	-0.8	$\pm$ 1.3	0.7	$\pm$ 1.6
Val	-1.2	$\pm$ 2.6	0.0	$\pm$ 2.8	-0.8	$\pm$ 2.1
Oleic acid	0.16	$\pm$ 0.09	0.29	$\pm$ 0.06	0.25	$\pm$ 0.1

**Table S2:** Mass isotopomer distribution of secreted lactate in untreated HL-1 cardiomyocytes and in cells treated with 0.01  $\mu\text{M}$  and 0.01  $\mu\text{M}$  DXR derived from  $[\text{U-}^{13}\text{C}_6]\text{glucose}$ . Mass distribution of secreted lactate was analysed by GC/MS. The data was used for calculation of mass isotopomer yields

Lactate mass distribution in untreated control				
t [h]	m+0	m+1	m+2	m+3
2	0.952	0.042	0.006	0.001
10	0.928	0.037	0.004	0.031
24	0.861	0.039	0.009	0.091
34	0.826	0.039	0.010	0.124
Lactate mass distribution (0.01 $\mu\text{M}$ DXR)				
t [h]	m+0	m+1	m+2	m+3
2	0.952	0.042	0.006	0.000
10	0.930	0.038	0.005	0.028
24	0.855	0.038	0.009	0.097
34	0.822	0.038	0.010	0.130
Lactate mass distribution (0.02 $\mu\text{M}$ DXR)				
t [h]	m+0	m+1	m+2	m+3
2	0.953	0.042	0.006	0.000
10	0.929	0.037	0.004	0.030
24	0.861	0.038	0.008	0.093
34	0.822	0.038	0.010	0.129

$m+0$ = unlabeled lactate,  $m+1$ = single labeled lactate,  $m+2$ = double labeled lactate,  $m+3$ = fully labeled lactate

**Table S3:** Mass isotopomer distribution of secreted lactate in untreated HL-1 cardiomyocytes and in cells treated with 0.01  $\mu\text{M}$  and 0.02  $\mu\text{M}$  DXR derived from  $[1,2\text{-}^{13}\text{C}_2]\text{glucose}$ . Mass distribution of secreted lactate was analysed by GC/MS. The data was used for calculation of mass isotopomer yields.

Lactate mass distribution in untreated control				
t [h]	m+0	m+1	m+2	m+3
2	0.952	0.042	0.007	0.000
10	0.943	0.039	0.018	0.000
24	0.905	0.040	0.055	0.000
34	0.888	0.042	0.070	0.000
Lactate mass distribution (0.01 $\mu\text{M}$ DXR)				
t [h]	m+0	m+1	m+2	m+3
2	0.952	0.042	0.006	0.000
10	0.943	0.038	0.019	0.000
24	0.907	0.040	0.052	0.000
34	0.888	0.042	0.070	0.001
Lactate mass distribution (0.02 $\mu\text{M}$ DXR)				
t [h]	m+0	m+1	m+2	m+3
2	0.953	0.041	0.006	0.000
10	0.942	0.038	0.020	0.000
24	0.902	0.040	0.057	0.000
34	0.887	0.042	0.070	0.001

$m+0$ = unlabeled lactate,  $m+1$ = single labeled lactate,  $m+2$ = double labeled lactate,  $m+3$ = fully labeled lactate

**Table S4:** Mass isotopomer distribution of secreted lactate in untreated HL-1 cardiomyocytes and in cells treated with 0.01  $\mu\text{M}$  and 0.02  $\mu\text{M}$  DXR derived from  $[\text{U-}^{13}\text{C}_5]\text{glutamine}$ . Mass distribution of secreted lactate was analysed by GC/MS. The data was used for calculation of mass isotopomer yields.

Lactate mass distribution in untreated control				
t [h]	m+0	m+1	m+2	m+3
2	0.952	0.042	0.006	0.000
10	0.949	0.041	0.005	0.004
24	0.942	0.044	0.007	0.007
34	0.940	0.045	0.008	0.007
Lactate mass distribution (0.01 $\mu\text{M}$ DXR)				
t [h]	m+0	m+1	m+2	m+3
2	0.953	0.042	0.006	0.000
10	0.951	0.041	0.005	0.004
24	0.942	0.044	0.007	0.007
34	0.940	0.045	0.008	0.007
Lactate mass distribution (0.02 $\mu\text{M}$ DXR)				
t [h]	m+0	m+1	m+2	m+3
2	0.953	0.041	0.005	0.000
10	0.950	0.041	0.005	0.004
24	0.942	0.044	0.007	0.007
34	0.940	0.045	0.008	0.007

*m+0= unlabeled lactate, m+1= single labeled lactate, m+2= double labeled lactate, m+3= fully labeled lactate*

**Table S5:** Intracellular fluxes in HL-1 cardiomyocytes upon exposure to doxorubicin at different sub-toxic concentrations. Cells were incubated for 34 h. Rates were determined by implementing  $^{13}\text{C}$  mass isotopomer fractions in lactate, obtained from incubating cells with  $[\text{U-}^{13}\text{C}_6]\text{glucose}$  and  $[1,2\text{-}^{13}\text{C}_6]\text{glucose}$  and  $[\text{U-}^{13}\text{C}_5]\text{glutamine}$ , into a metabolic network model. Rates were considered significantly different at  $p < 0.05$ .

reaction	specific rate [fmol cell <sup>-1</sup> h <sup>-1</sup> ]				
	untreated control	0.01 $\mu\text{M}$	<i>P</i>	0.02 $\mu\text{M}$	<i>P</i>
v1	298.4 ± 0.17	286.9 ± 0.12	<0.001	260.8 ± 0.4	<0.001
v2	298.2 ± 0.07	286.5 ± 0.05	<0.001	260.4 ± 0.2	<0.001
v3	595.4 ± 0.10	572.1 ± 0.07	<0.001	519.8 ± 0.3	<0.001
v4	591.1 ± 0.76	571.3 ± 0.97	<0.001	513.2 ± 1.4	<0.001
v5	30.7 ± 12.99	60.6 ± 15.16	<0.05	73.4 ± 55.8	n.s.
v18	16.0 ± 1.63	15.5 ± 1.23	<0.01	19.9 ± 3.1	n.s.
v20	14.6 ± 0.12	13.7 ± 0.63	<0.05	12.1 ± 2.8	n.s.
v21	560.7 ± 6.55	466.2 ± 13.97	<0.001	390.8 ± 36.3	<0.01
v23	4.3 ± 0.72	0.8 ± 0.95	<0.01	6.6 ± 1.4	<0.05
v30	0.3 ± 0.64	-2.6 ± 0.88	<0.01	2.3 ± 0.9	<0.05
v5	30.7 ± 12.99	60.6 ± 15.16	<0.05	73.4 ± 55.8	n.s.
v6	61.0 ± 7.02	142.6 ± 16.61	<0.01	148.0 ± 38.5	<0.05
v11	104.3 ± 8.18	163.5 ± 16.41	<0.01	167.6 ± 39.0	<0.05
v12	86.2 ± 8.18	144.1 ± 16.50	<0.01	147.5 ± 39.1	<0.05
v13	103.6 ± 9.09	176.2 ± 19.19	<0.01	177.7 ± 43.1	<0.05
v14	117.8 ± 9.29	183.2 ± 19.06	<0.01	181.8 ± 42.9	<0.05
v27	17.3 ± 1.56	32.1 ± 2.98	<0.001	30.2 ± 6.7	<0.05
v15	30.2 ± 13.64	81.9 ± 18.69	<0.01	74.6 ± 40.7	n.s.
v35	4.9 ± 0.62	2.1 ± 0.59	<0.01	2.1 ± 1.1	<0.05
v33	6.0 ± 0.57	2.9 ± 0.54	<0.001	1.1 ± 0.9	<0.001
v31	8.2 ± 0.53	4.1 ± 0.62	<0.001	3.0 ± 1.3	<0.01
v32	8.5 ± 0.64	4.2 ± 0.64	<0.001	4.2 ± 1.4	<0.01
v28	20.4 ± 1.10	35.4 ± 2.71	<0.001	37.8 ± 5.2	<0.01
v34	5.3 ± 0.61	5.3 ± 0.50	n.s.	2.9 ± 1.2	<0.05
v32	8.5 ± 0.64	4.2 ± 0.64	<0.001	4.2 ± 1.4	<0.01
v24	16.4 ± 13.44	62.1 ± 17.00	<0.05	61.3 ± 38.7	n.s.
v26	18.1 ± 0.30	19.4 ± 0.27	<0.01	20.2 ± 1.1	<0.05
v25	-0.4 ± 0.26	-0.1 ± 0.30	n.s.	0.9 ± 0.3	<0.01
v16	1.7 ± 13.34	-42.7 ± 17.10	<0.05	-41.1 ± 39.2	n.s.
v7	0.4 ± 0.16	0.4 ± 0.12	n.s.	0.4 ± 0.4	n.s.
v8	-0.1 ± 0.05	-0.2 ± 0.04	n.s.	-0.2 ± 0.1	n.s.
v9	-0.1 ± 0.05	-0.2 ± 0.04	n.s.	-0.2 ± 0.1	n.s.
v10	-0.1 ± 0.05	-0.2 ± 0.04	n.s.	-0.2 ± 0.1	n.s.

**Table S6:** List of reactions in the metabolic network model used for calculation of intracellular fluxes showing reactants, products, carbon transfer atom products and the metabolic pathway.

reactant	product	flux	Atomic mechanism		pathway
			reactant carbon	product carbon	
G6P <sub>in</sub>	F6P <sub>in</sub>	v1	[1*2*3*4*5*6]	[1*2*3*4*5*6]	Glycolysis
F6P <sub>in</sub>	GAP <sub>in</sub>	v2	[1*2*3*4*5*6]	[4*5*6]	Glycolysis
F6P <sub>in</sub>	GAP <sub>in</sub>	v2	[1*2*3*4*5*6]	[3*2*1]	Glycolysis
GAP <sub>in</sub>	3PG <sub>in</sub>	v3	[1*2*3]	[1*2*3]	Glycolysis
3PG <sub>in</sub>	gPYR <sub>in</sub>	v4	[1*2*3]	[1*2*3]	Glycolysis
gPYR <sub>in</sub>	mPYR <sub>in</sub>	v5	[1*2*3]	[1*2*3]	Glycolysis
mPYR <sub>in</sub>	gPYR <sub>in</sub>	v5r	[1*2*3]	[1*2*3]	Glycolysis
G6P <sub>in</sub>	P5P <sub>in</sub>	v7	[1*2*3*4*5*6]	[2*3*4*5*6]	PPP
P5P <sub>in</sub>	GAP <sub>in</sub>	v8	[1*2*3*4*5]	[0*0*0]	PPP
P5P <sub>in</sub>	GAP <sub>in</sub>	v8	[1*2*3*4*5]	[3*4*5]	PPP
P5P <sub>in</sub>	S7P <sub>in</sub>	v8	[1*2*3*4*5]	[0*0*1*2*3*4*5]	PPP
P5P <sub>in</sub>	S7P <sub>in</sub>	v8	[1*2*3*4*5]	[1*2*0*0*0*0*0]	PPP
GAP <sub>in</sub>	P5P <sub>in</sub>	v8r	[1*2*3]	[0*0*0*0*0]	PPP
S7P <sub>in</sub>	P5P <sub>in</sub>	v8r	[1*2*3*4*5*6*7]	[3*4*5*6*7]	PPP
GAP <sub>in</sub>	P5P <sub>in</sub>	v8r	[1*2*3]	[0*0*1*2*3]	PPP
S7P <sub>in</sub>	P5P <sub>in</sub>	v8r	[1*2*3*4*5*6*7]	[1*2*0*0*0]	PPP
GAP <sub>in</sub>	F6P <sub>in</sub>	v9	[1*2*3]	[0*0*0*1*2*3]	PPP
S7P <sub>in</sub>	F6P <sub>in</sub>	v9	[1*2*3*4*5*6*7]	[1*2*3*0*0*0]	PPP
GAP <sub>in</sub>	E4P <sub>in</sub>	v9	[1*2*3]	[0*0*0*0]	PPP
S7P <sub>in</sub>	E4P <sub>in</sub>	v9	[1*2*3*4*5*6*7]	[4*5*6*7]	PPP
F6P <sub>in</sub>	S7P <sub>in</sub>	v9r	[1*2*3*4*5*6]	[1*2*3*0*0*0*0]	PPP
E4P <sub>in</sub>	S7P <sub>in</sub>	v9r	[1*2*3*4]	[0*0*0*1*2*3*4]	PPP
F6P <sub>in</sub>	GAP <sub>in</sub>	v9r	[1*2*3*4*5*6]	[4*5*6]	PPP
E4P <sub>in</sub>	GAP <sub>in</sub>	v9r	[1*2*3*4]	[0*0*0]	PPP
P5P <sub>in</sub>	F6P <sub>in</sub>	v10	[1*2*3*4*5]	[1*2*0*0*0*0]	PPP
E4P <sub>in</sub>	F6P <sub>in</sub>	v10	[1*2*3*4]	[0*0*1*2*3*4]	PPP
P5P <sub>in</sub>	GAP <sub>in</sub>	v10	[1*2*3*4*5]	[3*4*5]	PPP
E4P <sub>in</sub>	GAP <sub>in</sub>	v10	[1*2*3*4]	[0*0*0]	PPP
F6P <sub>in</sub>	P5P <sub>in</sub>	v10r	[1*2*3*4*5*6]	[1*2*0*0*0]	PPP
GAP <sub>in</sub>	P5P <sub>in</sub>	v10r	[1*2*3]	[0*0*1*2*3]	PPP
F6P <sub>in</sub>	E4P <sub>in</sub>	v10r	[1*2*3*4*5*6]	[3*4*5*6]	PPP
GAP <sub>in</sub>	E4P <sub>in</sub>	v10r	[1*2*3]	[0*0*0*0]	PPP
mPYR <sub>in</sub>	mACA <sub>in</sub>	v6	[1*2*3]	[2*3]	TCA
mOAA <sub>in</sub>	mCIT <sub>in</sub>	v11	[1*2*3*4]	[4*3*2*0*0*1]	TCA
mACA <sub>in</sub>	mCIT <sub>in</sub>	v11	[1*2]	[0*0*0*2*1*0]	TCA
mCIT <sub>in</sub>	mAKG <sub>in</sub>	v12	[1*2*3*4*5*6]	[1*2*3*4*5]	TCA
mAKG <sub>in</sub>	mSUC <sub>in</sub>	v13	[1*2*3*4*5]	[2*3*4*5]	TCA
mSUC <sub>in</sub>	mOAA <sub>in</sub>	v14	[1*2*3*4]	[1*2*3*4]	TCA
mSUC <sub>in</sub>	mOAA <sub>in</sub>	v14	[1*2*3*4]	[4*3*2*1]	TCA
mOAA <sub>in</sub>	mSUC <sub>in</sub>	v14r	[1*2*3*4]	[1*2*3*4]	TCA
mOAA <sub>in</sub>	mPYR <sub>in</sub>	v15	[1*2*3*4]	[1*2*3]	Anaplerosis
mPYR <sub>in</sub>	mOAA <sub>in</sub>	v15r	[1*2*3]	[1*2*3*0]	Anaplerosis
CO2ixx	mOAA <sub>in</sub>	v15r	[1]	[0*0*0*1]	Anaplerosis

OAA <sub>in</sub>	gPYR <sub>in</sub>	v16	[1*2*3*4]	[1*2*3]	Anaplerosis
gPYR <sub>in</sub>	OAA <sub>in</sub>	v16r	[1*2*3]	[1*2*3*0]	Anaplerosis
CO2ixx	OAA <sub>in</sub>	v16r	[1]	[0*0*0*1]	Anaplerosis
OAA <sub>in</sub>	mOAA <sub>in</sub>	v24	[1*2*3*4]	[1*2*3*4]	Intracellular
mOAA <sub>in</sub>	OAA <sub>in</sub>	v24r	[1*2*3*4]	[1*2*3*4]	Intracellular
mCIT <sub>in</sub>	OAA <sub>in</sub>	v26	[1*2*3*4*5*6]	[6*3*2*1]	Intracellular
mCIT <sub>in</sub>	ACA <sub>in</sub>	v26	[1*2*3*4*5*6]	[4*5]	Intracellular
OAA <sub>in</sub>	mCIT <sub>in</sub>	v26r	[1*2*3*4*5*6]	[4*3*2*0*0*1]	Intracellular
ACA <sub>in</sub>	mCIT <sub>in</sub>	v26r	[1*2]	[0*0*0*2*1*0]	Intracellular
PYR <sub>in</sub>	gPYR <sub>in</sub>	v20	[1*2*3]	[1*2*3]	Intracellular Pyr
ALA <sub>in</sub>	gPYR <sub>in</sub>	v18	[1*2*3]	[1*2*3]	Intracellular Pyr
gPYR <sub>in</sub>	ALA <sub>in</sub>	v18r	[1*2*3]	[1*2*3]	Intracellular Pyr
gPYR <sub>in</sub>	LAC <sub>in</sub>	v21	[1*2*3]	[1*2*3]	Intracellular Pyr
mOAA <sub>in</sub>	ASP <sub>in</sub>	v25	[1*2*3*4]	[1*2*3*4]	AA Metabolism
ASP <sub>in</sub>	mOAA <sub>in</sub>	v25r	[1*2*3*4]	[1*2*3*4]	AA Metabolism
GLU <sub>in</sub>	mAKG <sub>in</sub>	v27	[1*2*3*4*5]	[1*2*3*4*5]	AA Metabolism
mAKG <sub>in</sub>	GLU <sub>in</sub>	v27r	[1*2*3*4*5]	[1*2*3*4*5]	AA Metabolism
3PG <sub>in</sub>	SER <sub>in</sub>	v23	[1*2*3]	[1*2*3]	AA Metabolism
SER <sub>in</sub>	3PG <sub>in</sub>	v23r	[1*2*3]	[1*2*3]	AA Metabolism
SER <sub>in</sub>	GLY <sub>in</sub>	v30	[1*2*3]	[1*2]	AA Metabolism
GLY <sub>in</sub>	SER <sub>in</sub>	v30r	[1*2]	[1*2*0]	AA Metabolism
MTFixx	SER <sub>in</sub>	v30r	[1]	[0*0*1]	AA Metabolism
GLN <sub>in</sub>	GLU <sub>in</sub>	v28	[1*2*3*4*5]	[1*2*3*4*5]	AA Metabolism
GLU <sub>in</sub>	GLN <sub>in</sub>	v28r	[1*2*3*4*5]	[1*2*3*4*5]	AA Metabolism
GLU <sub>in</sub>	PRO <sub>in</sub>	v29	[1*2*3*4*5]	[1*2*3*4*5]	AA Metabolism
PRO <sub>in</sub>	GLU <sub>in</sub>	v29r	[1*2*3*4*5]	[1*2*3*4*5]	AA Metabolism
ILE <sub>in</sub>	mACA <sub>in</sub>	v31	[1*2*3*4*5*6]	[5*6]	AA Metabolism
CO2ixx	mACA <sub>in</sub>	v31	[1]	[0*0]	AA Metabolism
ILE <sub>in</sub>	mSUC <sub>in</sub>	v31	[1*2*3*4*5*6]	[0*2*3*4]	AA Metabolism
CO2ixx	mSUC <sub>in</sub>	v31	[1]	[1*0*0*0]	AA Metabolism
LEU <sub>in</sub>	mACA <sub>in</sub>	v32	[1*2*3*4*5*6]	[1*2]	AA Metabolism
LEU <sub>in</sub>	mACA <sub>in</sub>	v32	[1*2*3*4*5*6]	[3*4]	AA Metabolism
LEU <sub>in</sub>	mACA <sub>in</sub>	v32	[1*2*3*4*5*6]	[5*6]	AA Metabolism
VAL <sub>in</sub>	mSUC <sub>in</sub>	v33	[1*2*3*4*5]	[2*3*4*5]	AA Metabolism
ARG <sub>in</sub>	GLU <sub>in</sub>	v34	[1*2*3*4*5]	[1*2*3*4*5]	AA Metabolism
LYS <sub>in</sub>	mACA <sub>in</sub>	v35	[1*2*3*4*5*6]	[2*3]	AA Metabolism
LYS <sub>in</sub>	mACA <sub>in</sub>	v35	[1*2*3*4*5*6]	[4*5]	AA Metabolism
LAC <sub>in</sub>	LAC <sub>ex</sub>	vext1	[1*2*3]	[1*2*3]	Secretion
ALA <sub>in</sub>	ALA <sub>ex</sub>	vext2	[1*2*3]	[1*2*3]	Secretion
GLU <sub>in</sub>	GLU <sub>ex</sub>	vext3	[1*2*3*4*5]	[1*2*3*4*5]	Secretion
PRO <sub>in</sub>	PRO <sub>ex</sub>	vext4	[1*2*3*4*5]	[1*2*3*4*5]	Secretion
SER <sub>in</sub>	SER <sub>ex</sub>	vext5	[1*2*3]	[1*2*3]	Secretion
GLN <sub>ex</sub>	GLN <sub>in</sub>	vinp2	[1*2*3*4*5]	[1*2*3*4*5]	Uptake
ARG <sub>ex</sub>	ARG <sub>in</sub>	vinp3	[1*2*3*4*5]	[1*2*3*4*5]	Uptake
ASP <sub>ex</sub>	ASP <sub>in</sub>	vinp4	[1*2*3*4]	[1*2*3*4]	Uptake
GLY <sub>ex</sub>	GLY <sub>in</sub>	vinp5	[1*2]	[1*2]	Uptake
ILE <sub>ex</sub>	ILE <sub>in</sub>	vinp6	[1*2*3*4*5*6]	[1*2*3*4*5*6]	Uptake



LEU <sub>ex</sub>	LEU <sub>in</sub>	vinp7	[1*2*3*4*5*6]	[1*2*3*4*5*6]	Uptake
LYS <sub>ex</sub>	LYS <sub>in</sub>	vinp8	[1*2*3*4*5*6]	[1*2*3*4*5*6]	Uptake
PYR <sub>ex</sub>	PYR <sub>in</sub>	vinp9	[1*2*3]	[1*2*3]	Uptake
VAL <sub>ex</sub>	VAL <sub>in</sub>	vinp10	[1*2*3*4*5]	[1*2*3*4*5]	Uptake

## Chapter 6

**Table S1:** List of reactions in the metabolic network model used for calculation of intracellular fluxes in untreated hESC-CM showing reactants, products, carbon transfer atom products and the metabolic pathway.

reactant	product	flux	Atomic mechanism		pathway
			reactant carbon	product carbon	
G6P <sub>in</sub>	F6P <sub>in</sub>	v1	[1*2*3*4*5*6]	[6*6]	Glycolysis
F6P <sub>in</sub>	G6P <sub>in</sub>	v1r	[1*2*3*4*5*6]	[6*6]	Glycolysis
F6P <sub>in</sub>	GAP <sub>in</sub>	v2	[4*5*6]	[6*3]	Glycolysis
F6P <sub>in</sub>	GAP <sub>in</sub>	v2	[3*2*1]	[6*3]	Glycolysis
GAP <sub>in</sub>	3PG <sub>in</sub>	v3	[1*2*3]	[3*3]	Glycolysis
3PG <sub>in</sub>	PYR <sub>in</sub>	v4	[1*2*3]	[3*3]	Glycolysis
PYR <sub>in</sub>	mACA <sub>in</sub>	v5	[2*3]	[3*2]	TCA
mOAA <sub>in</sub>	mCIT <sub>in</sub>	v6	[4*3*2*0*0*1]	[4*6]	TCA
mACA <sub>in</sub>	mCIT <sub>in</sub>	v6	[0*0*0*2*1*0]	[2*6]	TCA
mCIT <sub>in</sub>	mAKG <sub>in</sub>	v7	[1*2*3*4*5]	[6*5]	TCA
mAKG <sub>in</sub>	mSUC <sub>in</sub>	v8	[2*3*4*5]	[5*4]	TCA
mSUC <sub>in</sub>	mOAA <sub>in</sub>	v9	[1*2*3*4]	[4*4]	TCA
mSUC <sub>in</sub>	mOAA <sub>in</sub>	v9	[4*3*2*1]	[4*4]	TCA
mOAA <sub>in</sub>	mSUC <sub>in</sub>	v9r	[1*2*3*4]	[4*4]	TCA
mOAA <sub>in</sub>	PYR <sub>in</sub>	v10	[1*2*3]	[4*3]	Anaplerosis
PYR <sub>in</sub>	mOAA <sub>in</sub>	v10r	[1*2*3*0]	[3*4]	Anaplerosis
CO2 <sub>ixx</sub>	mOAA <sub>in</sub>	v10r	[0*0*0*1]	[1*4]	Anaplerosis
mCIT <sub>in</sub>	mOAA <sub>in</sub>	v11	[6*3*2*1]	[6*4]	Intracellular
mCIT <sub>in</sub>	ACA <sub>in</sub>	v11	[4*5]	[6*2]	Intracellular
mOAA <sub>in</sub>	mCIT <sub>in</sub>	v11r	[4*3*2*0*0*1]	[4*6]	Intracellular
ACA <sub>in</sub>	mCIT <sub>in</sub>	v11r	[0*0*0*2*1*0]	[2*6]	Intracellular
PYR <sub>in</sub>	LAC <sub>in</sub>	v12	[1*2*3]	[3*3]	Intracellular
mOAA <sub>in</sub>	ASPin	v13	[1*2*3*4]	[4*4]	AA metabolism
ASPin	mOAA <sub>in</sub>	v13r	[1*2*3*4]	[4*4]	AA metabolism
GLU <sub>in</sub>	mAKG <sub>in</sub>	v14	[1*2*3*4*5]	[5*5]	AA metabolism
mAKG <sub>in</sub>	GLU <sub>in</sub>	v14r	[1*2*3*4*5]	[5*5]	AA metabolism
PYR <sub>in</sub>	ALAIN	v15	[1*2*3]	[3*3]	AA metabolism
ALAIN	PYR <sub>in</sub>	v15r	[1*2*3]	[3*3]	AA metabolism
3PG <sub>in</sub>	SER <sub>in</sub>	v16	[1*2*3]	[3*3]	AA metabolism
SER <sub>in</sub>	3PG <sub>in</sub>	v16r	[1*2*3]	[3*3]	AA metabolism
SER <sub>in</sub>	GLY <sub>in</sub>	v17	[1*2]	[3*2]	AA metabolism
GLY <sub>in</sub>	SER <sub>in</sub>	v17r	[1*2*0]	[2*3]	AA metabolism
MTF <sub>ixx</sub>	SER <sub>in</sub>	v17r	[0*0*1]	[1*3]	AA metabolism
GLN <sub>in</sub>	GLU <sub>in</sub>	v18	[1*2*3*4*5]	[5*5]	AA metabolism
GLU <sub>in</sub>	GLN <sub>in</sub>	v18r	[1*2*3*4*5]	[5*5]	AA metabolism
GLU <sub>in</sub>	PRO <sub>in</sub>	v19	[1*2*3*4*5]	[5*5]	AA metabolism
PRO <sub>in</sub>	GLU <sub>in</sub>	v19r	[1*2*3*4*5]	[5*5]	AA metabolism
LEU <sub>in</sub>	mACA <sub>in</sub>	v21	[1*2]	[6*2]	AA metabolism
LEU <sub>in</sub>	mACA <sub>in</sub>	v21	[3*4]	[6*2]	AA metabolism
LEU <sub>in</sub>	mACA <sub>in</sub>	v21	[5*6]	[6*2]	AA metabolism

LYSin	mACAin	v23	[2*3]	[6*2]	AA metabolism
LYSin	mACAin	v23	[4*5]	[6*2]	AA metabolism
PHEin	TYRin	v24	[1*2*3*4*5*6*7*8*9]	[9*9]	AA metabolism
TYRin	mOAAin	v25	[6*7*8*9]	[9*4]	AA metabolism
TYRin	mACAin	v25	[4*5]	[9*2]	AA metabolism
TYRin	mACAin	v25	[2*3]	[9*2]	AA metabolism
ARGin	GLUin	v34	[1*2*3*4*5]	[5*5]	AA metabolism
ALAin	ALAx	vext1	[1*2*3]	[3*3]	Secretion
GLUin	GLUx	vext2	[1*2*3*4*5]	[5*5]	Secretion
LACin	LACx	vext3	[1*2*3]	[3*3]	Secretion
PROin	PROx	vext4	[1*2*3*4*5]	[5*5]	Secretion
PYRin	PYRx	vext5	[1*2*3]	[3*3]	Secretion
GLClab	G6Pin	vinp1	[1*2*3*4*5*6]	[6*6]	Norm Uptake
ARGnon	ARGin	vinp2	[1*2*3*4*5]	[5*5]	Uptake
ASPnon	ASPin	vinp3	[1*2*3*4]	[4*4]	Uptake
HISnon	HISin	vinp4	[1*2*3*4*5*6]	[6*6]	Uptake
LEUnon	LEUin	vinp5	[1*2*3*4*5*6]	[6*6]	Uptake
LYSnon	LYSin	vinp6	[1*2*3*4*5*6]	[6*6]	Uptake
PHEnon	PHEin	vinp7	[1*2*3*4*5*6*7*8*9]	[9*9]	Uptake
SERnon	SERin	vinp8	[1*2*3]	[3*3]	Uptake
TYRnon	TYRin	vinp9	[1*2*3*4*5*6*7*8*9]	[9*9]	Uptake
GLNnon	GLNin	vinp10	[1*2*3*4*5]	[5*5]	Uptake
GLYnon	GLYin	vinp11	[1*2]	[2*2]	Uptake

**Table S2:** List of reactions in the metabolic network model used for calculation of intracellular fluxes in hESC-CM treated with doxorubicin showing reactants, products, carbon transfer atom products and the metabolic pathway.

reactant	product	flux	Atomic mechanism		pathway
			reactant carbon	product carbon	
G6Pin	F6Pin	v1	[1*2*3*4*5*6]	[6*6]	Glycolysis
F6Pin	G6Pin	v1r	[1*2*3*4*5*6]	[6*6]	Glycolysis
F6Pin	GAPin	v2	[4*5*6]	[6*3]	Glycolysis
F6Pin	GAPin	v2	[3*2*1]	[6*3]	Glycolysis
GAPin	3PGin	v3	[1*2*3]	[3*3]	Glycolysis
3PGin	PYRin	v4	[1*2*3]	[3*3]	Glycolysis
PYRin	mACAin	v5	[2*3]	[3*2]	TCA
mOAAin	mCITin	v6	[4*3*2*0*0*1]	[4*6]	TCA
mACAin	mCITin	v6	[0*0*0*2*1*0]	[2*6]	TCA
mCITin	mAKGin	v7	[1*2*3*4*5]	[6*5]	TCA
mAKGin	mSUCin	v8	[2*3*4*5]	[5*4]	TCA
mSUCin	mOAAin	v9	[1*2*3*4]	[4*4]	TCA
mSUCin	mOAAin	v9	[4*3*2*1]	[4*4]	TCA
mOAAin	mSUCin	v9r	[1*2*3*4]	[4*4]	TCA
mOAAin	PYRin	v10	[1*2*3]	[4*3]	Anaplerosis
PYRin	mOAAin	v10r	[1*2*3*0]	[3*4]	Anaplerosis
CO2ixx	mOAAin	v10r	[0*0*0*1]	[1*4]	Anaplerosis
mCITin	mOAAin	v11	[6*3*2*1]	[6*4]	Intracellular
mCITin	ACAin	v11	[4*5]	[6*2]	Intracellular
mOAAin	mCITin	v11r	[4*3*2*0*0*1]	[4*6]	Intracellular
ACAin	mCITin	v11r	[0*0*0*2*1*0]	[2*6]	Intracellular
PYRin	LACin	v12	[1*2*3]	[3*3]	Intracellular
mOAAin	ASPin	v13	[1*2*3*4]	[4*4]	AA metabolism
ASPin	mOAAin	v13r	[1*2*3*4]	[4*4]	AA metabolism

GLUin	mAKGin	v14	[1*2*3*4*5]	[5*5]	AA metabolism
mAKGin	GLUin	v14r	[1*2*3*4*5]	[5*5]	AA metabolism
PYRin	ALAin	v15	[1*2*3]	[3*3]	AA metabolism
ALAin	PYRin	v15r	[1*2*3]	[3*3]	AA metabolism
3PGin	SERin	v16	[1*2*3]	[3*3]	AA metabolism
SERin	3PGin	v16r	[1*2*3]	[3*3]	AA metabolism
SERin	GLYin	v17	[1*2]	[3*2]	AA metabolism
GLYin	SERin	v17r	[1*2*0]	[2*3]	AA metabolism
MTFixx	SERin	v17r	[0*0*1]	[1*3]	AA metabolism
GLNin	GLUin	v18	[1*2*3*4*5]	[5*5]	AA metabolism
GLUin	GLNin	v18r	[1*2*3*4*5]	[5*5]	AA metabolism
GLUin	PROin	v19	[1*2*3*4*5]	[5*5]	AA metabolism
PROin	GLUin	v19r	[1*2*3*4*5]	[5*5]	AA metabolism
LEUin	mACAin	v21	[1*2]	[6*2]	AA metabolism
LEUin	mACAin	v21	[3*4]	[6*2]	AA metabolism
LEUin	mACAin	v21	[5*6]	[6*2]	AA metabolism
LYSin	mACAin	v23	[2*3]	[6*2]	AA metabolism
LYSin	mACAin	v23	[4*5]	[6*2]	AA metabolism
PHEin	TYRin	v24	[1*2*3*4*5*6*7*8*9]	[9*9]	AA metabolism
TYRin	mOAAin	v25	[6*7*8*9]	[9*4]	AA metabolism
TYRin	mACAin	v25	[4*5]	[9*2]	AA metabolism
TYRin	mACAin	v25	[2*3]	[9*2]	AA metabolism
ARGin	GLUin	v34	[1*2*3*4*5]	[5*5]	AA metabolism
ALAin	ALAex	vext1	[1*2*3]	[3*3]	Secretion
GLNin	GLNex	vext2	[1*2*3*4*5]	[5*5]	Secretion
GLUin	GLUex	vext3	[1*2*3*4*5]	[5*5]	Secretion
GLYin	GLYex	vext4	[1*2]	[2*2]	Secretion
LACin	LACex	vext5	[1*2*3]	[3*3]	Secretion
PROin	PROex	vext6	[1*2*3*4*5]	[5*5]	Secretion
PYRin	PYRex	vext7	[1*2*3]	[3*3]	Secretion
GLClab	G6Pin	vinp1	[1*2*3*4*5*6]	[6*6]	Norm Uptake
ARGnon	ARGin	vinp2	[1*2*3*4*5]	[5*5]	Uptake
ASPnon	ASPin	vinp3	[1*2*3*4]	[4*4]	Uptake
HISnon	HISin	vinp4	[1*2*3*4*5*6]	[6*6]	Uptake
LEUnon	LEUin	vinp5	[1*2*3*4*5*6]	[6*6]	Uptake
LYSnon	LYSin	vinp6	[1*2*3*4*5*6]	[6*6]	Uptake
PHEnon	PHEin	vinp7	[1*2*3*4*5*6*7*8*9]	[9*9]	Uptake
SERnon	SERin	vinp8	[1*2*3]	[3*3]	Uptake
TYRnon	TYRin	vinp9	[1*2*3*4*5*6*7*8*9]	[9*9]	Uptake

## List of publications:

### Journal articles

- Strigun, A.**, Wahrheit, J., Niklas, J., Heinzle, E., Noor, F. (2011). Doxorubicin increases oxidative metabolism in HL-1 cardiomyocytes as shown by  $^{13}\text{C}$ -metabolic flux analysis. **Toxicological Sciences**, doi: 10.1093/toxsci/kfr298
- Strigun, A.**, Noor, F., Pironti, A., Niklas, J., Yang, T.H., Heinzle, E. (2011). Metabolic flux analysis gives an insight on verapamil induced changes in central metabolism of HL-1 cells. **Journal of Biotechnology** **155**, 299– 307.
- Strigun, A.**, Wahrheit, J., Beckers, S., Heinzle, E., Noor, F. (2011). Metabolic profiling using HPLC allows classification of drugs according to their mechanisms of action in HL-1 cardiomyocytes. **Toxicology and Applied Pharmacology** **15**, 183-91.
- Beckers, S., Noor, F., Müller-Vieira, U., Mayer, M., **Strigun, A.**, Heinzle, E. (2010). High throughput, non invasive and dynamic toxicity screening on adherent cells using respiratory measurements. **Toxicology in Vitro** **24**, 686–694.
- Strigun, A.**, Wahrheit, J., Heinzle, E., Noor, F. (2012). EC<sub>50</sub>-dynamics for better understanding of cytotoxicity. In preparation.
- Strigun, A.**, Niklas, J., Heinzle, E., Noor, F. (2012). Characterisation of the central metabolism in cardiomyocytes derived from human embryonic stem cells and its changes due to exposure to Doxorubicin. In preparation.
- Hadjivassiliou, M., Aeschlimann, P., **Strigun, A.**, Sanders, D. S., Woodroffe, N., Aeschlimann, D. (2008). Autoantibodies in gluten ataxia recognize a novel neuronal transglutaminase. **Annals of Neurology** **64**, 332-343.

### Poster presentation

- Metabonomic Characterisation of Human Embryonic Stem Cell Derived Cardiomyocytes in Response to the Calcium Channel Blocker Verapamil. **Screening, MedChem and ADMET Europe** 23-25 February 2009, Berlin.

## Curriculum vitae

### Persönliche Angaben

Geburtstag: 25.11.1981  
Geburtsstadt: München

### Berufliche Tätigkeiten

04/2007 – voraus-  
sichtlich 01/2012

**Dissertation** am Institut für Technische Biochemie der Universität des Saarlandes bei Prof. Dr. Heinzle im Rahmen des EU-Projekts „Invitroheart“

06/2006 – 11/2006

**Wissenschaftlicher Mitarbeiter** an der School of Dentistry, Cardiff University, Wales, Großbritannien

11/2005 – 05/2006

„**Post-Ing**“-**Mitarbeiter** bei der Fa. N-Zyme BioTec GmbH (jetzt Zedira), Darmstadt, Deutschland

### Studium und Schule

04/2007 – voraus-  
Sichtlich 03/2012

**Promotionsstudium** an der Universität des Saarlandes

09/2001 – 01/2006

**Diplom-Ingenieur (FH)**  
Studium der Biotechnologie an der University of Applied Sciences, Darmstadt, Deutschland

03/2003 – 07/2003

**Betriebspraktisches Semester** bei der Fa. Immundiagnostik AG, Bensheim, Deutschland

06/2001

**Allgemeine Hochschulreife** an der Georg Büchner Schule, Darmstadt